NNT : 0000AIXM0000

THÈSE DE DOCTORAT

Soutenue à Aix-Marseille Université
le 25 Septembre 2024 par

Orion FARR

Mineral spirits: The redox transformations of CO_2 & CH_4 mediated by $Fe^{2+/3+}$oxyhydroxide "green rust" minerals

Discipline

PHYSIQUE ET SCIENCES DE LA MATIERE

Spécialité

Matière Condensée et Nanosciences

École doctorale

ED 352

Laboratoire/Partenaires de recherche

Bioénergétique et Ingénierie des Protéines (BIP), CNRS UMR 7281
Centre Interdisciplinaire de Nanoscience de Marseille (CINaM), CNRS UMR 7325

Composition du jury

François GUYOT	Président du jury, examinateur
Professeur, Muséum National d'Histoire Naturelle	
Abderrazak EL ALBANI	Rapporteur
Professeur, Université de Poitiers	
Laurent CHARLET	Rapporteur
Professeur Emérite, Université de Grenoble Alpes	
Anabella IVANCICH	Examinatrice
Directrice de Recherche, CNRS	
Christian RUBY	Examinateur
Professeur, Université de Lorraine	
Daniel FERRY	Directeur de thèse
Chargé de recherche, CNRS	
Wolfgang NITSCHKE	Co-encadrant de thèse
Directeur de recherche, CNRS	
Simon DUVAL	Membre invité
Chargé de recherche, CNRS	
Michael J. RUSSELL	Membre invité
Professeur Emérite, Université de Turin	

Affidavit

I, undersigned, Orion Farr, hereby declare that the work presented in this manuscript is my own work, carried out under the scientific supervision of Daniel Ferry, in accordance with the principles of honesty, integrity and responsibility inherent to the research mission. The research work and the writing of this manuscript have been carried out in compliance with both the French national charter for Research Integrity and the Aix-Marseille University charter on the fight against plagiarism.

This work has not been submitted previously either in this country or in another country in the same or in a similar version to any other examination body.

Place Marseille, date 9 juillet 2024



Cette œuvre est mise à disposition selon les termes de la Licence Creative Commons Attribution - Pas d'Utilisation Commerciale - Pas de Modification 4.0 International.

Liste de publications et/ou brevets et participation aux conférences

1) Liste des publications et/ou brevet [a] réalisés dans le cadre du projet de thèse :

1. **Farr, O.**, Gaudu, N., Truong, C., Duval., S., Russell, M. J. (2024). Green rusts offered ingestion and respiration channels for CO_2, CH_4, & thus life's emergence, *MILS,. In preparation*
2. Nitschke, W., **Farr, O.**, Gaudu, N., Truong, C., Guyot, F., Russell, M. J., & Duval, S. (2024). The Winding Road from Origin to Emergence (of Life). *Life*, *14*(5), 607. https://doi.org/10.3390/life14050607
3. **Farr, O.**, Gaudu, N., Danger, G., Russell, M., Ferry, D., Nitschke, W., Duval, S., Methanol on the rocks: Green rust transformation promotes transformation of methane, Journal of the Royal Society Interface 20, 206 (2023) http://dx.doi.org/10.1098/rsif.2023.0386
4. Gaudu, N., **Farr, O.**, Ona-Nguema, G., Duval, S., Dissolved metal ions and mineral-liposome hybrid systems, Biochemie (2023) https://doi.org/10.1016/j.biochi.2023.09.009
5. Nitschke, B.Schoepp-Cothenet, S. Duval, K. Zuchan, **O. Farr**, F.Baymann, F. Panico, A. Minguzzi, E. Branscomb, M. J. Russell., Aqueous electrochemistry; the toolbox for life's emergence from redox disequilibria, Electrochem Sci Adv.2022, 2100192. https://doi.org/10.1002/elsa.202100192

2) Participation aux conférences[b] et écoles d'été au cours de la période de thèse :

1. **Farr, O.,** Mineral Spirits: reactive nano-minerals catalyze CO_2 reduction, IPGP 2024, Paris, France (invited department talk)
2. **Farr, O.**, Nil, G., Danger, G., Russell, M., Ferry, D., Nitschke, W., Duval, S., "Methanol on the rocks: Green rusts promote redox cycling of greenhouse gasses", Goldschmidt 2023, Lyon, France (Poster)
3. **Farr, O.**, Nil, G., Danger, G., Russell, M., Ferry, D., Nitschke, W., Duval, S., "Methanol on the rocks: Naturally occurring reactive minerals catalyze methane oxidation to methanol and hydrocarbons, AGU 2022, Chicago, USA, (Oral)
4. **Farr, O.**, Reactive minerals promote CH_4 oxidation to methanol and hydrocarbons, CiNaM 2022, Cassis, France (poster)

[a] Cette liste comprend les articles publiés, les articles soumis à publication et les articles en préparation ainsi que les livres, chapitres de livre et/ou toutes formes de valorisation des résultats des travaux propres à la discipline du projet de thèse. La référence aux publications doit suivre les règles standards de bibliographie et doit être conforme à la charte des publications d'AMU.

[b] Le terme « conférence » est générique. Il désigne à la fois « conférence », « congrès », « workshop », « colloques », « rencontres nationales et/ou internationales » … etc.

Indiquer si vous avez fait une présentation orale ou sous forme de poster.

Résumé

Le métabolisme biologique existant est alimenté par le transfert efficace d'électrons entre les espèces carbonées et les atomes métalliques coordonnés dans des enzymes spécialement évoluées. Cependant, ce mécanisme d'oxydoréduction n'est pas unique à la biologie, car les métaux naturels et les structures minérales effectuent un transfert d'électrons cryptique dans l'environnement. Ce cycle abiotique d'oxydoréduction du carbone par les minéraux a conduit à l'évolution géochimique des environnements marins et terrestres avant la vie, et il est impliqué dans son émergence. L'homologie structurale entre la coordination du réseau de certains minéraux réactifs et les centres de réaction enzymatique suggère une transition géochimique entre les systèmes chimiques abiotiques et biologiques. Cette thèse explore cette hypothèse et identifie l'oxyhydroxyde nanominéral unique Fe^{2+}/Fe^{3+} en couches, la « rouille verte » (RV), comme un candidat potentiel pour cette transition en raison de son impressionnant transfert d'électrons et de ses propriétés d'échange ionique polyvalentes. Nous démontrons expérimentalement la nouvelle chimie redox des minéraux de rouille verte de l'oxyhydroxyde de fer en CO_2 et CH_4 sous différentes conditions (par exemple, pression, température, irradiation UV) et caractérisons les réactions par analyse spectroscopique et spectrométrique (par exemple, XRD, Raman, FTIR, XPS, RMN et GC-MS). Nous identifions divers produits formés à partir de la réduction du CO_2 et de l'oxydation du CH_4 médiée par la RV, soutenant l'hypothèse que la vie a pu émerger de minéraux réactifs qui médient des voies chimiques organiques complexes imitant les métabolismes de fixation du carbone existant. De plus, certains produits formés par l'oxydoréduction du carbone médiée par les RV ont de fortes implications sur le forçage climatique précoce et la nature des contrôles abiotiques sur le développement de la biosphère.

Mots clés : redox, oxyhydroxyde de fer, rouille verte, minéral réactif, oxydation du méthane, réduction du dioxyde de carbone, climat, origine de la vie

Abstract

Extant biological metabolism is powered by the efficient transfer of electrons between carbon species and coordinated metal atoms within specially evolved enzymes. However, this redox mechanism is not unique to biology as naturally occurring metals and mineral scaffolds conduct cryptic electron transfer throughout the environment. This abiotic redox cycling of carbon by minerals drove the geochemical evolution of marine and terrestrial environments prior to life, and it is implicated in its emergence. Structural homology between the lattice coordination of certain reactive minerals and enzymatic reaction centers suggests a geochemical transition between abiotic and biological chemical systems. This thesis explores this hypothesis and identifies the unique layered nanomineral Fe^{2+}/Fe^{3+} oxyhydroxide 'green rust' as a potential candidate for this transition due to its impressive electron transfer and versatile ionic exchange properties. We experimentally demonstrate the novel redox chemistry of Fe-oxyhydroxide green rust (GR) minerals towards CO_2 and CH_4 gases under a barrage of conditions (e.g. pressure, temperature, UV irradiation) and characterize the reactions via spectroscopic and spectrometric analysis (e.g. XRD, Raman, FTIR, XPS, NMR, and GC-MS). We identify various products formed from the reduction of CO_2 and oxidation of CH_4 mediated by Fe-oxyhydroxide GR, supporting the hypothesis that life emerged from reactive minerals that mediate complex organic chemistry pathways mimicking extant carbon fixation metabolisms. Additionally, certain products formed by GR mediated carbon redox have strong implications over early climate forcing and the nature of the abiotic controls over the development of the biosphere.

Key words: redox, iron oxyhydroxide, green rust, reactive mineral, methane oxidation, carbon dioxide reduction, climate, origin of life

Extended Summary in French

Le transfert d'électrons est une propriété thermodynamique fondamentale inhérente à diverses espèces chimiques naturelles, jouant un rôle essentiel dans les systèmes abiotiques et biologiques (Nitschke *et al*., 2022). La vie a exploité cette propriété redox au cours de l'évolution des centres redox enzymatiques composés de métaux de transition, qui effectuent des réactions biochimiques redox essentiel dans le métabolisme (P. Falkowski, 2015). Des structures de coordination des ions métalliques similaires à celles qui sous-tendent le métabolisme peuvent également être trouvées dans les réseaux minéraux purement abiotiques, et des travaux récents suggèrent que la structure a précédé la fonction (Farr *et al*., 2023). Les structures homologues peuvent être utilisées pour identifier des conditions environnementales similaires qui ont conduit à l'évolution de certains traits biologiques ou biochimiques, et dans le même ordre d'idées, l'identification de structures homologues dans les minéraux et les enzymes pourrait potentiellement fournir un aperçu de la transition géochimique à biochimique - l'évolution des centres de réaction enzymatiques à partir d'un ancêtre géochimique hypothétique (Farr *et al*., 2023; Preiner, Asche *et al*., 2020). Plusieurs hypothèses postulent que la vie a émergé de déséquilibres géochimiques inhérents aux interfaces entre l'océan primitif et la lithosphère serpentinisante (De Graaf et al., 2023 ; W. Martin et Russell, 2007 ; Nitschke et Russell, 2009 ; Preiner *et al*., 2019 ; Xavier *et al*., 2020). Ici, de forts gradients d'oxydoréduction, de pH et de concentration ont formé des environnements catalytiques capables de conduire et de maintenir une chimie organique complexe. Des recherches sur des équivalents modernes de ces environnements, les cheminées hydrothermales en eaux profondes, ont permis de découvrir diverses voies chimiques abiotiques pour la synthèse de matière organique (Koga & Naraoka, 2017 ; H.-E. Lee et al., 2023 ; W. Martin et Russell, 2007). Ces conditions sont dérivées d'interactions eau-roche serpentinisantes, où la confluence du magma, de la roche en subduction et de l'eau supercritique modifie le basalte pour générer des gaz réduits (e.g., H_2, CH_4) et des métaux solubilisés (e.g., Fe, Ni, Co, Mo, Zn, Cu et W) (Preiner *et al*., 2018).

Ces mêmes métaux confèrent le comportement redox catalytique nécessaire aux enzymes qui conduisent les métabolismes prédominants (par exemple, la photosynthèse, la chimiosynthèse) existant sur Terre aujourd'hui (P. G. Falkowski *et al*., 2008). Selon les hypothèses de l'émergence de la vie par le métabolisme, les protéines et les enzymes ont été les premières structures biochimiques à apparaître au début de la vie, car elles étaient nécessaires pour exploiter le déséquilibre thermodynamique présent dans l'environnement pour effectuer un travail (Preiner et al., 2019 ; M. J. Russell *et al*., 2013). Les protéines modernes partagent des séquences qui peuvent être retracées jusqu'à LUCA (dernier ancêtre commun) (Lane, 2017), et cette conservation indique que certains métabolismes (e.g. methanotrophy, methanogenesis, acetogenesis) sont anciens et ont probablement été les premiers à apparaître (Nitschke *et al*., 2013 ; Wimmer *et al*., 2021). Les cofacteurs des métaux de transition interviennent dans ces métabolismes, le fer en particulier jouant un rôle essentiel dans de nombreuses voies métaboliques (Nitschke et Russell, 2009 ; Sánchez *et al*., 2017). En biochimie, les complexes de fer peuvent assurer

un transfert efficace d'électrons entre les molécules à grandes distances allant jusqu'à 20 angströms, catalysant diverses réactions allant de la formation de radicaux, à la réduction des protons, au traitement des métabolites à la synthèse et à la réparation du matériel génétique, des vitamines, des coenzymes, des antibiotiques et des coenzymes (Frey et Reed, 2012 ; Sánchez *et al.*, 2017). Il existe une grande variété de centres métalliques (FeS, FeNI, FeFe) présents dans le vivant qui sont capables d'utiliser une grande diversité de substrats avec des gammes de potentiel redox allant de +360 à -650mV, capables d'effectuer des transferts redox nécessaires à la phosphorylation de l'ATP et à la chimiosmose. La polyvalence du transfert d'électrons basé sur le Fe est largement exploitée par la vie, mais comment ces systèmes se sont-ils développés à partir d'interactions chimiques apparemment abiotiques ?

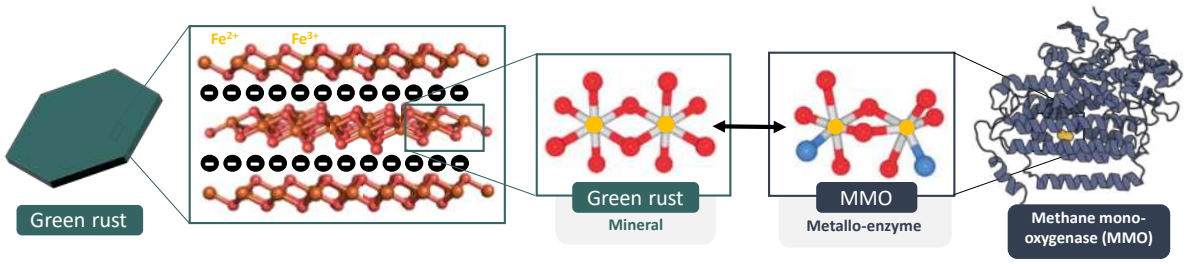


Figure 0.1: Diagramme comparant les similitudes structurelles entre la RG et la sMMO. De gauche à droite, une illustration d'un seul cristal GR, la structure du cation et de l'anion LDH du cristal, la coordination octaédrique des atomes de fer (jaune) et d'oxygène (rouge) dans la GR, la structure atomique analogue du centre de réaction MMO (azote = bleu), et un modèle de l'enzyme MMO

Un candidat proposé (Duval et al., 2019 ; M. Russell, 2018 ; M. J. Russell, 2023 ; Trolard *et al.*, 2022) pour répondre à ce problème est le groupe des rouilles vertes Fe-oxyhydroxide (GR), minéraux double hydroxyde en couches métastables, réactifs et naturellement formés, qui partagent certaines caractéristiques structurales et réactives communes avec les métalloenzymes (Figure 0.1). Ce groupe de minéraux à double (oxy)hydroxyde (LDH) en couches comprenant une structure à double couche composée d'une couche externe cationique chargée positivement de métaux Fe^{2+}/Fe^{3+} liés à des hydroxydes qui enveloppent des intercouches interchangeables chargées négativement contenant des anions tels que Cl^-, SO_4^{2-} ou CO_3^{2-} (Usman *et al.*, 2018). La rouille verte est réactive et se distingue comme une protoenzyme possible en raison des réactions uniques et polyvalentes qu'elle effectue facilement, telles que la réduction des métaux (ex. : Cu, As, U), des composés inorganiques (ex. : NO_3^-, ClO_4^-), des composés organiques (ex. : carbon tetrachloride, tetrachloroethylene, trichloromethane), (Buessecker et al., 2022 ; Choi et coll., 2012 ; Døssing *et al.*, 2011 ; Etique *et al.*, 2014 ; Jönsson et Sherman, 2008 ; Onoguchi *et al.*, 2019). Dans la nature, de telles réactions ne sont observées que dans divers métabolismes microbiens, mais la GR effectue facilement toutes ces réactions de transfert d'électrons, qui peuvent être catalysées ou inhibées si l'on modifie sa structure unique de cations multivalents chargés et octaédralement coordonnés (par exemple, Fe, Ni, Mg, Co, Al) prenant en sandwich des anions réactifs interchangeables (par exemple, CO_3^{2-}, $HCOO^-$, Cl^-, SO_4^{2-}) (Agnel et al., 2020; S. Lee *et al.*, 2023). En tant que nanomatériau métastable naturel avec des surfaces et des espaces internes catalytiquement actifs, la GR est représente un candidat viable pour l'hypothèse d'une émergence de la vie (Duval et al.,

2019 ; M. Russell, 2018). Cette polyvalence et cette configuration structurale mène à la proposition d'une comparaison directe avec les centres de réaction enzymatique (Figure 0.1). Dans cette thèse, nous démontrons expérimentalement la viabilité d'une rouille verte initiée par proto-métabolisme en testant son comportement catalytique vis-à-vis de CH_4 et du CO_2. Ces résultats révèlent des réactions d'oxydoréduction jusqu'alors inconnues avec les rouilles vertes et le cycle du carbone, ce qui a des implications environnementales importantes pour la Terre moderne et ancienne.

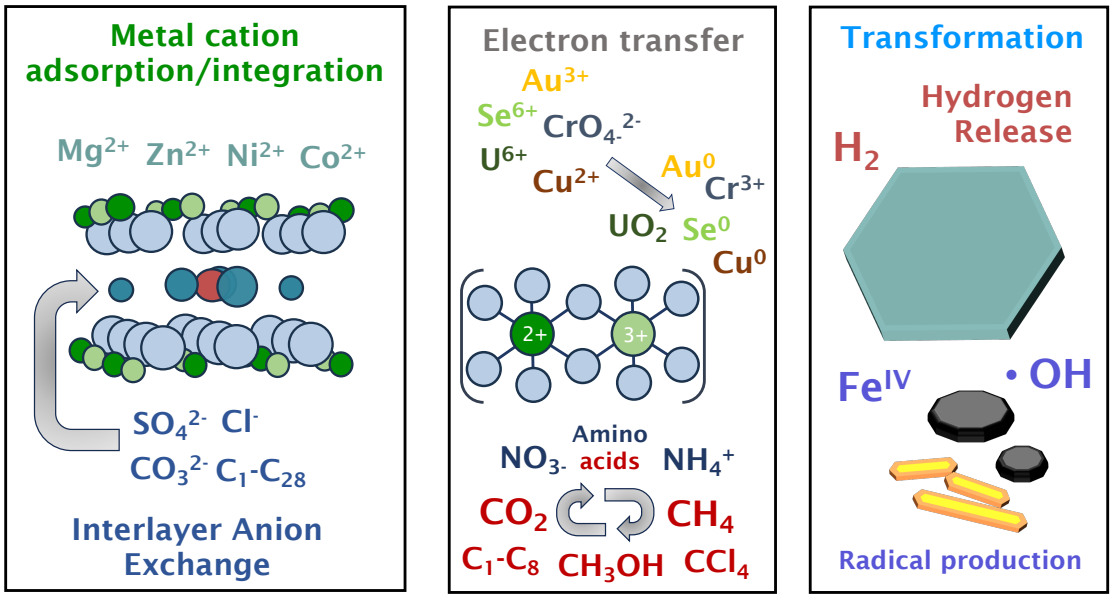


Figure 0.2: Schéma illustrant diverses interactions chimiques avec les minéraux d'oxyhydroxyde $Fe^{2+}/^{3+}$

Résultats

Nous avons exploré l'oxydation du méthane, puis les réactions de réduction du dioxyde de carbone avec les minéraux de rouille verte dans diverses conditions en utilisant de nombreuses analyses spectroscopiques et spectrométriques différentes. Nous pensons que la GR était abondante dans les anciens océans archéens, au niveau des cheminées hydrothermales où les bactéries méthanotrophes vivent aujourd'hui sous haute pression (Trolard et al., 2022). Les pressions élevées auraient été importantes pour catalyser cette réaction. De plus, nous pensons que le transfert d'électrons entre les sites de réaction du Fe aurait également joué un rôle dans le mécanisme réactionnel à l'origine de l'oxydation du CH4, ainsi que des espèces oxydatives telles que l'O2, le NO et les photons. C'est pour cela que nous avons testées ces conditions pour déterminer leur effet sur l'oxydation du CH4 (Q. Huang et al., 2023 ; C. Wang et al., 2023). En simulant des conditions hydrothermales, sous pression des GR avec du méthane et du dioxygène a entraîné la production de méthanol (MeOH) (Figure 0.3A) ainsi que de divers autres composés organiques, notamment le trichlorométhane (TCM) et le dichlorométhane (DCM). La GR est connue pour être fortement photoréactive et susceptible de se transformer (Liu, 2021 ; C. Wang et Chakrapani, 2023). Nos travaux utilisant la lumière UV pour catalyser

l'oxydation des RV démontrent que CH_4 est facilement oxydé en d'autres produits organiques tels que l'acétone et le benzène. De plus, ces processus peuvent être combinés pour produire des réactions d'auto-catalyse (X. He *et al.*, 2023). Ces résultats confirment l'oxydation du CH_4 par les réactions de transformation oxydative médiées par les GR. La coïncidence de la réaction avec la transformation des GR en diverses phases d'oxyhydroxyde de fer et d'oxydes suggère un mécanisme médié par les radicaux.

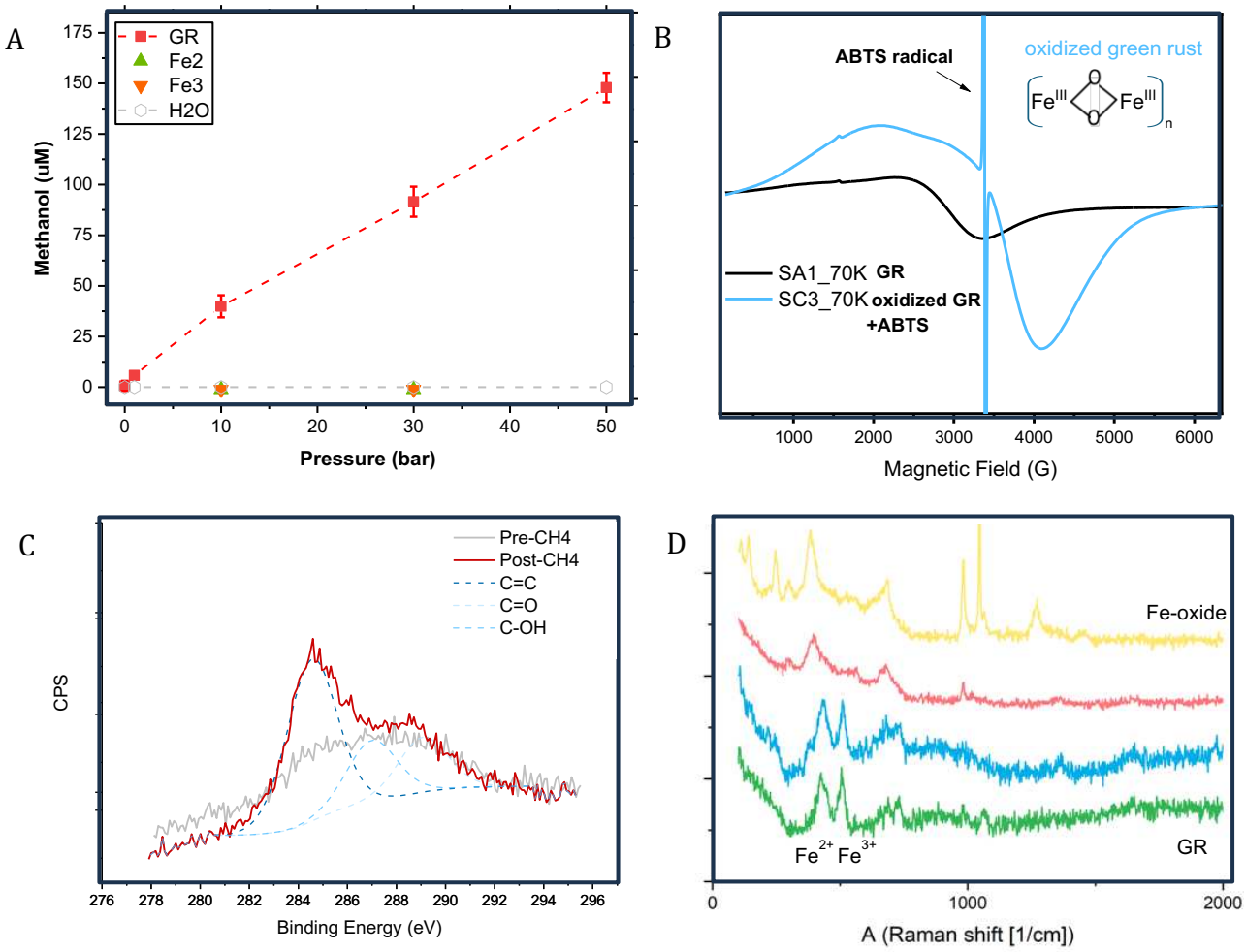


Figure 0.3 : Oxydation du méthane CH_4. **A-** augmentation de la concentration de CH_4 avec la pression dans la solution GR-CO_3. **B-** spectres EPR de GR-CO_3 avant (noir) et après oxydation (bleu) lorsque l'acide peracétique et un piège à radicaux ABTS sont utilisés. **C-** spectres XPS de la surface de GR-CO_3 avant (gris) et après (rouge) exposition à 1 bar de CH_4montrant l'augmentation de l'intensité de la bande correspondant aux liaisons C=C après exposition. **D-** spectres Raman de GR-CO_3 avant (vert) et après exposition à 2 heures (bleu) et 48 heures (rouge et jaune) de mélanges gazeux CH_4 +O_2.

La GR partage une géométrie de coordination similaire entre ses atomes de Fe coordinnés octaédriquement dans son réseau cristallin et le centre de réaction coordinné octaédriquement de la métalloenzyme sMMO. Ainsi, pour tester l'hypothèse selon laquelle la GR est non seulement structurallement mais également catalytiquement similaire à la sMMO, c'est-à-dire oxydant le CH_4 via un même mécanisme d'activation du Fe^{4+} une série d'expériences utilisant H_2O_2 et l'acide peracétique ont été développées. Cette expérience

a permis de tester l'existence d'une telle réaction dans la GR, et sa réactivité dans diverses conditions pour en améliorer son efficacité. Ces résultats (non illustrés) ont donné des quantités substantielles de méthanol et ont clairement indiqué le rôle des radicaux dans le mécanisme d'oxydation du CH_4. Par la suite, des expériences de RPE, donnant des informations sur la nature des interactions Fe^{3+}-Fe^{2+} dans le réseau cristallin de GR, ont été réalisées. Par cette technique nous avons également étudié la signature de la production de radicaux et de la formation de Fe^{4+} (Figure 0.3B). Ces informations nous permettrons par la suite de comparer avec les signaux de radicaux formés pendant l'oxydation de la GR, qui pourrait être les principaux facteurs de la réaction d'oxydation du CH4 et de production de méthanol. D'autres études spectroscopiques ont examiné les interactions entre le CH_4 et les surfaces des minéraux GR à l'aide de XPS (Figure 0.3C), Raman (Figure 0.3D), FTIR et XRD. Les expériences XPS (Chapitre 4) ont révélé des pics similaires correspondants aux liaisons C=C et C=O à la surface de $GRCO_3$ après adsorption du CH_4 par rapport au CO_2. Ces signaux peuvent refléter l'accumulation de phases organiques ou refléter des produits d'oxydation similaires à la formation de coke, mais lors de l'observation par spectroscopie Raman, aucune présence organique n'a été détectée sur les surfaces minérales. Cependant, la transformation des GR en divers oxydes a été enregistrée via Raman, avec une forte hétérogénéité des espèces minérales se formant à la surface minérale.

De l'autre côté de l'échelle redox, le CO_2 est déjà fortement oxydé. Les réactions entre les GR et le CO_2 ont déjà été étudiées en dehors d'un contexte de réduction du CO_2, car la transformation des GR par ajout de CO_2 a été utilisée pour synthétiser $GRCO_3$ à partir d'autres espèces précurseurs de GR en utilisant l'échange d'anions. En solution, le CO_2 existe sous forme de H_2CO_3, HCO_3^- et CO_3^{2-} compte tenu de l'augmentation du pH de la solution, et dans les intercouches GR, l'échange anionique se produit facilement, avec une forte préférence accordée au HCO_3^- par rapport aux autres anions (CO_3^{2-} >SO_4^{2-}>Cl^-) (Agnel et al., 2020). La GR n'est stable qu'au dessus d'un pH de ~6,5 (Bocher et al., 2004 ; Ruby et al., 2010) donc, compte tenu de l'excès de CO_2 dans une solution non tamponnée, la GR subira finalement une transformation en phases oxydées Fe^{3+} telles que la lépidocrocite, la magnétite, la chukanovite ou les minéraux sidérites. Pour la réduction du CO_2, qui est la réaction inverse, nous avons mené diverses expériences de la même manière que celles effectuées lors de l'oxydation du méthane. Nous avons introduit du CO_2 gazeux dans des solutions alcalines de GR pour constater que les GR réagissent facilement en absence de lumière et UV pour former une variété de composés (Figure 0.4A). Des solutions alcalines riches en HCO_3 de GR en bullant du CO_2 ont entraîné la production de diverses espèces organiques à une concentration de l'ordre de >100mM (S. Lee et al., 2023). On pense que la réduction du CO_2 se produit dans l'intercouche du minéral, de ce fait la solution saturée de HCO_3 rentre constamment à l'intérieur du minéral. Les réactions spontanées avec le CO_2 ont conduit à la production (>100 mM) de composés d'alcool de sucre riches en hydroxyles, à savoir l'érythritol, dont la présence confère une stabilité supplémentaire à la GR (Farr, 2024). D'autres études spectroscopiques des interactions de la phase gazeuse sur la surface minérale ont été menées à l'aide de XPS (Figure 0.4C),

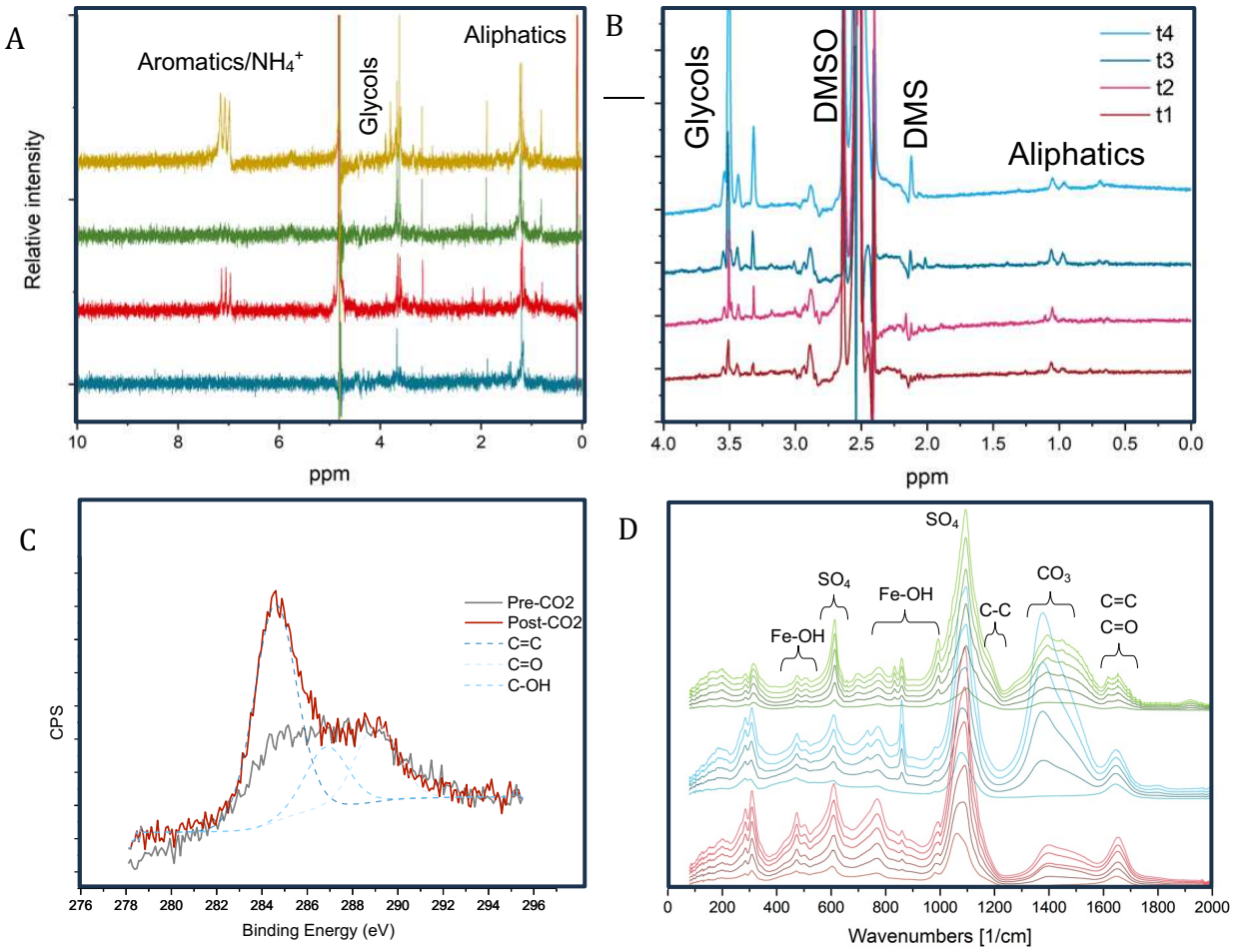


Figure 0.4 : Illustration de résultats obtenus à lors d'expériences de réduction du CO_2. **A-** spectres RMN détaillant l'effet de la sorption de différents gaz sur les solutions de RV-SO_4, où N_2 (bleu), CO_2 (rouge), CH_4 (vert) et CH_4 + NO (jaune) sont comparés. **B-** spectres RMN du DMSO introduit dans les solutions de RV-SO_4 au cours du temps. L'état initial (rouge) diffère de l'état final (bleu clair) où l'augmentation de la surface des pics à 2,1 et 3,6 ppm implique la production de DMS et de produits de réduction glycolique. **C-** spectres XPS de RV-CO_3 avant (gris) et après (rouge) l'introduction de CO_2. **D-** spectres FTIR de RV-SO_4 à pH=7 (rouge), pH=10 (bleu) et pH=10 avec K_2CO_3 (vert).

de Raman, de FTIR (Figure 0.4D) et de XRD. Des études de surface indiquent que le CO_2 est facilement adsorbé sur les sites de surface Fe-OH disponibles, avec diverses liaisons C-C, C-O et C-H présentes après l'adsorption du CO_2, indiquant une transformation rapide au contact (Farr, 2024 ; S. Lee et al., 2023). En fait, ces liaisons Fe-OH, en particulier leur longueur, sont impliquées dans la réactivité des hydroxydes de Fe envers les réactions de réduction catalytique (H. Li et al., 2024). Les modèles d'espèces minérales apparentées comme le Fe_3O_4 montrent de très fortes interactions de surface entre le CO_2 et ces sites Fe-OH communs dans les minéraux de fer (Santos-Carballal et al., 2018). Bien que le comportement catalytique des surfaces soit le plus évident, l'intercouche est également impliquée en tant que site de réaction, car Lee démontre en outre la réduction des espèces de SO_4 intercalaires en DMSO en présence de CO_2. Même les produits de réduction du CO_2 par la GR sont encore plus réduits par le minéral ; le DMSO peut être réduit en DMS (Figure 0.4B) et le pyruvate peut subir une amination réductrice en présence de NH_3 pour former des acides aminés (Barge et al., 2019). Ainsi, des voies de réaction assez complexes se forment à partir d'un apport de CO_2 dans la GR.

Implications

L'oxydoréduction abiotique du carbone peut avoir grandement influencé les conditions environnementales de la Terre ancienne en raison des fortes concentrations en CO_2 et CH_4 ainsi que des conditions océaniques ferrugineuses généralisées au cours de l'Hadéen (4,6-4 Ga), de l'Archéen (4-3,5 Ga) et du Protérozoïque inférieur (3,5-2 Ga) (Halevy et al., 2017 ; Poulton et Canfeld, 2011a ; Thibon et al., 2019). Ce carbone aurait probablement réagi avec les océans primitifs, et aurait donc carbonaté les précipités minéraux d'hydroxydes de fer présents. Selon les résultats de cette thèse, la réduction de l'oxydation du CO_2 et du CH_4 par les minéraux GR a produit des quantités uM à M de produits organiques, y compris du méthanol, des composés carbonés halogénés, des composés organosulfurés, ce qui signifie qu'une concentration non négligeable de carbone organique dissous peut avoir existé dans les eaux de surface de la Terre primitive en échange avec l'atmosphère. L'effet de ces voies de réaction spécifiques n'est pas encore quantifié. Cependant, ce cycle abiotique du carbone aurait pu avoir des impacts dramatiques sur la chimie environnementale primitive et l'émergence éventuelle de la vie.

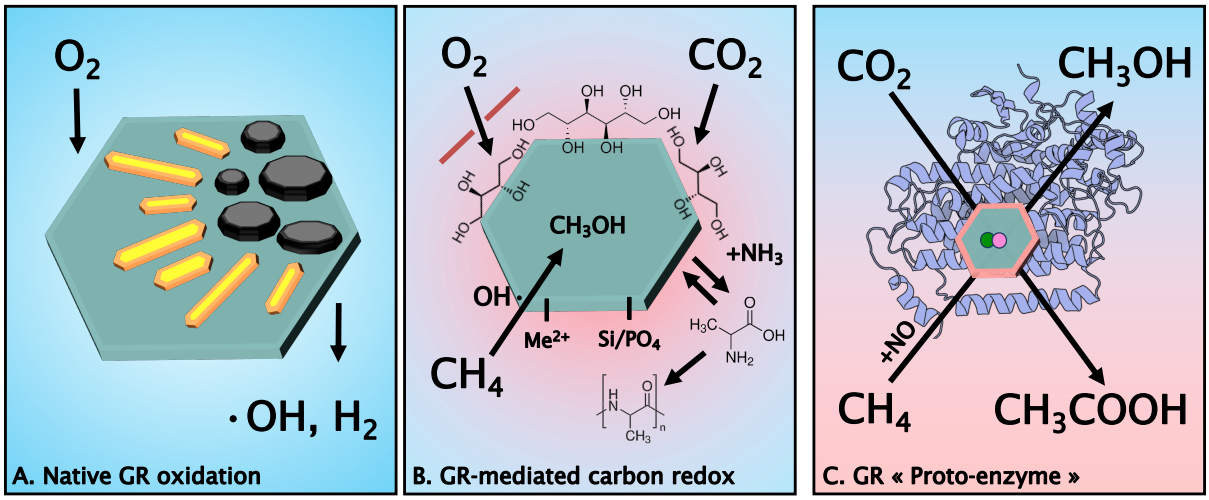


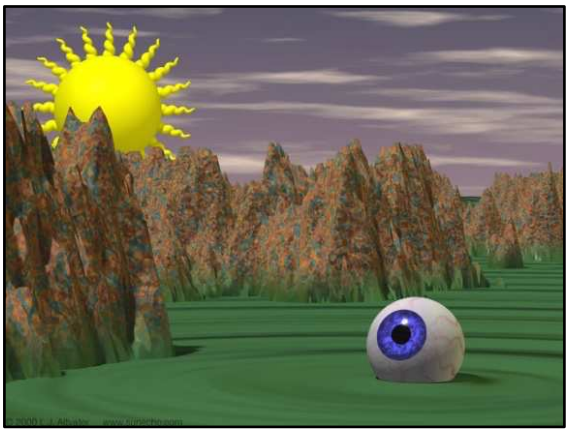
Figure 0.4: Démonstration de la réponse du GR aux espèces rédox externes à différents niveaux de complexité. Dans la section A, les GR sont susceptibles de transformation oxydative en présence d'O_2. En B, cela ne se produit plus en raison de la production de glycols protecteurs résultant de la réduction spontanée du CO_2. De nombreuses réactions peuvent être catalysées de manière non spécifique à ce niveau de complexité. Dans la diapositive C, en raison de pressions de sélection spécifiques, les molécules organiques se sont complexifiées en un hypothétique ligand polyamino qui sélectionne uniquement l'oxydation du CH_4 en CH_3OH, ressemblant à la fonction enzymatique existante du sMMO. La coloration rouge et bleue indique respectivement les niveaux relatifs de conditions réductrices et oxydantes.

Nous proposons que la réactivité vis-à-vis du CO_2/CH_4 inhérente aux minéraux de GR telle que décrite dans cette thèse fournit la preuve d'une voie viable vers l'émergence de systèmes autocatalytiques qui conduisent des réactions redox organiques et inorganiques au sein d'un minéral ou d'une membrane organique, précurseur direct du métabolisme biologique. Dans le cas de la réduction du CO_2 dans des conditions alcalines, la rouille verte carbonatée est capable de produire des composés riches en hydroxyles C2-C4 comme le glycérol, en grandes quantités (S. Lee *et al.*, 2023). Le glycérol et les composés similaires riches en hydroxyle sont connus pour retarder indéfiniment l'oxydation de la rouille verte (J.-M. R. Génin *et al.*, 2001 ; Y. Sun et al., 2023). Protéger les cristaux de l'oxydation

physique par un enrobage hydroxyle ou produire des hétérocycles antioxydants (par exemple des quinones) (Anschutz et Penn, 2005) pourrait constituer des formes innées d'autoconservation dynamique dans les systèmes chimiques autocatalytiques. De plus, comme les interactions organiques sont connues pour modifier la chimie de coordination des métaux (Q.-Q. Jia *et al*., 2024), la modification continue de la surface (Borrego-Sánchez *et al*., 2022 ; Hooks *et al*., 2020 ; Yin *et al*., 2017, 2018) augmente encore la réactivité et les capacités du système de rouille verte. Divers ajouts à la rouille verte, tels que la présence de phosphate adsorbé, augmentent la libération de radicaux lors de l'oxydation (L. Z. Huang *et al*., 2022), peut-être via la prévention de la résorption par le minéral lui-même, conférant à la rouille verte protégée des propriétés oxydatives catalytiques. Avec une polymérisation appropriée, la rouille verte commence à ressembler au centre métallique d'une enzyme ou d'une protéine entourée de ligands de cofacteurs (Gutierrez-Rus *et al*., 2023). Ce système évolue à partir d'une structure chimique innée qui a précédé sa fonction (Wong *et al*., 2023).

D'un point de vue général, la caractérisation, la réactivité et les implications des minéraux de rouille verte en tant que catalyseurs naturels vers l'oxydoréduction du CO_2 et du CH_4 ont été explorées pour la première fois. Nous avons observé que ces minéraux peuvent réagir spontanément ou être amenés à réagir avec des gaz carbonés en raison de propriétés chimiques distinctives inhérentes à leur structure multivalente d'oxyhydroxyde de fer double-couche. La RV comporte des couches bien organisées de cations métalliques prenant en sandwich des anions, ce qui lui permet de transférer des électrons, des anions et des protons pour mener une chimie redox complexe. Il en résulte la formation de plus de 22 composés lorsqu'ils sont exposés à des gaz tels que CH_4 et CO_2 dans une solution ayant un pH neutre ou alcalin. Si la production de ces différentes espèces organiques a été décrite dans ce travail, il reste un travail considérable à réaliser pour élucider soigneusement les mécanismes impliqués dans leur formation. Cependant, ces premiers résultats indiquent des voies de réaction possibles qui impliquent les minéraux réactifs de l'oxyhydroxyde de fer dans le cycle cryptique du carbone tout au long de l'histoire géochimique, et renforcent les hypothèses concernant leur rôle de précurseur, à l'origine ou à l'émergence de la vie.

Preface & Acknowledgements



L.J. Altvater, *PHF5* (1999)

"God got lonesome. So God said to some of the mud, "Sit up!" "See all I've made," said God, "the hills, the sea, the sky, the stars." And I was some of the mud that got to sit up and look around. Lucky me, lucky mud."

Kurt Vonnegut, *Cats Cradle* (1963)

This document is an ode to the tremendousness I've captured in a library of reaction vials over the last 5 years, recalling to life the primordial viridian blood of the Earth's ancient seas. For eons the ocean breathed an alien atmosphere, where reactive minerals akin to blood, transported electrons from the depths to the surface, and back again. The rhythmic cycling of Fe^{2+}/Fe^{3+} within green rust nanocrystals heralded the first heartbeats of life, which continue unbroken to this day.

I owe great thanks to my (co)advisors and collaborators Drs. Wolfgang Nitschke, Daniel Ferry, Simon Duval, and Michael Russell for their initial forays into this mineral-metabolism research and for their trust in me to lead it. I thank the BiP, CINaM, and PIIM teams for their wealth of technical, instructive, and cordial support. I highlight the immense experimental and technical expertise of Drs. Anabella Ivancich, Olivier Grauby, Philippe Parent, Carine Laffon, Gregoire Danger, Olivier Bornet, Vasile Heresanu, Frederic Brunel, Alexandre Altie, and Damien Chaudanson of which my work relied heavily upon. I thank our GR collaborators Francois Guyot, Christian Ruby, Georges Ona-Nguema, Mustapha Abdelmoula and Romain Coustel for enlightening discussions on GR chemistry. I thank Drs. Chartlet and El Alabani and all other members of my jury for agreeing to oversee my work. A special shout-out goes to Mr. Nil Gaudu, my fellow GR investigator in arms. I wish my BIP09 team members, Simon, Wolfgang, Barbara, Frauke, Nil, Kilian, Guilia, Jostin, Chloe, Yann, and Adriana well in their current and future endeavors, particularly in their continued search for the emergence of life. I thank Drs. Nathan Yee, Paul Falkowski, Jihua Hao, Rick Mortlock, Gail Ashley and many others for opening the doors that led me here today.

I hold a deep gratitude for my wonderful wife Sanna Sharp and her enduring love which kept me aloft during my thesis. I simply could not have done this without her. I have spent much time thinking about the emergence of life only to have it greet us directly with the forthcoming arrival of our child into the world. I have my family and friends, new and old, to thank for their continued and unyielding moral support and encouragement, of which I can never thank for enough.

This work received support from the French Government under the France 2030 investment plan, as part of the initiative d'Excellence d'Aix Marseille Université (A*MIDEX -AMX-21-PEP-039) as well as a grant from the French Agence Nationale pour la Recherche (ANR-22-CE30-0035-01).

Table of Contents

Affidavit 4
Liste de publications et/ou brevets et participation aux conférences 5
Résumé 6
Abstract 7
Extended Summary in French 8
Preface & Acknowledgements 16
Table of Contents 18
Chapter 1: An introduction to mineral-mediated carbon redox and the emergence of life 20
1.1. A geochemical history of the availability of Iron on Earth 21
1.2. Redox state changes on the Early Earth 23
1.3. Emergence of metabolism from geochemistry 24
1.4. Electron transfer in Fe-bearing minerals 26
1.5. Carbon redox in natural systems mediated by interactions with Iron 27
1.6. Redox behavior of $Fe^{2+/3+}$oxyhydroxide "Green rust" minerals 29
1.7. The role of green rust in the emergence of life 33
Chapter 2: Methanol on the rocks: Green rust transformation promotes the oxidation of methane 35
2.1. Abstract 36
2.2. Introduction 36
2.3. Methods 38
2.4. Results 39
2.5. Discussion: 43
2.6. Conclusion: 47
1.8. Supplementary material to original manuscript 48
2.7. Experimental addenda not included in original manuscript 56
Chapter 3: Probing $Fe^{2+}/^{3+}$ catalytic reactivity of Green Rust applying Electron Paramagnetic Resonance (EPR) spectroscopy. 60
3.1. Introduction 61
3.2. Material and Methods 62
3.3. Results and Discussion 63
3.4. Conclusion 67
Chapter 4: Further $Fe^{2+/3+}$ oxyhydroxide green rust redox reactions towards CO_2 and CH_4 analyzed by spectroscopy and mass spectrometry 68
4.1. Introduction 69

4.2. Methods 70
4.3. Results 72
4.3.2. Investigating reduction of CO_2 in alkaline solutions of K2CO3 76
4.3.3. Reduction of DMSO to DMS 79
4.3.4. Observations of GR during CO_2 and CH_4 redox using XPS, Raman, FTIR, and Mass spectrometry 83
4.4. Discussion 93
4.5. Conclusion 95
Chapter 5: Implications of reactive mineral mediated carbon redox for modern and ancient environments 96
5.1. Carbon redox mediated by reactive Fe-oxyhydroxide minerals 97
5.2. Natural industrial catalyst for carbon removal? 100
5.3. Mineral mediated carbon redox cycling in modern environments 102
5.4. GR mediated carbon redox cycling in ancient ferruginous environments 102
5.5. An inferred evolutionary transition from abiotic minerals to protoenzymes 105
5.6. Synthesizing alkaline vent emergence of life hypotheses with an abiotic Gaia 107
Conclusion 112
Bibliography 114
List of Figures 137

Chapter 1: An introduction to mineral-mediated carbon redox and the emergence of life

This chapter provides an introduction to the chemistry, geochemical conditions, and hypotheses relevant to the hypothesized transition between abiotic and biological metabolism proposed to have taken place within alkaline hydrothermal vents early in Earth's history. The proposed candidate, a LDH Fe^{2+}/Fe^{3+} (oxy)hydroxide « green rust » mineral, presents exceptional properties which indicate its suitability as a candidate for conducting protometabolism (e.g. electron transfer, reactivity towards carbon species, adsorption and integration of cation and anions, metastable transformation). This work builds upon past research and reveals novel pathways for mineral mediated carbon cycling in the context of protometabolism.

1.1. A geochemical history of the availability of Iron on Earth

Iron (Fe) is vital to life. From redox active reaction centers at the heart of ancient and extant metabolisms to the heme proteins in blood carrying oxygen throughout every human being, Fe serves as a versatile and essential electron transporter in almost all biochemical systems (Frey & Reed, 2012). Formed in the final stage of stellar nucleosynthesis, it is the 2nd most common element on the Earth behind carbon, the cycling of which is intrinsically linked that of Fe. It's availability on the surface of the earth, through geochemical and biogeochemical transport, has guided the evolution of life throughout Earth's history (Camprubi et al., 2017).

Iron today

On the surface of the Earth, iron is derived and made available from two main sources, continental weathering and hydrothermal vent effluent (Konhauser et al., 2017). Native iron is not common to the surface of the Earth due to prevailing oxidative conditions for the past 2.5 billion years oxidizing iron to Fe^{2+} and Fe^{3+} states, yet Fe^{0} can be formed via biological and abiotic redox reactions (Sánchez et al., 2017). The majority of Fe is associated with minerals locked within continental rock, constituting approximately 5% by mass (Sánchez et al., 2017). From this source, Fe minerals are eroded by weathering processes and are transported by glacial, riverine, and aeolian processes across the globe. Surface oceans are seeded with ~10 Gmol/yr of Fe dust as it is swept out to sea, serving as a source of limiting nutrient for photosynthetic algae in open ocean waters and fertilizing a carbon sink of 11-16 gT/yr (P. Falkowski et al., 2000; J. H. Martin, 1992; C. M. Moore et al., 2013). Aeolian Fe is also found to effect climate with the effect of particulates on shielding the surface of the Earth from incoming solar irradiation to interactions with various atmospheric species present in air. Aeolian Fe is known to catalyze various reactions with carbon bearing molecules such as methane (CH_4) or chloromethane (CH_3Cl)(Al-Abadleh, 2015), and likely influence climate.

Iron readily reacts with other elements, specifically electronegative species of oxygen and sulfur, forming iron oxides, sulfides, and silicate minerals. The biogeochemical cycling of Fe overlaps with the cycling of various other elements essential for life, including nitrogen, sulfur, carbon, and various metals (e.g., Ni, Zn, Cu, Mn, Mo)(Sánchez et al., 2017). Iron oxides are commonly recognized as rusts, the major mineral components of rusts are Fe-oxyhydroxides such as goethite and lepidocrocite, constituting a major component of soils and are involved in the sequestration, transport, and redox processing of various elements and nutrients throughout the environment (Bigham et al., 2018).

Iron yesterday

Iron minerals deposited during the Archean and Proterozoic eons serve as records of the chemical reactions and pathways that characterized the early Earth's transition

from anoxic to oxygenic alteration (Bolhar et al., 2004; Poulton & Canfeld, 2011; K. E. Yamaguchi et al., 2005). The oldest sedimentary rock formation currently known is dated to 3.85 Ga and is composed of iron and silicate minerals believed to have directly precipitated from the primordial Archean ocean (Konhauser et al., 2017; Nutman et al., 2007; Tosca et al., 2019). These minerals provide the earliest records of oceanic chemistry, depicting sea water saturated with iron and devoid of oxygen (Nutman et al., 2016; Poulton & Canfeld, 2011). Today Fe concentrations in surface oceans average to only 0.2nM due to the poor solubility of Fe under oxygenic conditions (X. Liu & Millero, 2002a; J. H. Martin, 1992). In the absence of O_2 as seen during the Archean, these concentrations existed two orders of magnitude greater at ~0.2 mM (Koeksoy et al., 2019a; X. Liu & Millero, 2002b; Poulton & Canfeld, 2011). This glut of Iron was introduced to the oceans via hydrothermal vents, where serpentization processes from the subduction of hot water traveling through fissures within the oceanic crust leached acidic metals out of ultra-mafic rock and supplied the primitive oceans with 1×10^{13} g/yr of iron (Tosca & Tutolo, 2023), much higher than modern due to higher mantle activity (Korenaga, 2013; Rosas & Korenaga, 2021). Dissolved Fe vented from these chimneys and saturated the oceans with Fe forming a variety of mineral species. At the effluent sites, the precipitation of minerals formed tall chimneys of composed of transition metal oxides, sulfides, silicates, and carbonates. These ancient towers were the sites of complex redox reactions (Möller et al., 2017), organic synthesis (Burcar et al., 2015; D. He et al., 2021; McDermott et al., 2015a; Ogasawara et al., 2000; Proskurowski et al., 2008; Purvis et al., 2024) geochemical (Rasmussen et al., 2021; Ungerhofer et al., 2024), and electrochemical (Ooka et al., 2019; Yamamoto et al., 2017) processes, which some believe to have been the birthplace of life or prebiotic chemistry (Kitadai et al., 2019; W. Martin & Russell, 2007; Trolard et al., 2022).

This ancient ocean underwent dramatic changes following the onset of oxygenic photosynthesis, a period known as the Great Oxidation Event (GOE) (Planavsky et al., 2014a). Throughout the GOE massive amounts of iron began being deposited as the Banded Iron Formations (BIF), a group of globally spanning deposits of banded Si and Fe-rich minerals (e.g. chert, hematite, magnetite) dated to have formed between 3.8 – 2.4 Ga (Bolhar et al., 2004; Konhauser et al., 2017). Fe minerals controlled the flux of light in surface oceans(Gauger et al., 2015), nutrients sorption (Hao et al., 2017; Zegeye et al., 2012), sequestering metals (Konhauser et al., 2009, 2015), and mineralizing carbon (Friese et al., 2021); all directly constraining the possible evolutionary pathways of early life. This transition from an anoxic to an oxygenic atmosphere and ocean had fundamentally changed the chemistry of the planet from a chemically reducing to an oxidative environment, opening new pathways for chemical and biological redox reactions(Hao et al., 2019).

The identities of these the precursor minerals that formed the BIF deposits are poorly constrained as Fe minerals are metastable and are subject to transformation due to heat, time, as well as inputs of trace metals, silica, phosphorus, and organic compounds (Farr et al., 2022; Hooks et al., 2020; A. M. Jones et al., 2009; C. Jones et al., 2015; Sumoondur et al., 2008; Tosca et al., 2016; Xiong et al., 2023). As such, various ferrous silicates (e.g. greenalite(Hinz et al., 2021; Tosca et al., 2016)), carbonates (e.g. siderite(Kim et al., 2013; Vuillemin et al., 2019)), and oxyhydroxides (e.g. green rust(Halevy et al., 2017; Koeksoy et al., 2019b; Sumoondur et al., 2008)) have all been proposed as progenitor minerals to

those mineral constituents found in BIFs (Konhauser et al., 2017; Y. L. Li et al., 2017a). However, in a solid solution between Fe and various other competing soluble components relevant to Archean conditions (e.g. Si, P, V, Mg, CO_3^{2-} , SO4), the common mineral phase to precipitate under all conditions would be mixed valent Fe-oxyhydroxides like GR (Bigham et al., 2018; Bourrié et al., 2019). Thus GR, and its transformation into other mineral phases, dominated the early Earth's oceans.

1.2. Redox state changes on the Early Earth

The Archean Earth (3.8 – 2.5 Ga) transitioned from an initial reducing to a final oxidizing redox state by the dawn of the Proterozoic (2.5-0.5 Ga), opening new pathways for the fate of essential elements of life (Hao et al., 2019).

Mineral shuttles for electron transfer

Charged surfaces of reactive mineral species (e.g. Iron sulfides, Iron oxyhydroxides) are attractive sites for the adsorption of free metals and organic compounds, and their sorption to minerals would have facilitated transport to and from reducing conditions at deep sea hydrothermal sites to oxidizing surface waters(Hao et al., 2019). Iron minerals have reactive surfaces which can be positively or negatively charged depending on the mineral's zero-point charge and the pH of the medium(Bigham et al., 2018). Precambrian ocean pH is believed to have increased from a pH of 6 to the modern 8, and within this range iron oxyhydroxides like ferrihydrite present a positive charge (Halevy & Bachan, 2017a). The adsorptive capability of iron minerals is thought to have been responsible for the sequestration of nickel, phosphate, and other resources essential to biological processes, thus limiting nutrient availability for early life (Farr et al., 2022; Konhauser, Lalonde, et al., 2007; M. Zhao et al., 2023). However, these early transport systems may have in turn accumulated the necessary catalysts for the transition from prebiotic to biotic chemistry.

Photochemical cycling of essential elements

Various elements are essential elements to life, including the big 6 (C, H, O, N, P, S) in addition to transition metals such as Fe, Ni, Zn, Mo, Cu, Co, and W. Their metabolism by microorganisms are ancient and intertwined with that of transition metals like Fe(Farr, Hao, et al., 2023; Rogers & Schulte, 2012; Tyrrell, 1999; Wong et al., 2017). As the sulfur isotope record implies the lack of an appreciable ozone layer(Farquhar et al., 2000), the Archean atmosphere would have likely allowed some UV-C light to reach the surface of the Earth, resulting in the photooxidation of the surface oceans bearing dissolved and precipitated reduced Fe species (Dodd et al., 2022; François, 1987). Studies have shown that the modelled rates of available photons would be enough to oxidize the surfaces of the ferruginous ocean (Dodd et al., 2022; Konhauser, Amskold, et al., 2007; Mauzerall, 1990). This would have impacted the redox state and thus cycling of various elements including sulfur (Hao et al., 2022), phosphorus(Farr, Hao, et al., 2023), Nitrogen(Bushaw-Newton & Moran, 1999; Schrauzer & Guth, 1976; C. Ye et al., 2016). Further interactions with radical species and reactive minerals could promote a complex sulfur redox chemistry in the absence of life (Farquhar et al., 2000; Koeksoy et al., 2019b; J. Wang et al., 2024).

Radical interactions

Various chemical oxidants could have been generated at the interface between primitive terrestrial, oceanic, and atmospheric chemistries. The discovery of geochemically generated radical species from the weathering of silicate bonds (Anipsitakis & Dionysiou, 2004; H. He et al., 2021; G. Zhao et al., 2023) demonstrates a new pathway for oxidation in the previously supposed anoxic Archean. Limited radical production at the surfaces of mineral faces weathered by rocks could produce x11 more than produced by UV interactions with the atmosphere (H. He et al., 2023). Critical interpretation of these hypotheses (Koppenol & Sies, 2023) posit that Fe^{2+} scavenging in ferruginous ocean would prevent any H_2O_2 from building up to appreciable concentrations, leading to a source of Fe oxidation. Futher complex chemistry taking place within the atmosphere itself could have generated various oxidized nitrogen species in substantial concentrations, primarily via lighting and meteoritic impacts in the absence of life. Recent experimental and theoretical work place nitrogen oxides (Buessecker et al., 2022; Wong et al., 2017), and nitrogen oxyanions (Barge et al., 2022; Ducluzeau et al., 2009) in the position to react with early Fe minerals and yield complex organic chemistry as a byproduct.

Life

The appearance of life on Earth dramatically altered the redox state of the environment, as life creates chemical and redox disequilibrium in metabolism's wake (Nitschke et al., 2024; Sagan, 1961; Ward et al., 2016). The ferruginous conditions that dominated the Eoarchean were nearly gone by the Proterozoic, and so too with it the reducing conditions and composition of the atmosphere in most part due to the expanse of photosynthetic life (Planavsky et al., 2014b; Poulton & Canfeld, 2011; Rochelle M. Soo, James Hemp, Donovan H. Parks, Woodward W. Fischer, 2017; Ward et al., 2016, 2019). The availability of the essential elements that power life limit its capacity to grow (Hao et al., 2017; Hao, Knoll, Huang, Schieber, et al., 2020; C. M. Moore et al., 2013; Zegeye et al., 2012), thus this limitation inspired the evolution of metabolisms which employ inherent properties of transition metals as inventive mechanisms thermodynamically difficult energy sources (P. G. Falkowski et al., 2008; Geisberger et al., 2019; E. K. Moore et al., 2017; Nitschke et al., 2013). As such, life has spread to the deepest environments on the planet (Ménez et al., 2012), only limited by intense temperatures (-201 to 22 C) (Clarke, 2014), prompting scientific questions that border the philosophical as to their origin.

1.3. Emergence of metabolism from geochemistry

An emergent property of life on Earth are the biogeochemical feedback loops which regulate the cycling of nutrients across the biosphere (P. G. Falkowski et al., 2008), which according to the Gaia hypothesis, functions very much like an organism (Lovelock & Margulis, 1974). How much of this self-regulating condition was present prior to the emergence of life? At what point was the transition separate from the processes that preceded it? Erwin Schrodinger described life as an "evasion from the decay to equilibrium" (Schrödinger E, 1944), and given certain hypotheses relating to life's origins,

namely at alkaline hydrothermal vents (W. Martin & Russell, 2007; M. J. Russell, 2023; M. J. Russell & Hall, 1997), this evasion from entropy may stem from life's initiation at a natural redox gradient (Nitschke et al., 2024).

The earth is an organics factory and carbon in its various forms are constantly undergoing redo transformations mediated by life as well as abiotic chemical systems throughout the environment (P. Falkowski et al., 2000; McDermott et al., 2015a). Such transformations likely occurred immediately following the formation of Earth, the precipitation of its oceans, and of course at the transition between non-living and biological metabolism. Several hypotheses posit that life emerged from geochemical disequilibria inherent to the interfaces between the primitive ocean and the serpentinizing lithosphere (De Graaf et al., 2023; W. Martin & Russell, 2007; Nitschke & Russell, 2009; Preiner et al., 2019; Xavier et al., 2020). Here, steep redox, pH, and concentration gradients formed catalytic environments capable of conducting and sustaining complex organic chemistry. Investigations into modern equivalents of these environments, the deep sea hydrothermal vents, have discovered various abiotic chemical pathways for the synthesis of organic material (Koga & Naraoka, 2017; H.-E. Lee et al., 2023; W. Martin & Russell, 2007). These conditions are derived from serpentinizing water-rock interactions, where the confluence of magma, subducting rock, and supercritical water hydrothermally alters basalt to generate reduced gasses (e.g. H2, CH_4) and solubilized metals (e.g. Fe, Ni, Co, Mo, Zn, Cu, and W)(Preiner et al., 2018). Due to strong temperature and redox gradients at the sea floor, this effluent precipitates out as transition metal and sulfide rich mineral chimneys with complex architecture with high surface area and porosity. It has been found that certain minerals present at these vents, specifically transition metal rich oxides, sulfides, and clays have a high affinity for the adsorption of organics and provide catalytic surfaces and scaffolds for reactions that aggregate and polymerize such molecules into more complex ones (Hazen & Sverjensky, 2010a). Experiments that replicate these reactions have produced significant amounts of polymerized amino acids and proteins as shown by the polymerization of amino acids by brucite or ferrihydrite (Grégoire et al., 2016, 2018; Matrajt & Blanot, 2004) and have been confirmed to occur in modern hydrothermal systems (Ménez et al., 2018a).

These environments offer conditions (e.g. redox gradients, variable temperature, pressure, electrochemistry) and plentiful reactants (e.g. CO_2, CH_4, HS, transition metals) for the catalyzation of reactions which produce simple to complex organic compounds (e.g. methanol, formic acid, formaldehyde, pyruvate, amino acids) from the reduction of CO_2 and the oxidation of CH_4 (Beyazay et al., 2023; Grosch et al., 2022; Kitadai et al., 2019; McDermott et al., 2015b; Ménez et al., 2018a). The similarities between the coordination and arrangement of transition metals within mineral lattices and those Fe-Fe, Fe-Ni, or Fe-Co metal pairs within enzyme reaction centers at the heart of the metabolism of methane, hydrogen, and carbon compounds respectively, inspire hypotheses that link the evolution of enzymatic metabolism to geochemical mineral analogues (Nitschke & Russell, 2013; Preiner et al., 2019, 2020; Xavier et al., 2020). Such a transition could occur at these alkaline hydrothermal vent environments, which provide all the necessary conditions for the emergence of complex proto-metabolism (Trolard et al., 2022).

1.4. Electron transfer in Fe-bearing minerals

Electron transfer is a fundamental thermodynamic property inherent to various naturally occurring chemical species, playing critical roles in abiotic and biological systems (Nitschke et al., 2022). Life has harnessed this redox property via the evolution of transition metal-based enzyme reaction centers, which perform biochemical redox reactions to power metabolism (P. Falkowski, 2015). Similar metal ion coordination structures to those that underpin metabolism can also be found in purely abiotic mineral lattices, and recent work suggests that structure preceded function (Farr, Gaudu, et al., 2023).

Minerals are naturally forming crystalline materials exhibiting a diverse array of chemical and structural properties. With over 5000 distinct mineral species divided into groups based on similar crystal and chemical structures(Hazen et al., 2013), some minerals are recognized for their catalytic nature towards various chemical redox reactions. This behavior has long been exploited within certain industrial or societal purposes throughout history. At the heart of this catalytic ability, is electron transfer within and between minerals and exogenous species (Q. Q. Jia et al., 2022; Piechota & Meyer, 2019). Several properties inherent to crystalline minerals make for good conductors or semi-conductors, namely the energy difference between their outer valence and conduction bands which is known as the bandgap. Given sufficient excitation, electrons can move across band gaps, which are determined by the degree overlapping by outer valence bands between atoms within a crystal lattice. Thus, crystals bearing transition metals closely coordinated with each other often exhibit lower band gaps than in those with larger interatomic distances, making them better agents of electron transfer (Qian et al., 2023; Yu, Qian, et al., 2024).

The most abundant element on Earth, Fe is widespread in terrestrial and marine environments and displays exceptional electron transfer capabilities when in the form of metal oxides, hydroxides, and oxyhydroxide minerals, which exist as Fe cations bind to O, OH, or both groups(Bigham et al., 2018). In iron oxides such as hematite (Fe_3O_4), Fe atoms form strong octahedral bonds with oxygen atoms, yielding dense crystals as opposed to Fe-hydroxides which coordinate with OH groups resulting in poor crystallinity (e.g. ferrihydrite). Oxyhydroxides share qualities of both materials, and often form layered metastable crystals which can bear interstitial anions (e.g., green rust and goethite). These materials can contain multiple oxidation states within the same crystal structure yielding semiconducting properties as exemplified in magnetite (Fe_3O_4) which serves as useful semi-conductors for industrial processes in the reforming of fossil fuel gas, the Haber-Bosch process for converting N_2 to NH_3, and in the past as primitive semi-conductors for electronics (Usman et al., 2018). It is able to be used in these contexts as it's electron potential allows for the transfer of electrons from Fe sites to other compounds to promote the hydrolysis of complex hydrocarbons or the reduction of N_2 under specific T/P conditions where the transfer is thermodynamically uninhibited.

Various materials properties control electron transfer. As transition metals can exist in a variety of oxidation states, they have different capacities for electron transfer during oxidation and reduction reactions. The mild reduction potential of certain transition

metals [Fe= ($E°_{Fe2+/Fe0}$ =-0.44V), Nickel ($E°_{Ni2+/Ni0}$ = −0.26 V), cobalt ($E°CO_{2+/Co0}$ = −0.28 V), manganese ($E°_{Mn2+/Mn0}$ = −1.17 V), and copper ($E°_{Cu2+/Cu0}$ = 0.34 V)] make for suitable electron transfer agents in a wide variety of redox reactions catalyzed in abiotic mineral systems, as well as those essential in biochemistry (Frey & Reed, 2012). In the case of Fe-oxides, the partial substitution of Fe with other transition metals can promote or decrease the efficiency of electron transfer by varying bandgap. How these transition metals are coordinated within crystal lattices determines the conductivity of electrons within the mineral and between the mineral and exogenous species present at the surface or within the local environment.

A diverse range of catalytic reactions inherent to Fe-minerals has been attributed to the reactivity of Fe^{2+} atoms (J. Huang et al., 2021). Fe^{2+} in minerals exist as sources of electrons for transfer to acceptors via reaction sites located at mineral surfaces, edges, and notably interlayer regions (Yu, Qian, et al., 2024). The length of the Fe-OH bonds at these surfaces control mineral catalytic efficiency (H. Li et al., 2024) toward the reduction of organic and halogenated species, with longer lengths increasing the relative ease of electron transfer. Interactions with adsorbed organics can further modify coordination and bond chemistry changing reaction rates and efficiency (Q.-Q. Jia et al., 2024). as high pressures are predicted to increase chemical electronegativity in minerals, which may explain the intensified production of organics during serpentization within the deep earth (Y. Li et al., 2023). The flexible configuration and rearrangement of electrons within multivalent minerals like $Fe^{2+/3+}$ -oxyhydroxides provides for versatile chemical characteristics (J. Huang et al., 2021) and can quickly transport electrons between cations to counter balance changing anion chemistry (Wander et al., 2007). Recent work has revealed the role of $Fe^{2+/3+}$ within Fe-bearing minerals (e.g. green rust, Fe-sulfide, lepidocrocite) towards radical formation (Anipsitakis & Dionysiou, 2004; L. Fang et al., 2021; R. Liu et al., 2023; Morin et al., 2023; Xue, 2009; G. Zhao et al., 2023). Oxidation of these cations result in cascading radical chain reactions between iron and oxygen radical species, such as in the Fenton reaction where redox cycling of Fe^{2+}, Fe^{3+}, and O_2 yields hydroxyl radicals and H_2O_2 (L. Fang et al., 2021; Hanna et al., 2010). Electron transfer from radical interactions can yield short lived high valent Fe^{4+} states (Yu, Ji, et al., 2024), which like the excitation of electrons (e.g. via photons), can catalyze thermodynamically unfavorable reactions by providing the energy to cross steep reaction barriers (Z. Wang et al., 2022). Overall, Fe-mineral chemistry presents diverse arrays of catalytic function and as such significantly influences environmental redox chemistry.

1.5. Carbon redox in natural systems mediated by interactions with Iron

Carbon species are constantly undergoing redox reactions within the environment, as biological and geochemical processes mediate the transfer of electrons between organic electron acceptors and donors. Approximately. 3.5 x 10^{12} mol/yr of Fe is involved in environmental reactions (J. Huang et al., 2021) up and down the redox chain.

Carbon dioxide (CO_2) is the most oxidized form of carbon, making up 0.041% of the atmosphere. It is constantly cycled throughout terrestrial and marine environments via abiotic (e.g. carbonation) and biological (e.g. respiration) components of the carbon cycle. The concentration of CO_2 in the atmosphere imposes controls over the pH and alkalinity dependent speciation of carbon (H_2CO_3, HCO_3^-, $CO3^{2-}$) of all aqueous systems. CO can react to carbonate metal ions and form various carbonate minerals, sequestering gaseous CO_2 into mineral form (Middelburg et al., 2020). In biochemistry, cellular respiration metabolizes CO_2 into organic compounds via reduction, and various enzymes rely on Fe, Fe-Ni, or other metal cofactors to power this transformation process (E. K. Moore et al., 2017). Under specific conditions, CO_2 can also be reduced by reactive minerals (Grosch et al., 2022; Hudson et al., 2020; X. Liu et al., 2022). To achieve CO_2 reduction CH_3OH an input of -0.38 V (at pH 7) must be exceeded (S. Fang & Hu, 2022). In non-reactive conditions, CO_2 is otherwise readily adsorbed to mineral surfaces (Santos-Carballal et al., 2018).

Methane (CH_4), exists as the second lowest oxidation state of carbon, and although currently present at only 1.9 ppm, is the major heat-trapping greenhouse gas in terms of its radiative forcing effect, having 80x the effect of CO_2 (Jackson et al., 2021). With four hydrogens, the central C atom is highly reduced. Methane oxidation to higher oxidation states, such as the CH_3 radical, is thermodynamically difficult due to the redox potential (0.17V) required (S. Fang & Hu, 2023), however methanotrophy is one of the oldest metabolisms present on Earth (Ducluzeau et al., 2009), and some naturally forming minerals have been found to conduct this reaction (this thesis). In methanotrophs, methane is oxidized to methanol by sMMO and its multivalent di-iron cofactor surrounded by a polyamino acid ligand. This iron cofactor is capable of existing in 3 oxidation states, Fe^{2+}, Fe^{3+}, Fe^{4+}. In the enzyme sMMO the Fe^{3+}:Fe^{3+} center is reduced by a reductase to Fe^{2+}:Fe^{2+}, whereO_2 can bind to iron. Then via proton transfer the Fe^{3+}:Fe^{3+} is oxidized to a diamond di(μ-oxo) Fe^{IV}_2 core, which is able to transfer electrons to methane and form methanol. This Fe^{4+} state is thermodynamically unstable but it is supported by the enzyme's structural ligands (Shu et al., 1997). Synthetic catalysts for methane oxidation have optimized structures for Fe^{4+} entrapment, as seen in HZM-5 zeolites, which efficiently guide CH_4 into high surface area pores for efficient oxidation. In natural minerals, Fe^{4+} states have only recently been identified (Yu, Ji, et al., 2024). Overall various mineral characteristics influence CO_2/CH_4 gas adsorption (e.g. surface area, hydration, composition) but gas pressure is the greatest control (Du et al., 2020).

Non-reactive minerals play a role in the transport and sequestration of various organic compounds in marine and terrestrial settings, interfacing with microbial life while reactive minerals share this function as well as modify the organic compounds via hydrolysis or redox reactions(Gledhiir & Buck, 2012; B. Li et al., 2024; Longman et al., 2022; Purvis et al., 2022). Many transition metal bearing minerals are known to conduct the degradation of natural and synthetic organic compounds in the environment, such as organic phosphorus, nitrogen, and particular interest has focused on the destruction of persistent pollutants such as organohalogens such as TCE and PFAS(Y. Chen et al., 2019; J.-M. R. Génin et al., 2001; Xue, 2009; Yao et al., 2022).

Several groups of iron minerals are implicated in the cycling of carbon, iron-sulfides, oxides and oxyhydroxides in particular display strong electron transfer capabilities towards organic carbon(J. Huang et al., 2021). Fe sites in these minerals can transfer

electrons to carbon bonds (Comba et al., 2015) to break them or by initiating Fenton radical production (J. Ye et al., 2024) resulting in the degradation of complex molecules into smaller compounds, as well as CO_2 and CH_4. This process is essential to the cycling of carbon through the environment(Friese et al., 2021; O. W. Moore et al., 2023). The cycle continues as contact with CO_2 or CH_4 can cause some minerals generate organic carbon (Purvis et al., 2022), which is subject to further reaction and modification by reactive mineral species (J. Huang et al., 2021; B. Li et al., 2024; Longman et al., 2022). Environmental conditions play a strong regulating role over the mineral carbon reactions, with temperature, pressure, radiation impose upon the thermodynamic properties of these minerals.

1.6. Redox behavior of $Fe^{2+/3+}$oxyhydroxide "Green rust" minerals

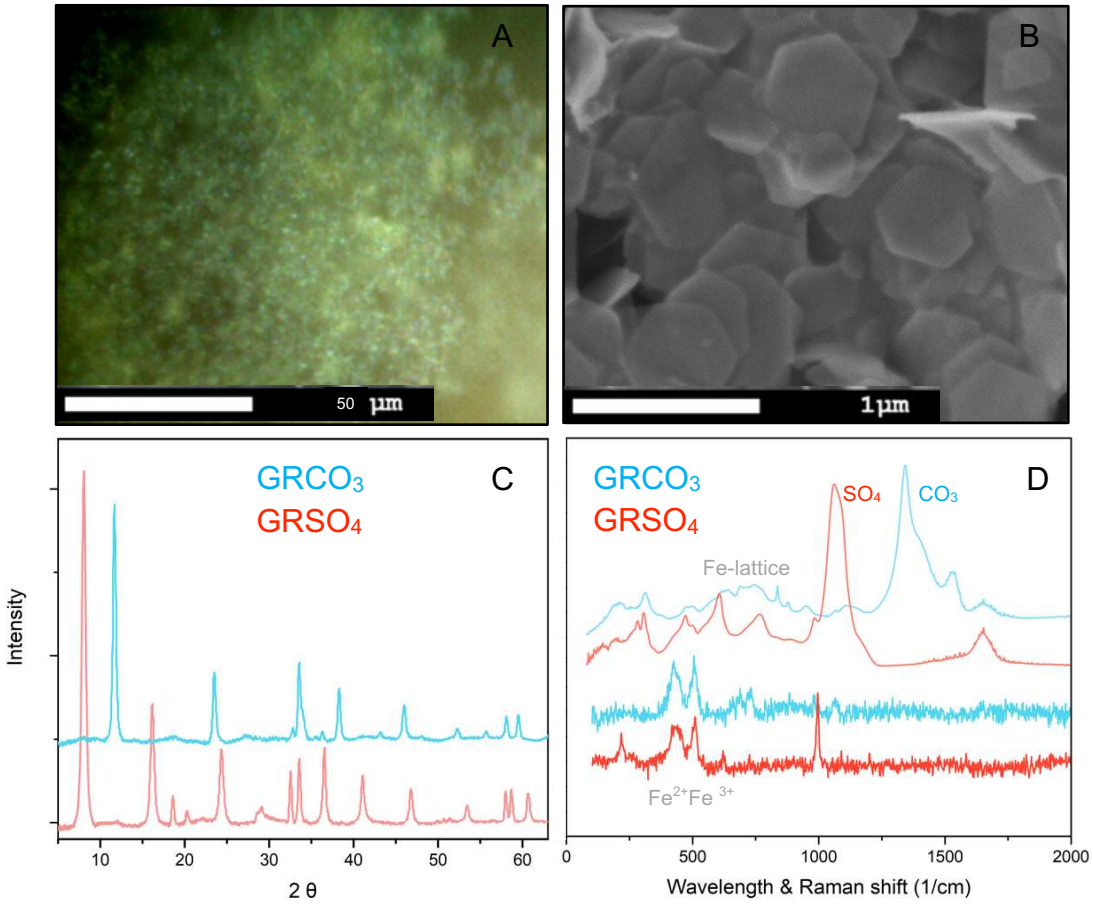


Figure 1.1: Section A displays a 20x magnification image of wet $GRCO_3$ minerals, demonstrating the intense green color and granular packing. Section B displays a SEM image of $GRCO_3$ minerals alongside a vial of freshly flocculated $GRSO_4$ for reference. Section C displays XRD crystallograph of $GRCO_3$ (blue) and GR SO_4 (red), while section D shows overlain IR, Raman spectra of $GRCO_3$ (blue) and SO_4 (red) minerals. Methods for collection are described in Chapter 3.

One group of minerals noted for its exceptional electron transfer capabilities and high reduction potential are "green rusts" which are the main subject of this thesis. $Fe^{2+/3+}$-oxyhydroxide green rust is a group of layered double (oxy)hydroxide (LDH) minerals comprising of double layered structure consisting of a positively charged cationic outer layer of Fe^{2+}/Fe^{3+} metals bound to hydroxides which envelope negatively charged interchangeable interlayers containing anions such as Cl^-, SO_4^{2-}, or CO_3^{2-} (Usman et al., 2018).

Characteristics

These high surface area (3.6-30.1 g/cm^2) (Usman et al., 2018) hexagonal minerals range in size from 10 nm to 100 um and have two distinct structures based on anionic component, GR1 and GR2. Green rust 1 (GR1) [Lattice parameters a = 0.3172 nm, c = 2.274 nm] is associated with planar and spherical anions, e.g., chloride $[Fe_5^{2+}Fe_2^{3+}(OH)_{14}]^{2+}[2Cl^-.3H_2O]^{2-}$, carbonate $[Fe^{2+}6Fe_2^{3+}(OH)_{16}]^{2+}.[CO_3^{2-}.5H_2O]^{2-}$, formate $[Fe_5^{2+}Fe_2^{3+}(OH)_{14}]^{2+}[2HCOO^-.3H_2O]^{2-}$; as opposed to GR2's [Lattice parameters a = 0.5524 nm, c = 1.1011 nm] three-dimensional hydrated anions such as sulfate $[Fe_4^{2+}Fe_2^{3+}(OH)_{12}]^{2+}.[SO_4^{2-}.8H_2O]^{2-}$ with tetrahedral structures requiring two layers of water (Legrand et al., 2004; Ruby et al., 2003). More complex arrangements can exist with the entry of large organic molecules of up to 24 carbon atoms has been reported (Ayala-Luis et al., 2010).

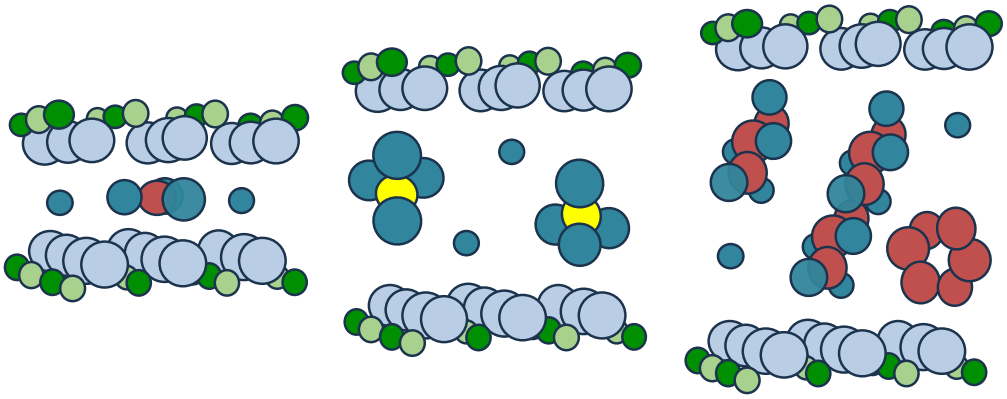


Figure 1.2 : Illustrative diagram of $Fe^{2+/3+}$ oxyhydroxide GRI, GRII, and inferred mineral crystalline lattices containing CO_3, SO4, or variable organic interlayer species. [$Fe^{2+/3+}$ are greens, O are blues, C is red, S is yellow]

Green rust occurs naturally as the oxygen sensitive mineral Fougérite $[Fe/Mg/Al^{2+}6Fe_2^{3+}(OH)_{16}]^{2+}.[CO_3^{2-}.5H_2O]^{2-}$ in suboxic soils, anoxic water (Jorand et al., 2011; Trolard et al., 1997; Zegeye et al., 2012), and is hypothesized to exist in deeper and more anoxic environments such as hydrothermal vents and diagenetic sediments (Farr et al., 2022; Trolard et al., 2022).

GR exists within a range of stabilities due to necessary charge balancing between cation and interlayer anions with the ratio of $Fe^{2+/3+}$ cations within the crystal structure ranges from (x= $Fe^{3+/2+}$; x = 0.25 - 0.33) (Refait & Génin, 1994; Ruby, Géhin, et al., 2006). Electrons freely flow across the cation basal planes in a constant reshuffling of $Fe^{2+/3+}$ sites (Wander et al., 2007). This is achieved due to limited hindrances to electron transport as of all analyzed Fe-oxide minerals analyzed, green rust has the smallest band

gap (S. Lee et al., 2023) Surface charge varies between types of GR, and is primarily controlled by pH (Guilbaud et al., 2013; Kozin, 2014). Changes to redox state (eH) have dramatic effects on the chemical properties of GR. Perturbations to these fragile conditions results in the transformation to various minerals (e.g. ferrihydrite, goethite, lepidocrocite, and magnetite) most commonly due to exposure to oxidizing species (Ayala-Luis et al., 2008; W. Liu, 2021; Ruby et al., 2010; C. Wang & Chakrapani, 2023b). This transformation is associated with the release of hydrogen via the Schikorr reaction and as well as radicals under oxidizing conditions. Factors that impair dissolution-recrystallization such changes to pH, temperature, or the adsorption of some metals, organic, or inorganic compounds can result in eventual transformation of the mineral (Farr et al., 2022; Perez et al., 2024; X. Wang et al., 2019). This variable capacity for structural reconfiguration, sorption, and electron transfer impart GR with enhanced reactivity towards a variety of compounds.

Electron transfer

The LDH oxyhydroxide structure, coordination, and atomic members of GR's crystal lattice allow for excellent electron transfer within GR and out to other species (Usman et al., 2018) leading to impressive redox capabilities in carrying out the reduction of various compounds (Yao et al., 2022). The multivalent octahedrally coordinated metal cation sheets that compose GR surfaces are highly catalytic towards the reduction of metals, organic, and inorganic compounds (Ruby, Upadhyay, et al., 2006). GR is a natural n-type semiconductor, displaying small band gap (1.6 eV) and relatively low electron affinity (~3.2 eV) compared to other transition metal minerals drives its donation of electrons in many redox reactions (S. Lee et al., 2023). Green rust has a pH dependent (zpc=~8-8.6) affinity towards the adsorption and surface layer incorporation of various metals (e.g. Ni, Zn, Cu, Si, As, W) and compounds (e.g. PO_4, NO_{3-}, amino acids) (Bearcock et al., 2011; Y. L. Li et al., 2017b; O'Loughlin, Kelly, Kemner, et al., 2003). Dense Fe-OH surface sites located on basal planes and edges preferentially adsorb molecules while the cations themselves can only replace Fe during synthesis or during recrystallization via Ostwald ripening (Chaves et al., 2009; Guilbaud et al., 2013).

Native metal as well as various metal compounds in contact with green rust minerals are found to be effectively reduced (e.g., Cu, As, U) under laboratory and environmental conditions, dramatically effecting their solubility and transport throughout aqueous systems (Inoue et al., 2008; O'Loughlin, Kelly, Cook, et al., 2003; Perez et al., 2024; Yan et al., 2018). This behavior extends to other inorganic compounds such as NO_3^- and ClO_4^- which are eventually fully converted into NH_3^- and Cl^- if left in solution (Buessecker et al., 2022; Z. Zhang et al., 2021). Many carbon bearing compounds are found to meet the same fate as even notoriously recalcitrant organic pollutants such as CCl_4, $CHCl_3$, C_2HCl_3 are eventually reduced to ethylene, chloromethane, and CH_4 given properly doped GR (Ai et al., 2022; Erbs et al., 1999; W. Lee & Batchelor, 2002; O'loughlin et al., 2022).

This capacity for electron transfer has several mechanisms implicated; small band gap, Fe-OH bond length, and radical generation. Bond length is regulated by Fe coordination, and modifications to this, such as amendment with exogenous metal or organic compounds (Q.-Q. Jia et al., 2024; Maithreepala & Doong, 2005; O'loughlin et al., 2022), manifest in changes to bond length between Fe and OH groups which result increased or decreased effectiveness towards electron transfer outside of the mineral (H. Li et al.,

2024). As these redox reactions result in the transfer of electrons that stabilize GR, without replenishment, the GR crystal transforms to other mineral phases.

Transformation

As previously mentioned, GR is only stable within a range of ratios between $Fe^{3+}/^{2+}$, and the presence of oxidants results in the perturbation of this stability leading to transformation (Antony et al., 2008; Inoue et al., 2007; Legrand et al., 2004; X. Wang et al., 2013). Various oxidants have been studied as agents of mineral transformation. Various Nitrogen, Chlorine, and Manganese oxides have been found to readily react with Fe^{2+} oxides, and GR resulting in mineral transformation. Interestingly, Mn can be integrated into the GR structure via adsorption and integration substituting for $Fe^{2/3+}$ sites in the mineral lattice at formation (C. Wang & Chakrapani, 2023a; X. Wang et al., 2019). Direct contact between oxidizing minerals implies electron transport may readily occur within heterogenous sediments. Additionally, Ultraviolet photons are highly energetic agents of electron transfer and have been shown to oxidize Fe^{2+} sites in GR and other reactive transition metal minerals in solution. Related to direct UV irradiation, UV produced radicals as a result of Fenton processes are also found to oxidize GR (Anipsitakis & Dionysiou, 2004; Dodd et al., 2022; L. Fang et al., 2021; Fubini et al., 1995; H. He et al., 2021; Z. Li et al., 2022; Matta et al., 2008).

GR has affinities towards the adsorption and integration of various metals and organic species. The sorption of metals resulted in decreased stability under oxidizing and increased temperature conditions (Farr et al., 2022; Tamaura, 1986; X. Wang et al., 2019). Surface binding or the replacement of structural Fe^{2+} with different transition metals may negatively impact the stabilizing effect of electron transport between iron atoms (cite wander e hopping). The sorption of various organic species which can transfer electrons such as quinones also results in destabilization of GR, again by disrupting the ratio of Fe $Fe^{2/3+}$ (Taran, 2017). Conversely the sorption of certain hydroxyl group rich organic molecules like glycerol or amino acids can protect GR from attack by electron acceptors likeO_2 (J. M. R. Génin et al., 2005).

While GR is thought to be stable at 25C, increasing temperature to 80°C in water baths has been shown to result in the spontaneous transformation to Fe_3O_4 (Farr et al., 2022; Tamaura, 1986; Tamaura et al., 1984). However, brief exposure to high temperatures is promoted as a method of increasing the crystallinity of GR and related mineral species. Therefore it is possible that interactions with excess metal ions, such as Fe^{2+} in solution can impair crystallization, thus promoting mineral transformation at higher temperatures. In nature, these conditions are representative of hydrothermal and diagenetic environments, where GR is liable to transformation changes playing a yet unquantified role in the geochemical cycling of sub-oxic subsurface environments (Farr et al., 2022; Trolard & Bourrié, 2008; Zegeye et al., 2012). GR's role as an agent of geochemical redox extends far back into geological history.

1.7. The role of green rust in the emergence of life

This thesis aims to reveal previously unrecognized reactions between naturally occurring green rusts and gaseous CO_2 and CH_4. As a naturally occurring metastable nanomaterial with catalytically active surfaces and internal spaces, GR presents a viable candidate for an-in-one emergence of life hypothesis (Duval et al., 2019; M. Russell, 2018).

Homologous structures can be used to identify similar environmental conditions that led to the evolution of certain biological or biochemical traits, and in the same vein, the identification of homologous structures in minerals and enzymes could potentially provide insight into the geochemical to biochemical transition - the evolution of enzymatic reaction centers from a hypothesized geochemical ancestor(Farr, Gaudu, et al., 2023; Preiner, Asche, et al., 2020). Enzymes are the central functioning unit of metabolism, responsible for the production and transformation of compounds to yield energy that can be used for biological functioning.(P. G. Falkowski et al., 2008) According to metabolism-first hypotheses, proteins and enzymes were the first biochemical structures to appear at the beginning of life, as they were all that was necessary to exploit thermodynamic disequilibrium present in the environment to perform work (Preiner et al., 2019; M. J. Russell et al., 2013). Modern proteins share structures that can be traced back to LUCA (last common ancestor)(Lane, 2017), and this conservation indicates that certain metabolisms H_2, CO_2, CH_4 are ancient and were likely the first to appear (Nitschke et al., 2013; Wimmer et al., 2021). Transition metal cofactors mediate these metabolisms, with iron in particular playing an outsized role in numerous metabolisms (Nitschke & Russell, 2009; Sánchez et al., 2017). In biochemistry, Iron complexes can mediate efficient electron transfer between molecules as well as large distances up to 20 angströms, catalyzing various reactions from radical formation, proton reduction, metabolite processing, to the synthesis and repair of genetic material, vitamins, coenzymes, antibiotics, and coenzymes (Frey & Reed, 2012; Sánchez et al., 2017). Varied structures, such as Fe-S complexes and Fe-Ni hydrogenases have strong reduction potentials from +360 to -650 mV, capable of carrying out redox transfers necessary for ATP phosphorylation and chemiosmosis. The reliability and versatility of Fe electron transfer was consequential to the development of metabolism, but how did these systems first develop from ostensibly abiotic chemical interactions?

A proposed candidate(Duval et al., 2019; M. Russell, 2018; M. J. Russell, 2023; Trolard et al., 2022) for the solution to this problem are the Fe-oxyhydroxide green rusts, a naturally forming, metastable, reactive, layered double hydroxide minerals that shares certain structural and reactive characteristics in common with metalloenzymes.

Green rust is reactive (the full catalogue of redox reactions mediated by GR were previously discussed in section 1.3.) and is distinguished as a protoenzyme candidate due to its unique and versatile reactions that it conducts, readily carrying out the reduction of metals (e.g., Cu, As, U), inorganic compounds (e.g., NO_3^-, ClO_4^-), organic compounds (e.g., CT, TCE, TCM), (Buessecker et al., 2022; Choi et al., 2012; Døssing et al., 2011; Etique et al., 2014; Jönsson & Sherman, 2008; Onoguchi et al., 2019). In nature such reactions are observed only in diverse microbial metabolisms yet GR readily conducts all these electron transfer reactions, which can further be catalyzed or inhibited given modifications to its

unique structure of a charged octahedrally coordinated multivalent cations (e.g., Fe, Ni, Mg, Co, Al) sandwiching interchangeable reactive anions (e.g., CO_3^{2-}, $HCOO^-$, Cl^-, SO_4^{2-}) (Agnel et al., 2020; S. Lee et al., 2023).

This versatility and structural configuration draws a direct comparison to enzyme reaction centers. For example, in Fe green rusts the octahedral coordination geometry of the di-valent iron lattice is comparable to the di-iron reaction center structure of sMMO (Duval et al., 2019; Farr, Gaudu, et al., 2023). This structure present in methanotrophs as well as synthetic catalysts is known to be the key site essential to the oxidation of methane. As this thesis demonstrates, this shared homology does indeed translate to catalytic function towards CH_4 (Farr, Gaudu, et al., 2023) and CO_2 (S. Lee et al., 2023). Furthermore, the modification of these enzyme-like mineral lattices by substituting metal species can confer additional catalytic behavior, encompassing a range of known catalytic abilities demonstrated by similar mineral species (Choi et al., 2012; de Graaf et al., 2023; O'loughlin et al., 2022; Thomas et al., 2020; Y. Zhang et al., 2018). GR is also able to integrate itself within organic membranes (Gaudu et al., 2023), situating itself in a similar position to membrane bound proteins. This versatility in structure and function parallels that of enzyme configuration and resultant metabolism (P. G. Falkowski et al., 2008; E. K. Moore et al., 2017).

In this thesis, we experimentally demonstrate the viability of a green rust initiated proto-metabolism by testing its catalytic behavior towards CH_4 and CO_2. These results uncover previously unrecognized redox reactions with green rusts and the carbon cycle, yielding significant environmental implications to the modern and ancient Earth.

Chapter 2:

Methanol on the rocks: Green rust transformation promotes the oxidation of methane

In this chapter, we describe various experiments conducted to determine the validity of hypotheses relating to the catalytic nature of green rust minerals towards methane oxidation, and the inferred relationship between homologous mineral lattice coordination and the coordination of the metallic cofactor at the heart of the methanotrophic enzyme sMMO. A large part of this chapter was used to produce the now published manuscript *Methanol on the rocks: Green rust transformation promotes transformation of methane,* (http://dx.doi.org/10.1098/rsif.2023.0386) and has been reproduced verbatim along with the supplementary material, however various additional content and experiments, which did not appear in the manuscript have been included in an additional section 1.5.

Methanol on the rocks: Green rust transformation promotes the oxidation of methane

Orion Farr[a,b], Nil Gaudu[b], Gregoire Danger[c], Michael Russell[d], Daniel Ferry[a], Wolfgang Nitschke[b], Simon Duval[b]

a. Aix-Marseille Univ, CNRS, CINaM, F-13009, Marseille, France
b. CNRS, BIP (UMR 7281), Aix Marseille Univ, Marseille, France
c. Aix-Marseille Univ, CNRS, PiiM, F-13013, Marseille, France
d. Dipartimento di Chimica, Università degli Studi di Torino, Italy

2.1. Abstract

Shared coordination geometries between metal ions within reactive minerals and enzymatic metal cofactors hints at mechanistic and possibly evolutionary homology between particular abiotic chemical mineralogies and biological metabolism. The octahedral coordination of reactive $Fe^{2+/3+}$ minerals such as green rusts, endemic to anoxic sediments and the early Earth's oceans, mirrors the di-iron reaction center of soluble methane monooxygenase (sMMO), responsible for methane oxidation in methanotrophy. We show that methane oxidation occurs in tandem with the oxidation of green rust to lepidocrocite and magnetite, mimicking radical mediated methane oxidation found in sMMO to yield not only methanol but also halogenated hydrocarbons in the presence of seawater. This naturally occurring geochemical pathway for CH_4 oxidation elucidates a previously unidentified carbon cycling mechanism in modern and ancient environments and reveals clues into mineral-mediated reactions in the synthesis of organic compounds necessary for the emergence of life.

2.2. Introduction

Methane (CH_4), although currently present at only 1.9 ppm, is the major heat-trapping greenhouse gas in terms of its radiative forcing effect, having 80x the effect of CO_2 (Jackson et al., 2021). Anthropogenic emissions of CH_4 now outweigh natural sources produced via biotic (organic degradation) and abiotic (serpentinization, mantle degassing) mechanisms. Natural sinks exist for CH_4 but are insufficient to offset growing anthropogenic output. In the biosphere, CH_4 is readily oxidized by methanotrophs, yielding methanol (MeOH), a key metabolic intermediate towards biomass formation (Chistoserdova et al., 1998; M. J. Russell & Nitschke, 2017). In many species this metabolism employs the enzyme soluble methane monooxygenase (sMMO) to react CH_4 with oxygen (O_2), N_2O, or H_2O_2 over an ephemeral di-Fe^{4+} intermediate reaction center to achieve the conversion of CH_4 to MeOH (Kopp & Lippard, 2002). A similar reaction mechanism takes place within man-made catalysts where Fe^{4+} reaction centers embedded

within mineral scaffolds are used to convert CH_4 to value-added products (Dummer et al., 2023; Nizova et al., 1997; Starokon et al., 2013). The oxidation state Fe^{4+}, which is only ephemeral in nature, is crucial to the energetically demanding partial oxidation of CH_4 for biological and industrial purposes (Banerjee et al., 2015; Dummer et al., 2023).

Methane is thought to have had an even larger role in climate regulation during the Hadean-Archean Eons 4.4 to 3.2 Ga, where the estimated atmospheric abundance of greenhouse gasses like CH_4, CO_2, and N_2O were orders of magnitude greater than modern, supplying ample CH_4 for the proliferation of primitive methanotrophs (Arney et al., 2016; Catling & Zahnle, 2020). This anerobic metabolism, along with various others, dominated the biosphere until the emergence of oxygenic photosynthesis during the great oxidation event (GOE) (Schirrmeister et al., 2015).

Of pertinence to the experiments and outcomes reported herein, the octahedral di-iron reaction center structure of sMMO shares similar coordination geometry to the octahedral di-valent iron lattice coordination in green rusts (GR) (Figure 2.1) (Duval et al., 2019). This group of naturally forming, metastable, reactive, layered double hydroxide (LDH) minerals are known for their redox capabilities in carrying out the reduction of metals (e.g., Cu, As, U), inorganic compounds (e.g., NO_3^-, ClO_4^-), and organic compounds (e.g., CT, TCE, TCM (Buessecker et al., 2022; Choi et al., 2012; Døssing et al., 2011; Etique et al., 2014; Jönsson & Sherman, 2008; Onoguchi et al., 2019). GR's unique structure consists of a charged octahedrally coordinated bilayer of divalent $Fe^{2+/3+}$ cations which can integrate other transition metals (e.g., Ni, Co, Zn, Mg, Al) and sandwich interchangeable anions (e.g., CO_3^{2-}, $HCOO^-$, Cl^-, SO_4^{2-}) (Usman et al., 2018). The mineral reacts with oxygen, radicals, and temperature to undergo pH- and redox-dependent transformations into other reactive minerals, namely magnetite and lepidocrocite, playing a yet unquantified role in the geochemical cycling of sub-oxic subsurface environments (Farr et al., 2022; Trolard & Bourrié, 2008; Zegeye et al., 2012). Of note is its proposed role in marine nutrient and metal geochemical cycling prior to the GOE at ~ 2.5Ga (Dodd et al., 2022; Halevy et al., 2017), and its hypothesized suitability as an "abiotic enzyme" linking geochemical proto-metabolism with the evolution of enzymatic biochemistry prior to the emergence of life (Barge et al., 2019; Duval et al., 2019; M. Russell, 2018; M. J. Russell, 2023).

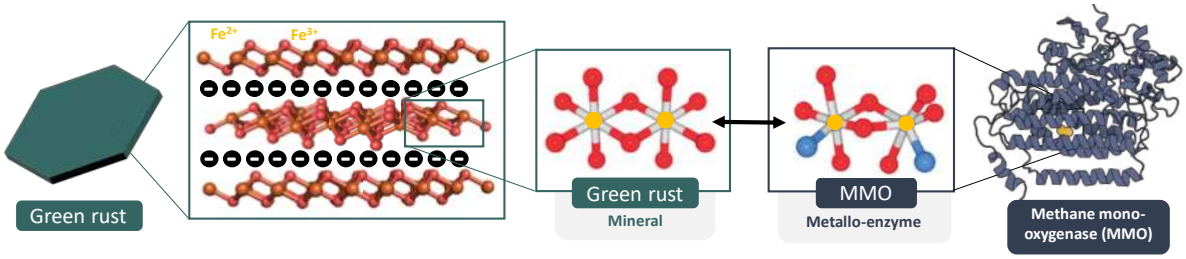


Figure **2.1:** A diagram comparing the structural similarities between GR and sMMO. From left to right, an illustration of a single GR crystal, the crystal's cation and anion LDH structure, the octahedral coordination of iron (yellow) and oxygen (red) atoms in GR, the analogous atomic structure of the MMO reaction center (nitrogen = blue), and a model of the enzyme MMO.

The di-iron structure present in sMMO and synthetic catalysts is known to be the key site essential in the oxidation of methane. Thus, the presence of an analogous structure in

GR suggests that it also has the potential to catalyze methane oxidation. In this study, we experimentally demonstrate the viability of this proposed analogous catalytic behavior by reacting green rust with CH_4 andO_2 to produce significant quantities of MeOH and halogenated organics. These results uncover previously unrecognized redox reactions with GR and the carbon cycle, yielding significant environmental implications to the modern and ancient Earth.

2.3. Methods

Mineral synthesis

Three GR species and their transformation products were synthesized following a procedure based on $GRCO_3$ syntheses outlined in Ruby (2003) and Bocher (2004). The main species of GR studied was a green rust intercalated with the carbonate anion ($GRCO_3$) and its synthesis is described below. Synthesis for $GRSO_4$ and GRCl is detailed in the supplementary section 1.

A concentrated stock solution of simulated seawater (80 ml) containing 150 mM $FeCl_2{\cdot}H_2O$, 50 mM $FeCl_3$, 50 mM of MgCl, and 400 mM of NaCl was prepared using deoxygenated ultra-purified water (milli-Q) and purged with N_2 gas for 30 minutes in a sealed 125 mL reactor vial. A solution (20 ml) of 300 mM NaOH and 30 mM Na_2CO_3 was then injected into the reactor via a N_2-purged needle syringe and the mixture was gently shaken. A dark green precipitate formed which was then confirmed to be $GRCO_3$ via powder X-ray diffraction (section d), which was stable indefinitely. The total Fe concentration in this stock solution was 200 mM and final pH was ~7.

Methane oxidation reactions

The pressurized reactions took place inside a 200 ml Parr autoclave reactor pressurized to 0, 1, 10, 30, 50 bar CH_4 (Linde Gas 99.99%), 0-3 bar O_2 (Linde), 1 bar NO (Linde Gas 5%), at 25°C. Within the reactor 20-100 ml glass vials with stirrers, butyl or screw top caps, and needle-perforated septa were used to contain the replicate mineral suspensions. These vials were then removed and stored under anoxic conditions before their headspaces were analyzed using GC-MS.

Headspace Analysis

GC gas chromatography coupled to an ISQ mass spectrometer (ThermoFisher Scientific). The sampling was performed by headspace (HS) using an RSH auto-sampler (ThermoFisher Scientific). 5 mL of each sample was deposited on a 20 mL HS vial with screwtop PTFE septas. Each vial was then incubated during 6 min at 55°C under agitation. The HS sampling was performed by collecting 2 mL of the gas phase. It was then injected into the GC via an injector at 250°C, a split at 10 mL/min and a column flow of 1.1 mL/min. The column was a Stabilwax-DA from Restek (length 30m, diameter 0.25 mm, film thickness 0.5µm). Analyses were performed with the temperature gradient that starts with a 1 min isotherm at 35°C and proceeds with a gradient at 25°C/min up to 220°C ending with a 2 min isotherm. The detection was performed with the MS in full scan or SIM mode using an electron impact ionization at 70eV. MS transfer line and ion source

temperatures were set at 250°C. For the full scan analyses, the m/z range was 20-300 au, meanwhile for the SIM m/z 31 and 84 were isolated for MeOH and TCM identification (Supplementary Figure S2.6).

Mineral characterization

Mineral transformation over the course of the reaction was monitored using X-ray diffraction (XRD), transmission electron microscopy (TEM), and scanning electron microscopy (SEM). Samples were centrifuged, decanted, and dried under a stream of N_2 gas. For XRD analysis glycerol was added prior to analysis to prevent oxidation and the paste was transferred into a glass ampule for XRD analysis in a Rigaku RU 200BH diffractometer with Cu anode (λ = 1.5418Å), scanning from 2 theta values of 2-80 degrees. For TEM analysis, an aliquot of dried mineral was deposited on a copper grid coated with a holey carbon film (AGAR Scientific, S147-3). Grids were then transferred to a Jeol-JEM2010 electron microscope operated at 200 kV and GR particles were observed in bright field mode. For SEM analysis, an aliquot of dried mineral was deposited on an aluminum sample holder and then transferred to a Jeol JSM-7900F electron microscope and analyzed using accelerating voltages ranging from 5 to 15 kV.

2.4. Results

The pressurization of GR with CH_4 and O_2 resulted in the production of MeOH along with various other compounds, including trichloromethane (TCM) and dichloromethane (DCM). Various conditions were tested to optimize the yield of MeOH.

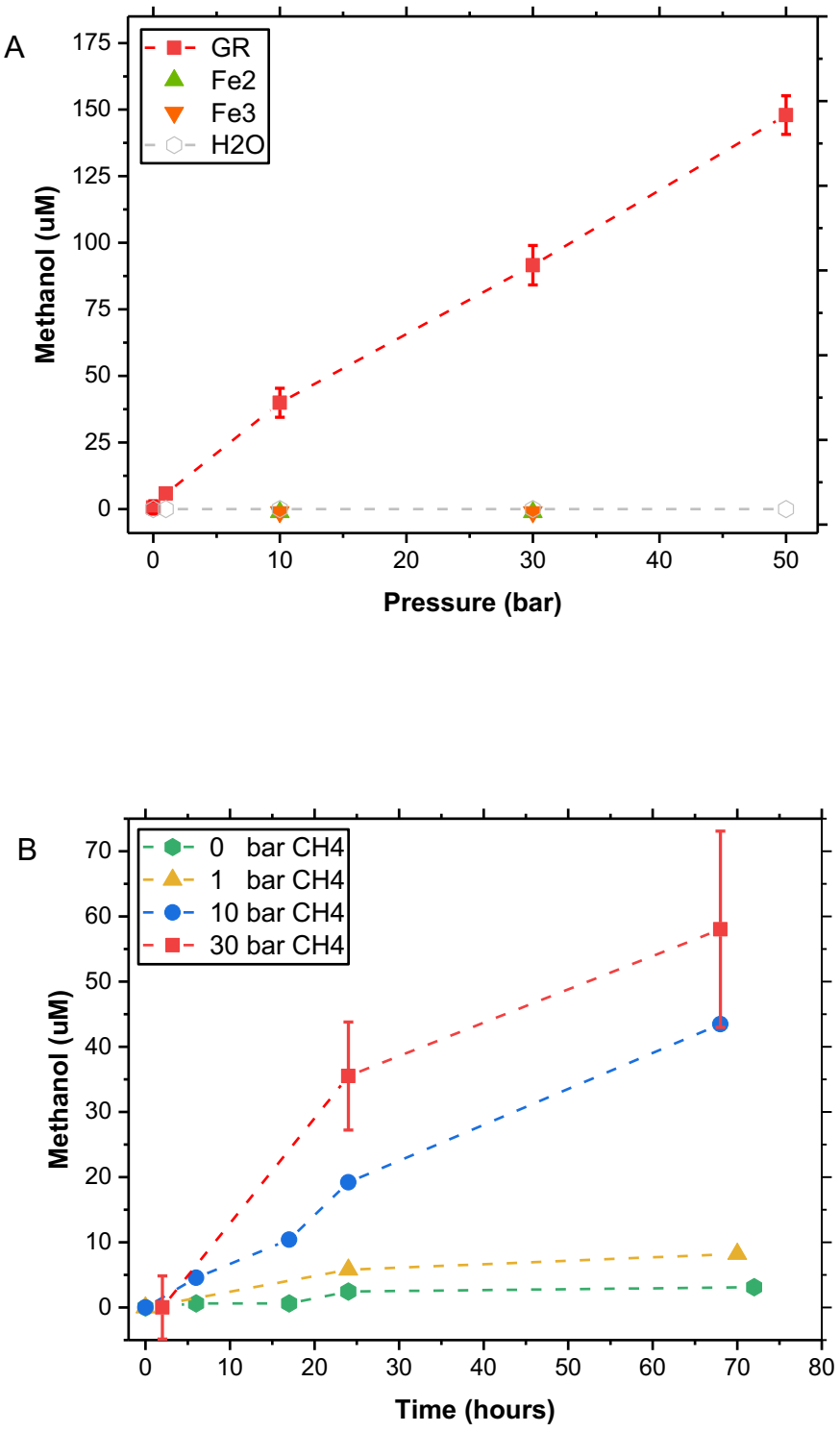


Figure 2.2: Graph A displays methanol concentrations at given CH_4 partial pressure following 24 hours of reaction time in solutions containing $GRCO_3$, $FeCl_2$, $FeCl_3$, and H_2O. Graph B displays a related set of experiments conducted at [Fe] = 30 mM, showing methanol production over time.

Figure 2.2A shows MeOH concentrations in solutions of $GRCO_3$ ([Fe]=200mM) following 24 hours of pressurization to 0, 1, 10, 30, and 50 bars of CH_4 mixed with 0.2 bar O_2. There is a significant increase in MeOH concentration with increasing pressure. At 10 bar CH_4, solutions of $GRCO_3$ with a total [Fe]= 200mM yield 30μM MeOH which increases 5-fold with a corresponding 5-fold increase to 50 bar CH_4. Thus MeOH concentration increases with a linear relationship with pressure [y = (2.88E-6)x + 5.30E-6)]. Multiple concentrations were examined and the relationship between [MeOH]/[Fe] is compared (Supplementary Figure S2.5). MeOH is only detected with GR in the initial solution, as solutions containing $FeCl_2$, $FeCl_3$, or H_2O did not produce detectable levels of MeOH under the same conditions. No MeOH is detected without the added oxidants. Substitutes forO_2, NO and H_2O_2, were tested and found to produce products of CH_4 oxidation (Supplementary Figure S1.7).

Figure 2.2B shows the production of MeOH over time in solutions of $GRCO_3$ ([Fe]=30mM) with partial pressures of CH_4 from 0 to 30 bar mixed with 0.2 barO_2. These experiments were conducted at lower concentrations of Fe than Figure 2.2 (30 vs 200mM). No MeOH is detected in solutions of GR not exposed to CH_4. With 1 bar CH_4 there is a mild increase to ~5μM of MeOH. At 10 bars CH_4 there is an increase from 0 to ~40μM of MeOH by 80 hours. At 30 bar of CH_4 we show an increase from 0 to ~55μM of MeOH by 68 hours of reaction time. The addition of 0.2 bar O_2 and subsequent MeOH production resulted in changes to solution pH, which was recorded to drop from an initial value of 7 to 6 by 24 hours and 5 by ~70 hours. Additional experiments were attempted with 1 bar O_2 and 10 bar CH_4, leading to rapid mineral transformation yet no measurable MeOH production.

Coinciding with MeOH production was the production of various organic compounds produced in μM quantities. The most prevalent compounds detected other than MeOH were halogenated organics, mainly TCM and DCM (Supplementary Figure S2.2). The concentration of TCM and DCM increased in response to increased pressure, however DCM was the primary organohalogen detected at higher pressures (30 bar) versus TCM dominating at lower pressures. Trace amounts of TCM were also detected without the presence of O_2 in aged $GRCO_3$ solutions exposed to CH_4. However, TCM was also produced in solutions of $FeCl_2$ when exposed to CH_4. Other organic products were produced but were not easily replicated and thus were not quantified: these compounds included C_1-C_{12} hydrocarbons, butanal, pentanal, paraformaldehyde, acetaldehyde, and dimethyl ether.

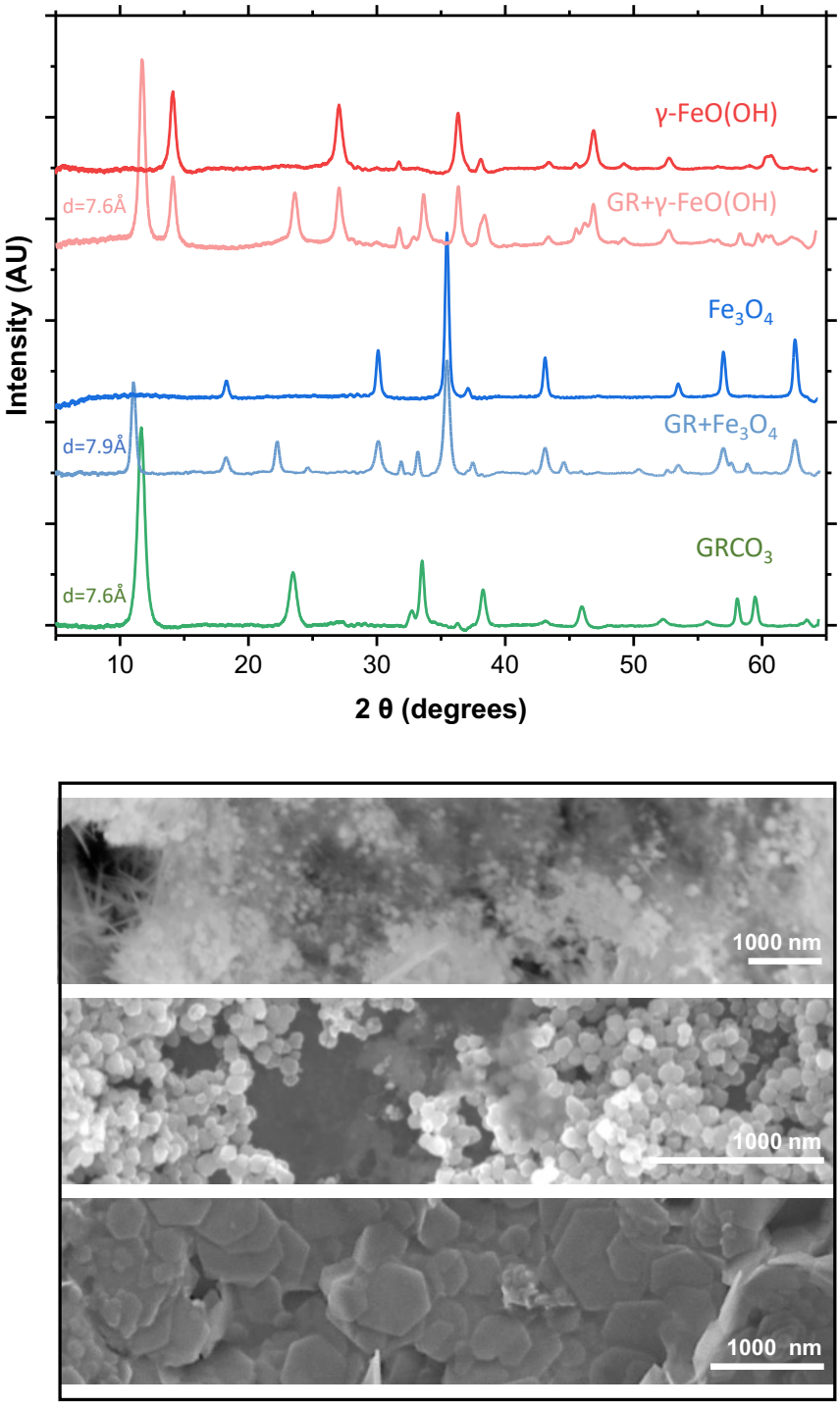


Figure 2.3 : Section A displays the XRD diffractograms of the mineral species produced following the exposure of $GRCO_3$ to pressurized CH_4/O_2 atmospheres. Magnetite (Fe_3O_4) and lepidocrocite (γ-FeO(OH)) were the primary transformation products of GR corresponding to low (~0.1 bar) and high (>0.1 bar) O_2 content respectively. Partially transformed products are displayed below the primary product, with the residual GR's low 2θ d-spacing listed adjacent. Section B displays the corresponding SEM images of the pure mineral phases characterized in section A.

GR undergoes transformation to two mineral phases following the exposure to pressurized CH_4 and O_2 mixtures, oxidizing to either magnetite (Fe_3O_4) or lepidocrocite (γ-FeO(OH)) according to XRD (Figure 2.3A). The presence of O_2 (0-1 bar) at the start of the reaction resulted in different transformation product yields, with increased O_2 selecting for γ-FeO(OH) over Fe_3O_4. In the case of transformation to Fe_3O_4, d spacing for the low 2θ peak shifts from 7.6 A to 7.9 A. Full transformation takes place within 68 hours of reaction. SEM (Figure 2.3B) images show distinct transformation from GR's characteristic 10 to 500 nM hexagonal platelets, through an intermediate phase with hexagonal plates studded with <100 nM spheroid assemblages or <100nm irregular acicular crystals, to a fully transformed phase with only spheroids or acicular crystals. The transformation of GR results in a decrease from an initial average pH of 7 to 5.

2.5. Discussion:

Our experiments show that the oxidative transformation of GR in the presence of CH_4 results in the oxidation of CH_4, to a variety of products. In section a, we discuss the analysis of MeOH, as well as the other compounds (e.g. TCM, DCM) detected in significant quantities.

The concurrent oxidation of green rust and methane

The production of MeOH at various pressures and over time is depicted in Figure 2.2, showing significant quantities are produced in solutions of GR pressurized to 1-50 bar over 60 hours, given the initial presence of 0.2 bar of O_2 at the start of the experiment. However, in the absence of oxygen, the introduction of CH_4 to GR resulted in little to no MeOH production. Substitutes for O_2 were tested, using H_2O_2 (Supplementary Figure S2.5) and NO (Supplementary Figure S2.7) in separate experiments, yielding MeOH and butanal respectively. The presence of a sufficient oxidant is therefore implicated in the successful oxidation of methane using GR.

Increasing CH_4 pressure resulted in a linear increase in MeOH concentration over a range of [Fe] (200, 100, 30 mM). Increasing the concentration of Fe results in higher yield of MeOH, however the efficiency of the production of MeOH/Fe falls dramatically (Supplementary Figure S2.5). GR's affinity to hydrophilic O_2 and as well as radical scavenging likely dominates surface interactions versus hydrophobic gases like CH_4. The reaction rate is thus dependent on how much CH_4 is in contact with the mineral surface, which is controlled by the concentration of dissolved CH_4 in solution (Figure 2.2). CH_4 solubility is controlled by pressure and chloride concentration due to CH_4's low solubility in distilled water at STP (25 C:1 bar) – solubility increases 42% from 1 to 50 bars but is decreased by 20% with the addition of 0.4 M Cl^- (Duan et al., 1992). The solubilization of CH_4 is one route for aqueous mineral reactions, however within pore spaces common to sediments and hydrothermal systems where this reaction would occur, direct contact with trapped CH_4 bubbles would offer a more direct mineral-to-gas interface, increasing the reaction rate.

The substitution of interlayer anions is known to affect GR reactivity (Agnel et al., 2020) and our investigation of Cl^-, CO_3^{2-}, and SO_4^{2-} (Supplementary Figure S2.4) shows an

unexpected trend in reactivity with CO_3^{2-}>Cl^->SO_4^{2-}. With prior work in GR, redox reactions involving the various anions show clear preference for Cl^- and SO_4^{2-} over CO_3^{2-} reactions (Usman et al., 2018). A shift in d-spacing (Figure 2.3) from 7.6A to 7.9A corresponds to a shift in interlayer anion species from CO_3^{2-} to Cl^- during transformation from GR to Fe_3O_4(Usman et al., 2018). As the $GRCO_3$ and GRCl solutions were conducted in simulated seawater, a mixed or transitory interlayer phase of CO_3^{2-}+Cl^- could conceivably be responsible for increased reactivity towards CH_4 oxidation. The increased MeOH production could also be linked to the reduction of interlayer bound CO_3^{2-} during the reaction (S. Lee et al., 2023).

The production of halogenated organic molecules was observed (Supplementary Figure S2.2): GR appears to catalyze CH_4 chlorination as TCM and DCM are products in solutions containing GR and NaCl. GR and magnetite are known to reduce halogenated organics (Erbs et al., 1999), which may explain the preference for DCM over TCM at higher pressure. Given time, this reduction should continue to methyl chloride and CH_4. Chlorine could likely be replaced by other environmentally relevant halogens such as iodine or bromine, indicating a general abiotic link between Fe redox and halogen cycling in the environment.

MeOH was not detected in parallel experiments using solutions of H_2O, NaCl, or $FeCl_2$, or $FeCl_3$ in place of GR. Since no MeOH is formed without GR or without O_2, GR must be producing a short-lived reactant during oxidation necessary for the reaction to proceed over GR or its oxide transformation products; ferric green rust, magnetite, or lepidocrocite.

Radicals and Fe^{4+} mediated oxidation mechanism

The presence of radicals and Fe^{4+} oxidation states are routinely implicated in CH_4 oxidation research as a main mechanism for achieving the energetically difficult partial oxidation of methane over transition metal bearing mineral catalysts such as zeolites (Dummer et al., 2023; Starokon et al., 2013). These high surface area aluminosilicate minerals bear Fe^{2+}-Fe^{3+} reaction sites which readily react with oxidative species such asO_2, H_2O_2, N_2O, UV, or radicals to create short lived reactive Fe^{4+} oxidation states which can effectively conduct CH_4 oxidation (Dummer et al., 2023; Nizova et al., 1997; Szécsényi et al., 2018). This Fe^{4+} state is likewise responsible for CH_4 oxidation in microbial methanotrophy, where the enzyme sMMO uses oxidant-activated Fe^{4+} reaction centers to transform CH_4 to MeOH (Kopp & Lippard, 2002). Correspondingly, in GR, it's oxidative transformation is known to produce a significant amount of hydroxyl radicals, H_2O_2, and Fe^{4+} sites (L. Fang et al., 2021; Z. Li et al., 2022) which have been observed to promote the degradation of complex organic molecules (Hanna et al., 2010; Matta et al., 2008).

Given the known relationship between radical production, Fe^{4+} sites, and methane oxidation, we propose that GR mediates CH_4 oxidation via radical mediated oxidation pathway over short-lived Fe^{4+} sites in a manner similar to sMMO (Banerjee et al., 2015) or Fe-ZSM zeolites (Starokon et al., 2013). To further test this hypothesis, we replicated the experimental conditions for $GRCO_3$ at 1 bar CH_4 and replaced O_2 with 1 mM of H_2O_2 which yielded a significant amount of MeOH even without high pressures (Supplementary Figure S2.5). This indicates the reaction is dependent on the interaction between hydroxyl

radicals, iron, and CH_4 (Anipsitakis & Dionysiou, 2004). Furthermore, MeOH serves as a radical scavenger resulting in its own oxidation to formaldehyde (which was detected), formate, and CO_2 (Alshehri, 2013). The production of organohalogens in the presence of Cl^- anions, likely through a radical chlorination pathway (Rabiu & Yusuf, 2013), adds further evidence to the radical-based hypothesis. In this case, the Cl^- radical ion substitutes for the hydroxyl radical to oxidize CH_4 yielding methyl chloride (MC), DCM, and TCM, instead of MeOH, which was observed in our experiments.

Implications

The discovery of a naturally occurring mineral-based mechanism for CH_4 oxidation is novel and hints at large scale geochemical processes that have been overlooked with past research.

Feasibility and environmental relevance

The conditions simulated within the pressure reactor (GR in contact with pressurized CH_4) provided optimal conditions for the reaction in addition to serving as an analogue to environmental conditions where GR could conceivably interact with sources of CH_4 at depth. GR has been isolated in deep anoxic ferruginous lakes (Zegeye et al., 2012) and is speculated to form at hydrothermal vents and (Trolard et al., 2022) where oxygen-poor hydrothermal fluids meet cold oxygen-rich sea water. In both locales, abiotic and biotic sources of CH_4, pressurized at depths (e.g. 100 m depth = 10 bar pressure) would fall within the range of conditions we tested. For environments closer to STP, such as wetland sediments, soils, and ground water, our experimental results still demonstrate GR's reactivity towards CH_4 oxidation, albeit one accelerated by pressure. We observed both MeOH and halogenated organics at 1 bar CH_4, though in low concentrations, indicating that mineral based CH_4 oxidation will take place even under STP. The discovery of naturally occurring mineral-based mechanism for CH_4 oxidation is novel and hints at global geochemical processes that have been previously overlooked.

Implied role of green rust in carbon and halogen cycling in modern environments

Green rusts are well studied for their use in the degradation of organohalogen pollutants in the environment (Choi & Lee, 2008; Maithreepala & Doong, 2005; O'Loughlin & Burris, 2022; Yao et al., 2022), however they have never been linked to organohalogen formation via CH_4 oxidation. Recent observations revealed that salt plains, rainforests, and soils are the source of abiotic emissions of chloromethanes (Bahlmann et al., 2019; Huber et al., 2009; Redeker & Kalin, 2012; Sattler et al., 2019; Wittmer et al., 2015). Of note is the isotopic fractionation of some of these signatures, implying an abiotic source (Bahlmann et al., 2019). As mentioned previously, GR is common in these types of waterlogged environments (Trolard et al., 1997) and within anoxic regions of stratified bodies of water and rivers with high iron content (Jorand et al., 2011; Zegeye et al., 2012). In soils, Fe is already known to halogenate decaying organic matter (Huber et al., 2009), the direct oxidation of CH_4 has not yet been observed in the environment. Our experiments show that it is feasible for GR to be oxidatively transformed to reactive Fe-oxides in the presence of CH_4, thus catalyzing abiotic CH_4 oxidation and chloromethane production. As CH_4, halomethane, and halogen flux greatly affect climate forcing (Q. Li et

al., 2022) uncovering the role reactive minerals play in these cycles may help constrain their input over climate change. Overall, the further study of these environments should take care to identifyO_2-sensitive minerals like GR, to understand the extent of their influence over the geochemical cycling of carbon and halogens.

Methane oxidation on the ancient Earth

Abiotic CH_4 oxidation may have played a greater role in the deep past as long periods of ferruginous oceans characterized the Archean (4-3.5 Ga) and Proterozoic (3.5-2 Ga) eons (Halevy et al., 2017; Poulton & Canfeld, 2011; Thibon et al., 2019). During these periods GRs are thought to have been abundant and likely shepherded marine geochemistry at the interface between land, air, and sea (Halevy et al., 2017; Koeksoy et al., 2019b; Zegeye et al., 2012). Prior to the GOE and the subsequent proliferation ofO_2 in marine environments; geochemically generated radical species (Anipsitakis & Dionysiou, 2004; Ernst et al., 2023; H. He et al., 2021, 2023; G. Zhao et al., 2023), thermochemical processes (Farr et al., 2022; Q. Huang et al., 2023), natural electrochemical processes (S. Lee et al., 2023; Nitschke et al., 2022; Ooka et al., 2019), photochemistry (Dodd et al., 2022; Ernst et al., 2023), nitrogen oxides (Buessecker et al., 2022; Wong et al., 2017), and nitrogen oxyanions (Barge et al., 2022; Ducluzeau et al., 2009), may have served as potential surrogates for the oxidation of GR and thus CH_4, creating a CH_4 sink within the ancient Archean ocean. AsO_2 concentrations increased following the GOE, the oxidation of GR-bearing oceans may have played a role in the drawdown of atmospheric CH_4 concentrations (Catling & Zahnle, 2020), impacting climate throughout the Proterozoic (Guilbaud et al., 2015; Jaziri et al., 2022).

As halomethanes exert strong influences over the greenhouse effect (Q. Li et al., 2022), the effect of their production by a GR saturated ocean on the Archean climate is currently unstudied. As such, the detection of exoplanet halomethane signatures may not necessarily indicate the presence of life, as was recently suggested (Leung et al., 2022). However, as life is thought to have emerged sometime in the late Hadean to early-Archean, the oxidation of abundant CH_4 (Catling & Zahnle, 2020) to more biochemically accessible compounds such as MeOH, hydrocarbons, and halogenated organics may have played important roles both before and after its emergence.

More specifically, our results strengthen an emergence-of-life hypothesis that invokes a pathway for GR-mediated protocell synthesis (Duval et al., 2019; M. Russell, 2018; M. J. Russell, 2023; M. J. Russell & Nitschke, 2017), where hydrothermal CH_4 is oxidized to multi-carbon compounds within GR-saturated mineral membranes precipitated at the redox boundary between reducing alkaline vent effluent and oxidizing acidic ocean water – the type of disequilibria considered to have driven life into being (M. J. Russell et al., 2013). Just as in the biological metabolism of methanotrophy, methane would thereby serve both as a feedstock for production of organics and as a source of a cascade of increasingly reducing electrons derived from the further oxidation of MeOH, formaldehyde etc, as discussed in (Nitschke et al., 2022; M. J. Russell & Nitschke, 2017). As pointed out previously, such entropy-decreasing processes are prerequisites for thermodynamically meaningful emergence-of-life scenarios (Branscomb & Russell, 2018). Given the similarities between sMMO's di-iron reaction center and GR's atomic lattice coordination, a proposed evolutionary link between minerals and enzymes is

suggested (Nitschke et al., 2013). Because GR has a uniquely versatile structure which allows for chemical exchange; integrating several essential metals (e.g., Co, Ni, Zn, Mo) and anionic (e.g., NO^{3-}, formate, linear carbon chain) species, it is suggested that its reactive surfaces and bilaterally active interlayers served as sites for organic synthesis and concentration (Helmbrecht et al., 2022) at early submarine alkaline hydrothermal vents, and that these interlayers also compartmentalized and guided the free-energy converting proto-metabolic processes which led to the emergence of life (Duval et al., 2019; M. Russell, 2018; M. J. Russell, 2023).

2.6. Conclusion:

We demonstrate that the oxidative transformation of green rust in the presence of methane yields methanol, along with organohalogens and various other organic compounds. This newly discovered behavior implies the existence of previously undetected links between iron, carbon, and halogen redox cycling in modern and ancient environments mediated by reactive minerals. Furthermore, the oxidation of CH_4 mediated by an abiotic GR mineral invites further research into the relationship between the evolution of primitive microbial metabolisms and the abiotic geochemical processes that preceded them.

Acknowledgements:

This work received support from the French Government under the France 2030 investment plan, as part of the initiative d'Excellence d'Aix Marseille Université (A*MIDEX -AMX-21-PEP-039) as well as a grant from the French Agence Nationale pour la Recherche (ANR-22-CE30-0035-01).

We thank Vasile Heresanu for performing XRD measurements, Alexandre Altié and Damien Chaudanson for SEM/TEM support, Frederic Brunel for lending us the pressure reactor, and Olivier Grauby for helpful discussions on green rust.

Authors contributions

OF designed and performed experiments. OF, NG, GD, MR, DF, WN, SD contributed to the manuscript.

1.8. Supplementary material to original manuscript

Supporting Information Text

1. Expanded syntheses.

The synthesis procedures for the additional green rust species and Fe solutions are as follows.

$GRSO_4$:
A 100 ml solution containing 150 mM $FeSO_4 \cdot 7H_2O$ (GR-SO_4) and 25 mM $Fe_2(SO_4)_3$ (GR-SO_4) was prepared using 80 ml deoxygenated ultra-purified water (milli-Q) and purged with N_2 gas for 30 minutes in a sealed 125 mL reactor vial. 20ml 3 M of NaOH was added dropwise.

GRCl:
A 100 ml solution containing 150 mM $FeCl_2 \cdot 4H_2O$ and 25 mM $Fe_2(Cl)_3$ was prepared using 80 ml deoxygenated ultra-purified water (milli-Q) and purged with N_2 gas for 30 minutes in a sealed 125 mL reactor vial. 20 ml 3 M of NaOH was added dropwise.

$FeCl_2$:
A 100 ml solution containing 200 mM $FeCl_2 \cdot 4H_2O$ was prepared using deoxygenated ultra-purified water (milli-Q) and purged with N_2 gas for 30 minutes in a sealed 125 mL reactor vial.

$FeCl_3$:
A 100 ml solution containing 200 mM $FeCl_3$ was prepared using deoxygenated ultra-purified water (milli-Q) and purged with N_2 gas for 30 minutes in a sealed 125 mL reactor vial.

2. Supplementary Data

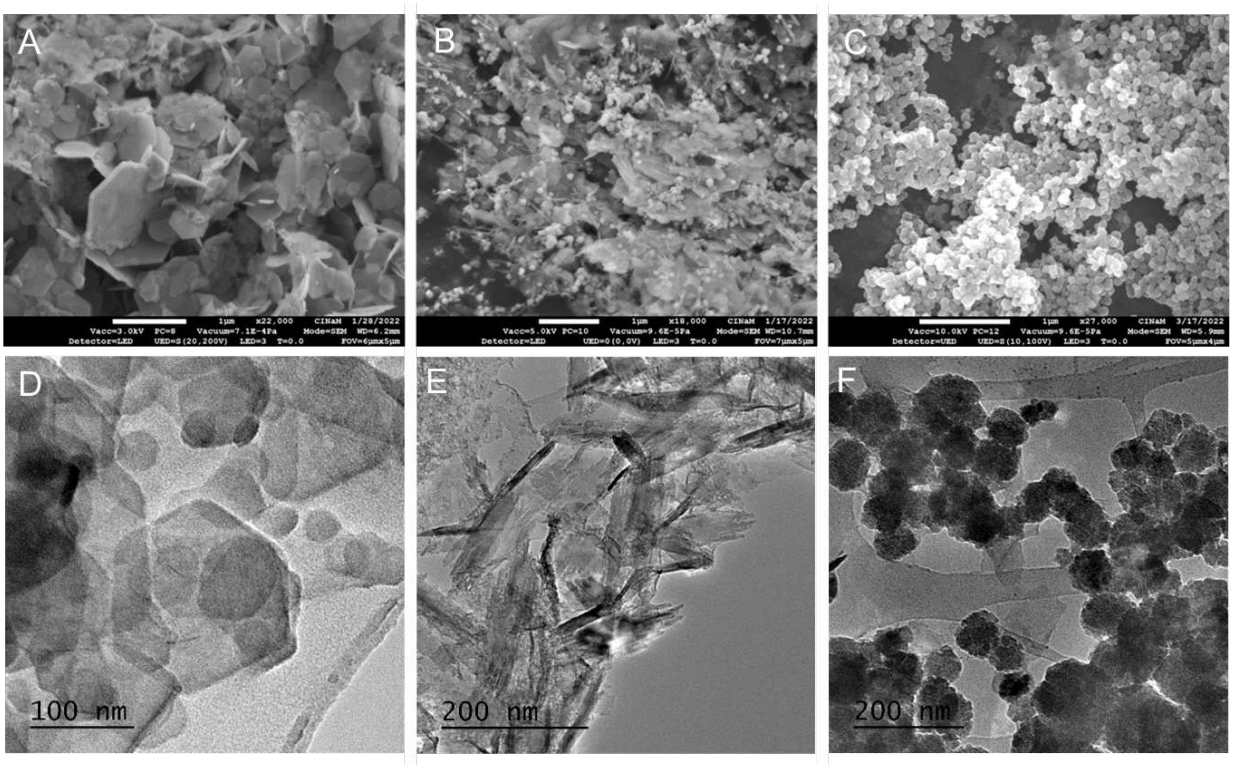


Figure S2.1 : Two rows of images from SEM (top row) and TEM (bottom row) observations of the mineral phases detected within our experiments. Image A and D show Green Rust Carbonate ($GRCO_3$) freshly prepared and observed under SEM and TEM respectively. Image B and E show partially oxidized $GRCO_3$ following exposure to CH_4/O2 mixture. Visible are GR crystals studded with FeOOH (B, E) and Fe_3O_4 minerals (B). Image D and F shows the complete transformation of GR into Fe_3O_4 following GR's exposure to CH_4/O2 mixture.

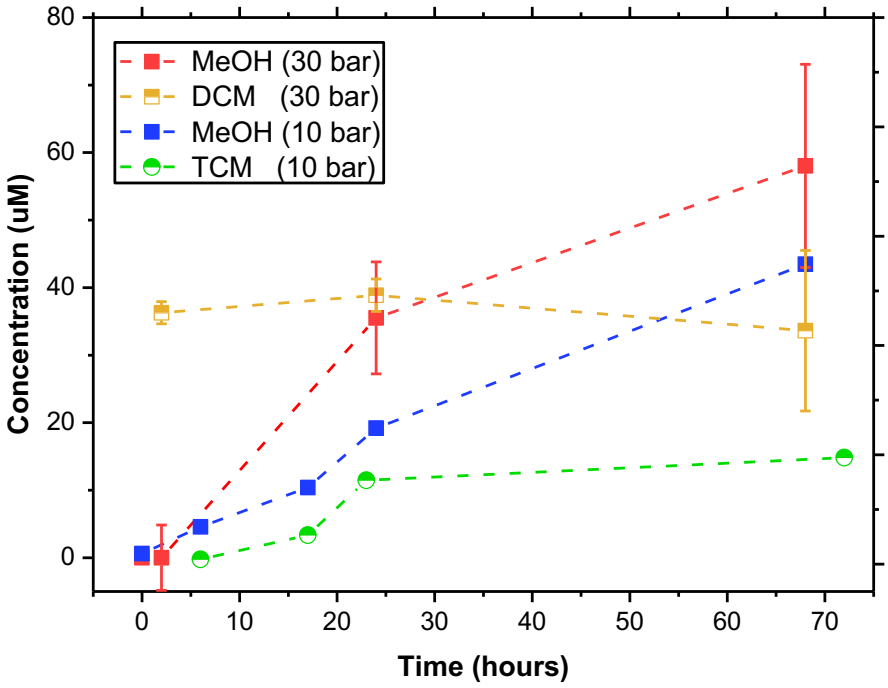


Figure S2.2 : Graph displaying GR's ([Fe] = 30 mM) production of MeOH and chlorocarbons (TCM, DCM) under two pressure conditions, 10 and 30 bar CH_4.

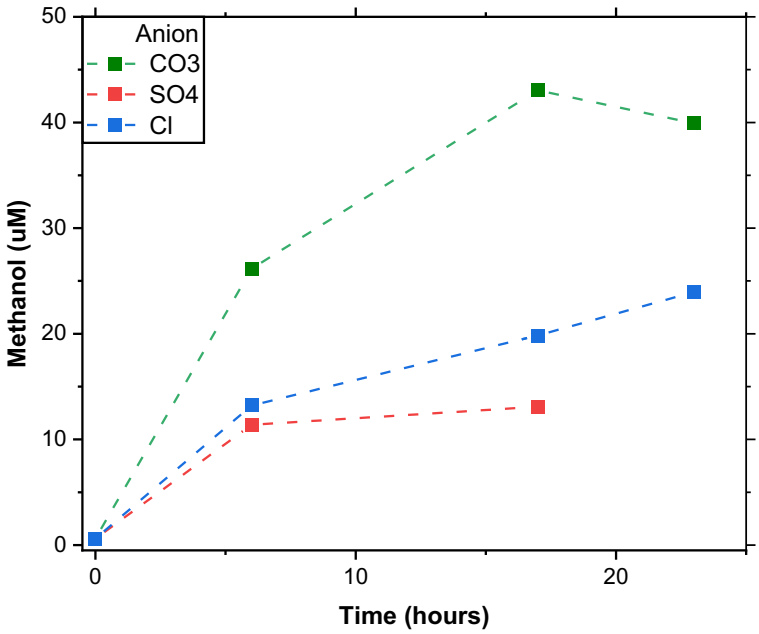


Figure S2.3: Graph displays difference in the production of MeOH with different GR ([Fe] = 30 mM) species.

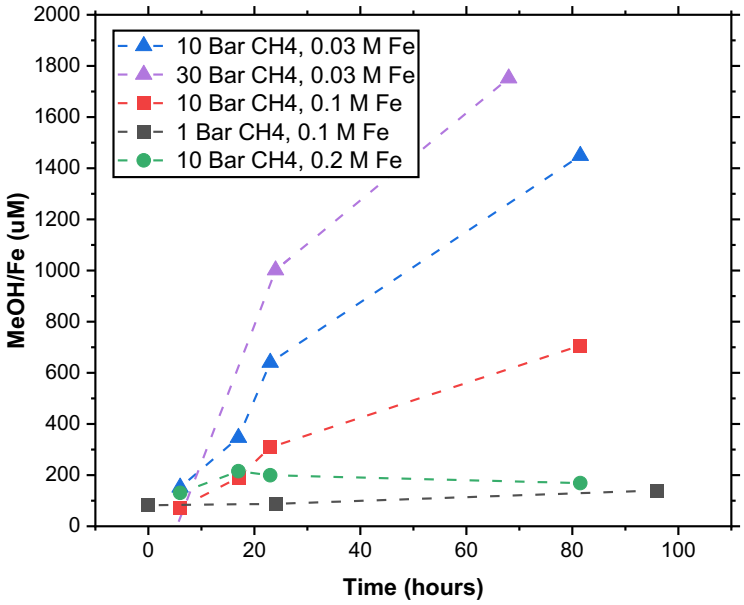


Figure S2.4: Graph displaying the relative efficiencies of MeOH production at a given concentration of Fe (MeOH/Fe).

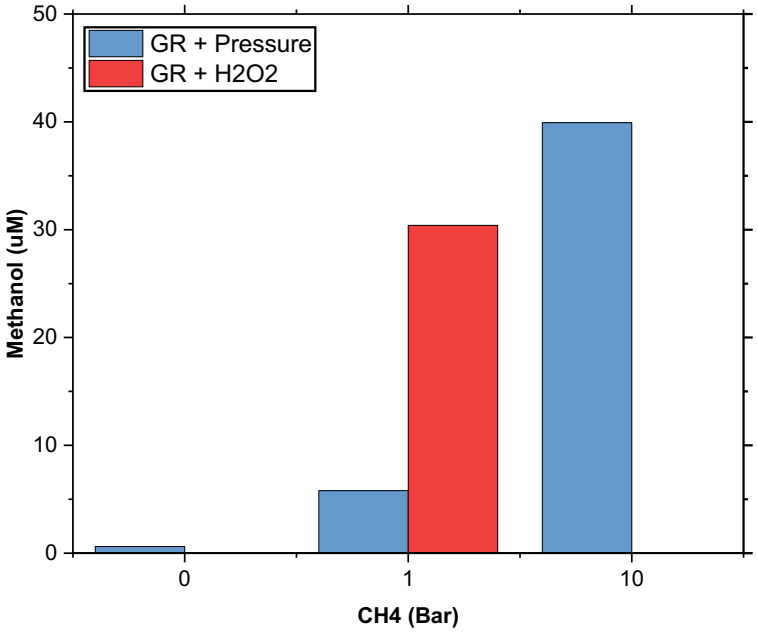


Figure S2.5: Graph displaying the influence of 1 mM H2O2 on the production of methanol by GR ([Fe] = 30 mM) compared to the pressure experiments.

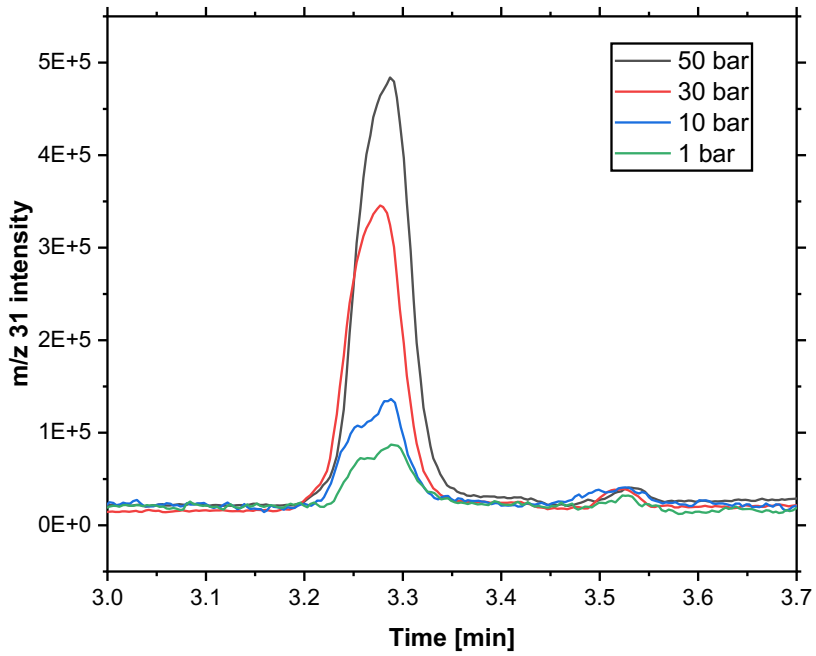


Figure S2.6 : Graph shows observed growth in GC-MS peak area at t = 3.28 min associated with m/z 31. MeOH concentration corresponds to 31 m/z peak area.

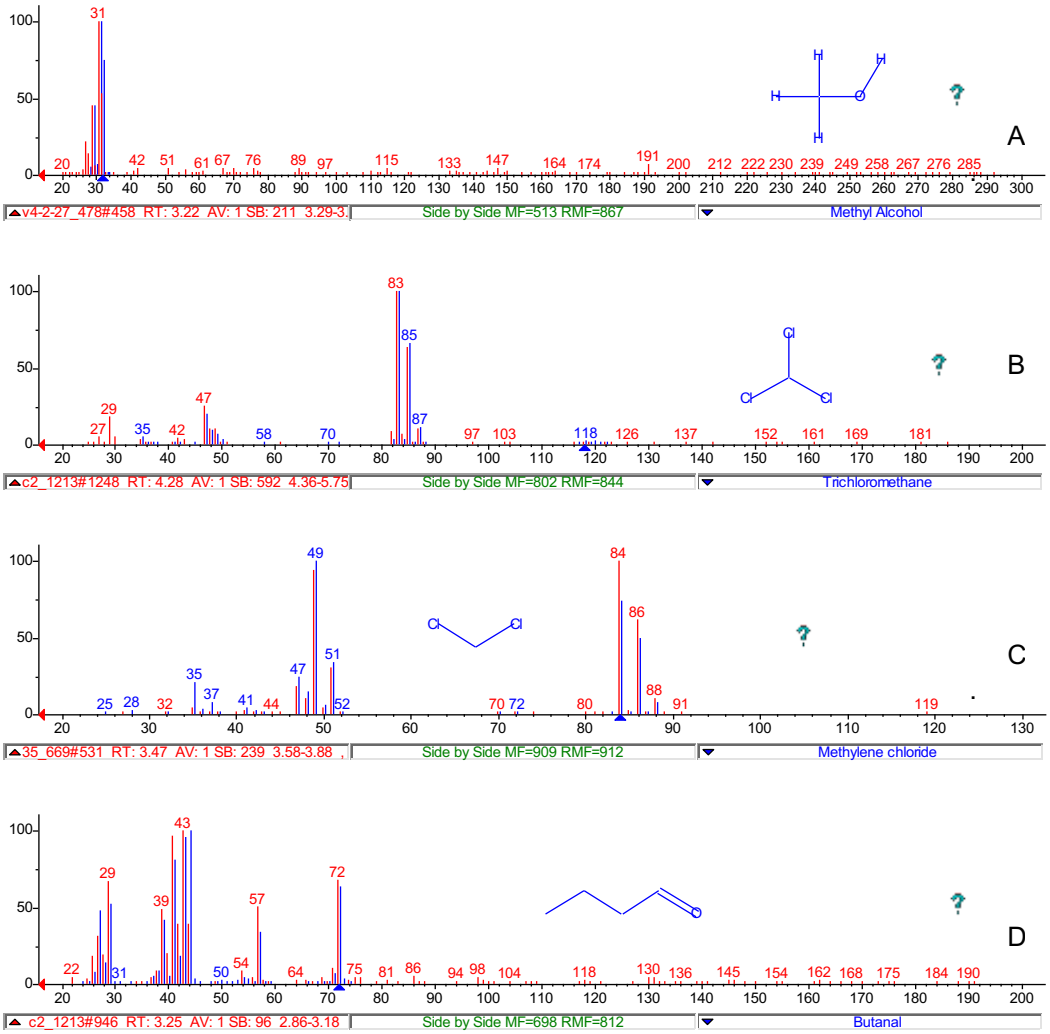


Figure S2.7 : Graph shows observed growth in GC-MS peak area at t = 3.28 min associated with m/z 31. MeOH concentration corresponds to 31 m/z peak area.

2.7. Experimental addenda not included in original manuscript

Certain experiments related to GR mediated methane oxidation were conducted yet not included in the final manuscripts due to time constraints, limited relevance, and lack of replicates. However, these experiments do provide interesting glance into the versatility of the GR system, and other methods for the analysis or the experimental procedure to conduct methane oxidation.

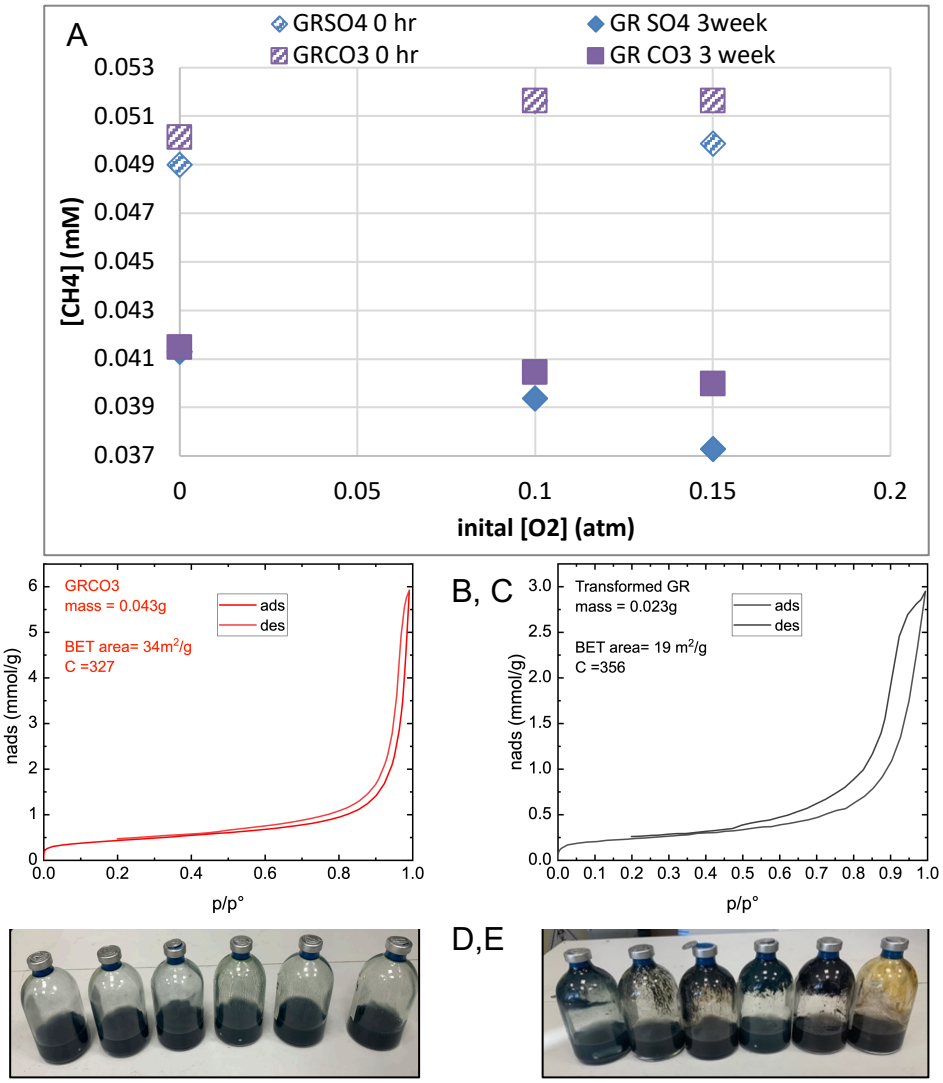


Figure SS2.1 : Graph A depicts recovered CH_4 concentrations from GR $GRSO_4$ and $GRCO_3$ suspensions incubated with ~1 bar CH_4 and 0, 0.1, 0.15 atmO_2. Graphs B and C show BET analysis using N2 adsorption on $GRCO_3$ and its transformation product Fe2O3. Images D and E are the before and after images of $GRSO_4$ and $GRCO_3$ (respectively).

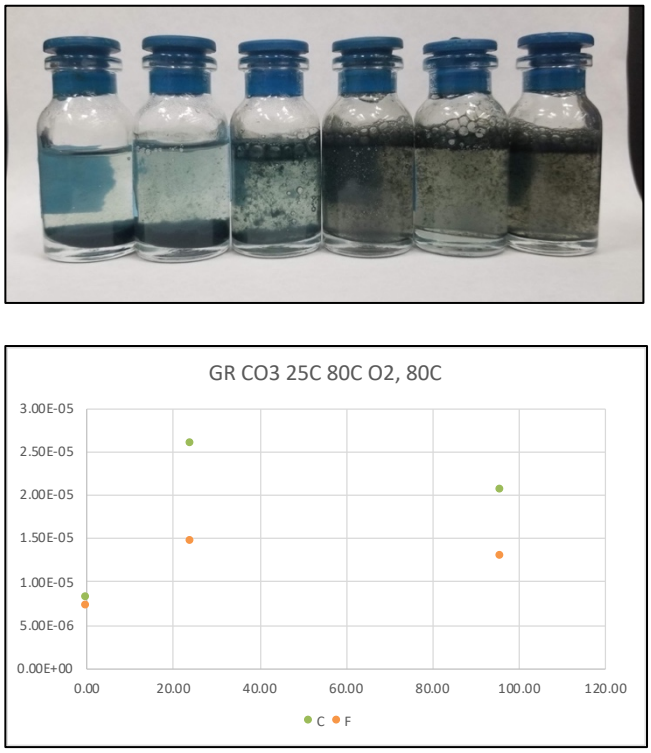


Figure SS2.2 : A image depicting morphological changes associated with the transformation of solutions of GR via heating at 80C, and a graph demonstrating the corresponding effect of heat over methane oxidation to methanol.

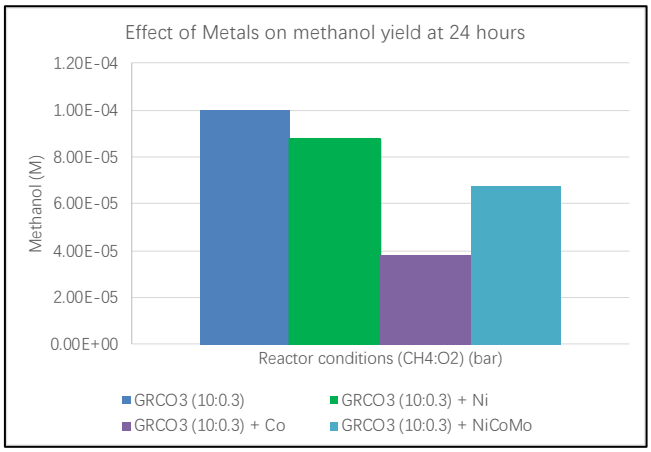


Figure SS2.3 : Amendment of GR solutions with transition metals modified methanol production.

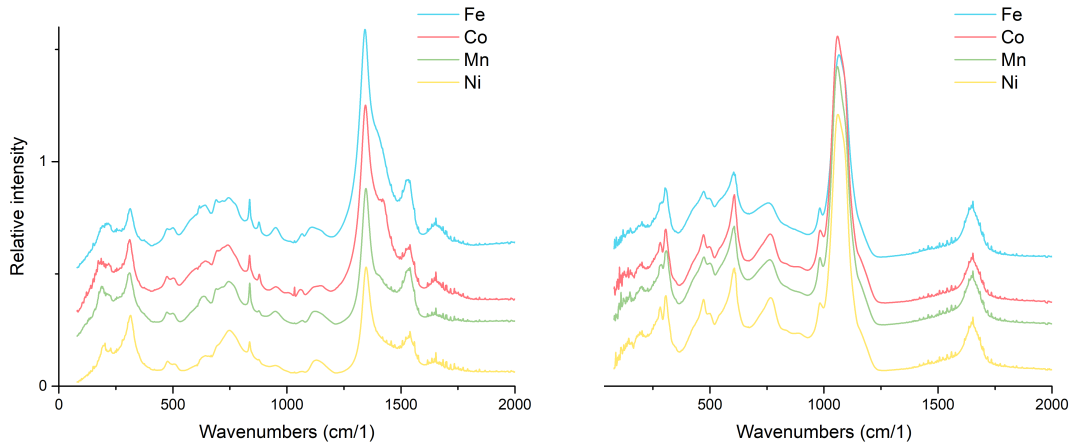


Figure SS2.4: The formation of 10% metal cation substituted $GRSO_4$ and $GRCO_3$ with Co, Mn, Ni. Little effect on FTIR is observed with a relatively small (10%) amount of Fe replaced with similarly sized transition metal species.

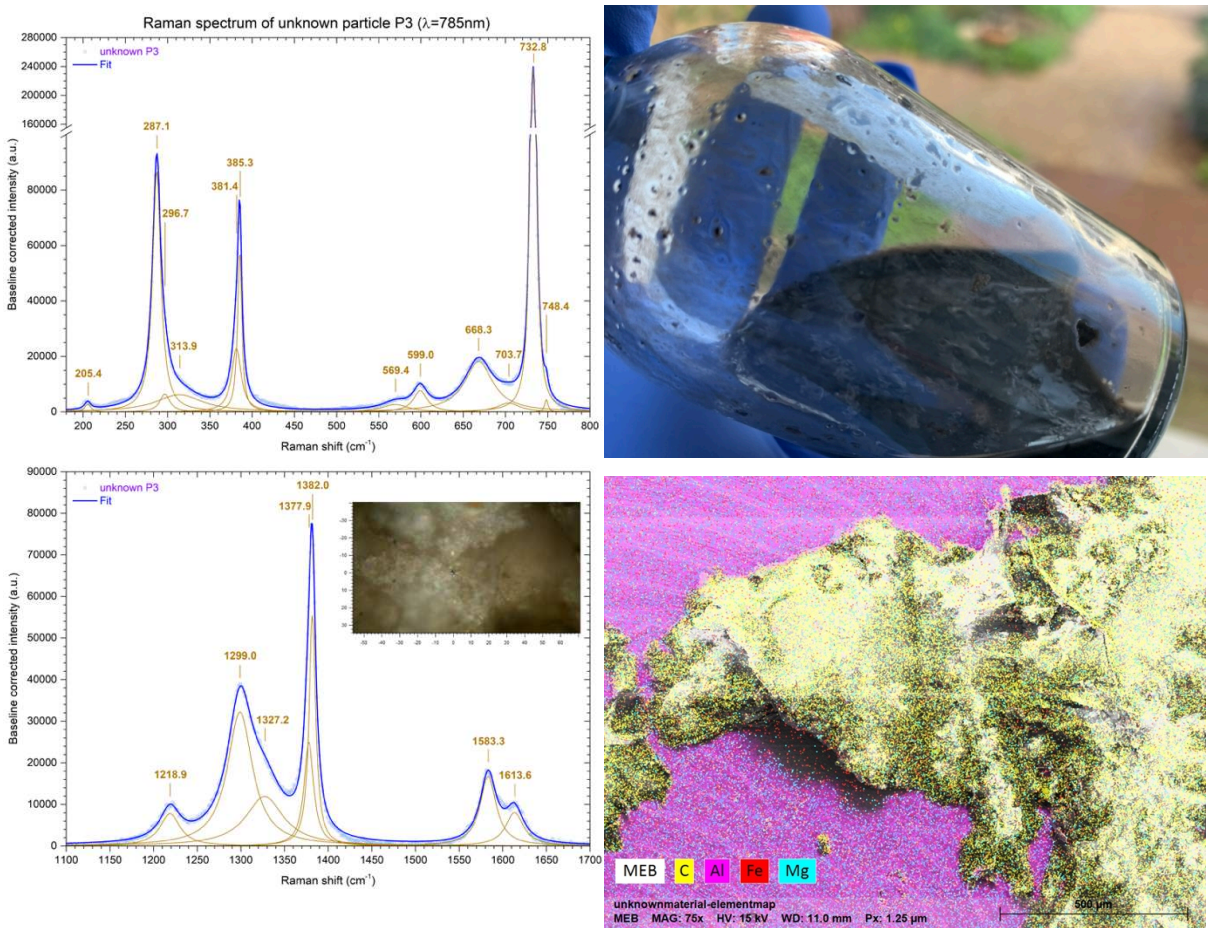


Figure SS2.5 : Raman spectra of unknown solid. Image of solids adhered to glass surface and floating on mineral suspension under SEM.

Discussion

Prior to the locating of a GCMS for high precision analyses of product formation of methane oxidation, enzymatic methanol kits (Sigma aldritch, MAK353) were used to determine the concentration of methanol in solution. To ascertain the drawdown of CH_4 via the oxidation of GR minerals 6 vials $GRSO_4$ and $GRCO_3$ suspensions were incubated with 0, 1, 1.5 bar of O_2 (Figure SS2.1). After 1 month samples exposed to .1 and .15 atm O_2 had significantly less CH_4 concentrations. This trend was explained as CH_4 being oxidized during the oxidation of the green rust minerals. However, given the high quantity of Fe in these solutions, interference possibly led to inaccurate results. Later GCMS analyses confirmed the presence of methanol, at similar concentrations.

Attempts to increase reactivity at low pressure included heat and metal amendment. Heating $GRCO_3$ and SO_4 samples in 20 ml vials inside of an 80C oven resulted in the transformation to magnetite. Temperature induced transformation of GR was studied as a mechanism for methane oxidation with and without oxygen (Figure SS2.2). Heating vials of GR to 80C over 100 hours yielded a significant increase in MeOH formation to 2.5uM. A set of experiments were conducted at elevated temperatures to determine the effect of temperature on the oxidation of methane at 1 bar CH_4 pressure. Methanol concentrations as measured by GCMS increased from baseline at 20 hours 2.5E-5 M, however decreased to 2E-5 by 100 hours. This experiment did not replicate well, with difficulties in obtaining consistent results. Heating and subsequent transformation of GR likely lead to the formation of compounds other than methanol.

Solutions of transition metal chlorides (Ni, Co, Mo) were added to GR prior to pressurization. The results suggest that metals decrease methanol formation, however this does not indicate the effect upon CH_4 oxidation itself. It is possible that the amendment of GR with various metals could have no or increased effect upon the oxidative ability of GR towards CH_4, however it does appear to modify the products formed during the reaction. Ni and Co are known to catalyze various reactions with primary alcohols under pressure and it is likely that the compounds formed were not detectable within the headspace, but instead the solution.

During extended contact between GR solutions and CH_4 headspaces a hydrophobic solid sometimes would appear on the surface of the solution. Collecting the solids and analyzing them under Raman and SEM revealed a carbon rich material with raman peaks at 287, 385, 599, 668, 732, 1218, 1299, 1382, 1583, and 1613 cm^{-1}. This spectra displays a mix of signals corresponding to known fe-oxides (e.g. magneitite), and indicates a pathway for redox mediated mineral precipitation that occurs over time in GR solutions in the presence of an electron donor like methane.

These data suggest surface area, gas composition, heat, and metals all likely influence the reaction pathway, supporting our hypotheses on the versatility of the GR mediated emergence of life scenario, yet dedicated experiments must be designed to truly discern how.

Chapter 3:

Probing $Fe^{2+}/^{3+}$ catalytic reactivity of Green Rust applying Electron Paramagnetic Resonance (EPR) spectroscopy.

The following experiments and findings described in this chapter were undertaken to assess the putative catalytic oxidation reactivity of Green Rust minerals driven by the array of mixed-valence μ-oxo Fe^{2+} Fe^{3+} dimers, which features a metalloprotein-like catalytic mechanism as in the case of methane monooxygenases (MMOs). The EPR experiments were supervised and chiefly conducted by Dr. Anabella Ivancich, CNRS Research Director (UMR 7281, CNRS, Marseille).

3.1. Introduction

Radicals are highly reactive chemical species bearing unpaired electrons which are predisposed to spontaneous oxidation reactions, playing pivotal roles in biochemical, environmental, and geochemical redox cycles. The oxidation of various minerals, specifically transition metal bearing oxyhydroxides is a source of radical generation via the so-called Fenton reaction (Winterbourn, 1995) and related radical chain mechanisms (Chen et al., 2022; Fang et al., 2021; R. Liu et al., 2023; Morin et al., 2023; Vijay et al., 2023). Of these minerals, Fe-oxyhydroxide green rusts, present a viable candidate for a geochemical origin to life, one mediated by proton and electron transfer (Duval et al., 2019; Nitschke et al., 2022; M. J. Russell, 2023).

$$Fe^{2+} + H_2O_2 \rightarrow Fe^{3+} + {}^{\bullet}OH + OH^-$$

(or $Fe^{2+} + H_2O_2 \rightarrow Fe^{4+} + 2\ OH^-$)

$$Fe^{3+} + H_2O_2 \rightarrow Fe^{2+} + HOO^{\bullet} + H^+$$

The oxidation of Fe^{2+} cations within green rust minerals by oxygen, and its resultant transformation to various Fe^{3+} dominated oxide, hydroxide, and oxyhydroxide products has been well described (Guilbaud et al., 2013; Legrand et al., 2004; Refait & Génin, 1994). The ratios of Fe^{2+} and Fe^{3+} in such minerals have been explored via XPS, Raman, XFAS, and Mossbauer spectroscopies (Usman et al., 2018), yet only recently has experimental evidence suggested the formation of short-lived Fe^{4+} sites during oxidation as the source of radical formation in GR and related Fe-minerals (Z. Li et al., 2022; Yu, Ji, et al., 2024). High energy photons can catalyze radical formation in GR systems (J. Wang et al., 2024). Further interactions between radicals and dissolved species, such as carbonate or sulfate can generate other radicals bearing unique properties (Vijay et al., 2023). *Ab initio* calculations investigated the structure and room-temperature hopping dynamics of hole polarons from iron site to iron site in green rust materials. The predicted "to side" hopping frequency was consistent with distinct Fe^{2+} and Fe^{3+} valences observed experimentally using Mössbauer spectroscopy at low temperature. Intersheet hopping was predicted to be slow in vacuum, but such process may become feasible if interlayer molecules and ions facilitate the intersheet electron transfer (Wander et al., 2007).

The prior chapter (2) dealt with the formation of methanol as a result of CH_4 oxidation via a proposed radical-mediated reaction pathway. Similar mechanisms for methane oxidation exist in man-made catalysts (Simons et al., 2021) as well as methanotrophic enzymes (Kopp & Lippard, 2002). The research work done during my Thesis showed that methane oxidation occurs in tandem with the oxidation of green rust to lepidocrocite and magnetite, mimicking radical-mediated methane oxidation featured by sMMO enzymes, to yield not only methanol but also halogenated hydrocarbons in the presence of seawater (Farr et al., 2023). Accordingly, we identified the previously proposed radical-generating Fenton reactions mediated by GR (Fang et al., 2021; Z. Li et al., 2022; Morin et al., 2023) as the preceding step to methane oxidation in this GR catalyzed system.

In this study, we applied 9-GHz EPR spectroscopy to characterize the $GRCO_3$ spectra before and after reaction with oxidants, as well as in the presence of a substrate, in order to investigate the putative formation of sMMO-like high-valent intermediates and the GR catalytic oxidation of a substrate by a Fe^{3+} Fe^{4+} intermediate, the later formed by the $2e^-$ oxidation with peroxyacetic acid in anaerobic conditions and in order to exclude the Fenton reactions in the presence of oxygen.

3.2. Material and Methods

Electron Paramagnetic Resonance (EPR) spectroscopy.

The 9-GHz EPR spectra of the green rust samples were recorded on a Bruker EleXsys E500 spectrometer, equipped with a standard rectangular Bruker (ST) cavity and a liquid helium cryostat (Oxford Instruments, ESR 900). Typically, the following instrumental parameters were used for recording EPR spectra: microwave frequency, 9.482 GHz; microwave power, 5 mW; modulation amplitude, 1 G; 4 scans; temperature, 10 K to 70 K. GR samples were measured in 4mm quartz EPR tubes.

Preparation of samples

Green rust samples with carbonate ($GRCO_3$) were synthesized anaerobically (see Methods in Chapter 2) five days before the EPR experiments. Resonance Raman experiments showed a 2:1 Fe^{2+}-Fe^{3+} content in the samples used for EPR experiments. Anaerobic EPR samples of green rust (estimated final concentration of 7.5 mM total iron content) were prepared by resuspending the synthetized green rust into 0.05 M TRIS-maleate buffer pH 7 (or pH 9) directly in 4-mm quartz EPR tubes and degassed. For reactivity experiments targeted to obtain the high valent intermediates, green rust was mixed anaerobically, at room temperature with chosen molar excess of peroxyacetic acid (PAA) or hydrogen peroxide as oxidants, in plastic vials and prior to the transfer into EPR tubes. The EPR tubes were than immediately frozen in a cold bath at -80 °C, prior to flash freezing them in liquid nitrogen. The stock solutions of PAA or H_2O_2 were each pre-prepared in degassed 0.05 M TRIS-maleate buffer pH 7, at desired concentrations

Further tests of the "enzyme-like" reactivity of the high valent intermediates putatively formed by mixing green rust with PAA (or H_2O_2) were performed by using 2,2'-azino-bis(3-ethylbenzothiazoline-6 sulfonic acid (ABTS) as substrate, and taking advantage of the relatively high stability of its $1e^-$ oxidized product, the ABTS cationic radical ($ABTS^{\bullet+}$), readily trapped and detected by its characteristic EPR signal. Different ratios of molar excess of oxidant and molar excess of ABTS substrate were tested.

XRD

Mineral transformation over the course of the reaction was monitored using X-ray diffraction (XRD), transmission electron microscopy (TEM), and scanning electron microscopy (SEM). Samples were centrifuged, decanted, and dried under a stream of N_2 gas. For XRD analysis glycerol was added prior to analysis to prevent oxidation and the paste was transferred into a glass ampule for XRD analysis in a Rigaku RU 200BH diffractometer with Cu anode (λ = 1.5418Å), scanning from 2 theta values of 2-80 degrees.

For TEM analysis, an aliquot of dried mineral was deposited on a copper grid coated with a holey carbon film (AGAR Scientific, S147-3). Grids were then transferred to a Jeol-JEM2010 electron microscope operated at 200 kV and GR particles were observed in bright field mode. For SEM analysis, an aliquot of dried mineral was deposited on an aluminum sample holder and then transferred to a Jeol JSM-7900F electron microscope and analyzed using accelerating voltages ranging from 5 to 15 kV.

Raman spectroscopy/ Mass spectrometry
The Raman analysis are carried out with a Renishaw Invia Reflex microspectrometer equipped with a Leica DM2500M microscope. The characterizations were carried out at 633 nm with ×25 magnification, an 1800-line grating and a CCD detector. The samples were enclosed in a X reactor chamber hooked up to N_2 flux.

3.3. Results and Discussion

Electron Paramagnetic Resonance (EPR) is a spectroscopic technique that is sensitive to the presence of unpaired electrons and, therefore, is a powerful tool for the study of metal containing systems. When a magnetic field is applied to a transition metal-containing system with unpaired electrons and the sample is irradiated with microwaves, a spin transition can be observed. The detailed analysis of the resulting EPR spectrum provides information about the electronic environment of the unpaired electrons found on the metal centers(Fielding et al., 2008).

The 9-GHz EPR spectrum of the as-synthetized green rust ($GRCO_3$) was recorded as a function of temperature in the range of 10 K to 70K (Figure 3.1A and 3.1B). Despite the recorded broad scan (6000 G), the entire spectrum could not be detected, as indicated by the EPR signal not going to the zero baseline (black dotted lines in Figure 3.1A and 3.1B) for the lower fields. The observed very broad spectrum centered at $g \cong 2$ (Figure 3.1A) was consistent with superparamagnetic species, for which the EPR signal shifts to the low magnetic fields with decreasing temperatures as previously reported (Petrakovskii et al., 1983). Interestingly such a shift was observed between 70 K and 30 K (Figure 3.1B), but the 10 K spectrum did not seem to follow the trend (Figure 3.1A). Most possibly, this difference is due to contribution of different EPR signals to the overall spectrum, arising from iron centers with various antiferromagnetic interactions being distance dependent. Such a case has been previously reported for iron-exchanged beta-zeolites (Zhilinskaya et al., 2003). Changes in temperature could alter the local environment surrounding the Fe ions, such as ligand or structural changes within the material, leading to broadening and shifting of the EPR signals. This reflects a more dynamic and less ordered chemical environment around the Fe ions. Species present in solution, including coordinated water molecules, hydroxide ions, and carbonate ions, can influence the magnetic resonance properties of the Fe ions.

It is of note that the previously reported 9-GHz EPR spectrum of the metal site in the MbnBC enzyme complex shows a rhombic EPR signal with g = (1.94, 1.88, 1.76), average g value $\cong$ 1.9 and overall width of *ca.* 1000 G that has been attributed to an

antiferromagnetically coupled dinuclear $Fe^{2+}Fe^{3+}$ center with an S = 1/2 ground state (Park et al., 2022) Accordingly, the significant broadening observed for the as-isolated $GRCO_3$ spectrum is totally consistent with the presence of several interacting dinuclear centers.

The contribution of a narrow signal with effective g value g_{eff} = 4.3 (Figure 3.1A, dotted ellipses) characteristic of "rhombic" S = 5/2 Fe^{3+}, that is an isolated species in aqueous environment most possibly arises from ions in solution that were not incorporated in the green rust layers. The relative intensity of such narrow EPR signal increased with sample concentration (data not shown).

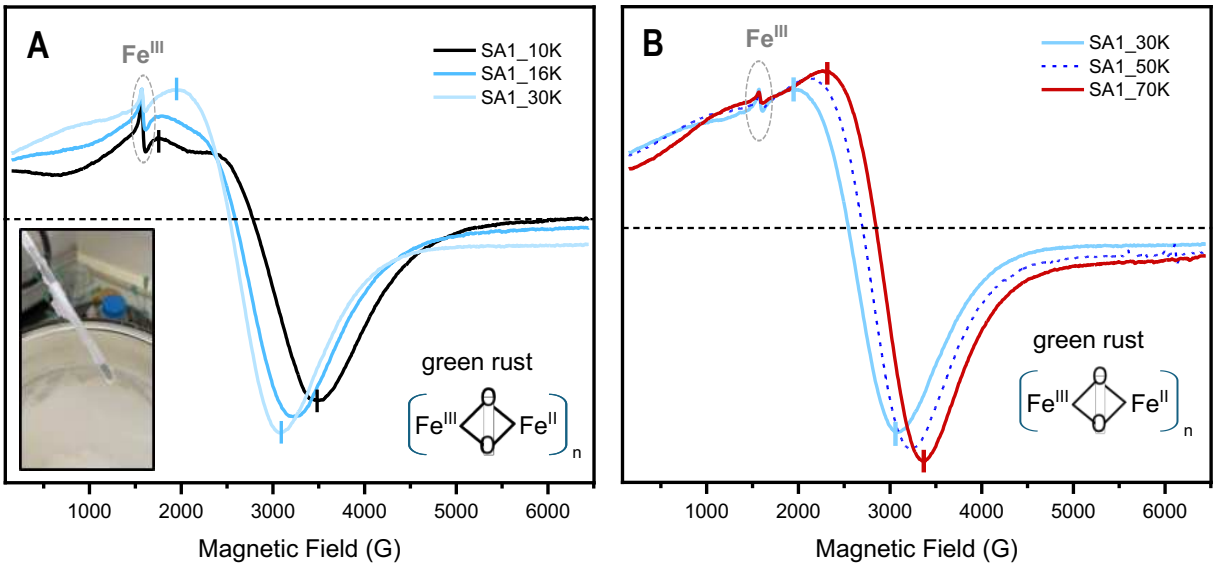


Figure 3.1: 9-GHz EPR spectrum of $GRCO_3$ (x=.33) recorded as a function of temperature. The very broad signal is consistent with superparamagnetic species arising from exchange interactions of the Fe^{2+} and Fe^{3+} ions. Experimental conditions for sample preparation and measurements are described in the Materials and Methods section. The inset shows a sample of $GRCO_3$ in the EPR tube being frozen in liquid nitrogen.

In order to test a putative catalytic reactivity of green rust in an enzyme-like fashion, that is cycling through high valent intermediates that could oxidize ABTS as substrate (Switala et al., 2024) we used peroxyacetic acid (PAA) as an alternative $2e^-$ oxidant to hydrogen peroxide and which has the advantage of not liberating molecular oxygen in the solution upon reaction, as is the case of hydrogen peroxide. We mixed anaerobically the green rust sample with the ABTS substrate (Figure 3.2A, black trace), then added PAA. It was found that the use of PAA during the oxidation of ABTS also oxidizes green rust fully, transforming it into a yellow Fe-oxide. The resulting broad EPR spectrum (Fig. 3.2A, light blue trace) showed clear differences, both in shape and intensity, to that of the as-synthetized $GRCO_3$ sample. If considering that the Fe^{2+} species are EPR silent, the increase in signal intensity indicated that the resulting oxidation state of the sample was $Fe^{3+}Fe^{3+}$. The new narrow EPR signal (peak-to-trough of 9 G) at g ≅ 2 in the EPR spectrum of the reacted sample (Figure 3.2A, light blue trace) is consistent with the oxidized product of

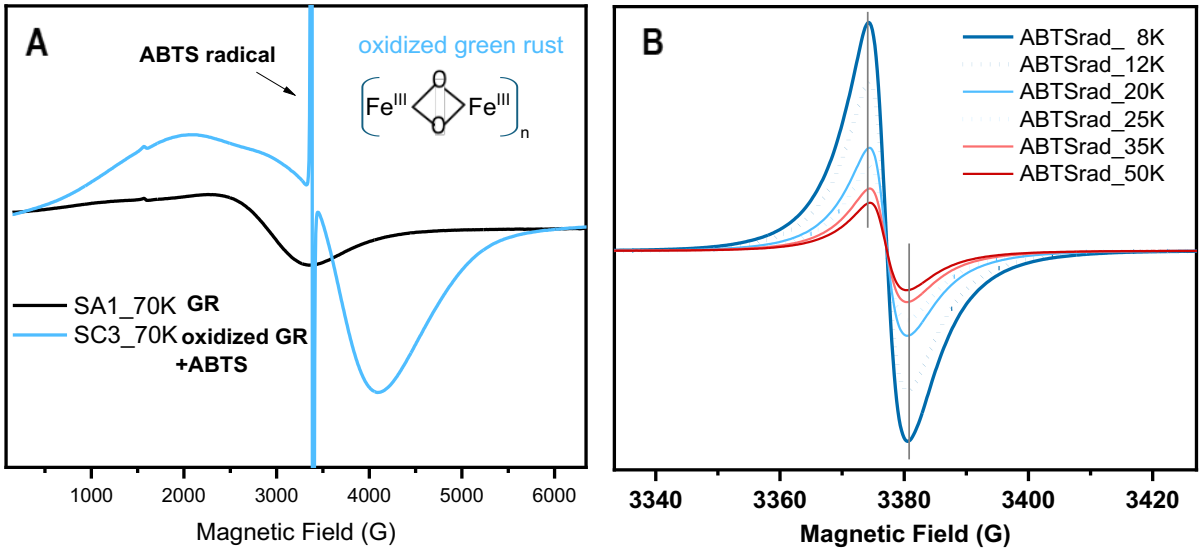


Figure 3.2: Panel A: 9 GHz EPR spectrum of $GRCO_3$ (x=.33) upon reaction with PAA as oxidant and ABTS as substrate. Panel B: Temperature dependent EPR spectrum of the ABTS radical product of the reaction.

the substrate, that is the ABTS radical formed as product of the catalytic oxidation reaction. The EPR spectrum of the ABTS radical, recorded in non-saturating conditions and as a function of temperature (Figure 3.2B), showed no broadening of the EPR signal at lower temperatures, thus indicating that the ABTS radical is not in interaction with the Fe ions.

A plausible catalytic cycle to rationalize the resulting EPR spectrum in Fig. 2A includes the formation of the $Fe^{3+}Fe^{4+}$ intermediate by the $2e^-$ oxidation of the as-synthetized $Fe^{2+}Fe^{3+}$ green rust (Figure 3.3). The high-valent $Fe^{3+}Fe^{4+}$ intermediate would readily oxidize the ABTS substrate ($1e^-$ oxidation reaction) thus resulting in the $Fe^{3+}Fe^{3+}$ species.

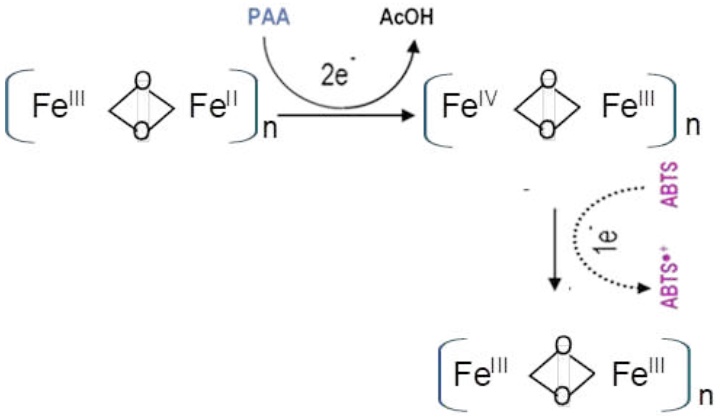


Figure 3.3 : Proposed reaction mechanism for the 2 electron oxidation of $Fe^{2+}(^{3+})$ green rust dimers to a metastable Fe^{4+} state which conducts electron transfer to ABTS back down to Fe^{3+}.

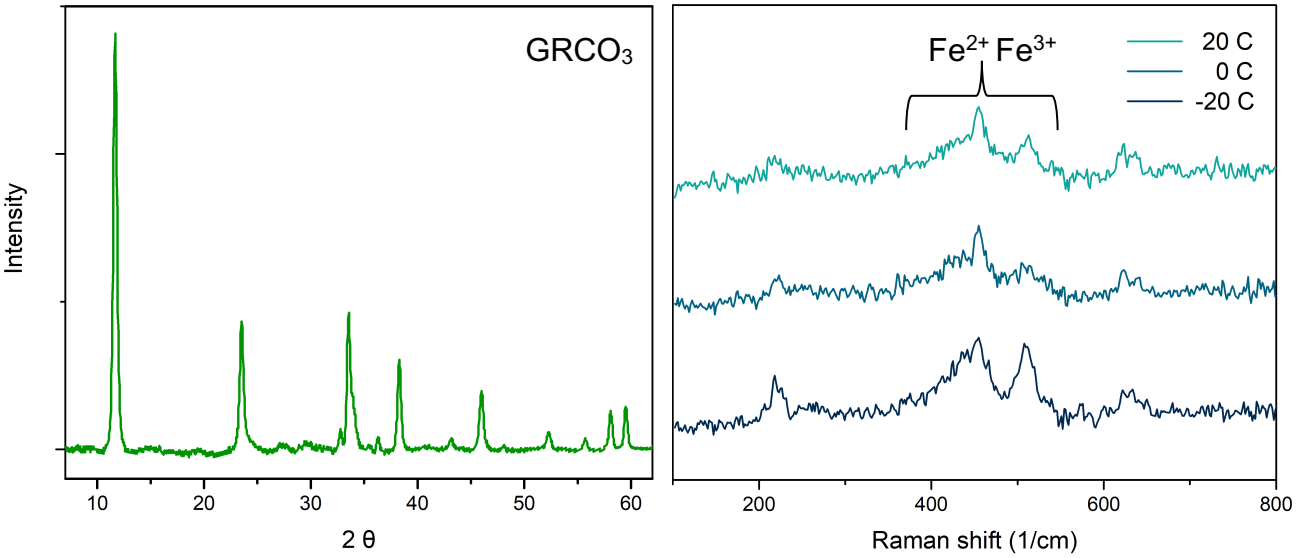


Figure 3.4: Spectroscopic characterization of $GRCO_3$ (x=0.33) system at 25°C with XRD (A) and at -20, 0, 20 °C with Raman(B)

The analyses were replicated using variations in GR1 mineral phases with varying carbonate and chloride concentrations. Similar EPR results/trends were observed for a "fougèrite" (GR Cl/CO_3 mixed phase, Chapter 2) type synthesis, that was performed in order to assess whether the interlayer arrangement has an effect on the paramagnetic interactions of the proposed $Fe^{2+}Fe^{3+}$ dimers at longer distances and possibly on the reactivity. In both CO_3^{2-} and Cl^- concentrated test cases ABTS was oxidized in the presence of PAA and green rust. Yet, the broadening of the ABTS radical indicated that the substrate is located in closer position to the iron centers and consistent with the differences in the layers packing induced by the NaCl. Preliminary EPR experiments using H_2O_2 as oxidant, and which results in the release of O_2 in the sample solution indicated that such dissolved O_2 has an effect on the oxidation state of the iron centers, and this is well supported with our findings on using H_2O_2 as an oxidant for CH_4 oxidation in Chapter 2. A more detailed study on the reactions is ongoing in our lab.

Figure 3.4 depicts the Raman and XRD spectra of a selected sample of $GRCO_3$ synthesized for the EPR experiments. XRD analyses confirmed the quality of mineral produced, and the Raman experiments depicted a mild temperature dependence between room temperature and frozen samples dependence given the variation in peak area of the peak associated with Fe^{2+} (450 cm^{-1}) and Fe^{3+} (510 cm^{-1}). It was found that minor variations in sample synthesis, such as the concentration of carbonate in solution, the quality of Fe powder, humidity, and temperature at time of synthesis (8 to 30°C) resulted in the broadening of the EPR signals, leading to initial difficulty in signal replication. The broadening of the $Fe^{2+/3+}$ interactions may indicate far more Fe-Fe interactions are taking place as compared to the relatively small contributions between Fe atoms under ideal conditions. We hypothesize that these differences could be due to changes in the $Fe^{2+/3+}$ ratio and thus differences in the paramagnetic interactions of the iron centers as well as

structural changes to the GR crystals which would impact the behavior of Fe-O-Fe and Fe-Fe bonding. Other points of failure may be due to the chaotic metastable nature of GR which is constantly undergoing dissolution-reprecipitation in solution. It was found that briefly sonicating mineral suspensions prior to freezing aided signal replication, indicating that mineral flocculation or intergrowth may impact signal quality. Such effects are not easily detected by XRD characterization, but changes to oxidation state are detectable via Raman and colorimetric Fe^{2+} determination.

3.4. Conclusion

For the first time $GRCO_3$ Fe^{2+}/Fe^{3+} magnetic interactions have been characterized via EPR, demonstrating strong association between Fe within crystalline GR. The 2-electron oxidation of GR by peroxyacetic acid and the resulting oxidation of ABTS demonstrate the production of a high valent Fe^{4+} site. These findings correspond well to recent attempts at characterizing similar Fe-mineral systems and implicate the formation of ephemeral high valent states in the observed redox reactivity of these mineral systems towards organic compounds. However, variability in signal broadness indicate unknown factors controlling Fe-Fe bond interactions. Further exploration of Fe-Fe magnetic interactions is required to fully elucidate this dynamic system. We propose that this electron transfer mechanism is responsible for the methane oxidation activity observed in our previous experiments with green rust mediated redox chemistry.

Chapter 4:

Further $Fe^{2+/3+}$ oxyhydroxide green rust redox reactions towards CO_2 and CH_4 analyzed by spectroscopy and mass spectrometry

This section details further investigations into the surface chemistry and organic production during CO_2 and CH_4 mediated redox reactions using XPS, Raman, and FTIR spectroscopies. We describe the formation of various organic products from CO_2 and CH_4 oxidation under spontaneous and UV-irradiated conditions and propose mechanisms which have strong implications over conditions in the past and present environment as well as the emergence of life.

4.1. Introduction

Mineral interactions with oxidized (e.g. CO_2) or reduced (e.g. CH_4) carbon species play significant roles in the geochemical cycling of carbon in terrestrial and marine environments as well as the exploitation of carbon species for chemical synthesis, energy production and storage by research and industry. These physical and chemical interactions (e.g. adsorption, redox, hydrolysis) occur at the interface between mineral surfaces and solid or gaseous carbon, where surface chemistry governs the fate and mobility of carbon (Hazen & Sverjensky, 2010b). Surface chemistry relates the interactions between surficial lattice atoms, their bonds between one another, and the types of bonds formed with the external environment and the carbon species present. For a mineral oxide or hydroxide, metals such as iron (Fe) are covalently bonded to oxygen (O) or hydroxide (OH) species, (e.g. Fe-O-Fe or Fe-OH-Fe) conformation (Smith, 1999). Surficial Fe-OH "hydroxyl" groups serve as hydrogen bonding sites for carbon species which can form various carbon functional groups (e.g. methyl (-C), carbonyl (C=O), carboxyl (-COOH)). The likelihood of binding or transferring electrons to CO_2 and CH_4 on material surfaces are dictated by thermodynamic properties of both the adsorbent and the adsorber (Du et al., 2020; Santos-Carballal et al., 2018). CH_4 is infamous for being difficult to efficiently oxidize to methanol (MeOH)(Dummer et al., 2023). Properties inherent to certain materials (e.g. mechanistically confining reaction site, small band gap) can decrease the required activation energy through physical and chemical interactions which decrease the entropic cost. Furthermore, environmental conditions such as increased heat and pressure can further decrease the necessary energies required for activation. Probing crystal and surface chemistry through spectroscopic analytical techniques can provide detailed information regarding the electronic states of carbon and the mineral surface before, during, and after interaction with material surfaces.

Our previous work (Farr, Gaudu, et al., 2023) uncovering the nature of the interactions between CH_4 and Fe-oxyhydroxide green rust (GR) minerals implied further carbon redox chemistry mediated by GR, and that CO_2 reduction could occur simultaneously with CH_4 oxidation. This was recently demonstrated (S. Lee et al., 2023) to occur spontaneously in alkaline solutions and within electrochemical systems. Several naturally occurring minerals have also been found to catalyze CO_2 reduction (Beyazay et al., 2023; Grosch et al., 2022; Hudson et al., 2020; Varma et al., 2018; A. Yamaguchi et al., 2014), however due to the particularly interesting properties of GR minerals which make it suitable candidate for emergence/origin of life hypotheses (e.g. layered interchangeable cations/anions, electron transfer, proton transport) we propose that carbon redox mediated by GR could have been the direct progenitor to metabolism (Duval et al., 2019; Farr, Gaudu, et al., 2023; Nitschke et al., 2024).

In this section, CO_2 and CH_4 redox reactions were further explored using spectroscopic and spectrometric analyses. Several implications of GR mediated carbon redox are explored, including the production of climatologically relevant organosulfur compounds (DMSO and DMS).

4.2. Methods

Synthesis

Both $GRCO_3$ and $GRSO_4$ their transformation products were synthesized following procedures outlined in Farr, 2023 and Lee, 2023. A concentrated stock solution of water (80 ml) containing 150 mM $FeSO_4 \cdot 7H_2O$, 50 mM $Fe2(SO4)_3$ was prepared using deoxygenated ultra-purified water (milli-Q) and purged with N_2 gas for 30 minutes in a sealed 125 mL reactor vial. A solution (20 ml) of 300 mM NaOH was then injected into the reactor via a N_2-purged needle syringe and the mixture was gently shaken. A dark green precipitate formed, and was confirmed to be $GRSO_4$ via powder X-ray diffraction. For $GRCO_3$ synthesis, 100 mM Na_2CO_3 was introduced to replace the SO_4 ion over 24 hours. Afterwards, samples were centrifuged, decanted, and washed. Samples were confirmed to be $GRCO_3$ which was stable for ~1-2 weeks before transformation to Fe_3O_4. The total Fe concentration in this stock solution was 200 mM and final pH was ~10.For the headspace replacements, N_2, CO_2, CH_4, and NO, gas was flushed through the headspace for 10 minutes before beginning gas experiments.

XRD

Mineral transformation over the course of the reaction was monitored using X-ray diffraction (XRD), transmission electron microscopy (TEM), and scanning electron microscopy (SEM). Samples were centrifuged, decanted, and dried under a stream of N_2 gas. For XRD analysis glycerol was added prior to analysis to prevent oxidation and the paste was transferred into a glass ampule for XRD analysis in a Rigaku RU 200BH diffractometer with Cu anode (λ = 1.5418Å), scanning from 2 theta values of 2-80 degrees. For TEM analysis, an aliquot of dried mineral was deposited on a copper grid coated with a holey carbon film (AGAR Scientific, S147-3). Grids were then transferred to a Jeol-JEM2010 electron microscope operated at 200 kV and GR particles were observed in bright field mode. For SEM analysis, an aliquot of dried mineral was deposited on an aluminum sample holder and then transferred to a Jeol JSM-7900F electron microscope and analyzed using accelerating voltages ranging from 5 to 15 kV.

XPS

XPS experiments are carriedouton a custom platform at CINaM using two X-ray sources (the Kα line from aluminum at 1486.6 eV and the Kα line from magnesium at 1253.6 eV). XPS spectra are obtained with a Resolve 120 hemispheric analyzer operating with a pass energy of 100 eV for survey spectra. The Fe2p line is detailed to determine the valence states of iron (pass of 50 eV) and chemical speciation of oxygen and carbon from O1s &C1s lines (pass of 20 eV). All analyses were carried out using the photoemission spectra obtained with the Al Kα source, except for the O1s line that requires the Mg Kα source to avoid the overlapping of Na Auger lines. Samples obtained at a depth of 1 nm. Due to surface carbon contamination the surface was cleaned with an ion beam prior to gas exposure. This carbon line is fixed at 284.6 eV and used to calibrated the binding energies.

Raman/ Mass spectrometry

The Raman analysis are carried out with a Renishaw Invia Reflex microspectrometer equipped with a Leica DM2500M microscope. The characterizations were carried out at 633 nm with ×25 magnification, an 1800-line grating and a CCD detector. The samples were enclosed in a X reactor chamber hooked up to N_2 flux. A HAL RC 201 HIDEN mass spectrometer was attached to the raman system via a custom made vacuum pump system.

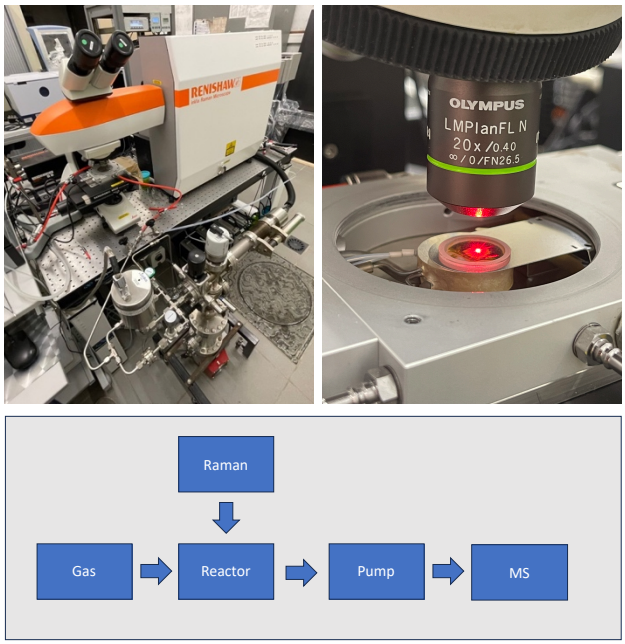


Figure 4.1 : Custom built MS experimental set up attached to high pressure reaction cell integrated into Raman microscope

Fourier transform infrared (FTIR) spectroscopy

Samples were analyzed under N_2 flushing at a resolution of 4 cm^{-1} in the wavenumber range of 900 to 3800 cm^{-1}. Measurements were achieved by using a MIRacle (PIKE Technologies) attenuated total reflectance (ATR) accessory mounted in a Vertex 70 spectrometer (Bruker) equipped with a DLaTGS detector.

GCMS

GC gas chromatography coupled to an ISQ mass spectrometer (ThermoFisher Scientific). The sampling was performed by headspace (HS) using an RSH auto-sampler (ThermoFisher Scientific). 5 mL samples was deposited in 20 mL HS vials with screwtop PTFE septas. Each vial was then incubated during 5 min at 80°C under agitation. The HS sampling was performed by collecting 2 mL of the gas phase. It was then injected into the GC via an injector at 250°C, a split at 10 mL/min and a column flow of 1.1 mL/min. The column was a Stabilwax-DA from Restek (length 30 m, diameter 0.25 mm, film thickness 0.5µm). Analyses were performed with the temperature gradient that starts with a 1 min isotherm at 35°C and proceeds with a gradient at 25°C/min up to 220°C ending with a 2 min isotherm. The detection was performed with the MS in full scan mode using an electron impact ionization at 70eV. MS transfer line and ion source temperatures were set at 250°C. For the full scan analyses, the m/z range was 10-300 au.

NMR spectroscopy

Samples were titrated with 1 M NaOH to precipitate out transition metal species, centrifuged, and filtered using 0.2 µm PTFE syringe filters. Prior to analyses, 10 µl of D_2O was added to 50 µl samples. All NMR experiments were performed at 298 K on a Bruker Avance III 600 MHz spectrometer equipped with a cryogenically cooled (1H) 5 mm probe. The data were processed using Bruker Topspin.

4.3. Results

4.3.1. Effect of gasses (N2, CO_2, CH_4, CH_4+NO) on GR organic production under dark and UV-irradiated conditions

Several experiments were conducted to investigate the capability of GR towards CO_2 reduction. It is known that exposure to oxidants such as O_2, CO_2, NO, and UV photons have a destabilizing effect upon the multivalent charge balance within GR lattices, resulting in its eventual transformation into Fe^{3+} rich oxyhydroxides (Dodd et al., 2022; W. Liu, 2021; C. Wang & Chakrapani, 2023b). However, investigations into whether these reactions result in the formation of organics have not been investigated. Here, we demonstrate simple experiments where stirred GR solutions were put into contact with various gasses under dark and UV irradiated conditions and had their aqueous phases analyzed by NMR and gas phases by GC-MS.

Dark gas reactions:

In the control samples (Figure 4.2A), no noticeable visual changes to the initial viridian green mineral solution occurred following 24 hours of incubation with the different gas species. However, the 1H NMR spectra show distinct differences depending on the gas environment. The N_2 (blue) serves as the baseline with peaks primarily around 0.9 ppm, 1.2-1.5 ppm, and 3-4 ppm indicating existing organic compounds within $GRSO_4$ solutions, residual solvents, or impurities without significant evolution within the mineral suspension. It should be noted that the control system evolved slightly over 48 hours, leading to intensification of the peaks present, and the appearance of a few new peaks (Figure 4.3A). The CO_2 (red) sample exhibits similar peaks in the aliphatic region but additionally presents minor peaks around 7 ppm, suggesting the initial formation of aromatic compounds. The CH_4 (brown) sample shows similar peaks to the control, indicating little reactivity under pure CH_4. The most complex spectrum is seen in the CH_4 + NO (green) sample, with significant peaks around 7 ppm, indicating the formation of nitro compounds or aromatic products due to interactions between methane and nitric oxide, while GCMS confirmed butanol as a significant product.

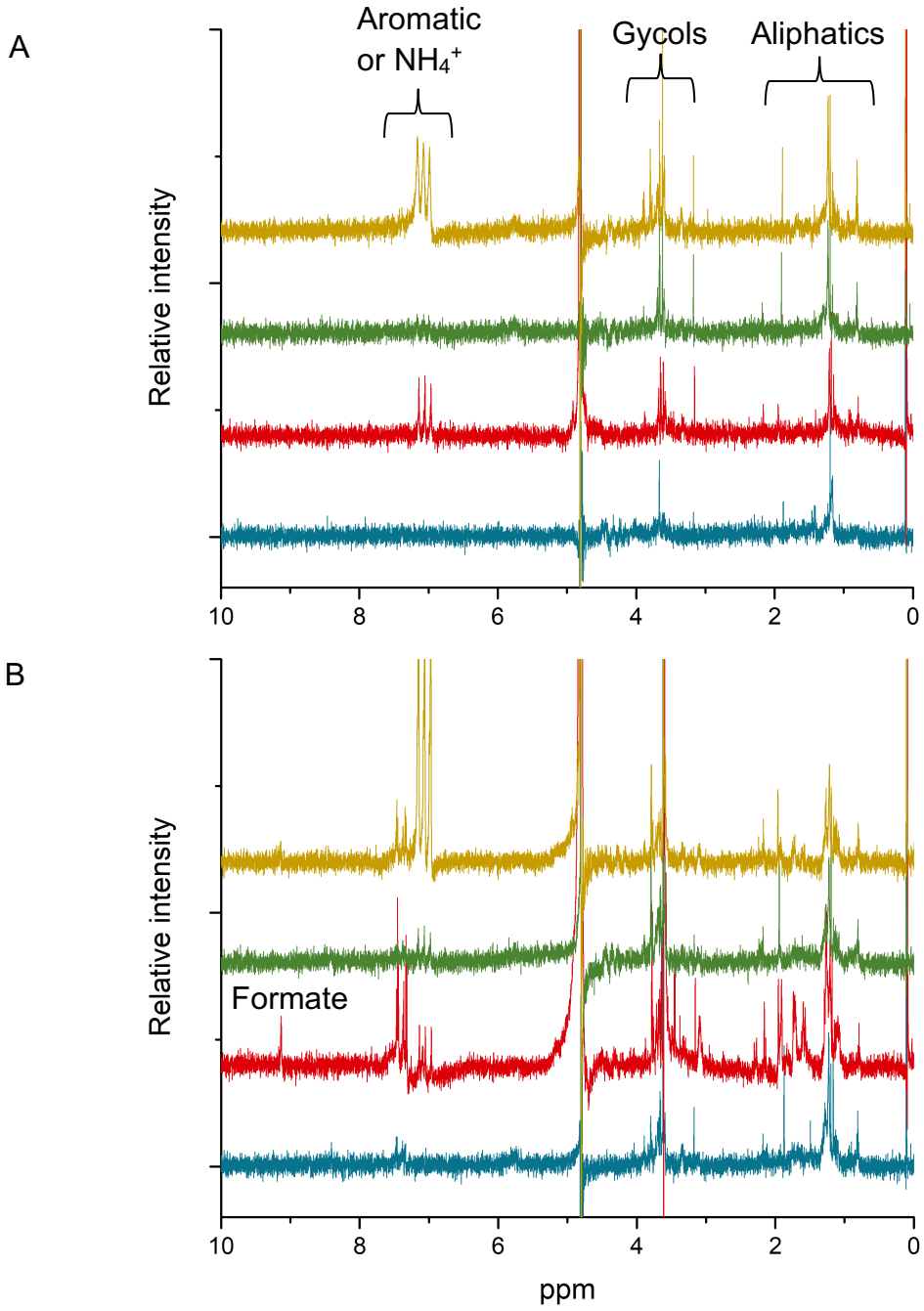


Figure 4.2: Exposure of $GRSO_4$ to N2, CO_2, CH_4, CH_4+NO atmospheres before (A) and after (B) UV irradiation. The two figures show NMR spectra of solutions of 0.2M $GRSO_4$ at pH 10 with different head space compositions under dark UV irradiation conditions for 48 hours. Blue = N2, Red = CO_2, Green = CH_4 , Yellow = CH_4 + NO. Changes to the spectra indicate formation of organic compounds.

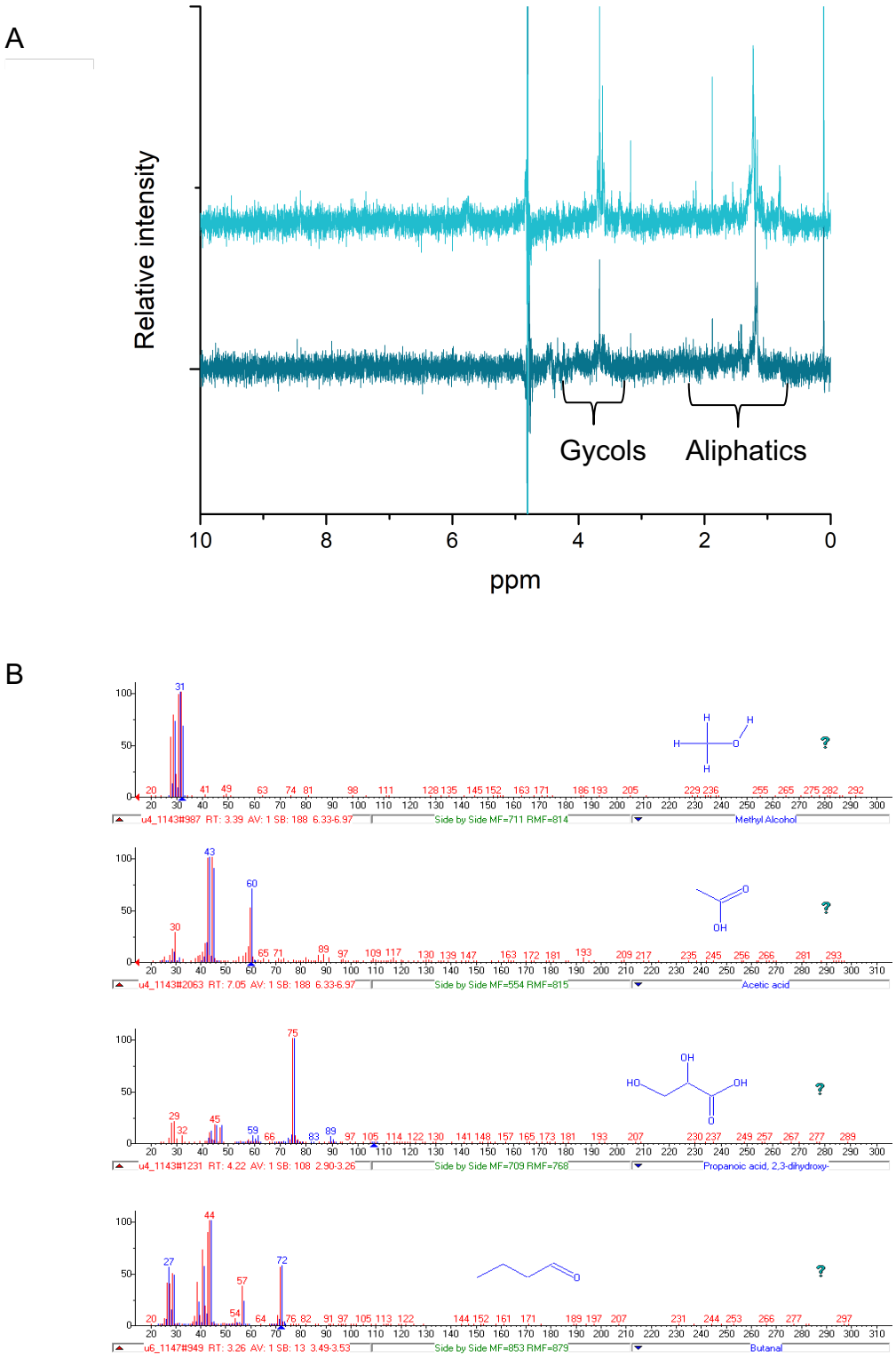


Figure 4.3: Figure (A) demonstrates evolution of N2 control over 48 hours. Figure (B) are m/z obtained via headspace GCMS analysis. Methanol, proponic acid, and acetic acid were common products between experiments while butanal were associated with exposure to NO.

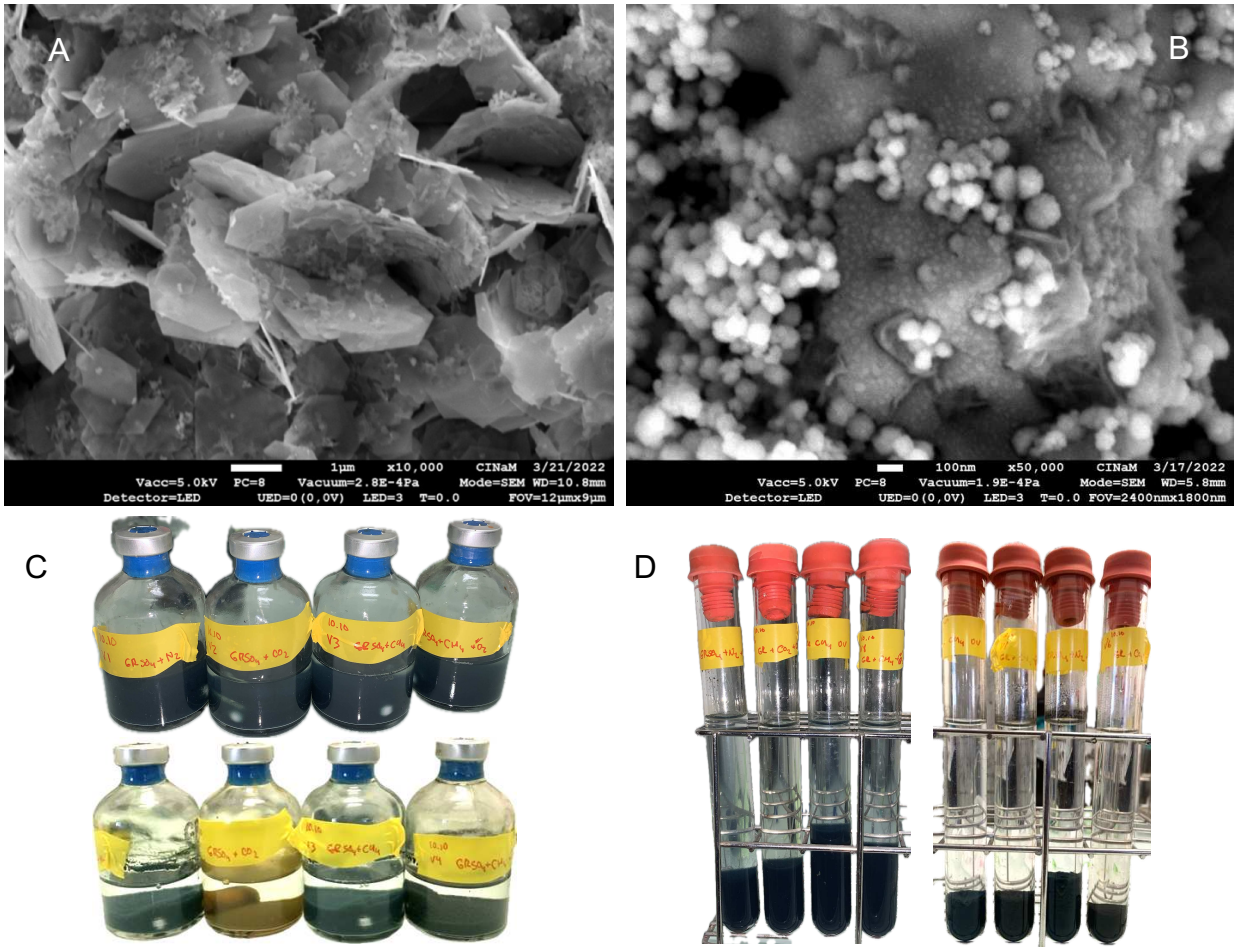


Figure 4.4 : A & B are SEM images of $GRSO_4$ crystals following exposure to 6 and 48 hours of UV irradiation. Minerals are studded with oxides. C & D are pictures of GR solutions with N_2, CO_2, CH_4, CH_4+ NO after 48 hours of incubation in dark and UV irradiation conditons. The control (N_2) was green and the addition of CO_2 and CH_4 +NO resulted in visible mineral transformation given color change. In all tests the UV experiments led to visible transformation to black Fe-oxide minerals.

UV-Irradiated gas reactions:

After 48 hours of UV irradiation (Figure 4.2B), distinct visual changes occurred to all mineral suspensions, indicating transformation of GR minerals to either mixtures or pure Fe^{3+}-oxide phases (Figure 4.4). Sample 1 (N_2) and 3 (CH_4) were partially transformed into a dark green/black phase, likely a mix of $Fe^{2+/3+}$ minerals. Samples 2 (CO_2) and 4 (CH_4 + NO) were more fully transformed to magnetite given the volume reduction and magnetic character of the black precipitate formed (Figure 4.4D). The dissolution of CO_2 and NO into the GR solutions likely resulted in lower solution pH during irradiation which led to magnetite formation, while N_2 and CH_4 did not experience as great of a decrease in pH, thus leading to the mixed oxyhydroxide phases.

All 1H NMR spectra show pronounced changes, particularly in the CO_2, CH_4, CH_4+NO samples. The N_2 (blue) shows the appearance of faint peaks in the aromatic region as well

as an intense peak at ~3.6ppm suggesting alcohol, dioxane, or ether formation, which is present in all irradiated samples. This was reflected in GCMS analysis as low-level methanol peaks were present in all irradiated samples (Figure 4.3B). The CO_2 (red) shows increased complexity around 2-4 ppm and enhanced peaks near 7 ppm, indicating further formation of various reduced carbon species such as alcohols, polyols, and aromatics driven by UV-induced CO_2 reduction. The CH_4 (brown) exhibits small but similar new peaks around 7 ppm, consistent with the formation of aromatic oxidized methane products. The CH_4 + NO (green spectrum) undergoes significant changes, with increased peak intensity and number across both aliphatic (0.5-3 ppm) and aromatic regions (6-8 ppm), suggesting that complex photochemical reactions led to various oxidation and nitration products. GCMS again detected butanol as a product of NO CH_4 interaction, but did not observe nitrated species (Figure 4.3B). The 3 peaks at ~7 ppm could also correspond to aqueous ammonium ion resonance which could result from the reduction of formed NO_3 or N_2 which was previously found to occur in photochemical Fe-oxide systems (Brandes et al., 1998; Schrauzer & Guth, 1976; Zang et al., 2022).

Conclusion:

Our experimental results indicate that various carbon redox compounds form in pH 10 $GRSO_4$ suspensions when exposed to N2, CO_2, CH_4, and NO gases as well as UV light irradiation. The primary processes include CO_2 reduction and CH_4 oxidation leading to simple alcohol, aldehyde formation which interact and can lead to the formation of larger more complex compounds. The presence of NO alongside CH_4 activates CH_4 oxidation, especially under UV irradiation, leading to the formation of nitrogen bearing compounds and aromatic products. UV irradiation significantly enhances these reactions, promoting the formation of various carbon redox species and altering the mineral chemistry.

4.3.2. Investigating reduction of CO_2 in alkaline solutions of K2CO3

Anion chemistry has been cited as a factor controlling CO_2 reduction (S. Lee et al., 2023; Yoo et al., 2023). The prior experiment observed organic compound formation in pH 10 solutions of $GRSO_4$ titrated with NaOH. The following experiments demonstrated modified organic production by replacing the titrant with K_2CO_3. The effect of temperature change and metal amendment over CO_2 reduction was explored.

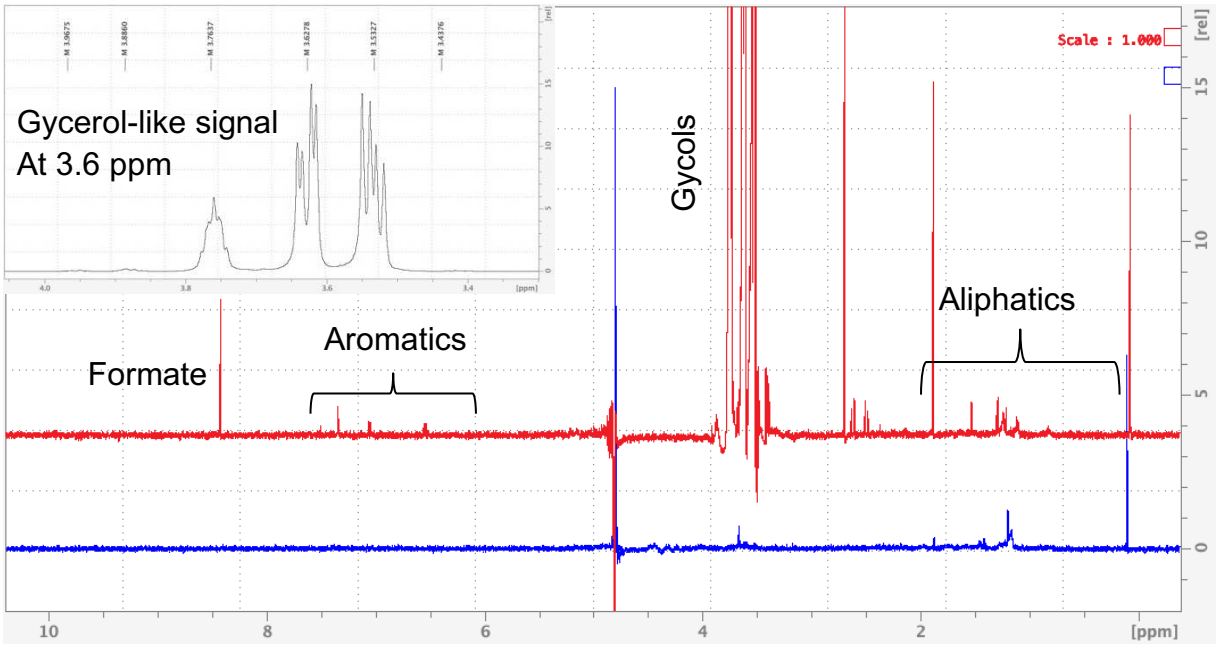


Figure 4.5 : Confirmation of glycol NMR signature following K_2CO_3 addition. In the main figure , blue signal corresponds to $GRSO_4$ prior to anionic replacement by $K2CO_3$, while the red is $GRCO_3$ synthesized via K_2CO_3 replacement. The grey spectra is centered on the glycol signal (3.6 ppm) which corresponds to Erythritol.

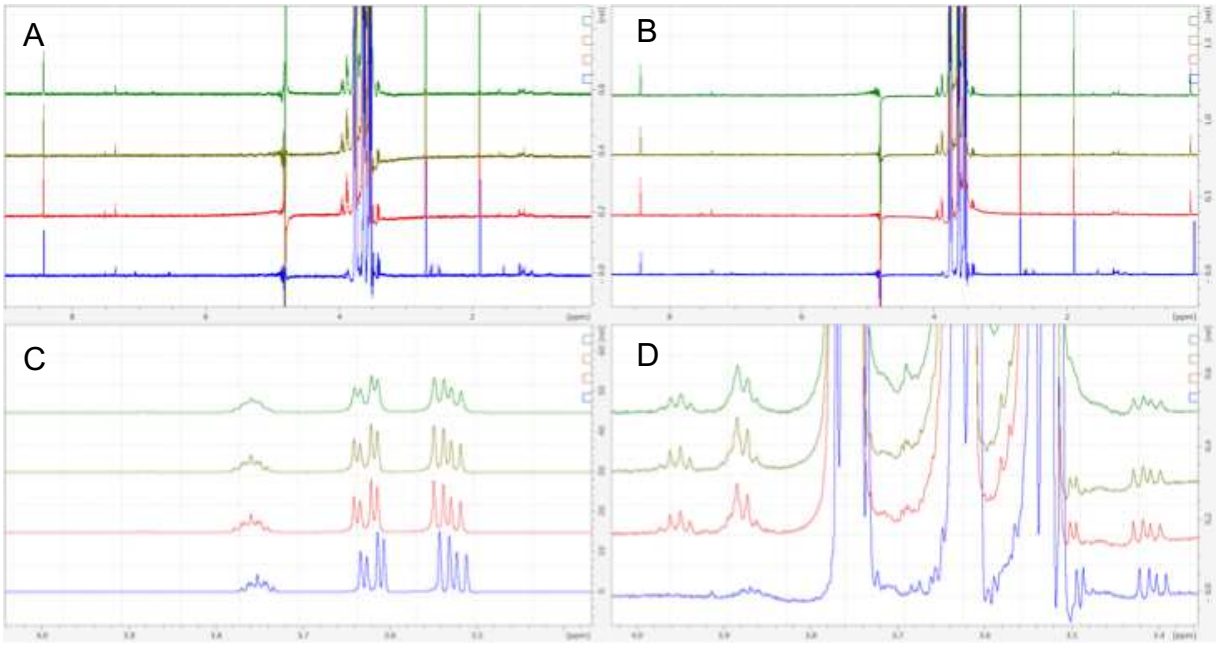


Figure 4.6: Stacked spectra from a CO_2 reduction experiment where the effect of time (0, 10, 30, 60 min corresponding to blue, red, brown, green) and heat (25-80°C corresponding to A,C,D and B respectively) was explored during the bubbling of CO_2. Approximately 1 week elapsed between sample collection and analysis by NMR. All samples displayed almost identical NMR spectra. Bubbling of CO_2 increased two triplet signatures between 4-3.8 ppm with no other significant changes to spectra.

In Figure 4.5, the blue spectrum corresponds to relatively newly synthesized $GRSO_4$ at pH 7. Few peaks in the aliphatic region indicate a small amount of organic product is already present, likely from contamination during synthesis. The red spectra shows the effect on the addition of concentrated K_2CO_3 to $GRSO_4$ to replace the SO_4^{2-} anion with CO_3^{2-} anion. This resulted in the formation of a multitude of organic compounds not found in the original solution. No additional CO_2 was bubbled through this solution. This indicates that aqueous CO_3^{2-} concentration influences the production of organic molecules in otherwise stable GR conditions. The large signal at 3.4-4 ppm corresponds to 1 or more glycol compound similar to the glycerol and erythritol. However, this compound and others were present in all other samples and conditions tested (Figure 4.2, 4.3A, 4.5, 4.6).

This time lag is a possible point of failure where the filtered solutions evolved in the time between experiment and analysis. This evolution interfered with further experiments investigating the effect of time, heat, and metal amendment with K_2CO_3 buffered systems as all solutions analyzed contained nearly identical molecules. However, this point of failure in experimental design still revealed interesting information regarding the GR-K_2CO_3 system, as GR will spontaneously reduce K_2CO_3 in solution with or without added CO_2. The only difference between solutions exposed to CO_2 for longer periods of time was the progressive formation of additional couplets at 3.9-4 ppm. This is associated with additional carbons added to the glycol compounds.

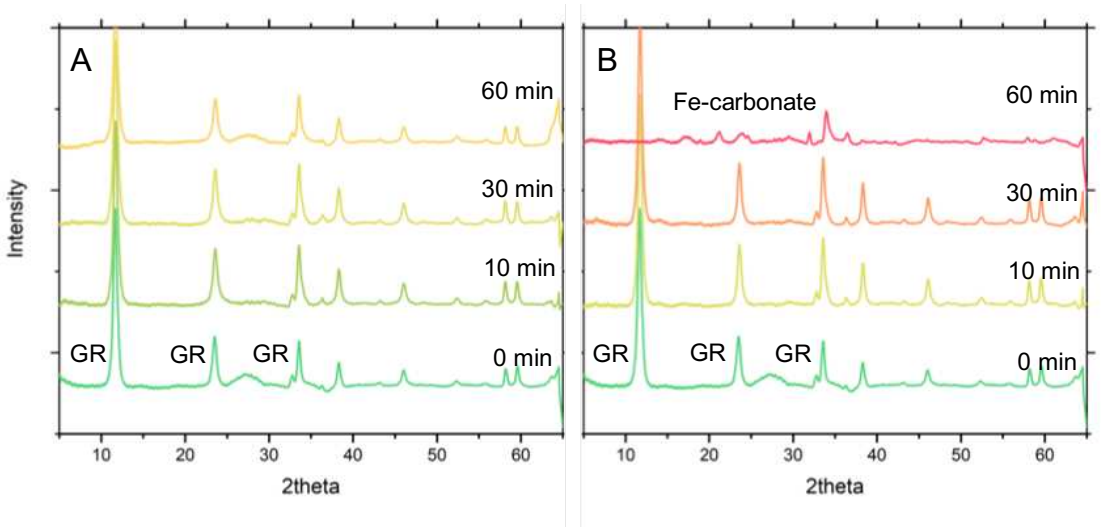


Figure 4.7: XRD crystallograms of the two temperature experiments (A:25C, B:80C) conducted using $GRCO_3$ in 1M KCO3. In both cases, 30 minutes of CO_2 bubbling did not significantly alter the crystal structure of $GRCO_3$. By 60 minutes, the heated experiment resulted in the loss of crystallinity of the sample and the formation of Fe-carbonate

This production corresponds with observed stability of GR (Figure 4.7) under continuous CO_2 addition after 60 minutes at 25C (Figure 4.7A). Only in the heated sample (Figure 4.7B) did GR eventually transform into light green poorly crystalline Fe-oxides after being left to equilibrate for 24 hours. It is known that extended exposure to CO_2 decreases the pH of GR solutions, resulting in its transformation (Legrand et al., 2004). The pH did decrease significantly with CO_2 exposure, from 12 to 6. This suggests that CO_2 reduction imparts some degree of oxidative and thermal stability to GR minerals, likely through the protective nature of adsorbed hydroxyl rich products.

Conclusion

Green rust reacts with anionic carbon species present in solution to form a variety of organic products at alkaline pH. These compounds impart oxidative and thermal stability to the GR mineral. Further, timely, and careful analysis of this system is required to reveal the intricacies of CO_2 reduction, preferably with in-situ analysis during reactions.

4.3.3. Reduction of DMSO to DMS

In CO_3^{2-} rich alkaline solutions, GR minerals intercalated with sulfate anions have been shown to produce DMSO (S. Lee et al., 2023). This organosulfur compound is a product of sulfate reduction in the presence of carbonate anion, possibly a reaction entirely contained within GR interlayers. DMSO is an organic sulfoxide compound relevant to environmental biochemistry chemistry, and contains a liable oxygen species that is reducible by microbial life to produce DMS, an environmentally significant climate forcing volatile compound (Charlson et al., 1987; Lovelock & Margulis, 1974; Pozzer et al., 2022). We proposed that GR could naturally achieve the same reduction through similar mechanisms employed in its well characterized reduction of organic compounds.

Dark reactions

We exposed solutions containing 200 mM $GRSO_4$ to 1M DMSO and left to react over 3 weeks. In the dark unirradiated experiment (Figure 4.8A), we observed the transformation of the DMSO and GR solution over time. Initially, at T=0, corresponding to the initial starting conditions, the spectrum exhibited an extremely strong signal centered at δ = 2.4-2.8 ppm, characteristic of a saturated DMSO signal. This peak existed throughout the incubation period as it was in large excess. Samples at 0, 1, 10, and 17 days were collected corresponding to samples T0, T1, T2, T3, and T4. Over a 17-day incubation period, several new peaks emerged, reflecting the formation of various new compounds.

Peaks between 2.1-2.3 adjacent to DMSO in continuously increased in area suggesting the formation of dimethyl sulfide (DMS), a common reduction product of DMSO and an important molecule in the biogeochemical controls over climate. DMS is not known to be abiotically formed on Earth. The spectrum also suggested the formation of methanol (3.4 ppm) and methanesulfonic acid (MSA) or methanesulfinic acid (MSIA) (2.8 and 3.1 ppm) with a number of peaks between becoming more pronounced over time, indicative of further degradation of the DMSO molecule. Additionally, glycolic compounds (3.0 - 3.7 ppm) observed in prior CO_2 reduction experiments are seen forming, suggesting a common reaction with exposure to carbon containing compounds or ambient CO_2. These observations indicate that GR is able to reduce DMSO to DMS and other products in aqueous solution.

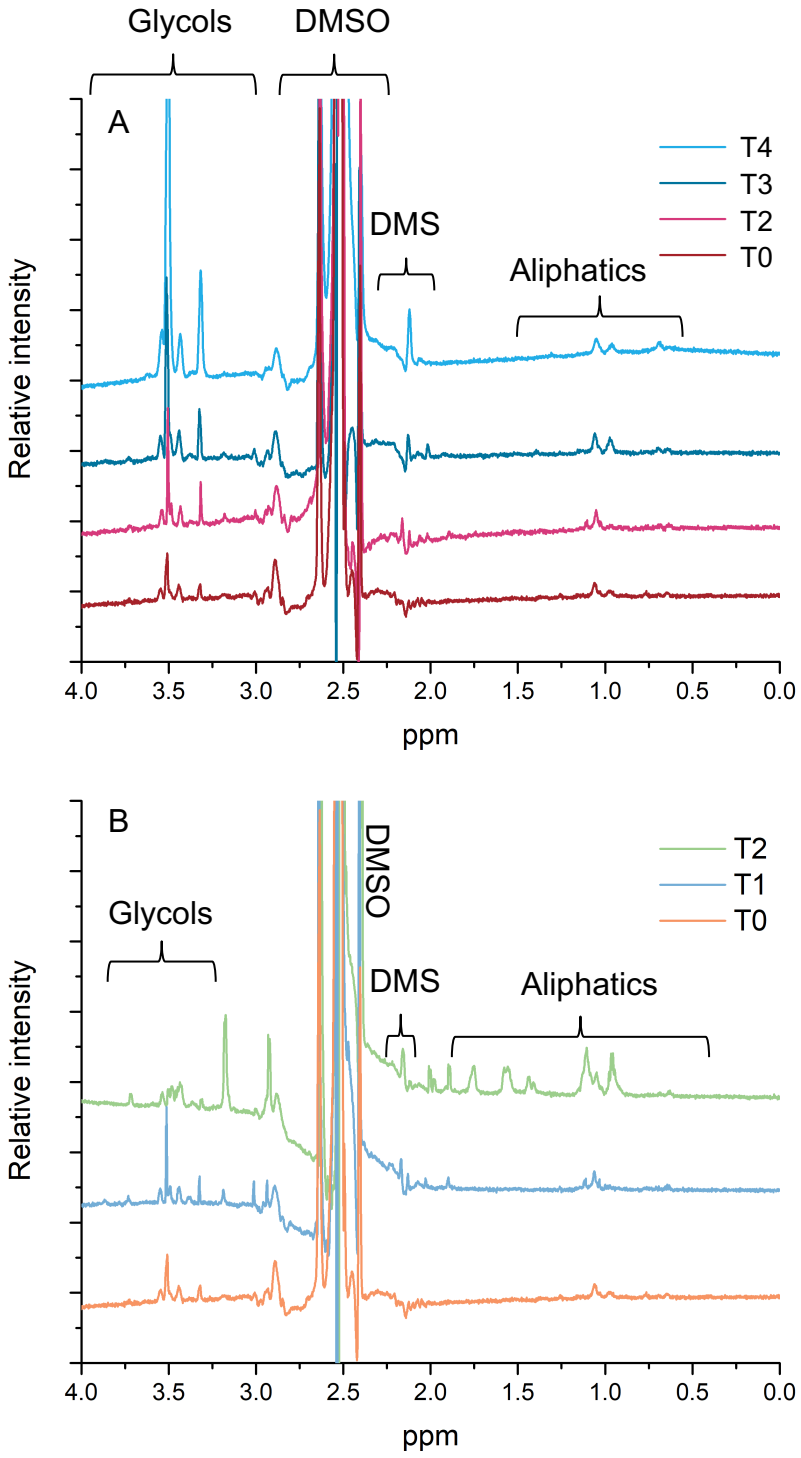


Figure 4.8: (A) NMR spectra of solutions of 0.2M $GRSO_4$ incubated with 1M DMSO. There are 4 timepoints taken during the reactions where T0 (0days) = red corresponds to a new solution of GR exposed to DMSO (2.6 ppm) while the T2 (1day) = pink, T3 (10 days) = dark blue spectra, and T4 (17 days) = light blue demonstrate the appearance and increases in a peak size at (3-3.7, 3, and 2.1 ppm) which corresponds to the production of DMSO degradation products. (B) Depicts GR+DMSO mixture exposed to UV irradiation for 48 hours, with T0 (0 hours) = orange, T1 (1 day) = blue, and T3(2 days) = green yielding new peaks associated with UV decomposition products of DMSO

GR and DMSO Irradiated Experiment

The irradiation of GR solutions containing DMSO revealed more pronounced chemical transformations than under controlled conditions (Figure 4.8B). At t=0, the NMR spectrum displayed the characteristic DMSO peaks between 2.2-2.8 ppm, but by T = 24 hr new peaks across the spectrum have appeared. By day 7, the peaks in the 3.0 - 3.7 ppm region further changed with the grouping centered at 3.5 ppm disappearing while a peak at 3.2 ppm increased, suggesting the continued degradation of DMSO and other products due to UV-induced reactions possibly yielding another degradation product methanesulfonic acid (MSIA) at ~3.2 ppm. Significant changes were also observed in the region 1.0 - 2.5 ppm, where increased peak intensity and complexity suggest the formation of new aliphatic compounds (alcohols, carbon chains). Additionally, the presence of peaks around 2.1 ppm indicated again the formation of dimethyl sulfide (DMS).

Product recovery with mass spectrometry

A mass spectrometer connected to an enclosed Raman pressure cell was used to explore the products of this DMSO reduction. Solutions of new and aged GR + DMSO suspensions were comparatively analyzed (Figure 4.9). It was found that accurate DMSO signals (A) (63, 78 m/z) are recoverable from GR solutions under high vacuum. However, in samples aged to 3 months (B) these signals are no longer present, and instead signals (52, 60 m/z) are detected. These are close to signals associated with DMS (m/z = 42, 61) and may imply further reactions have taken place over time. It is possible that given extended contact with GR, DMS itself is reduced to HS^-, however mineral samples were not analyzed via XRD. It is also possible that the small quantity of DMS produced is highly volatile and could have escaped during sample preparation.

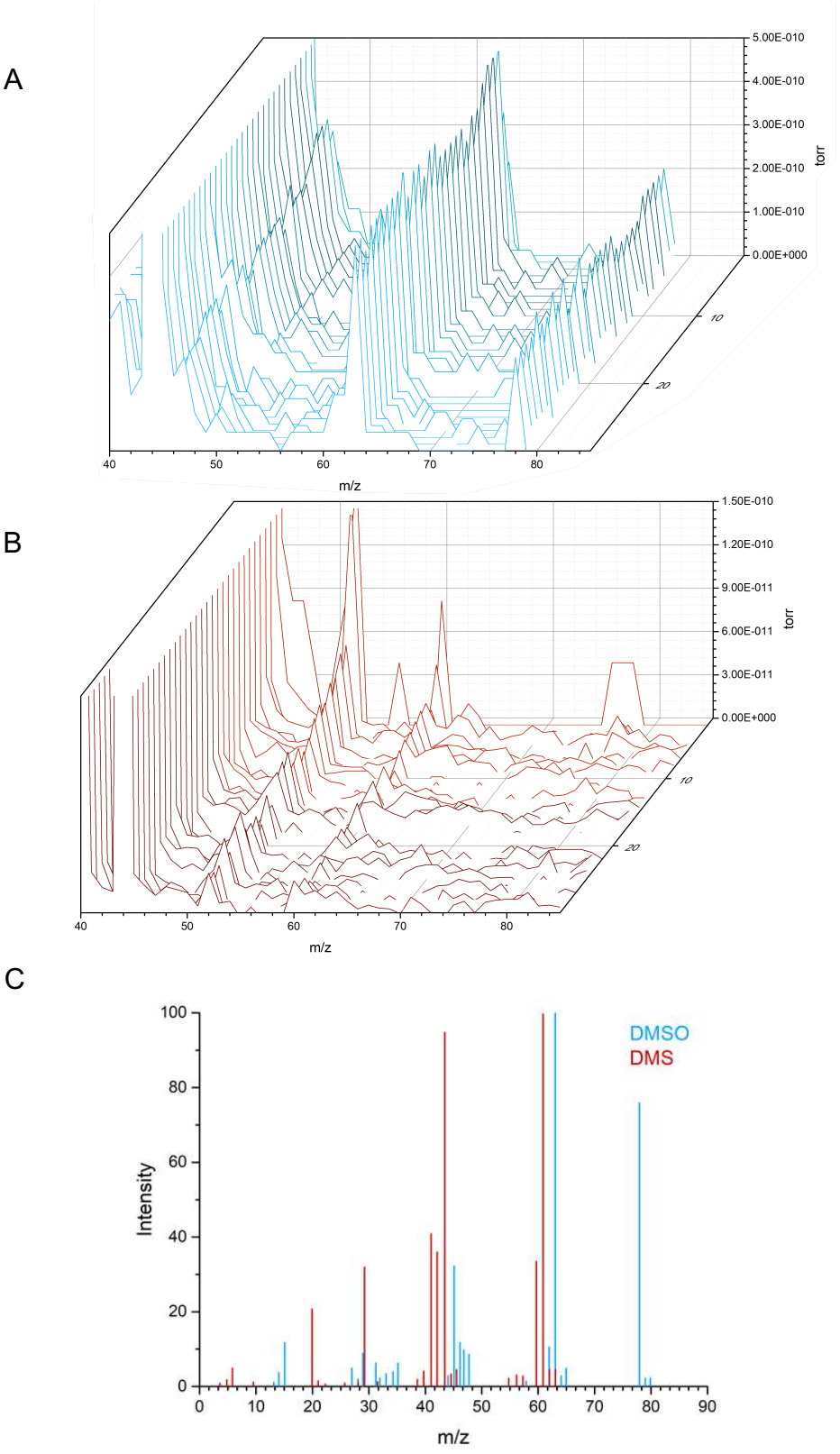


Figure 4.9 : MS measurements of GR DMSO incubation experiments. Graph A shows DMSO recovered from $GRSO_4$ suspension while B shows similar solution that has been aged 3 months. A new signal is weakly detectable (m/z = 52, 64, 80) but is difficult to distinguish if it related to the DMS or DMSO signal (C).

Conclusion

Overall, both the dark and irradiated experiments demonstrate the unique redox chemistry mediated by GR minerals towards DMSO, as well as the catalyzing effect of UV light on such reactions. These findings highlight the dynamic nature of a chemical environment influenced by Fe and CO_2 rich conditions under UV irradiation. DMSO undergoes various degradation mechanisms resulting in a diverse set of entirely abiotic reaction products. This implies strong environmental and climatological implications for a ferruginous early Earth Ocean subject to CO_2 reduction.

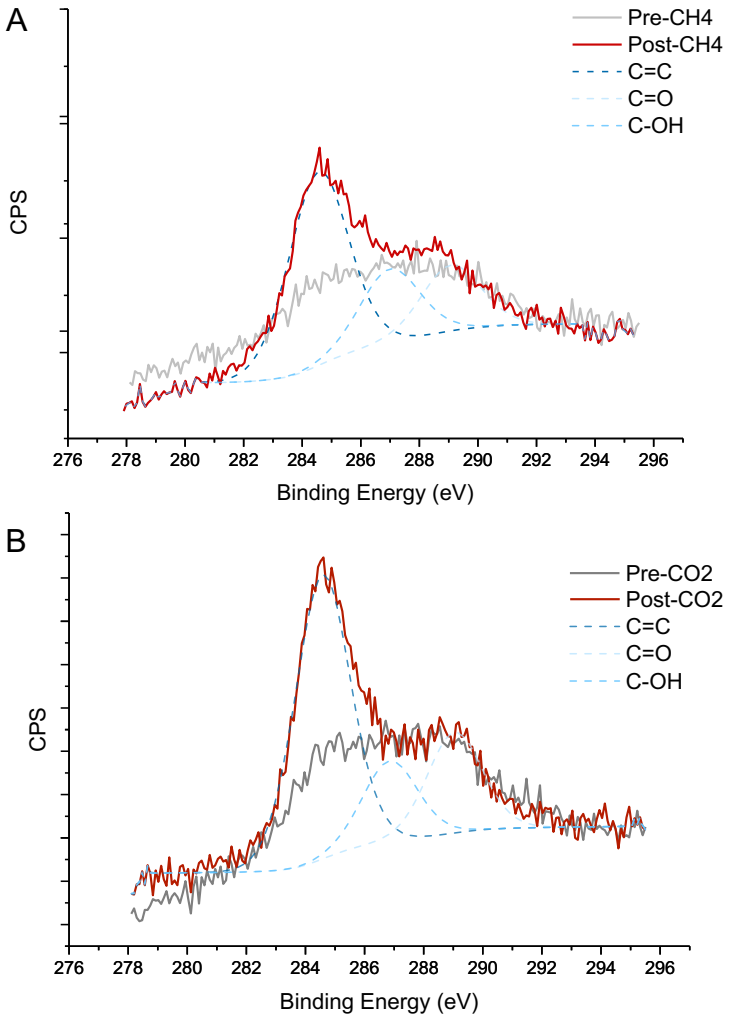
4.3.4. Observations of GR during CO_2 and CH_4 redox using XPS, Raman, FTIR, and Mass spectrometry

As product formation as a result of CO2 reduction and CH4 oxidation has been confirmed to occur when GR is exposed to CO2 or CH4 under various pressures and oxidant concentrations, we sought to better understand the mechanisms involved with product formation. Using spectroscopy, we are able to recover information regarding the type of interactions at the point of contact between the carbon gasses and the mineral surface. In these sets of experiments, we examined the surface chemistry of GR exposed to CO_2 and CH_4 under a variety of conditions (e.g. high vacuum, 1 bar, 10 bar pressure) to probe the reactivity of the mineral towards CO_2 and CH_4 redox.

Surface carbon binding with XPS

Using XPS, we examined the surface chemistry of GR exposed to CO_2 and CH_4 under ultra-high vacuum to better understand the processes that could occur during carbon redox. Such conditions differ as compared to aqueous solution; however general reactivity of the mineral surfaces can be explored.

$GRCO_3$ samples were exposed to 1 bar CO_2 or CH_4 prior to introduction to sample chamber. Figure 10 shows the results of these experiments on Cl modified $GRCO_3$ show marked differences before and after gas adsorption experiments under both 1 bar CH_4 and CO_2. Before exposure to the gases (grey spectra of figure 4.10A&B) each component has a similar intensity. The band at 284.6 eV is the signature of C=C bonds, that at 286.9 eV to C-O bonds, and that at 289 eV to carbonate (or to carboxyl functions O=C-O). Following 1 hour of gas exposure at 1 bar (red spectra of Figure 4.10A&B), the band at 284.6 eV increases which indicates a carbonaceous deposit on the surface , indicating the formation of C=C bonds in both CO_2 and CH_4 conditions.



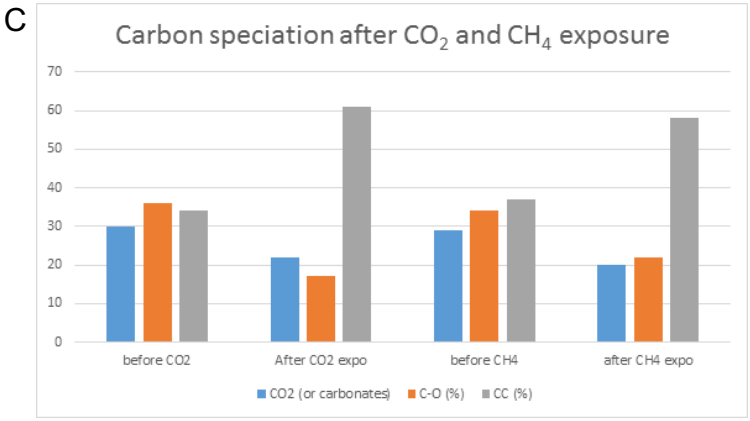


Figure 4.10: XPS spectra of $GRCO_3$ samples comparing of C1s spectra before (bottom) and after exposure to CO_2 (A) and CH_4(B). Graph C depicts percent composition of surface species.

In this experiment CH_4 shows similar carbon speciation as CO_2, with C=C bonding comprising ~60% of the carbon species following sorption. The layering of carbon species at surface of GR may under go reaction with Fe-OH sites, polymerizing them.
CH_4 demonstrates less intense surface adhesion than CO_2, aligning with experimental studies on similarly structured montmorillonite clays (Du et al., 2020). These experiments confirm the sorption of carbon species to GR surfaces, and imply a reactivity towards carbon species regardless of oxidation states.

Raman/IR analysis of CO_2 surface interactions

As the surface of GR was found to be saturated with a layer of C=C bonds following CO_2/CH_4 adsorption via XPS, we sought to further characterize the surface chemistry of GR minerals during exposure to CO_2/CH_4 gasses via FTIR and raman analyses.

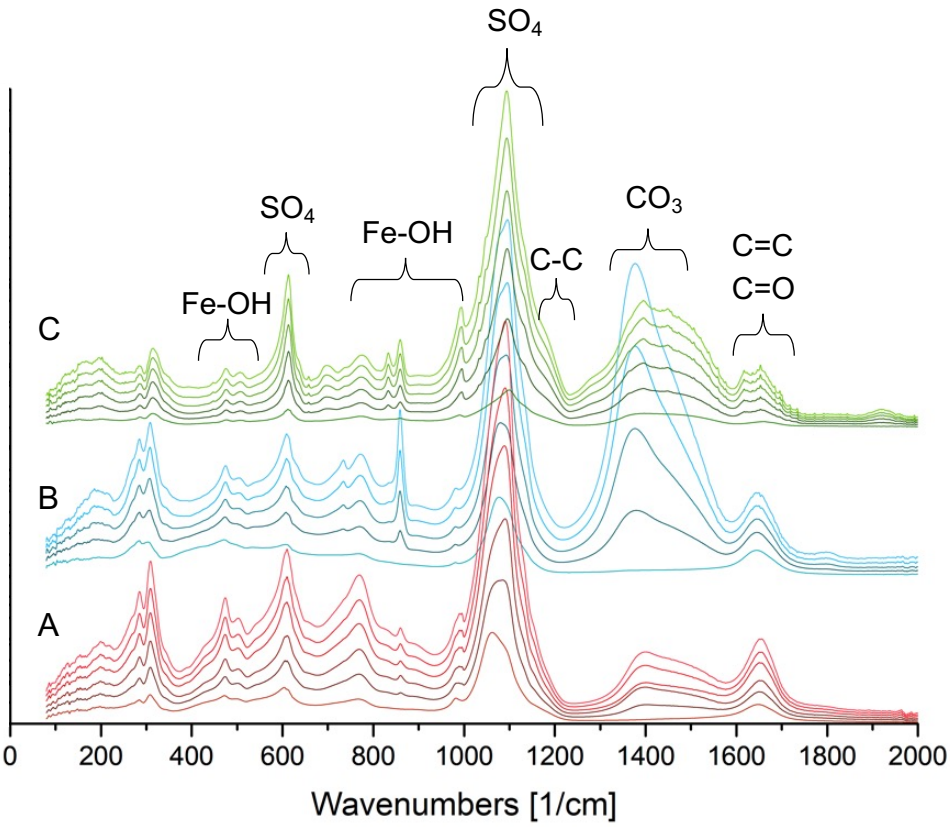


Figure 4.11: IR spectra of of (a) $GRSO_4$ pH 7, (b) $GRSO_4$ pH10, (c) $GRSO_4$ 10 + K_2CO_3 ambient exposure to CO_2 and (d) $GRSO_4$ ph 7 over 48 hours of exposure to CH_4 andO_2 . Larger carbonate formation occurs at higher pH, while modification with K_2CO_3 appears to modify carbonate signal.

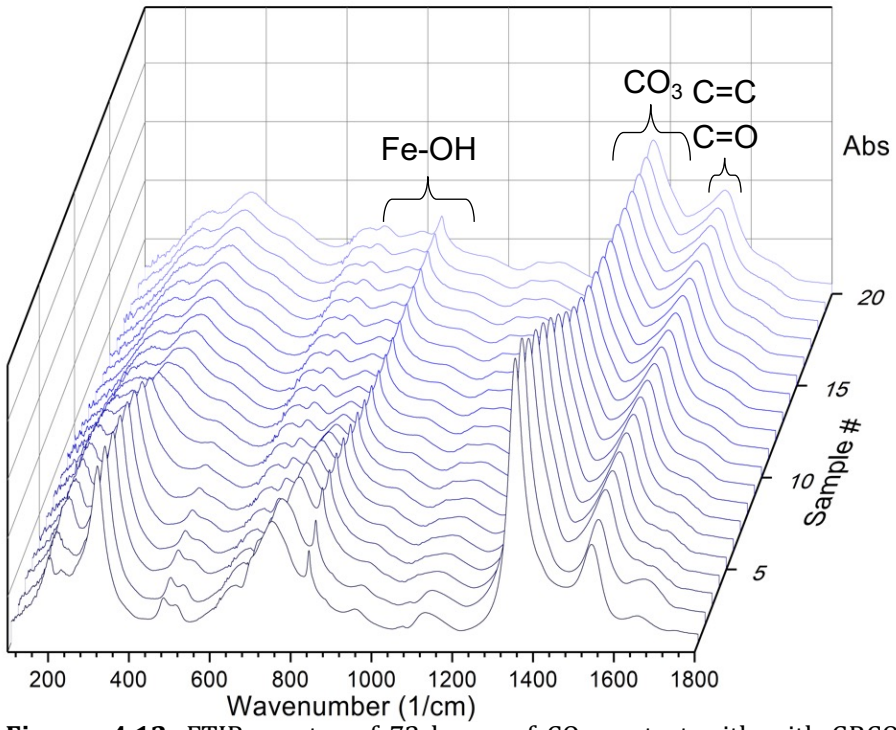


Figure 4.12: FTIR spectra of 72 hours of CO_2 contact with with $GRCO_3$, resulting in its destabilization and transformation into a mix of Fe-oxides and carbonate minerals

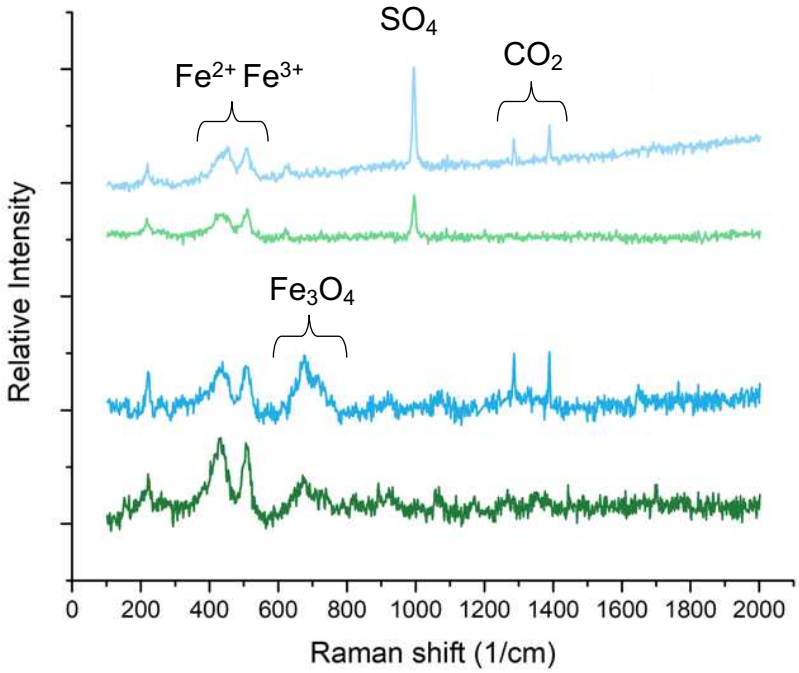


Figure 4.13 : Raman spectra of $GRSO_4$ minerals exposed to N_2 and CO_2 at 25°C (dark green and blue) and -25°C temperatures.(light green and blue) Surface loading of CO_2 appears as two distinct bands between 1200-1400 cm^{-1}.

Investigating the interactions between GR and CO_2 under FTIR spectroscopy (Figure 11) demonstrates a pH dependent uptake of CO_2 in the transformation of $GRSO_4$ to $GRCO_3$, with more intense carbonate peak formation at 1300-1550 cm^{-1} occurring at pH = 10 vs pH = 7. This aligns with the solubility and transformation of CO_2 to HCO_3^- under alkaline conditions, but also align with peaks (1410, 1625 cm^{-1}) associated with CO_2 reduction products in related Fe minerals (e.g. FeS, FeNiS) (J.-E. Lee et al., 2021). The presence of K_2CO_3 at pH 10 did not translate into an equivalent higher peak formation as pH 10 alone, possibly indicating that additional sorption of CO_2 is not translated into HCO_3^- production. Instead, CO_2 may be directly reduced to the various organic products as demonstrated by the appearance of peaks at 850 in both pH = 7 and 10, yet additional faint peaks at and 1790 cm^{-1} in pH 10. Appearances of new peaks in all samples at ~770 cm^{-1} suggests modification of Fe-OH bonding due to CO_2 sorption or organic compound formation. This behavior changes given extended time (>48 hours). Over extended time (Figure 12) $GRCO_3$ in the presence of CO_2 will transform and lose peaks associated with Fe-OH (790-900 cm^{-1}).

Under analysis by Raman microscopy (Figure 13), no direct evidence for CO_2 reduction is found throughout the spectrum 100-4000 cm^{-1} given extended exposure to CO_2. Only peaks associated with CO_2, 1350 and 1400 appear. The exposure of GR to CO_2 results in the increase of a peak at 650 cm^{-1}, associated with oxide formation. Decreasing the temperature of the mineral decreases the oxidation effect and still shows CO_2 sorption as evidenced by the 1350 and 1400 peaks. The CO_2 peaks are able to be removed once the reactor headspace is flushed with N_2.

In a different set of experiments, samples of $GRCO_3$ (green) were doped (orange) with concentrated erythritol (red) to observe the interactions between the mineral surface and the compound, and compared to CO_2 doped GR (blue). Under IR, it was found that regions 1200-1000 and 1500-1400 cm^{-1} were influenced by interaction with erythritol. This region is associated with C-OH stretching and CH_3 or CH_2 bending and could arise from the hydroxyl groups and carbon chain layered on the surface of GR. In the CO_2 modified GR similar changes occur in these regions, albeit with less intensity. There is also a noticeable shift in the peak at 780 to 800 which is not observed in the erythritol doped sample. This corresponds to shifting lattice Fe-OH sites (Perez et al., 2024), possibly due to bond length changes associated with Fe-O-C bond formation. This suggests unique changes to GR surface structure associated with CO_2 sorption.

Under observation using Raman spectroscopy, erythritol doping results in a complexified signal from GR-Erythritol which does not match CO_2 modified GR. Peaks associated with C-C, C-O-C, CH_2, and CH_3 are abundant, reflecting interactions between the compound and the surface sites atop GR. Increases in 150-250 cm^{-1} may be associated with Fe-O bonding or changes to interlayer chemistry. On the other hand, CO_2 exposure to GR did not result in intense peak formation other than those associated with the transformation of GR to magnetite as evidenced by the appearance of a strong peak at 700 cm^{-1}. CO_2 surface adhesion is apparent with the two peaks at 1400 and 1300 cm^{-1}. A peak at 210 cm^{-1} may be related again to Fe-O or interlayer changes.

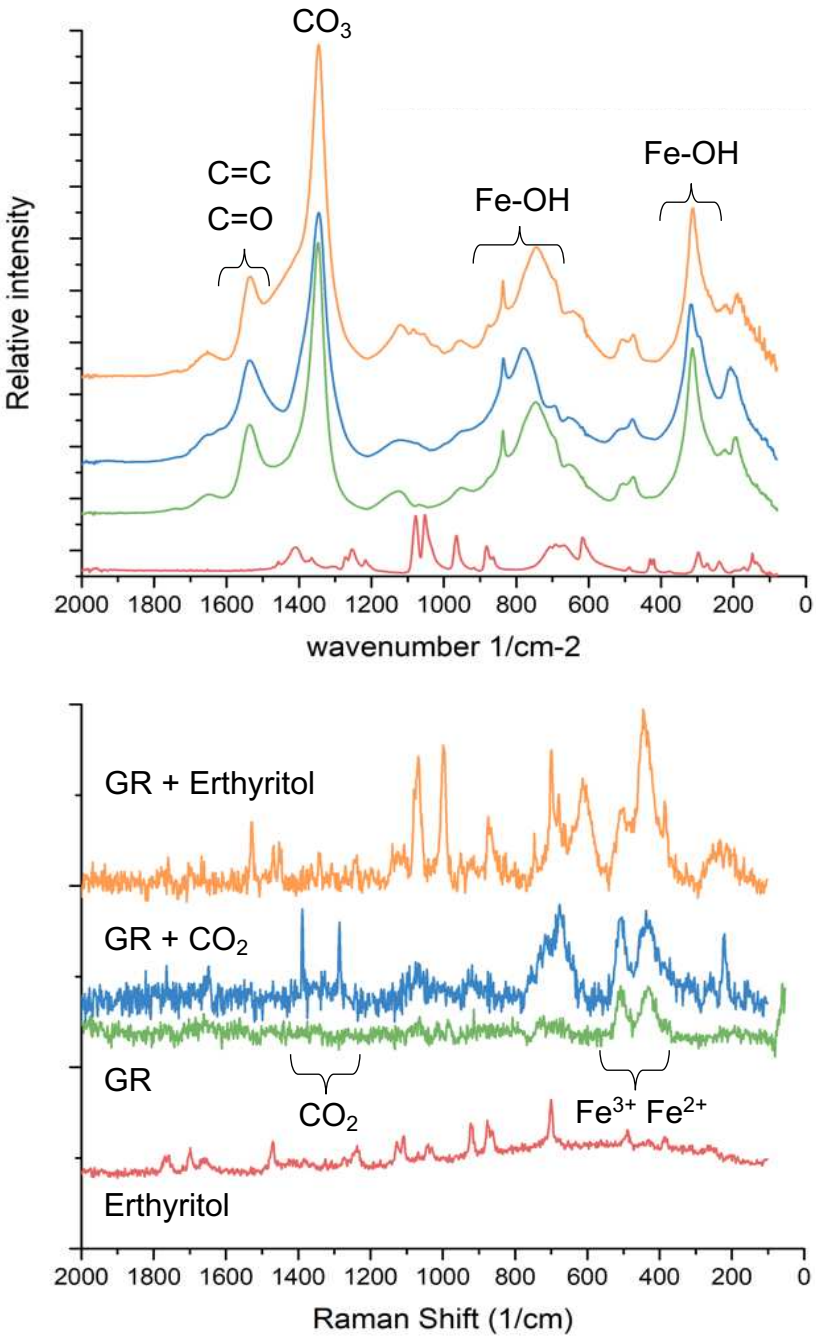


Figure 4.14: IR (A) and Raman (B) spectra of Erythritol (red), $GRCO_3$ (green), $GRCO_3$ + CO_2 24 hours (blue), $GRCO_3$+Erythritol.

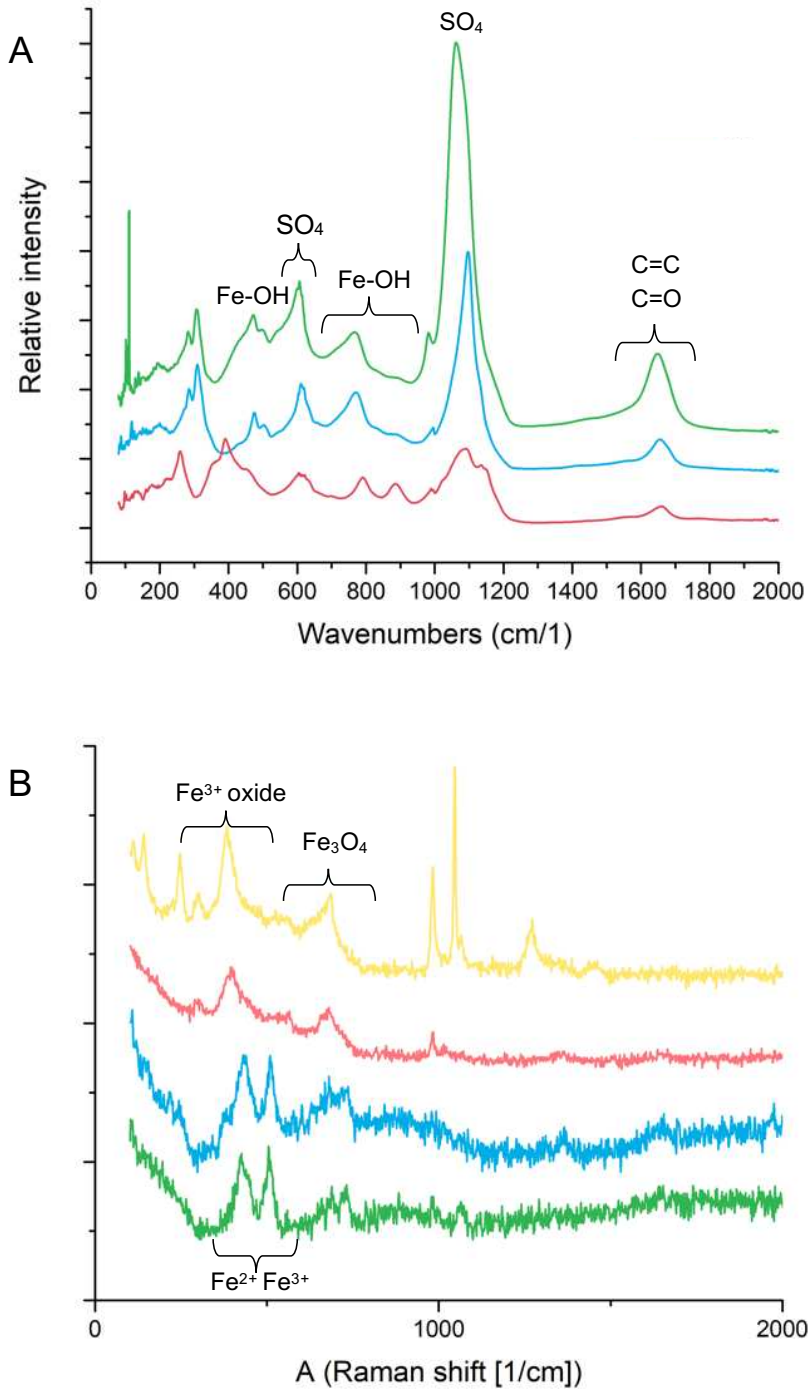


Figure 4.15: FTIR (A) and Raman (B) spectra of $GRSO_4$ exposed to 1 bar CH_4 and 0.2 barO_2. $GRSO_4$ (green), $GRSO_4$ + CH_4/O2 2 hr (blue), 48 hr (red & yellow)

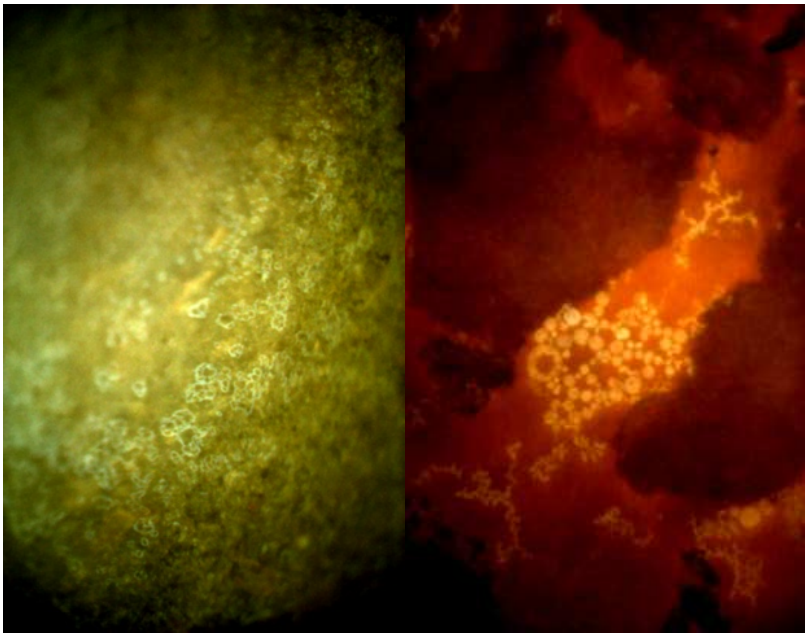
Analysis of GR and CH_4 interactions showed that GR is stable under CH_4 atmospheres indefinitely, however given an introduction of O_2 GR will oxidize and transform into various oxidized as explored in chapter 2 (Figure 4.15). We observed this transformation under 1 bar of CH_4 and 0.2 bar O_2 in FTIR and Raman. Under FTIR $GRSO_4$ peaks lost fidelity from initial (green) to 12 (blue) to 48 (red) hours of oxidation. This was also observed with Raman as initial green rust conditions gave away to oxide formation. These oxides however displayed variation in peaks by 48 hours, with peaks from 900-1500 cm^{-1} appearing. In addition by 48 hours the sample was highly fluorescent in some regions past 1200 cm^{-1} which made analysis difficult at times and possibly indirectly suggests organic formation. No peaks were located at 2000-4000 other than those associated with water (~3000 cm^{-1}). Curiously, CH_4 absorption was only directly detected sometimes at ~2900 cm^{-1}. An interesting morphological observation was the formation of spherical structures at the surface of liquid GR solutions following oxidation under CH_4 atmospheres (Figure 16A). Raman analysis demonstrated fluorescent spectra of Fe-SO4 with CH_4 absorbed.

Mass spectrometry of GR mediated CH_4 oxidation

With the mass spectrometer attached to the Raman cell, investigations were conducted to ascertain the existence of volatile intermediates and products of CH_4 oxidation in the presence of O_2 (Figure 4.17). Solutions of GR were exposed to 8 bar of CH_4 and 1 bar O_2 within the Raman cell result resulted in increases to m/z = 28, 32,34,40,44,50, 55, 56, and various peaks to 100 m/z. Compounds of interest as intermediates of CH_4 oxidation are CO (28 m/z) and CO_2 (44m/z). It is possible that CH_4 is oxidized to a CO intermediate upon exposure to oxidants, which would yield Fischer-Tropsch pathways for hydrocarbon product formation. Given the detection of various hydrocarbon species (Chapter 2) (Figure 4.17B) this could be a dominant mechanism alongside the direct oxidation of CH_4 to methanol and other species. However, as air contains N_2 (28m/z) and CO_2 it is difficult to distinguish between 28 and 44 m/z introduced and those associated with leaks. Decreases in peaks associated with CH_4 (16,15,14,12 m/z) indicate that CH_4 is consumed in a reaction or is lost during leaking.

Figure 4.17 demonstrates an interesting result as compounds greater than 44 m/z are shown to form immediately following air introduction as well as 48 hours later. It is difficult to distinguish these peaks from noise, however given the repetition in peak presence between 50-60, 65-70, 80-90 m/z it may indicate relatively stable concentrations of higher mass compounds. These compounds could correspond to the various hydrocarbon products detected during the initial methane oxidation experiments in Chapter 1. Potential products in this range include dimethyl ether (46.04 m/z), chloromethane (49.0 m/z), cyclobutene (56.06 m/z), acetone (58 m/z), and furan (68 m/z). It should be noted that these experiments were the first test case of the in-situ analysis of reactor headspace via MS that we developed, and serves as a proof of concept for future, more methodical, exploration of this GR carbon redox system.

A



B

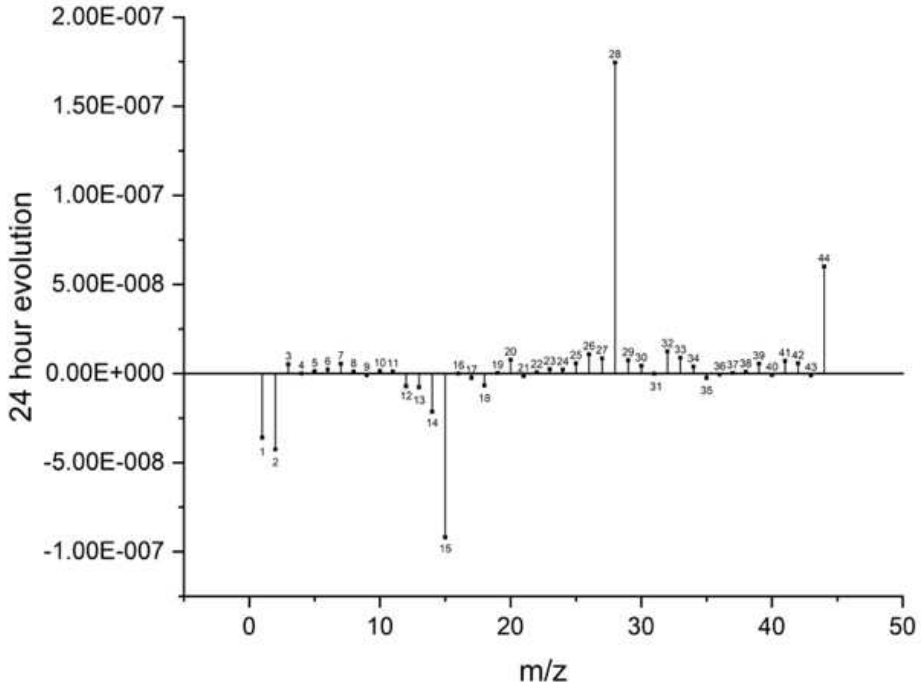


Figure 4.16 : Results from experiment where a headspace containing 8 bar CH_4 and 0.1ml $GRCO_3$ was introduced to 1 bar air. Part A shows GR solution (20x magnification) before and after oxidation. B shows the difference in m/z of 0-44 m/z over 24 hours adjusted to 16 m/z

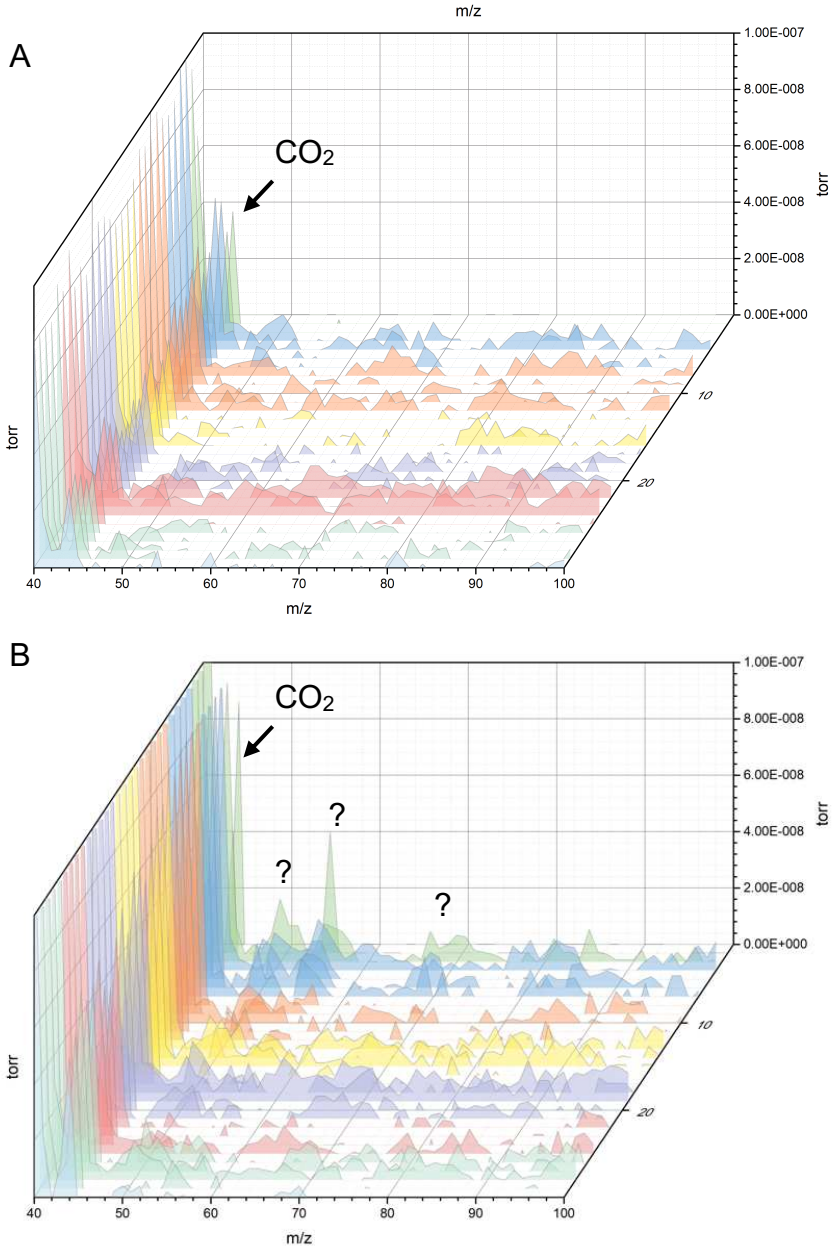


Figure 4.17 : Results from experiment where a headspace containing 8 bar CH_4 and 0.1ml $GRCO_3$ in sea water was introduced to 1 bar air. A & B compares initial and final m/z collected from 40-100 m/z range. Marked differences in m/z diversity are apparent when comparing T = before and 48 hours after O_2 introduction.

4.4. Discussion

Our findings confirm the redox capabilities of GR minerals towards CO_2 reduction and CH_4 oxidation in solution and probe further into reaction mechanisms, surface chemistry, and the broader biogeochemical implications of these processes.

Carbon dioxide reduction or carbonate reduction?

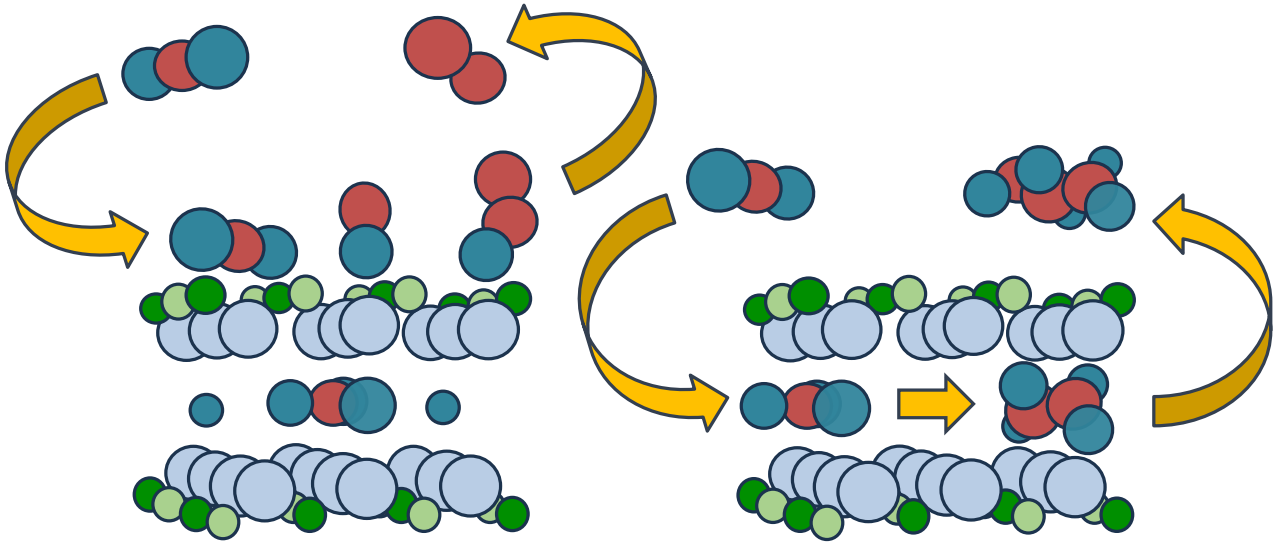


Figure 4.18: An illustrative diagram depicting possible reaction pathways for CO_2 reduction over $GRCO_3$ surfaces forming C-C bonds (a) or within its interlayer forming gycols (b).

We find that under alkaline conditions (pH = 10) GR in saturated with bubbles of CO_2 results in the formation of various organic compounds. These compounds are products of CO_2 reduction. The products detected via NMR and GCMS were various carbon compounds, including formate, alcohols, aldehydes, and multi-carbon polyols similar to glycerol and erythritol as first identified by Lee (2023). The production of organics is accelerated in the presence of concentrated K_2CO_3 versus NaOH. This aligns well with observations suggesting that both the interlayer CO_3^{2-} anions and carbon species introduced participate in the reaction (Farr, Gaudu, et al., 2023; S. Lee et al., 2023). It was found that exposure to concentrated CO_3^{2-} was sufficient to induce carbonate reduction, and added CO_2 only played a minor role in an already saturated system. Temperature (25-80°C) changes did not noticeably affect products formed during CO_2 reduction, but did eventually transform the mineral phase. At 25°C GR maintained its crystal structure with the addition of 1M K_2CO_3 during the bubbling of CO_2 over 1 hour. At increased temperatures (25°C, 80°C) resulted in the eventual transformation to Fe-carbonate by 1 hour. The increased temperature and transformation did not noticeably affect the formation of products. Exposure of alkaline solutions of $GRSO_4$ without added carbonate to N2, CO_2, CH_4, CH_4+NO demonstrated the reactivity of GR towards gas phase mediated reactions, particularly CO_2 and CH_4/NO combinations. Further irradiation of these solutions produced a variety of additional compounds through both UV and GR catalyzed interactions.

Evidence of these products were visible during IR but not Raman analysis. Interlayer bound CO_2 is very stable in LDH (Sasai et al., 2019) materials, however Lee, 2023 suggests that the interlayer anion plays a significant role during CO_2 reduction reactions. As there exists greater CO_2 adsorption related carbonate peak formation in OH titrated GR vs K_2CO_3 titrated GR at pH 10, prior saturation may prevent further incorporation.

We have found that even under careful preparation $GRCO_3$ is more unstable than $GRSO_4$ unless amended. The addition of chloride or magnesium during synthesis or the addition of K_2CO_3 after synthesis assisted in the preservation of GR mineral suspensions. $GRCO_3$ is known to be unstable without careful preparation, such as with phosphate adsorption or anion substitution(Agnel et al., 2020; Bocher et al., 2004). Perhaps it is possible by coating the crystal edges and faces with an inorganic molecule further interlayer interaction with the environment are halted, preventing eventual destabilization due to equilibrating interlayer chemistry.

Production and reduction of DMSO

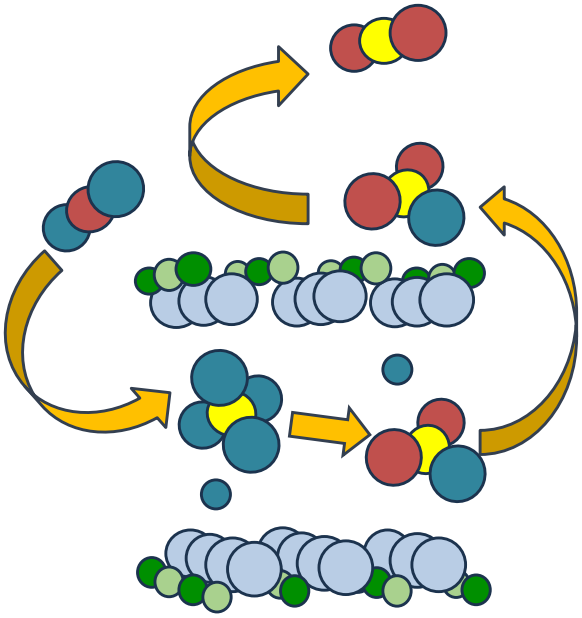


Figure 4.19 : An illustrative diagram depicting possible reaction pathway for reduction of CO_2 to DMSO and DMS within and outside the $GRSO_4$ interlayer.

The formation of DMSO and its commensurate reduction and degradation by UV light in GR containing solutions were investigated, finding that GR is able to reduce DMSO to DMS and other compounds spontaneously. The addition of UV to the reaction results in further, more complex degradation chemistry. Observation of the mixtures with Raman did not detect DMSO or DMS signatures once mixed into mineral samples. Lee 2023 reported that the formation of DMSO relies on interlayer interactions during CO_2 reduction, thus it is possible that DMSO exists, at least momentarily, within the interlayer of GR which is a known to exfoliate some LDH materials (Y. Zhao et al., 2011). Other sulfur compounds, such as sulfonates (Perez et al., 2018) have been found to exchange within

the interlayer of GR. The catalytic reduction of DMSO to DMS or oxidation to $DMSO_2$ likely are different processes. GR's reductive electron transfer is well studied and DMSO sorbed to its surface could provide the necessary conditions for its reduction. Meanwhile, $DMSO_2$ is likely a result of the production and mediated oxidation by radicals during GR transformation (Maciuca et al., 2007).

Sulfur is known to have been cycled by mineral and photo chemistry in the Archean (Hao et al., 2022), but this specific set of reactions prove novel with great implications on early Earth chemistry as DMS is purported indicator of biological activity and is used as a biosignature in spectroscopic observations of exoplanets(Domagal-Goldman et al., 2011; Hanni et al., 2024; Leung et al., 2022; Malaterre et al., 2023a). In addition, DMS and other organosulfur compounds are greenhouse gasses and affect the formation of clouds and thus climate(Farquhar et al., 2000; Lovelock & Margulis, 1974; Young et al., 2023). Popular hypotheses regarding the biogeoregulation of the biosphere implicate DMS as an important control over Earth's habitability (Lovelock & Margulis, 1974). As such, the completely abiotic production of DMSO, DMS, and various other climate affecting compounds by GR reveal a cryptic regulation of climate by abiotic reactive minerals like GR. This carbon redox system thus is important to the evolution of the biosphere on Earth, and potentially elsewhere in the cosmos.

4.5. Conclusion

The organic chemistry of green rust systems appears to be more complicated than previously imagined. What was assumed to be inert mineral species under controlled conditions presents various organic species when introduced to air, CO_2, K2CO3, and conceivably other additives. How these organic species manifest and interact with the mineral structure is poorly understood. Further work must carefully elucidate the mechanisms and conditions (e.g. temperature, pH, eH, ionic potential) by which organic compounds are synthesized from GR solutions. It is possible that previous studies examining GR-organic reactions may have results that were inadvertently influenced by this type of chemistry. More precise understanding of how stable interlayer chemistry would benefit the domains of environmental chemistry, remediation, catalysis, and emergence of life studies.

However, this work implies that green rusts play an interesting role in the redox cycles of carbon sulfur and halogens, with strong implications for geochemical controls over Archean, Proterozoic environmental chemistry. Such reactions may have provided and guided for the conditions that led to life's emergence.

Chapter 5:

Implications of reactive mineral mediated carbon redox for modern and ancient environments

This chapter reviews and discusses the work on GR carbon redox conducted in this thesis and connects it to the literature available on Fe-mineral mediated redox in the contemporary and ancient environment, revealing new insights into GR and the geochemical systems that it is highly involved within. The redox processing of the two major sources of carbon on the Earth, CO_2 and CH_4 implies a strong abiotic influence over atmospheric, environmental, and emergence of life chemistry. Parts of this section are directly used in the in-press chapter for *Metals in Life Sciences* titled "Green rusts offered ingestion and respiration channels for CO_2, CH_4, & thus life's emergence".

5.1. Carbon redox mediated by reactive Fe-oxyhydroxide minerals

Products	CO_2 reduction	CH_4 Oxidation
C1		
Methanol	X	X
Acetaldehyde		X
Formaldehyde		X
Formate	X	
C2		
Ethylene		X
Ethanol	X	X
Peracetate	X	
Acetate	X	
C3		
Acetone	X	X
Pyrvuvate	X	
2-Propanol	X	X
Propanone		X
Glycerol	X	
Malonate	X	
Lactate	X	
C4		
Glycolate	X	
Butanone		X
Erythritol	X	
Dioxane	X	
C>4		
Pentanone		X
Benzene		X
Hydrocarbons		X
C-Cl,N,S		
Chloroform		X
Dichloromethane		X
Tetrachloromethane		X
Nitromethane		X
Methylnitrate		X
DMSO	X	
DMS	X	

Table 5.1: Known products of CO_2 reduction and CH_4 oxidation as reported by Lee (2023) and Farr (2023,2024).

The cycling of carbon on the surface of the Earth today is primarily mediated by life via cellular respiration, processing 10^3 –10^6 gT of carbon in a planetary scale redox conversion of carbon species into higher and lower oxidation states utilizing highly evolved yet primitively conserved systems of electron transfer (P. Falkowski et al., 2000). The metabolisms that conduct these reactions are mediated by enzymes with transition metal cores readily reacting with rising (>400 ppm) levels of CO_2 to form the complex sugars (e.g. DNA) that form the backbone to all of biology (P. G. Falkowski et al., 2008).

Parallel to this biologically mediated cycling of carbon, completely abiotic naturally forming mineral systems are found to readily conduct the same type of reactions that life exhibits (de Graaf et al., 2023). Several studies of protometabolic systems where pure metals or metal-bearing minerals conduct CO_2 reduction under spontaneous, photochemical, and pressurized conditions have been recently described (Beyazay et al., 2023; Grosch et al., 2022; Hudson et al., 2020; Rauscher & Moran, 2022; Varma et al., 2018). Efforts to describe fully the reactivity of minerals towards CO_2 reduction is of interest to the wider emergence of life field and its applications in society as similar mineral-mediated reactions have long been exploited by industry for their catalytic behaviors. Catalytic materials species (e.g. Zeolites) are essential components of in the processing of natural gas or the production of commodity chemicals (Usman et al., 2018). However, these minerals, if naturally occurring, generally lack characteristics conducive to emergence of life hypotheses - of which GR exemplifies.

GR exhibits a combination of properties inherent to the aforementioned materials, bearing a clay-like envelope of catalytic variable valence metal sheets containing hydrated channels of anionic reactants. For example, fougèrite (naturally occurring GR) clusters and nanocrystals exchange metallic ions one for another known to be vital to life (eg., Ni, Co, Zn with Fe); can absorb anions into their nanometric aqueous interlayers (e.g., Cl^-, CO_3^{2-} HCO_3^-, $HCOO^-$,MoO_4^{2-} and many organic ions). The anions in some $Fe^{2+/3+}$ hydroxysalt green rusts (carbonate, oxalate, methanoate) can act as both electron acceptor and donor in reactions that induce conformational change (Antony et al., 2008; J. M. R. Génin et al., 2005; Ruby, Géhin, et al., 2006; Wander et al., 2007). As such, GR mediates catalytic electron transfers towards organic compounds in solution, from the degradation of organics such as trichloroethylene or phenols (Matta et al., 2008) to the reduction of nitrogen oxides and the amination of carbonic or keto acids to alanine and glycine (Barge et al., 2019, 2022). GR represents a natural mineral that could enable chemical disequilibria ("free" energy) conversion – a natural entity with mechanochemical potential (Arrhenius, 2003; Duval et al., 2019; Nitschke & Russell, 2013; M. J. Russell, 2023).

While the transformation of GR in the presence of oxidizing of gasses such as O_2, CO_2, and NO has been well characterized (Legrand et al., 2004; Ruby et al., 2010; P. Wang et al., 2021; Yoshino et al., 2013), only two studies (Farr, Gaudu, et al., 2023; S. Lee et al., 2023) have explored the redox behavior of GR with CH_4 and CO_2 gasses. They reveal over 20 organic compounds formed from simple interactions between the mineral and the gasses under ambient to high pressures, electrochemical impulse, and UV irradiation. Many of the products are precursors to or direct products of the metabolic pathways for carbon fixation.

One conceit in these experimental tests of protometabolic reactions is that we expect green rust minerals to act as similar to active enzymes enabling life's emergence, yet in this work we have only been able to follow the redox reactions through the formation of stable products by analyzing solution chemistry around GR minerals or by the direct dissolution of the mineral. Thus, the full reaction pathway mediated by interlayer chemistry along with intermediates have not yet been revealed.

Experimental findings

Reactions between GR and CO_2 have been previously studied outside of a CO_2 reduction context as the transformation of GR via CO_2 addition has been used to synthesize $GRCO_3$ from other GR precursor species using anion exchange. In solution CO_2 exists as H_2CO_3, HCO_3^-, and CO_3^{2-} given increasing solution pH, and within GR interlayers anionic exchange readily occurs with high preference given to HCO_3^- over other anions (CO_3^{2-}>SO_4^{2-}>Cl^-) (Agnel et al., 2020). GR is only stable above a pH of ~6.5 (Bocher et al., 2004; Ruby et al., 2010) thus given excess CO_2 in an unbuffered solution GR will eventually undergo an additional transformation to Fe^{3+} oxide phases such as lepidocrocite, magnetite, chukanovite, or siderite minerals.

In contrast, HCO_3^- rich alkaline solutions of GR bubbled with CO_2 resulted in the production of various organic species in the >100mM range (S. Lee et al., 2023). The reduction of CO_2 is thought to occur within the interlayer of the mineral, with the saturated HCO_3 solution constantly replenishing the mineral's interior. The spontaneous reactions with CO_2 led to (>100mM) production of hydroxyl-rich sugar alcohol compounds, namely Erythritol, the presence of which lends further stability to GR (Chapter 4). Surface studies indicate that CO_2 is readily adsorbed to available Fe-OH surface sites, with various C-C, C-O, and C-H bonds present following CO_2 adsorption indicating rapid transformation upon contact (Chapter 4) & (S. Lee et al., 2023). In fact, those Fe-OH bonds, specifically their length, are implicated in the reactivity of Fe-hydroxides towards catalytic reduction reactions (H. Li et al., 2024). DFT models of related mineral species like Fe_3O_4 show very strong surface interactions between CO_2 and these Fe-OH sites common to iron minerals (Santos-Carballal et al., 2018), and under these conditions CO_2 has a predisposition to OH mediated reduction (Martins-Costa & Ruiz-Lopez, 2024). While the catalytic behavior of the surfaces is apparent, the interlayer also is implicated as a reaction site as Lee further demonstrates the reduction of interlayer SO_4 species to DMSO in the presence of CO_2. Even products of CO_2 reduction by GR are further reducible by the mineral; as DMSO can be reduced to DMS (Chapter 4) and pyruvate can undergo reductive amination in the presence of NH_3 to form amino acids (Barge et al., 2019). Thus, fairly complex reaction pathways form given a supply of CO_2 and GR.

In contrast to CO_2, the bubbling of pure CH_4 does not produce any significant organic products (Farr, Gaudu, et al., 2023). The redox active bilayers of metal cations promote reduction, not oxidation reactions under stable conditions. GR is capable of catalyzing the oxidation of CH_4 during its own oxidation by O_2, NO, or H_2O_2 (Farr, 2023), which is hypothesized to occur due to the proliferation of radicals and/or formation of Fe^{4+} sites during GR oxidation (L. Fang et al., 2021; Z. Li et al., 2022). The role of oxidants in the activation of methane over GR surfaces was explored (Chapter 2), where O_2, NO, and H_2O_2 were found to promote the formation of methanol, hydrocarbons, organochlorides, and organonitrates from GR mixtures under 10-50 bar CH_4. The reaction coincided with the transformation of GR to various Fe-oxyhydroxide and oxide phases, providing evidence for the radical mediated hypothesis. XPS experiments (Chapter 4) revealed similar patterns of C=C and C=O bonding on the surface of $GRCO_3$ following adsorption of CH_4 compared to CO_2. These signals may reflect the accumulation of organic phases in a similar fashion to coke or soot formation as a result of incomplete oxidation processes.

GR shares structural homology between its octahedrally coordinated Fe atoms within its crystal lattice and the octahedrally coordinated reaction center of the metallo-enzyme

sMMO. Thus to probe the hypothesis that GR is not only structurally but catalytically similar to sMMO, oxidizing CH_4 using the same mechanistic principle of Fe^{4+} activation a series of experiments were developed to test the viability of said reaction, to probe its reactivity under various conditions, and to enhance its efficiency. EPR experiments probing the nature of Fe^{3+}-Fe^{2+} interactions within the crystal lattice of GR were performed to characterize the interactions for the first time and to isolate the signature of radical production and Fe^{4+} formation. Our EPR findings add further evidence to the existence of high valent intermediate production in transition metal minerals, and demonstrate that radical production does in fact occur without the need of phosphate sorption (L. Fang et al., 2021; L. Z. Huang et al., 2022), which likely was only required to block reuptake in order to be detectable under specific experimental conditions. This discovery implies that GR is able to catalyze CH_4 oxidation and likely other reactions in a similar high valent Fe^{4+} intermediate catalyzed mechanism as utilized by extant and likely ancient enzymes, such as sMMO.

Green rust was believed to have been abundant within the ancient Archean oceans at hydrothermal vents where methanotrophic bacteria today live under high pressures (Trolard et al., 2022). Thus, high pressures were thought to be important to catalyze this reaction. In addition, electron transfer between Fe reaction sites were thought to also have played a role in the reaction mechanism behind CH_4 oxidation, and so oxidative species such as O_2, NO, and photons were tested to determine their effect on the oxidation of CH_4 (Q. Huang et al., 2023; C. Wang et al., 2023). Simulating hydrothermal conditions, the pressurization of GR with CH_4 and O_2 resulted in the production of MeOH along with various other organic compounds, including trichloromethane (TCM) and dichloromethane (DCM). These results confirm the transformation of CH_4 by oxidative transformation reactions mediated by GR. Our further investigations using UV light to catalyze the oxidation of GR demonstrate that CH_4 is readily oxidized to acetone among other organic products such as benzene in the presence of GR under UV irradiation. GR is known to be strongly photoactive and liable to transformation (Liu, 2021; C. Wang & Chakrapani, 2023b). Moreover, such processes can be combined to yield self-catalyzing reactions (X. He et al., 2023).

The experiments in this thesis were designed to probe questions into a hypothesized transition from geochemical to metabolic chemical pathways. As such, as the results strengthen the arguments presented by Russell, Nitschke, and Duval for a green rust mediated transition from a purely abiotic system to ancient metabolism. These findings have great impacts on how the ancient Archean environment and chemistry should be interpreted.

5.2. Natural industrial catalyst for carbon removal?

Carbon dioxide is the most prevalent greenhouse gas at 426 ppm, whose greenhouse effect is dwarfed 25x by CH_4 which only exists at 1.8 ppm(Calvin et al., 2023). Further exploration of mineral-carbon interactions may reveal efficient sorbents for CO_2 and CH_4 sequestration.

Mirroring the revolution by oxygen producing cyanobacteria during the GOE and the ensuing inhospitable terrestrial conditions for anaerobic prokaryotes that followed; mankind's technological capacity following the industrial revolution and the subsequent and continued production of CO_2 that outproduces the sequestering capacities of natural geochemical sinks presents certain ecological impediments to the continued survival of the human species (P. Falkowski, 2015).

Thus, solutions to capture atmospheric or emitted CO_2 that optimize materials characteristics such as surface area, stability, reactivity, and especially cost are desperately needed to be deployed. Currently, various methods of carbon sequestration are being deployed in test and commercial scale sequestration projects (Dziejarski et al., 2023). Direct air capture (DAC) projects yet rely on calcium oxide or amine based solvent swing adsorption techniques which have thermodynamic limits to possible efficiency and potential impact on total global CO_2 emissions. Enhancing the sustainability of the carbon capturing industrial process will rely on the development of novel catalysts capable of efficiently performing CO_2 reduction or overcoming the unfavorable partial oxidation of CH_4 of without the use of expensive metal catalysts (Au, Rf, Pt, Pd, etc) obtained from environmentally damaging extraction or high pressure/temperatures activation conditions which contribute to increasing global carbon emissions (Calvin et al., 2023).

GR's reductive capabilities towards CO_2 and its ability of oxidize CH_4 present an interesting opportunity for a natural relatively cheap method of carbon redox. It's demonstrated capabilities towards CO_2 reduction in particular demonstrates high selectivity towards products of interest to industry. Methane on the other hand is not easily oxidized, and requires specific pressure or radical forming conditions to be met. In terms of viability for a renewable bioinspired catalyst, the experimental methods used in this paper, while interesting, are not currently viable due to low yields and lack of reaction specificity. Similar LDH materials, however calcined, have been shown to achieve relatively high rates of efficiency for CH_4/CO_2 redox (Fan et al., 2024), indicating GR's role as a precursor to useful catalysts. Furthermore, being highly versatile and modifiable materials could ostensibly be modified for much greater reaction specificity and efficiency. Similar synthetic LDH's, specifically Al-Zn or Ni based, have achieved significant yields with MeOH production (Fan et al., 2024; H. Wang et al., 2019; J. Zhao et al., 2022). In addition, due to the sensitivity of green rust to oxidation under surface conditions provides some added difficulty in scaling up the reaction, but methods of preparing O_2 resistant or O_2 stable green rusts also exist (Tahawy et al., 2021). Similar LDH's are also known to evolve O_2 and H_2 from the direct splitting of H_2O (B. W. Xue et al., 2020; Zhou et al., 2018), which could further oxygenate carbon redox products. However, creating composites with other materials with high surface areas (>1000m2/g) and adsorption properties, such as metal organic frame works (MOF), surface may lead to enhanced anion storage or catalytic capabilities towards CO_2 reduction (Song et al., 2024). Additionally, other methods of carbon sequestration such as ocean fertilization or alkalinity enhancement may be improved by the use of reactive mineral phases such as Fe-oxyhydroxides (Babakhani et al., 2022).

Maximizing efficiency and reducing the energy costs of carbon sequestering processes have called for unconventional bio-inspired approaches to catalysis, and the fact that a

natural and versatile platform like green rust exists and can conduct such an economically important reaction demands further investigations and optimizations.

5.3. Mineral mediated carbon redox cycling in modern environments

Green rust is found today in water logged and oxygen poor sediments in the form of the mineral fougèrite, alongside various other transition metal carbonates, sulfides, and oxyhydroxides. At these oxygen minimum zones, $Fe^{2+/3+}$ minerals are shuttles for microbial electron transport, and serves as a redox couple for the lithotrophic metabolism of sulfur, nitrogen, and carbon species. Fe minerals play a large role in the transport and recycling cycling of carbon in the environment (Comba et al., 2015; Hädeler et al., 2023; J. Huang et al., 2021). This cycle overlaps with those of other essential elements. Nitrogen (Doane, 2017), phosphorous (Klein et al., 2024), sulfur (Wu et al., 2019), and halogens (Comba et al., 2015) in various forms are cycled by redox interactions with Fe minerals. These reactions proceed via degradation (e.g. hydrolysis, radical mediated degradation) (J. Ye et al., 2024) or preservation pathways (e.g. mailard reaction, polymerization) (O. W. Moore et al., 2023) leading to the sequestration of carbon through mineralization.

Given the impressive redox properties of GR towards CO_2 and CH_4 new insights into microbial interactions and geochemical cycling of elements can be inferred. As CO_2 reduction forms various sugar like compounds which can serve as electron donors, the association of GR with microbial colonies (Jorand et al., 2011; Zegeye et al., 2005, 2010) would not be limited to purely inorganic electron transfer, but the GR themselves would offer an attractive source for organic products to metabolize. Evidence for the evolution of O_2 and H_2 from transition metal materials in addition to our findings provide evidence that GR-type LDH's could potentially sustain a fuel source of O_2, H_2, and now multi-carbon compounds for microbes at these redox transition zones (Dionigi et al., 2020; Ju et al., 2023; Ou et al., 2023; Sweetman et al., 2024). Evidence for unique isotopic fractionation of C, Fe, or O by these Fe-oxyhydroxide mediated reactions exists (Bahlmann et al., 2019; Gueguen et al., 2018; Nie et al., 2017), meaning that such GR mediated redox reactions leave behind a signature in the geochemical record. Much work remains to elucidate the signatures of this cryptic carbon redox pathway.

5.4. GR mediated carbon redox cycling in ancient ferruginous environments

Abiotic carbon redox may have greatly influenced the environmental conditions on the ancient Earth due to high concentrations of CO_2 and CH_4 alongside widespread ferruginous oceanic conditions during the Hadean (4.6-4 Ga), Archean (4-3.5 Ga) and early Proterozoic (3.5-2 Ga) eons (Halevy et al., 2017; Poulton & Canfeld, 2011; Thibon et al., 2019). This carbon was likely reacting with the primitive oceans, and thus carbonating the precipitating iron mineral hydroxides present (Ernst et al., 2023). CO_2 reduction by

GR (S. Lee et al., 2023) and other minerals (Grosch et al., 2022; Hudson et al., 2020) occurs spontaneously under the right conditions, meaning a substantial concentration of dissolved organic carbon may have existed in Early Earth surface waters or at depth in hydrothermal sites, given alkaline (>8 pH) conditions. Evidence for such interactions may be preserved within graphitic layers Eoarchean rock record (Dodd et al., 2019; Guo et al., 2024; L. Sun et al., 2022).

Reduction

As ocean chemistry evolved from acidic to more alkaline conditions by the early Archean (Halevy & Bachan, 2017b), so too would the conditions suitable to carbon redox which would have shifted optimal reaction conditions for GR-mediated organic production (pH>8) from vents to open water. The chemical evolution of the early environment could have been greatly influenced by the sequestration of CO_2 by GR minerals and its commensurate transformation by GR to volatile organic halogen (e.g. $CHCl_3$, CH_2Cl_2, CH_3Cl) and sulfur species (e.g., DMSO, $DMSO_2$, DMS) (Farr, Gaudu, et al., 2023)) exerting strong influences over the greenhouse effect (Charlson et al., 1987; Q. Li et al., 2022), the effect of their production by a GR saturated ocean on the Archean climate is currently unstudied. Today, these compounds are biologically produced, and have strong controls over climate. Their abiotic production in deep time would have exerted strong controls over the evolution of the biosphere. As such, the detection of exoplanet signatures corresponding to these compounds may not necessarily indicate the presence of life (Malaterre et al., 2023b), as putative biosignatures may be evidence of the natural evolution of planetary ocean and atmospheric chemistry guided by redox sensitive minerals.

Oxidation

Ambient methane oxidation at the surface and at hydrothermal sites also presents another route for carbon redox transformation on the early Earth. According to Farr 2023, CH_4 can be oxidized to methanol under ambient conditions as well as under pressure as given sufficient oxidizing species. Chemical oxidants have previously been thought to been rare during the Archean (4-3.5 Ga), however recent research points to several candidates that would have been naturally produced prior to the GOE and the subsequent proliferation ofO_2 in marine environments.

The discovery of geochemically generated radical species from the weathering of silicate bonds (Anipsitakis & Dionysiou, 2004; H. He et al., 2021; G. Zhao et al., 2023) demonstrates a new pathway for oxidation of GR in the allegedly anoxic Archean. Limited radical production at the surfaces of mineral faces weathered by rocks could produce x11 more than produced by UV interactions with the atmosphere (H. He et al., 2023). Critical interpretation of these hypotheses (Koppenol & Sies, 2023) posit that Fe^{2+} scavenging in ferruginous ocean would prevent any H_2O_2 from building up to appreciable concentrations. If so then the interface between weathered Si-minerals and GR could be redox active and lead to runaway Fenton reactions given GR's propensity to further produce radical species, serving as a base to autocatalytic oxidation and reduction based organic synthesis on itself or other mineral surfaces. Another source of autochthonous formation of oxygen is that naturally occurring redox potentials present at hydrothermal environments (Kitadai et al., 2021) could conceivably catalyze oxygen evolution reactions (OER) yielding O_2 via water splitting over GR related LDH minerals (Ou et al., 2023), as

recently found in Fe & Mn rich benthic polymetallic nodules (Sweetman et al., 2024). This would yield a self-catalyzing oxidation process given certain concentrations and fluxes of OER catalyzing metals (e.g. S, Ni, Mn, or Mo)(Kitadai & Maruyama, 2018).

Further sources of oxidants such as oxidized nitrogen species are hypothesized to have been produced through lighting and meteoritic impacts in the absence of life, and recent experimental and theoretical work place nitrogen oxides (Buessecker et al., 2022; Wong et al., 2017), and nitrogen oxyanions (Barge et al., 2022; Ducluzeau et al., 2009) in the position to react with GR in early marine environments. Such interactions with GR demonstrate the type of reactions instigated by NO and NO_2^- oxidizers with GR and CH_4 and imply new natural mechanisms for nitrogenated organic synthesis.

Photochemistry

The late Hadean to early Archean atmosphere would have likely allowed some UV-C light to reach the surface of the Earth, resulting in the photooxidation or photoreduction of the surface oceans bearing GR species (Dodd et al., 2022; C. Wang & Chakrapani, 2023), dramatically affecting the composition of surface organic species formed especially so given our findings on GR mediated photochemical organic synthesis (Table 5.1)(Chapter 4). Limited continental exposure at this time diminished possible weathering rates and thus limited the marine flux of essential nutrients necessary for the emergence and proliferation of early metabolism (Hao et al., 2017; Hao, Knoll, Huang, Hazen, et al., 2020). However, it is believed that ultraviolet irradiation was able to recycle some of these limited limiting nutrients (Farr, Hao, et al., 2023; Hao et al., 2022). As we demonstrated (Chapter 2 & 4) the GR mediated production of methanol, chloromethane, dimethyl sulfide, and potentially other cloud seeding or ozone depleting volatile compounds could have directly enforced controls over early climate and cloud cover, thus determining surficial UV-irradiation flux and thus the availability of nutrients for early metabolism. The production of volatile organic compounds by early life has been suggested to have linked the evolution of early metabolism to the early atmosphere (Ledford & Meredith, 2024), in a manner similar to the influence of microbial DMS production over modern climate regulation as proposed by the CLAW and Gaia hypotheses (Lovelock & Margulis, 1974; Vallina & Simó, 2007).

Warming from the sun may even contribute to the thermochemical processes known to modify GR's transformation rates as increased temperatures are now known to catalyze the transformation of GR to magnetite (Farr et al., 2022). However, these processes likely would have most impact within hydrothermal settings or diagenetic environments where temperatures exceed 80°C, where these processes are already thought to occur (Q. Huang et al., 2023). The Hadean and early Archean were subject to 40-30% less solar irradiation according to the faint young sun hypothesis(Catling & Zahnle, 2020). Greenhouse gasses such as CH_4 and CO_2 are implicated in the warming of the early Earth above freezing temperatures, however miscible organic molecules with lower freezing points like methanol could have served as an antifreeze for primitive oceans, which could possibly still exist below the surface of Mars, Ceres, Encedeldus, and Europa (Egea-González et al., 2024; Weber et al., 2024). With the discovery of new greenhouse gasses able to be formed by GR chemistry, further climatological modifications could have prevailed.

Overall, a ferruginous ocean bearing GR minerals would have had dramatic effects and controls over early environmental chemistry, resulting in a factory of organic production that presaged the emergence of metabolism.

5.5. An inferred evolutionary transition from abiotic minerals to protoenzymes

Life as an emergent property of geochemistry

At some point under these conditions geochemistry transitioned into biochemistry (M. J. Russell et al., 2013; Wimmer et al., 2021), and the links between the analogous structures and catalytic ability inherent to redox sensitive minerals and metallo-protein reaction centers invokes hypotheses relating to a mineral origin of enzymes (Goldman et al., 2023; X.-L. Huang, 2024; Nitschke & Russell, 2013). Extant biochemistry displays various examples of bio-mineral relationships, such magnetite serving as microbial electron transporters (F. Liu et al., 2015) or within the P-amended ferrihydrite core of ferritin (García-Prieto et al., 2016). Further parallels can be drawn between enzymatic metal cofactors and organic ligands with green rust's capacity to be modified by metallic and organic species, notably its increased reactivity in the presence of certain metals (O'Loughlin et al.; Choi et al., 2012; Zhang et al., 2018; Thomas et al., 2020; O'Loughlin and Burris, 2022; Farr et al., 2022) or its increased stability in the presence of inorganic and organic moieties (Bocher et al., 2004; L. Z. Huang et al., 2022).

In the case of CO_2 reduction under alkaline conditions, carbonate green rust is able to produce C2-C4 hydroxyl rich compounds like glycerol in high quantities (S. Lee et al., 2023). Glycerol and similar hydroxyl rich compounds are known to retard the oxidation of green rust indefinitely (J.-M. R. Génin et al., 2001; Y. Sun et al., 2023). Shielding crystals from physical oxidation by hydroxyl coating or producing anti-oxidant heterocycles (e.g. quinones) (Anschutz & Penn, 2005) could constitute innate forms of dynamic self-preservation in autocatalytic chemical systems. Furthermore, as organic interactions are known to modify coordination chemistry of metals (Q.-Q. Jia et al., 2024), continued surface modification (Borrego-Sánchez et al., 2022; Hooks et al., 2020; Yin et al., 2017, 2018) further augments the reactivity and capabilities of the green rust system. Various additions to green rust, such as metals (e.g., Ni, Co, Cu, Zn, Mo) can modify the reaction mechanism and products formed during CH_4 oxidation or CO_2 reduction. Sorbed inorganic species such as silicon or phosphate are known to protect GR from oxidation (Bocher et al., 2004; Perez et al., 2024), and the presence of adsorbed phosphate species specifically are known increase the release of radicals during oxidation (L. Z. Huang et al., 2022) possibly via the prevention of resorption by the mineral itself, granting the protected green rust with catalytic oxidative properties.

Given appropriate polymerization (Lambert, 2008; Shanker et al., 2012), GR morphologically and functionally and begins to resemble (Figure 5.1) a metallic center of

a ancestral enzyme or protein surrounded by cofactor ligands (Gutierrez-Rus et al., 2023). This system evolves from an innate chemical structure that preceded its function (Wong et al., 2023).

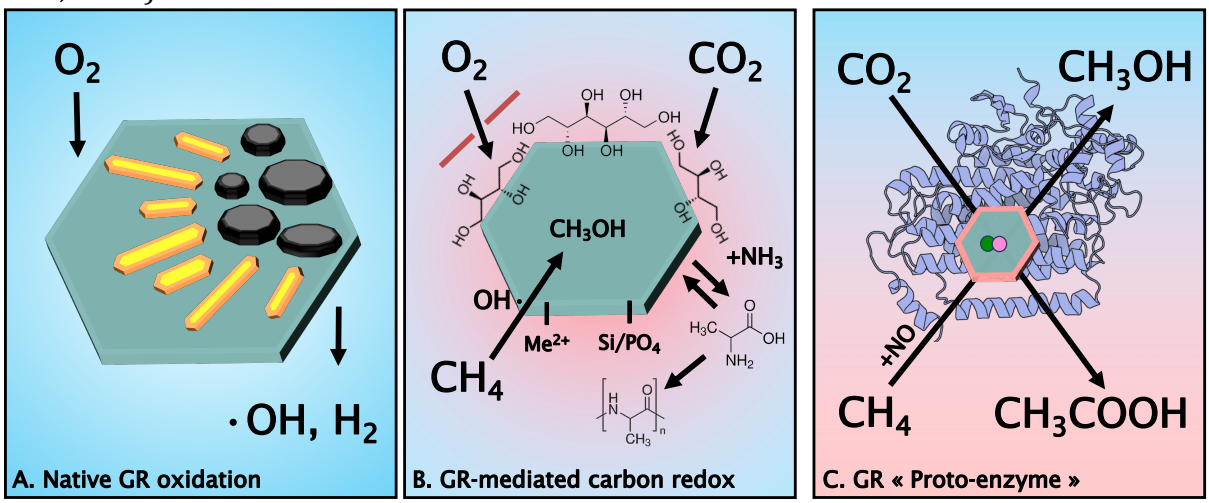


Figure 5.1: Demonstration of GR's response to external redox species at different levels of complexity. In section A, GR is liable to oxidative transformation in the presence of O_2. In B, this no longer occurs due to the production of protective glycols as a result of spontaneous CO_2 reduction. Many reactions can be nonspecifically catalyzed at this level of complexity. In slide C, due to specific selection pressures the organic molecules complexified into a hypothetical polyamino ligand that selects for only the oxidation of CH_4 to CH_3OH, resembling the extant enzymatic function of sMMO. Red and blue coloration indicate relative levels of reducing and oxidizing conditions, respectively.

In the diagram, this green rust mineral spontaneously converts CO_2 into protective glycolic sugar alcohol species (Chapter 4) including pyruvate which then can be further modified with the addition of ammonia to conduct reductive amination (Barge et al., 2019) to produce the amino acid alanine. This product can be used as a feedstock for further organic synthesis, or be used to reactivate GR that has been deactivated by Si/P adsorption (Yin et al., 2018) by competing with blocked surface sites. The next step in uncovering this hypothesized primordial metabolism is the polymerization and functionalization of glycols and amino acids to more complex proteins and organic membranes, which has been shown to occur over various mineral surfaces (Burcar et al., 2015; Lambert, 2008; Ogasawara et al., 2000; Shanker et al., 2012). From there, the autocatalytic production of polymerized amino acids ligands that both protect the mineral cofactor from oxidation and increase the reactivity towards certain reactions could arise, as demonstrated by GR surrounded by SMMO's ligands for the catalysis of CH_4 oxidation in the 3rd part of the diagram where GR begins to resemble a protoenzyme in form and function (Henriques Pereira et al., 2022) as it conducts a particular role in a complex system, possibly at a redox gradient. Biochemical enzymes share features in common with reactive mineral species like GR, and given the appropriate conditions whereby GR modified with various metals, inorganic compounds, polyamino acid chains, could have its reactivity selectively tuned, much like an enzyme, to service specific reaction mechanisms, such as CH_4 oxidation to methanol. The relationship between inorganic proto-enzymes as described and the initial biochemical enzymes to emerge from similar environments is not known, but it is possible that reactive organo-mineral assemblies

produced (Mamajanov & Cody, 2017) or served as (Rasmussen et al., 2020) the templates for their production and replication.

Furthermore, the phosphorylation of produced glycolic compounds by metals to form lipid membranes (Aleksandrova et al., 2023; Madanan et al., 2024) presents a pathway for this GR mediated proto-metabolic system to further encapsulate reactions, concentrate products, and preserve itself from perturbations from the outside world. Observed liposome-like morphological features preserved in Eoarchean BIFs reflect possible fossil evidence of simple organic membranes (Dodd et al., 2017; Jordan et al., 2023; Kanaparthi et al., 2024) or mineral membranes (McMahon, 2019). Lipid synthesis would rely on pathways for phosphorylation, and Fe-oxyhydroxides have been implicated in the hydrolysis of P from organic phosphates (Klein et al., 2024), but a phosphorylation system has also been observed in GR and other mineral systems to form pyrophosphates (Akouche et al., 2017; Barge et al., 2014; Q. Wang et al., 2019). If these polyphosphates could be transferred to the glycolic and amino acid products, then pathways to lipid membrane and nucleotide synthesis would arise from very simple starting conditions. In the functionalization of these membranes, GR and other minerals have been demonstrated to integrate within liposomes (Gaudu et al., 2023), opening the door to the chemiosmotic exploitation (Milshteyn et al., 2019) of proton gradients to do work, a necessary hallmark of life (Nitschke et al., 2022).

This GR protometabolic system would be able to exploit processes inherent to the reactivity of Fe-minerals, such as nitrogen redox. GR is well known to catalyze nitrate and nitrite reduction to ammonia (Barge et al., 2022; Choi et al., 2012; Etique et al., 2014) yet its oxidation from nitrogenous oxides (NO, NO_2^-) to nitromethane, and methylnitrate (Farr, Gaudu, et al., 2023) are poorly constrained and moreover its role in the geochemical cycling of nitrogen has only been recently discussed (Buessecker et al., 2022). These extraordinarily reactive members, precursors to TNT, can readily react to form nitrogen bearing heterocycles, and hypotheses regarding the evolution of nitrogenous nucleotides (Kadyshevich & Ostrovskii, 2023) posit that such compounds led directly to their synthesis over minerals. Heterocycles are known to interface and reduce Fe-minerals (Anschutz & Penn, 2005; Taran, 2017), potentially functioning as anti-oxidant, signaling, or proto-replicative molecules in early GR-protometabolic systems. Genetic or protogenetic replication of these systems could follow from the chiral formation of molecules from mineral surfaces serving as “templates” for future reciprocally-coupled reaction pathways to follow (Carter & Wills, 2021; Rasmussen et al., 2020). As we demonstrated GR’s tendency to form aromatic or potential aromatic compounds, such interactions must be further investigated. Alongside N redox, the plethora of organic and inorganic redox reactions mediated by GR chemistry could serve as possible fuel sources for early protometabolism.

5.6. Synthesizing alkaline vent emergence of life hypotheses with an abiotic Gaia

Here (Figure 5.2) we iterate upon previous alkaline vent hypotheses and connect new findings on the GR carbon redox to a global geochemical perspective (Duval et al., 2019, 2020; W. Martin & Russell, 2007; Nitschke et al., 2024; Trolard et al., 2022).

Situated within a Hadean or Eoarchean hydrothermal vent pore, the interface between cold oxidized acidic seawater and hot alkaline reduced effluent results in the precipitation of dissolved metal ions as silicates, sulfates, sulfide and oxyhydroxide nano- to micro-minerals. Such a network of Fe, Ni, Mg, Zn, Co, Mn, Mo, and W precipitates, loosely bound by intermolecular forces, serve as a semipermeable membrane separating the redox disequilibria inherent to the outside and inner environments (Glaab et al., 2012; Nitschke & Russell, 2009; Q. Wang et al., 2019). Here, green rust goes to work. As a metastable state of iron, green rust comes in and out of existence as suitable pH fronts advance and retreat due to oscillatory variations in pressure at these active sites (Elderfield & Schultz, 1996). GRs transformation to magnetite and goethite due to heat, redox, or oxidation, or to greenalite and vivianite due to Si or P fluxes, yields different pathways for the fate of dissolved cations and anions (Perez et al., 2024; Xiong et al., 2023; Zegeye et al., 2012). Carbon dioxide and nitric oxides dissolved within sea water and methane from the effluent meet this mixed micro-fluidized bed system and are thereby transformed by GR and/or FeS to formate, acetate, malonate, succinate, glycols, and amino acids (Barge et al., 2019; Farr, Gaudu, et al., 2023; Grosch et al., 2022; Hudson et al., 2020; S. Lee et al., 2023). The transport of compounds introduced or produced within the hydrothermal vents rely on the affinity or charge of the mineral species present, which depend on pH. With transformation comes the production of H_2 and radicals, introducing new players in the synthesis and modification of produced or adsorbed species (L. Fang et al., 2021; Z. Li et al., 2022).

The synthesis and accumulation of organic anions and compounds within vent pores would likely lead to the polymerization of amino acids and sugars (Ménez et al., 2018b; Ogasawara et al., 2000; Shanker et al., 2012), thus yielding simple proteinaceous matter. The mineral membranes are thus rendered near impermeable and thereby highly selective as to what can enter and exit these primitive chemical garden-like cells, so influencing the encapsulated reaction networks within (Hazra et al., 2023; D. He et al., 2021; Konn et al., 2009; Mccollom et al., 1999; Purvis et al., 2024). Protons are transported across membranes via green rust interlayers, yielding primitive chemiosmotic systems (Milshteyn et al., 2019; Nitschke & Russell, 2009). Electrons are transported through the semiconducting mineral layers, connecting chemiosmotic reactors distributed throughout the hydrothermal vents via ramified mineral plumbing (Goldman et al., 2023). This vent system that converts NO_3^- and CO_2 into reduced compounds and CH_4 and H_2 into oxidized ones, portending energy metabolism and life – life that emerges spontaneously as a result of geochemical thermodynamic disequilibria.

From these alkaline vents there are possible routes to a biosphere. A “deep” biosphere produced as the first living cells expand downward and laterally into the oceanic crust and sediments where the same minerals occur, though admittedly the flux rates are much reduced (M. J. Russell, 2023; M. J. Russell & Hall, 1997). Alternatively, similar nanocrysts and chemical complexes issue into the ocean where flocs of these same entities reach the surface and are subsequently modified and energized by UV light to living systems. Either way GR reacts with a methane and carbon-rich atmosphere to

produce organic fractions (Ernst et al., 2023; Farr, Gaudu, et al., 2023), including methanol, chloroform, and DMS, with profound implications over the evolution and emergent behavior of global marine, atmospheric, emergent biochemistry. At this point, the story is unfinished and awaits integration into the geochemical and biological literature. Further analysis of mineralogical and isotopic evidence may reveal more clues as to the extent to which this ferruginous ocean interacted with the atmosphere.

In 1974, James Lovelock proposed a startling hypothesis, mooting that the Earth's biosphere self-organizes to produce an emergent self-regulating system known he named Gaia (Lovelock & Margulis, 1974). Assuming this model, the questions arise: how much of this self-regulating condition was present prior to the emergence of life, and at what point was the transition separate from the processes that preceded it? Our work demonstrates the versatility of purely abiotic chemical systems to transform the environment in a manner that beckons towards life.

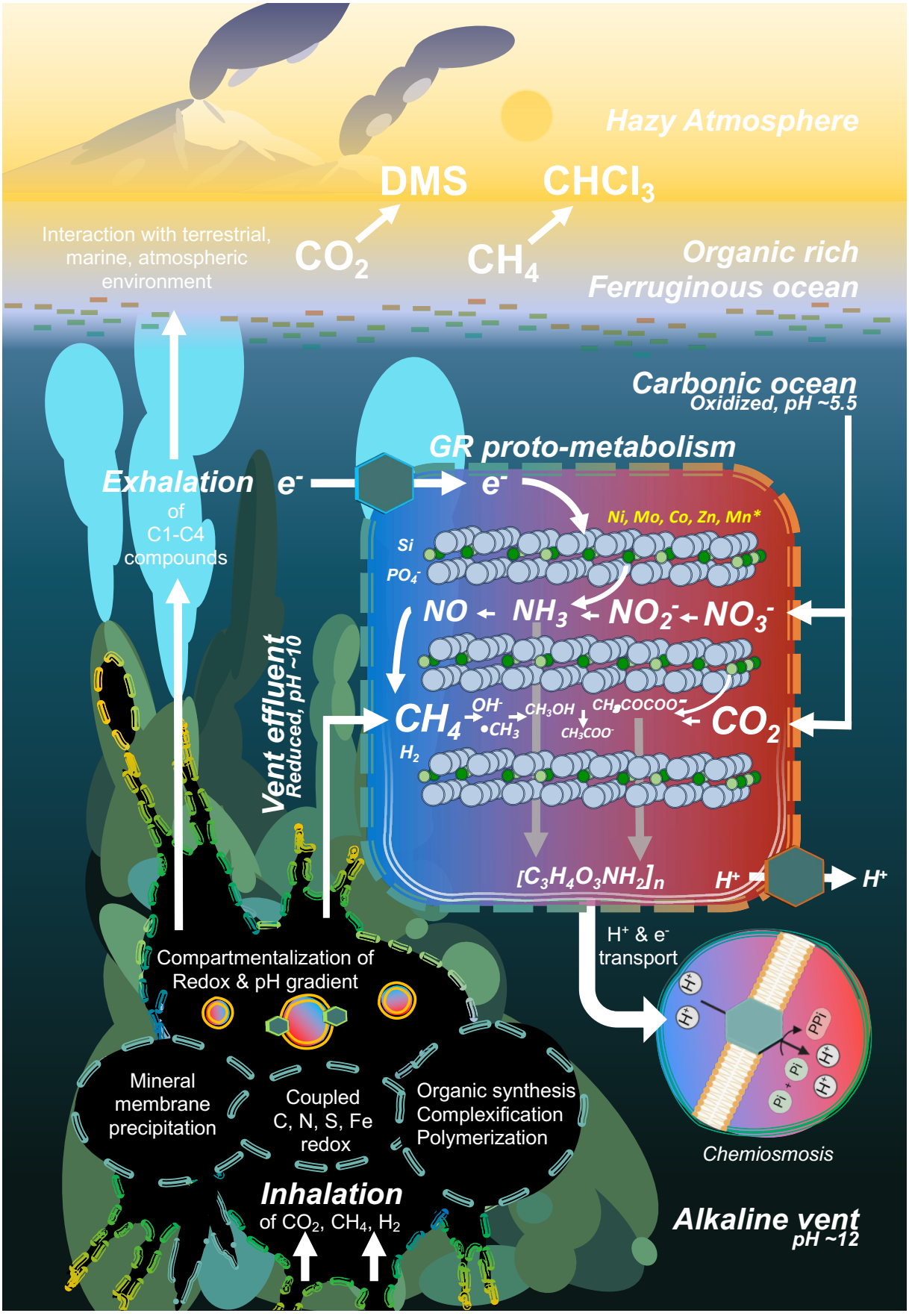

Hazy Atmosphere
DMS
CHCl3
CO2
CH4
Interaction with terrestrial, marine, atmospheric environment
Organic rich Ferruginous ocean
Carbonic ocean
Oxidized, pH ~5.5
GR proto-metabolism
Exhalation
of C1-C4 compounds
e-
e-
Ni, Mo, Co, Zn, Mn*
Si
PO4-
NO ← NH3 ← NO2- ← NO3-
CH4
OH-
•CH3
CH3OH
CH3COCOO-
CH3COO-
CO2
H2
Vent effluent
Reduced, pH ~10
[C3H4O3NH2]n
H+
H+
H+ & e- transport
Compartmentalization of Redox & pH gradient
Mineral membrane precipitation
Coupled C, N, S, Fe redox
Organic synthesis Complexification Polymerization
Inhalation
of CO2, CH4, H2
PPi
Pi
Chemiosmosis
Alkaline vent
pH ~12

Figure 5.2 : An illustrative diagram depicting the various chemical reaction pathways mediated by GR redox chemistry at early hydrothermal vent environments. The *inhalation* of dissolved and gaseous species from serpentization processes naturally leads to redox disequilibria with cold oxidized sea water at these mineral mounds, precipitating reactive mineral species like GR. These minerals conduct C, N, S, Fe redox which leads to the formation of simple organic compounds which complexify and polymerize in high surface area mineral pores. Here GR's particular characteristics, namely anionic transport and organic integration, are shown to cross organic membranes and conduct H+ and e- transport, leading to local disequilibria in a kind of protometabolism. This pH and redox gradient developing into a chemiosmotic system capable of phosphorylation is hypothesized to be necessary for life to emerge (Duval et al., 2019; M. J. Russell, 2023). Beyond this, the products yielded from redox reactions (e.g. DMS, $CHCl_3$) undergo *exhalation* from the vent environment out into the ocean and interact with surface ocean and atmospheric chemistry.

Conclusion

"*Everything is everywhere,* but, *the environment selects*"
Dr. Baas Becking, 1934

In this thesis the characterization, reactivity, and implications of green rust minerals as natural catalysts towards the redox of CO_2 and CH_4 were explored for the first time. We found that these minerals can spontaneously react or be coaxed into reaction with carbon gasses due to distinguishing chemical properties inherent to their multivalent LDH oxyhydroxide structure. GR bears well organized layers of metal cations sandwiching anions allowing it to transfer electrons, anions, and protons to conduct complex redox chemistry. This results in the formation of over 22 compounds when exposed to CH_4 and CO_2 gasses under neutral to alkaline pH. While the production of these various organic species has been described in this work, considerable work remains in the careful elucidation of the mechanisms involved in their formation. However, these initial findings point towards possible reaction pathways that implicate reactive Fe-oxyhydroxide minerals in the cryptic cycling of carbon throughout geochemical history as well as strengthen hypotheses regarding their shepherding role at the origin, or emergence, of life.

I find that this work neatly bridges experimental gaps in the literature concerning the mechanisms by which "prebiotic" chemistry at alkaline vents could have led to the emergence of life. While carbon dioxide and methane are the most relevant gasses to study in contemporary chemistry as they impose great danger due to the greenhouse effect, comparatively little exploration of their redox chemistry has been undertaken using naturally occurring reactive minerals as catalysts under conditions relevant to the early Earth. The relative ease of the spontaneous formation of CO_2 reduction products demonstrated by green rust highlights the utility of simple experiments to provide evidence for more complex hypotheses. Green rust, along with a few other minerals of this category (e.g. mackinawite, gregite, greenalite) lie at the center of various hypotheses related to the origin of life for good measure as their reactivity towards organic compounds and their structural homology with enzymatic reaction centers imply a geochemical origin to life. The systems investigated in this thesis are capable of the redox transformation of all the essential elements for life and are thought to naturally self-organized under ancient environmental conditions.

Further work remains to truly understand how mineral chemistry transitioned into biochemistry. Promising avenues opened by this work are the modification and optimization of carbon redox through the tuning of environmental conditions (e.g., pressure, irradiation, aqueous chemistry), the implementation of catalytic transition metals into the structure of green rust, situating mineral membranes along concentration, thermal, pH, and redox gradients, and the in-situ monitoring of solution chemistry during reactions. Additional field exploration of extant and fossil hydrothermal vents as well as

the careful interpretation of geochemical signatures within the rock record may reveal clues as to the former presence of green rust or related primary mineral phases prior to diagenesis. These records are not limited to Earth as hydrothermal activity is thought to occur on Mars, Ceres, Europa, Enceladus, and many other icy bodies within our solar system. The discovery of such systems would imply a universal nature to the emergence of life mediated by reactive mineral chemistry along redox gradients.

Bibliography

Agnel, M. I., Grangeon, S., Fauth, F., Elkaïm, E., Claret, F., Roulet, M., Warmont, F., & Tournassat, C. (2020). Mechanistic and Thermodynamic Insights into Anion Exchange by Green Rust. *Environmental Science and Technology*, *54*(2), 851–861. https://doi.org/10.1021/acs.est.9b05632

Ai, J., Chr. Bruun Hansen, H., Dideriksen, K., & Tobler, D. J. (2022). Fine-tuning green rust – bone char composite synthesis for efficient chlorinated ethylene remediation. *Chemical Engineering Journal*, *446*. https://doi.org/10.1016/j.cej.2022.136770

Akouche, M., Jaber, M., Maurel, M. C., Lambert, J. F., & Georgelin, T. (2017). Phosphoribosyl Pyrophosphate: A Molecular Vestige of the Origin of Life on Minerals. *Angewandte Chemie - International Edition*, *56*(27), 7920–7923. https://doi.org/10.1002/anie.201702633

Al-Abadleh, H. A. (2015). Review of the bulk and surface chemistry of iron in atmospherically relevant systems containing humic-like substances. In *RSC Advances* (Vol. 5, Issue 57, pp. 45785–45811). Royal Society of Chemistry. https://doi.org/10.1039/c5ra03132j

Aleksandrova, M., Rahmatova, F., Russell, D. A., & Bonfio, C. (2023). Ring Opening of Glycerol Cyclic Phosphates Leads to a Diverse Array of Potentially Prebiotic Phospholipids. *Journal of the American Chemical Society*, *145*(47), 25614–25620. https://doi.org/10.1021/jacs.3c07319

Alshehri, A. (2013). Methanol oxidation on transition elements oxides. *PhD Thesis - Cardiff University*. http://ethos.bl.uk/OrderDetails.do?uin=uk.bl.ethos.571733

Anipsitakis, G. P., & Dionysiou, D. D. (2004). Radical Generation by the Interaction of Transition Metals with Common Oxidants. *Environmental Science & Technology*, *38*(13), 3705–3712. https://doi.org/10.1021/es035121o

Anschutz, A. J., & Penn, R. L. (2005). Reduction of crystalline iron(III) oxyhydroxides using hydroquinone: Influence of phase and particle size. *Geochemical Transactions*, *6*(3), 60–66. https://doi.org/10.1063/1.2037887

Antony, H., Legrand, L., & Chaussé, A. (2008). Carbonate and sulphate green rusts-Mechanisms of oxidation and reduction. *Electrochimica Acta*, *53*(24), 7146–7156. https://doi.org/10.1016/j.electacta.2008.05.008

Arney, G., Domagal-Goldman, S. D., Meadows, V. S., Wolf, E. T., Schwieterman, E., Charnay, B., Claire, M., Hébrard, E., & Trainer, M. G. (2016). The Pale Orange Dot: The Spectrum and Habitability of Hazy Archean Earth. *Astrobiology*, *16*(11), 873–899. https://doi.org/10.1089/ast.2015.1422

Arrhenius, G. O. (2003). Crystals and life. *Helvetica Chimica Acta*, *86*(5), 1569–1586. https://doi.org/10.1002/hlca.200390135

Ayala-Luis, K. B., Koch, B. C., & Hansen, H. C. B. (2008). The standard gibbs energy of formation of Fe(II)Fe(III) hydroxide sulfate green rust. *Clays and Clay Minerals*, *56*(6), 633–644. https://doi.org/10.1346/CCMN.2008.0560604

Ayala-Luis, K. B., Koch, C. B., & Hansen, H. C. B. (2010). One-pot synthesis and characterization of FeII-FeIII hydroxide (green rust) intercalated with C9-C14 linear alkyl carboxylates. *Applied Clay Science*, *50*(4), 512–519. https://doi.org/10.1016/j.clay.2010.10.002

Babakhani, P., Phenrat, T., Baalousha, M., Soratana, K., Peacock, C. L., Twining, B. S., & Hochella, M. F. (2022). Potential use of engineered nanoparticles in ocean fertilization for large-scale atmospheric carbon dioxide removal. *Nature Nanotechnology*, *17*(12), 1342–1351. https://doi.org/10.1038/s41565-022-01226-w

Bahlmann, E., Keppler, F., Wittmer, J., Greule, M., Schöler, H. F., Seifert, R., & Zetzsch, C. (2019). Evidence for a major missing source in the global chloromethane budget from stable carbon isotopes. *Atmospheric Chemistry and Physics*, *19*(3), 1703–1719. https://doi.org/10.5194/acp-19-1703-2019

Banerjee, R., Proshlyakov, Y., Lipscomb, J. D., & Proshlyakov, D. A. (2015). Structure of the key species in the enzymatic oxidation of methane to methanol. *Nature*, *518*(7539), 431–434. https://doi.org/10.1038/nature14160

Barge, L. M., Doloboff, I. J., Russell, M. J., Vandervelde, D., White, L. M., Stucky, G. D., Baum, M. M., Zeytounian, J., Kidd, R., & Kanik, I. (2014). ScienceDirect Pyrophosphate synthesis in iron mineral films and membranes simulating prebiotic submarine hydrothermal precipitates. *Geochimica et Cosmochimica Acta*, *128*, 1–12. https://doi.org/10.1016/j.gca.2013.12.006

Barge, L. M., Flores, E., Baum, M. M., Velde, D. G. V., & Russell, M. J. (2019). Redox and pH gradients drive amino acid synthesis in iron oxyhydroxide mineral systems. *Proceedings of the National Academy of Sciences of the United States of America*, *116*(11), 4828–4833. https://doi.org/10.1073/pnas.1812098116

Barge, L. M., Flores, E., Weber, J. M., Fraeman, A. A., Yung, Y. L., VanderVelde, D., Martinez, E., Castonguay, A., Billings, K., & Baum, M. M. (2022). Prebiotic reactions in a Mars analog iron mineral system: Effects of nitrate, nitrite, and ammonia on amino acid formation. *Geochimica et Cosmochimica Acta*, *336*, 469–479. https://doi.org/10.1016/j.gca.2022.08.038

Bearcock, J. M., Perkins, W. T., & Pearce, N. J. G. (2011). Laboratory studies using naturally occurring "green rust" to aid metal mine water remediation. *Journal of Hazardous Materials*, *190*(1–3), 466–473. https://doi.org/10.1016/j.jhazmat.2011.03.074

Beyazay, T., Belthle, K. S., Farès, C., Preiner, M., Moran, J., Martin, W. F., & Tüysüz, H. (2023). Ambient temperature CO2 fixation to pyruvate and subsequently to citramalate over iron and nickel nanoparticles. *Nature Communications*, *14*(1), 570. https://doi.org/10.1038/s41467-023-36088-w

Bigham, J. M., Fitzpatrick, R. W., & Schulze, D. G. (2018). *Iron Oxides* (pp. 323–366). https://doi.org/10.2136/sssabookser7.c10

Bocher, F., Géhin, A., Ruby, C., Ghanbaja, J., Abdelmoula, M., & Génin, J. M. R. (2004). Coprecipitation of Fe(II-III) hydroxycarbonate green rust stabilised by phosphate adsorption. *Solid State Sciences*, *6*(1), 117–124. https://doi.org/10.1016/j.solidstatesciences.2003.10.004

Bolhar, R., Kamber, B. S., Moorbath, S., Fedo, C. M., & Whitehouse, M. J. (2004). Characterisation of early Archaean chemical sediments by trace element signatures. *Earth and Planetary Science Letters*, *222*(1), 43–60. https://doi.org/10.1016/j.epsl.2004.02.016

Borrego-Sánchez, A., Gutiérrez-Ariza, C., Sainz-Díaz, C. I., & Cartwright, J. H. E. (2022). The Effect of the Presence of Amino Acids on the Precipitation of Inorganic Chemical-Garden Membranes: Biomineralization at the Origin of Life. *Langmuir*, *38*(34), 10538–10547. https://doi.org/10.1021/acs.langmuir.2c01345

Bourrié, G., Ben Nacib, J., Ona-Nguema, G., & Trolard, F. (2019). *Absence of solid solution between Fe(II) and Mg(II) hydroxides and consequences on formation of fougerite and smectites; Absence of solid solution between Fe(II) and Mg(II) hydroxides and consequences on formation of fougerite and smectites*. 98. https://doi.org/10.1051/e3sconf/20199804003ï

Brandes, J. A., Boctor, N. Z., Cody, G. D., Cooper, B. A., Hazen, R. M., & Yoder, H. S. (1998). Abiotic nitrogen reduction on the early Earth. *Nature*, *395*(6700), 365–367. https://doi.org/10.1038/26450

Branscomb, E., & Russell, M. J. (2018). Frankenstein or a Submarine Alkaline Vent: Who is Responsible for Abiogenesis?: Part 2: As life is now, so it must have been in the beginning. In *BioEssays* (Vol. 40, Issue 8). John Wiley and Sons Inc. https://doi.org/10.1002/bies.201700182

Buessecker, S., Imanaka, H., Ely, T., Hu, R., Romaniello, S. J., & Cadillo-Quiroz, H. (2022). Mineral-catalysed formation of marine NO and N2O on the anoxic early Earth. *Nature Geoscience*, *15*(12), 1056–1063. https://doi.org/10.1038/s41561-022-01089-9

Burcar, B. T., Barge, L. M., Trail, D., Watson, E. B., Russell, M. J., & McGown, L. B. (2015). RNA Oligomerization in Laboratory Analogues of Alkaline Hydrothermal Vent Systems. *Astrobiology*, *15*(7), 509–522. https://doi.org/10.1089/ast.2014.1280

Bushaw-Newton, K. L., & Moran, M. A. (1999). *Photochemical formation of biologically available nitrogen from dissolved humic substances in coastal marine systems* (Vol. 18).

Calvin, K., Dasgupta, D., Krinner, G., Mukherji, A., Thorne, P. W., Trisos, C., Romero, J., Aldunce, P., Barrett, K., Blanco, G., Cheung, W. W. L., Connors, S., Denton, F., Diongue-Niang, A., Dodman, D., Garschagen, M., Geden, O., Hayward, B., Jones, C., … Ha, M. (2023). *IPCC, 2023: Climate Change 2023: Synthesis Report. Contribution of Working Groups I, II and III to the Sixth Assessment Report of the Intergovernmental Panel on Climate Change [Core Writing Team, H. Lee and J. Romero (eds.)]. IPCC, Geneva, Switzerland.* https://doi.org/10.59327/IPCC/AR6-9789291691647

Camprubi, E., Jordan, S. F., Vasiliadou, R., & Lane, N. (2017). Iron catalysis at the origin of life. *IUBMB Life*, *69*(6), 373–381. https://doi.org/10.1002/iub.1632

Carter, C. W., & Wills, P. R. (2021). Reciprocally-coupled gating: Strange loops in bioenergetics, genetics, and catalysis. In *Biomolecules* (Vol. 11, Issue 2, pp. 1–22). MDPI AG. https://doi.org/10.3390/biom11020265

Catling, D. C., & Zahnle, K. J. (2020). The Archean atmosphere. *Science Advances*, *6*(9). https://doi.org/10.1126/sciadv.aax1420

Charlson, R. J., Lovelockt, J. E., & Warren, S. G. (1987). *Oceanic phytoplankton, atmospheric sulphur, cloud albedo and climate*.

Chaves, L. H. G., Curry, J. E., Stone, D. A., Carducci, M. D., & Chorover, J. (2009). Nickel incorporation in Fe(II, III) hydroxysulfate Green Rust: effect on crystal lattice spacing and oxidation products. *Revista Brasileira de Ciência Do Solo*, *33*(5), 1115–1123. https://doi.org/10.1590/s0100-06832009000500005

Chen, N., Geng, M., Huang, D., Tan, M., Li, Z., Liu, G., Zhu, C., Fang, G., & Zhou, D. (2022). Hydroxyl radical formation during oxygen-mediated oxidation of ferrous iron on mineral surface: Dependence on mineral identity. *Journal of Hazardous Materials*, *434*. https://doi.org/10.1016/j.jhazmat.2022.128861

Chen, Y., Gao, S., Liu, Z., Shao, S., Yin, W., Fang, Z., & Huang, L. Z. (2019). Prolonged persulfate activation by UV irradiation of green rust for the degradation of organic pollutants. *Environmental Chemistry Letters*, *17*(2), 1017–1021. https://doi.org/10.1007/s10311-018-0815-7

Chistoserdova, L., Vorholt, J. A., Thauer, R. K., & Lidstrom, M. E. (1998). C1 Transfer Enzymes and Coenzymes Linking Methylotrophic Bacteria and Methanogenic Archaea. *Science*, *281*(5373), 99–102. https://doi.org/10.1126/science.281.5373.99

Choi, J., Batchelor, B., Won, C., & Chung, J. (2012). Nitrate reduction by green rusts modified with trace metals. *Chemosphere*, *86*(8), 860–865. https://doi.org/10.1016/j.chemosphere.2011.11.035

Choi, J., & Lee, W. (2008). Enhanced degradation of tetrachloroethylene by green rusts with platinum. *Environmental Science and Technology*, *42*(9), 3356–3362. https://doi.org/10.1021/es702661d

Clarke, A. (2014). The thermal limits to life on Earth. *International Journal of Astrobiology*, *13*(2), 141–154. https://doi.org/10.1017/S1473550413000438

Comba, P., Kerscher, M., Krause, T., & Schöler, H. F. (2015). Iron-catalysed oxidation and halogenation of organic matter in nature. In *Environmental Chemistry* (Vol. 12, Issue 4, pp. 381–395). CSIRO. https://doi.org/10.1071/EN14240

de Graaf, R., De Decker, Y., Sojo, V., & Hudson, R. (2023). Quantifying Catalysis at the Origin of Life**. *Chemistry - A European Journal*, *29*(53). https://doi.org/10.1002/chem.202301447

De Graaf, R., Yannick,], Decker, D., Sojo, V., & Hudson, R. (2023). *Quantifying Catalysis at the Origin of Life***. https://doi.org/10.26434/chemrxiv-2022-xhmzj

Dionigi, F., Zeng, Z., Sinev, I., Merzdorf, T., Deshpande, S., Lopez, M. B., Kunze, S., Zegkinoglou, I., Sarodnik, H., Fan, D., Bergmann, A., Drnec, J., Araujo, J. F. de, Gliech, M., Teschner, D., Zhu, J., Li, W. X., Greeley, J., Roldan Cuenya, B., & Strasser, P. (2020). In-situ structure and catalytic mechanism of NiFe and CoFe layered double hydroxides during oxygen evolution. *Nature Communications*, *11*(1). https://doi.org/10.1038/s41467-020-16237-1

Doane, T. A. (2017). The Abiotic Nitrogen Cycle. *ACS Earth and Space Chemistry*, *1*(7), 411–421. https://doi.org/10.1021/acsearthspacechem.7b00059

Dodd, M. S., Papineau, D., Grenne, T., Slack, J. F., Rittner, M., Pirajno, F., O'Neil, J., & Little, C. T. S. (2017). Evidence for early life in Earth's oldest hydrothermal vent precipitates. *Nature*, *543*(7643), 60–64. https://doi.org/10.1038/nature21377

Dodd, M. S., Papineau, D., She, Z. B., Manikyamba, C., Wan, Y. S., O'Neil, J., Karhu, J. A., Rizo, H., & Pirajno, F. (2019). Widespread occurrences of variably crystalline 13 C-depleted graphitic carbon in banded iron formations. *Earth and Planetary Science Letters*, *512*, 163–174. https://doi.org/10.1016/j.epsl.2019.01.054

Dodd, M. S., Wang, H., Li, C., Towner, M., Thomson, A. R., Slack, J. F., Wan, Y. sheng, Pirajno, F., Manikyamba, C., Wang, Q., & Papineau, D. (2022). Abiotic anoxic iron oxidation, formation of Archean banded iron formations, and the oxidation of early Earth. *Earth and Planetary Science Letters*, *584*. https://doi.org/10.1016/j.epsl.2022.117469

Domagal-Goldman, S. D., Meadows, V. S., Claire, M. W., & Kasting, J. F. (2011). Using biogenic sulfur gases as remotely detectable biosignatures on anoxic planets. *Astrobiology*, *11*(5), 419–441. https://doi.org/10.1089/ast.2010.0509

Døssing, L. N., Dideriksen, K., Stipp, S. L. S., & Frei, R. (2011). Reduction of hexavalent chromium by ferrous iron: A process of chromium isotope fractionation and its relevance to natural environments. *Chemical Geology*, *285*(1–4), 157–166. https://doi.org/10.1016/j.chemgeo.2011.04.005

Du, X., Guang, W., Cheng, Y., Hou, Z., Liu, Z., Yin, H., Huo, L., Lei, R., & Shu, C. (2020). Thermodynamics analysis of the adsorption of CH4 and CO2 on montmorillonite. *Applied Clay Science*, *192*. https://doi.org/10.1016/j.clay.2020.105631

Duan, Z., Møller, N., Greenberg, J., & Weare, J. H. (1992). The prediction of methane solubility in natural waters to high ionic strength from 0 to 250°C and from 0 to 1600 bar. *Geochimica et Cosmochimica Acta*, *56*(4), 1451–1460. https://doi.org/10.1016/0016-7037(92)90215-5

Ducluzeau, A. L., van Lis, R., Duval, S., Schoepp-Cothenet, B., Russell, M. J., & Nitschke, W. (2009). Was nitric oxide the first deep electron sink? *Trends in Biochemical Sciences*, *34*(1), 9–15. https://doi.org/10.1016/j.tibs.2008.10.005

Dummer, N. F., Willock, D. J., He, Q., Howard, M. J., Lewis, R. J., Qi, G., Taylor, S. H., Xu, J., Bethell, D., Kiely, C. J., & Hutchings, G. J. (2023). Methane Oxidation to Methanol. *Chemical Reviews*, *123*(9), 6359–6411. https://doi.org/10.1021/acs.chemrev.2c00439

Duval, S., Baymann, F., Schoepp-Cothenet, B., Trolard, F., Bourrié, G., Grauby, O., Branscomb, E., Russell, M. J., & Nitschke, W. (2019). Fougerite: The not so simple progenitor of the first cells. *Interface Focus*, *9*(6), 16–20. https://doi.org/10.1098/rsfs.2019.0063

Duval, S., Branscomb, E., Trolard, F., Bourrié, G., Grauby, O., Heresanu, V., Schoepp-Cothenet, B., Zuchan, K., Russell, M. J., & Nitschke, W. (2020). On the why's and how's of clay minerals' importance in life's emergence. *Applied Clay Science*, *195*, 105737. https://doi.org/10.1016/j.clay.2020.105737

Dziejarski, B., Krzyżyńska, R., & Andersson, K. (2023). Current status of carbon capture, utilization, and storage technologies in the global economy: A survey of technical assessment. *Fuel*, *342*. https://doi.org/10.1016/j.fuel.2023.127776

Egea-González, I., Mckay, C. P., Hallsworth, J. E., Jiménez-Díaz, A., & Ruiz, J. (2024). Ammonia or methanol would enable subsurface liquid water in the Martian South Pole Antifreeze and liquid water on Mars. *RXiv*.

Elderfield, H., & Schultz, A. (1996). Mid-ocean ridge hydrothermal fluxes and the chemical composition of the ocean. *Annual Review of Earth & Planetary Sciences*, *24*, 191–224. https://doi.org/10.1146/annurev.earth.24.1.191

Erbs, M., Hansen, H. C. B., & Olsen, C. E. (1999). Reductive dechlorination of carbon tetrachloride using iron(II) iron(III) hydroxide sulfate (green rust). *Environmental Science and Technology*, *33*(2), 307–311. https://doi.org/10.1021/es980221t

Ernst, L., Barayeu, U., Hädeler, J., Dick, T. P., Klatt, J. M., Keppler, F., & Rebelein, J. G. (2023). Methane formation driven by light and heat prior to the origin of life and beyond. *Nature Communications*, *14*(1), 4364. https://doi.org/10.1038/s41467-023-39917-0

Etique, M., Zegeye, A., Grégoire, B., Carteret, C., & Ruby, C. (2014). Nitrate reduction by mixed iron(II-III) hydroxycarbonate green rust in the presence of phosphate anions: The key parameters influencing the ammonium selectivity. *Water Research*, *62*(May 2014), 29–39. https://doi.org/10.1016/j.watres.2014.05.028

Falkowski, P. (2015). *Life's Engines: How Microbes Made Earth Habitable*. Princeton University Press.

Falkowski, P. G., Fenchel, T., & Delong, E. F. (2008). The microbial engines that drive earth's biogeochemical cycles. In *Science* (Vol. 320, Issue 5879, pp. 1034–1039). https://doi.org/10.1126/science.1153213

Falkowski, P., Scholes, ; R J, Boyle, ; E, Canadell, ; J, Canfield, ; D, Elser, ; J, Gruber, ; N, Hibbard, ; K, Högberg, ; P, Linder, ; S, Mackenzie, ; F T, Iii, ; B Moore, Pedersen, ; T, Rosenthal, Y., Seitzinger, ; S, Smetacek, ; V, & Steffen, ; W. (2000). The Global Carbon Cycle: A Test of Our Knowledge of Earth as a System. In *New Series* (Vol. 290, Issue 5490).

Fan, Y., Wei, K., Jin, B., & Liang, Z. (2024). In-situ metal doping to boost the reactivity of layered double hydroxide derived Mg-Fe-Al-O oxygen carriers for chemical looping CH4 reforming with CO2 reduction. *Chemical Engineering Science*, *298*, 120347. https://doi.org/10.1016/j.ces.2024.120347

Fang, L., Xu, L., Deng, J., Gao, S., & Huang, L. Z. (2021). Induced generation of hydroxyl radicals from green rust under oxic conditions by iron-phosphate complexes. *Chemical Engineering Journal*, *414*(November 2020), 128780. https://doi.org/10.1016/j.cej.2021.128780

Fang, S., & Hu, Y. H. (2022). Temperature, pressure, and adsorption-dependent redox potentials: I. Processes of CO2 reduction to value-added compounds. *Energy Science and Engineering*, *10*(12), 4520–4543. https://doi.org/10.1002/ese3.1287

Fang, S., & Hu, Y. H. (2023). Temperature, pressure, and adsorption-dependent redox potentials: Ⅱ. Processes of CH4 oxidation to value-added compounds. *Energy Science and Engineering*, *11*(2), 762–782. https://doi.org/10.1002/ese3.1361

Farquhar, J., Bao, H., & Thiemens, M. (2000). Atmospheric influence of Earth's earliest sulfur cycle. *Science*, *289*(5480), 756–758. https://doi.org/10.1126/science.289.5480.756

Farr, O., Elzinga, E. J., & Yee, N. (2022). Effect of Ni2+, Zn2+, and Co2+ on green rust transformation to magnetite. *Geochemical Transactions*, *23*(1), 3. https://doi.org/10.1186/s12932-022-00080-y

Farr, O., Gaudu, N., Danger, G., Russell, M. J., Ferry, D., Nitschke, W., & Duval, S. (2023). Methanol on the rocks: green rust transformation promotes the oxidation of methane. *Journal of The Royal Society Interface*, *20*(206). https://doi.org/10.1098/rsif.2023.0386

Farr, O., Hao, J., Liu, W., Fehon, N., Reinfelder, J. R., Yee, N., & Falkowski, P. G. (2023). Archean phosphorus recycling facilitated by ultraviolet radiation. *Proceedings of the National Academy of Sciences of the United States of America*, *120*(30). https://doi.org/10.1073/pnas.2307524120

Fielding, A. J., Singh, R., Boscolo, B., Loewen, P. C., Ghibaudi, E. M., & Ivancich, A. (2008). Intramolecular Electron Transfer versus Substrate Oxidation in Lactoperoxidase: Investigation of Radical Intermediates by Stopped-Flow Absorption Spectrophotometry and (9−285 GHz) Electron Paramagnetic Resonance Spectroscopy. *Biochemistry*, *47*(37), 9781–9792. https://doi.org/10.1021/bi801032k

François, L. M. (1987). Reducing power of ferrous iron in the Archean Ocean, 2. Role of FEOH + photooxidation. *Paleoceanography*, *2*(4), 395–408. https://doi.org/10.1029/PA002i004p00395

Frey, P. A., & Reed, G. H. (2012). The ubiquity of iron. In *ACS Chemical Biology* (Vol. 7, Issue 9, pp. 1477–1481). https://doi.org/10.1021/cb300323q

Friese, A., Bauer, K., Glombitza, C., Ordoñez, L., Ariztegui, D., Heuer, V. B., Vuillemin, A., Henny, C., Nomosatryo, S., Simister, R., Wagner, D., Bijaksana, S., Vogel, H., Melles, M., Russell, J. M., Crowe, S. A., & Kallmeyer, J. (2021). Organic matter mineralization in modern and ancient ferruginous sediments. *Nature Communications*, *12*(1). https://doi.org/10.1038/s41467-021-22453-0

Fubini, B., Mollo, L., & Giamello, E. (1995). Free radical generation at the solid/liquid interface in iron containing minerals. *Free Radical Research*, *23*(6), 593–614. https://doi.org/10.3109/10715769509065280

García-Prieto, A., Alonso, J., Muñoz, D., Marcano, L., Abad Díaz De Cerio, A., Fernández De Luis, R., Orue, I., Mathon, O., Muela, A., & Fdez-Gubieda, M. L. (2016). On the mineral core of ferritin-like proteins: Structural and magnetic characterization. *Nanoscale*, *8*(2), 1088–1099. https://doi.org/10.1039/c5nr04446d

Gaudu, N., Farr, O., Ona-Nguema, G., & Duval, S. (2023). Dissolved metal ions and mineral-liposome hybrid systems: Underlying interactions, synthesis, and characterization. In *Biochimie* (Vol. 215, pp. 100–112). Elsevier B.V. https://doi.org/10.1016/j.biochi.2023.09.009

Gauger, T., Konhauser, K., & Kappler, A. (2015). Protection of phototrophic iron(II)-oxidizing bacteria from UV irradiation by biogenic iron(III) minerals: Implications for early archean banded iron formation. *Geology*, *43*(12), 1067–1070. https://doi.org/10.1130/G37095.1

Geisberger, T., Diederich, P., Steiner, T., Eisenreich, W., Schmitt-Kopplin, P., & Huber, C. (2019). Evolutionary steps in the analytics of primordial metabolic evolution. *Life*, *9*(2). https://doi.org/10.3390/life9020050

Génin, J. M. R., Aïssa, R., Géhin, A., Abdelmoula, M., Benali, O., Ernstsen, V., Ona-Nguema, G., Upadhyay, C., & Ruby, C. (2005). Fougerite and FeII-III hydroxycarbonate green rust; Ordering, deprotonation and/or cation substitution; Structure of hydrotalcite-like compounds and mythic ferrosic hydroxide Fe(OH)(2+x). *Solid State Sciences*, *7*(5), 545–572. https://doi.org/10.1016/j.solidstatesciences.2005.02.001

Génin, J.-M. R., Refait, P., Bourrié, G., Abdelmoula, M., & Trolard, F. (2001). Structure and stability of the Fe(II)–Fe(III) green rust "fougerite" mineral and its potential for reducing pollutants in soil solutions. *Applied Geochemistry*, *16*(5), 559–570. https://doi.org/10.1016/S0883-2927(00)00043-3

Glaab, F., Kellermeier, M., Kunz, W., Morallon, E., & García-Ruiz, J. M. (2012). Formation and Evolution of Chemical Gradients and Potential Differences Across Self-Assembling Inorganic Membranes. *Angewandte Chemie International Edition*, *51*(18), 4317–4321. https://doi.org/10.1002/anie.201107754

Gledhiir, M., & Buck, K. N. (2012). The organic complexation of iron in the marine environment: A review. *Frontiers in Microbiology*, *3*(FEB). https://doi.org/10.3389/fmicb.2012.00069

Goldman, A. D., Weber, J. M., LaRowe, D. E., & Barge, L. M. (2023). Electron transport chains as a window into the earliest stages of evolution. *Proceedings of the National Academy of Sciences of the United States of America*, *120*(34). https://doi.org/10.1073/pnas.2210924120

Grégoire, B., Erastova, V., Geatches, D. L., Clark, S. J., Greenwell, H. C., & Fraser, D. G. (2016). Insights into the behaviour of biomolecules on the early Earth: The concentration of aspartate by layered double hydroxide minerals. *Geochimica et Cosmochimica Acta*, *176*, 239–258. https://doi.org/10.1016/j.gca.2015.12.026

Grégoire, B., Greenwell, H. C., & Fraser, D. G. (2018). Peptide Formation on Layered Mineral Surfaces: The Key Role of Brucite-like Minerals on the Enhanced Formation of Alanine Dipeptides. *ACS Earth and Space Chemistry*, *2*(8), 852–862. https://doi.org/10.1021/acsearthspacechem.8b00052

Grosch, M., Stiebritz, M. T., Bolney, R., Winkler, M., Jückstock, E., Busch, H., Peters, S., Siegle, A. F., van Slageren, J., Ribbe, M., Hu, Y., Trapp, O., Robl, C., & Weigand, W. (2022). Mackinawite-Supported Reduction of C 1 Substrates into Prebiotically Relevant Precursors . *ChemSystemsChem*, *4*(5). https://doi.org/10.1002/syst.202200010

Gueguen, B., Sorensen, J. V., Lalonde, S. V., Peña, J., Toner, B. M., & Rouxel, O. (2018). Variable Ni isotope fractionation between Fe-oxyhydroxides and implications for the use of Ni isotopes as geochemical tracers. *Chemical Geology*, *481*(November 2017), 38–52. https://doi.org/10.1016/j.chemgeo.2018.01.023

Guilbaud, R., Poulton, S. W., Butterfield, N. J., Zhu, M., & Shields-Zhou, G. A. (2015). A global transition to ferruginous conditions in the early Neoproterozoic oceans. *Nature Geoscience*, *8*(6), 466–470. https://doi.org/10.1038/NGEO2434

Guilbaud, R., White, M. L., & Poulton, S. W. (2013). Surface charge and growth of sulphate and carbonate green rust in aqueous media. *Geochimica et Cosmochimica Acta*, *108*, 141–153. https://doi.org/10.1016/j.gca.2013.01.017

Guo, Z., Papineau, D., O'Neil, J., Rizo, H., Chen, Z.-Q., Qiu, X., & She, Z. (2024). Abiotic synthesis of graphitic carbons in the Eoarchean Saglek-Hebron metasedimentary rocks. *Nature Communications*, *15*(1), 5679. https://doi.org/10.1038/s41467-024-50134-1

Gutierrez-Rus, L. I., Gamiz-Arco, G., Gavira, J. A., Gaucher, E. A., Risso, V. A., & Sanchez-Ruiz, J. M. (2023). Protection of Catalytic Cofactors by Polypeptides as a Driver for the Emergence of Primordial Enzymes. *Molecular Biology and Evolution*, *40*(6). https://doi.org/10.1093/molbev/msad126

Hädeler, J., Velmurugan, G., Lauer, R., Radhamani, R., Keppler, F., & Comba, P. (2023). Natural Abiotic Iron-Oxido-Mediated Formation of C_1 and C_2 Compounds from Environmentally Important Methyl-Substituted Substrates. *Journal of the American Chemical Society*. https://doi.org/10.1021/jacs.3c06709

Halevy, I., Alesker, M., Schuster, E. M., Popovitz-Biro, R., & Feldman, Y. (2017). A key role for green rust in the Precambrian oceans and the genesis of iron formations. *Nature Geoscience*, *10*(2), 135–139. https://doi.org/10.1038/ngeo2878

Halevy, I., & Bachan, A. (2017). The geologic history of seawater pH. *Science*, *355*(6329), 1069–1071. https://doi.org/10.1126/science.aal4151

Hanna, K., Kone, T., & Ruby, C. (2010). Fenton-like oxidation and mineralization of phenol using synthetic Fe(II)-Fe(III) green rusts. *Environmental Science and Pollution Research*, *17*(1), 124–134. https://doi.org/10.1007/s11356-009-0148-y

Hanni, N., Altwegg, K., Muller, D., Rubin, M., & Wampfler, S. (2024). Is dimethylsulfide a good biomarker? *EGU General Assembly 2024*, 14–19.

Hao, J., Knoll, A. H., Huang, F., Hazen, R. M., & Daniel, I. (2020). Cycling phosphorus on the Archean Earth: Part I. Continental weathering and riverine transport of phosphorus. *Geochimica et Cosmochimica Acta*, *273*(January), 70–84. https://doi.org/10.1016/j.gca.2020.01.027

Hao, J., Knoll, A., Huang, F., Schieber, J., Hazen, R., & Daniel, I. (2020). *Phosphorus Limitation on Primary Production in Archean Ecosystems*. 955–955. https://doi.org/10.46427/gold2020.955

Hao, J., Liu, W., Goff, J. L., Steadman, J. A., Large, R. R., Falkowski, P. G., & Yee, N. (2022). Anoxic photochemical weathering of pyrite on Archean continents. In *Sci. Adv* (Vol. 8). https://www.science.org

Hao, J., Sverjensky, D. A., & Hazen, R. M. (2017). Mobility of nutrients and trace metals during weathering in the late Archean. *Earth and Planetary Science Letters*, *471*, 148–159. https://doi.org/10.1016/j.epsl.2017.05.003

Hao, J., Sverjensky, D. A., & Hazen, R. M. (2019). Redox states of Archean surficial environments: The importance of H2,g instead of O2,g for weathering reactions. *Chemical Geology*, *521*(October 2018), 49–58. https://doi.org/10.1016/j.chemgeo.2019.05.022

Hazen, R. M., & Sverjensky, D. A. (2010). Mineral surfaces, geochemical complexities, and the origins of life. *Cold Spring Harbor Perspectives in Biology*, *2*(5), 1–21. https://doi.org/10.1101/cshperspect.a002162

Hazen, R. M., Sverjensky, D. A., Azzolini, D., Bish, D. L., Elmore, S. C., Hinnov, L., & Milliken, R. E. (2013). Clay mineral evolution. *American Mineralogist*, *98*(11–12), 2007–2029. https://doi.org/10.2138/am.2013.4425

Hazra, B., Prasad, M., Das, S., Mandal, R., Sardar, A., Dewangan, N., & Tarafdar, P. K. (2023). Phosphate-Based Amphiphile and Lipidated Lysine Assemble into Superior Protocellular Membranes over Carboxylate and Sulfate-Based Systems: A Potential Missing Link between Prebiotic and the Modern Era? *Langmuir*, *39*(48), 17031–17042. https://doi.org/10.1021/acs.langmuir.3c01617

He, D., Wang, X., Yang, Y., He, R., Zhong, H., Wang, Y., & Han, B. (2021). *Hydrothermal synthesis of long-chain hydrocarbons up to C 24 with NaHCO 3 -assisted stabilizing cobalt*. 1–7. https://doi.org/10.1073/pnas.2115059118/-/DCSupplemental.Published

He, H., Wu, X., Xian, H., Zhu, J., Yang, Y., Lv, Y., Li, Y., & Konhauser, K. O. (2021). An abiotic source of Archean hydrogen peroxide and oxygen that pre-dates oxygenic photosynthesis. *Nature Communications*, *12*(1). https://doi.org/10.1038/s41467-021-26916-2

He, H., Wu, X., Zhu, J., Lin, M., Lv, Y., Xian, H., Yang, Y., Lin, X., Li, S., Li, Y., Teng, H. H., & Thiemens, M. H. (2023). A mineral-based origin of Earth's initial hydrogen peroxide and molecular oxygen. *Proceedings of the National Academy of Sciences of the United States of America*, *120*(13). https://doi.org/10.1073/pnas.2221984120

He, X., Zhang, L., Chen, J., Liu, H., Su, Y., Li, H., Cao, Y., Dral, P. O., & Wang, C. (2023). Photo-Driven Aerobic Methane Nitration. *Inorganic Chemistry*, *62*(26), 10343–10350. https://doi.org/10.1021/acs.inorgchem.3c01210

Helmbrecht, V., Weingart, M., Klein, F., Braun, D., & Orsi, W. D. (2022). White and green rust chimneys accumulate RNA in a ferruginous chemical garden. *ArXiv*, 1–25. https://doi.org/10.48550/arXiv.2212.02793

Henriques Pereira, D. P., Leethaus, J., Beyazay, T., do Nascimento Vieira, A., Kleinermanns, K., Tüysüz, H., Martin, W. F., & Preiner, M. (2022). Role of geochemical protoenzymes (geozymes) in primordial metabolism: specific abiotic hydride transfer by metals to the biological redox cofactor NAD+. *FEBS Journal*, *289*(11), 3148–3162. https://doi.org/10.1111/febs.16329

Hinz, I. L., Nims, C., Theuer, S., Templeton, A. S., & Johnson, J. E. (2021). Ferric Iron Triggers Greenalite Formation In Simulated Archean Seawater. *Geology*, *49*(8), 905–909. https://doi.org/10.1130/G48495.1

Hooks, M. R., Webster, P., Weber, J. M., Perl, S., & Barge, L. M. (2020). Effects of Amino Acids on Iron-Silicate Chemical Garden Precipitation. *Langmuir*, *36*(21), 5793–5801. https://doi.org/10.1021/acs.langmuir.0c00502

Huang, J., Jones, A., Waite, T. D., Chen, Y., Huang, X., Rosso, K. M., Kappler, A., Mansor, M., Tratnyek, P. G., & Zhang, H. (2021). Fe(II) Redox Chemistry in the Environment. In *Chemical Reviews* (Vol. 121,

Issue 13, pp. 8161–8233). American Chemical Society. https://doi.org/10.1021/acs.chemrev.0c01286

Huang, L. Z., Zhang, X., Liu, R., & Fang, L. (2022). The redox chemistry of phosphate complexed green rusts: Limited oxidative transformation and phosphate release. *Chemical Engineering Journal*, *429*. https://doi.org/10.1016/j.cej.2021.132417

Huang, Q., Jiang, S.-Y., Pi, D.-H., Konhauser, K. O., Wen, X.-P., Lu, L.-Y., & Yan, H. (2023). Thermochemical oxidation of methane by manganese oxides in hydrothermal sediments. *Communications Earth & Environment*, *4*(1), 224. https://doi.org/10.1038/s43247-023-00891-6

Huang, X.-L. (2024). Unveiling the Role of Inorganic Nanoparticles in Earth's Biochemical Evolution through Electron Transfer Dynamics. *IScience*, 109555. https://doi.org/10.1016/j.isci.2024.109555

Huber, S. G., Kotte, K., Schöler, H. F., & Williams, J. (2009). Natural abiotic formation of trihalomethanes in soil: Results from laboratory studies and field samples. *Environmental Science and Technology*, *43*(13), 4934–4939. https://doi.org/10.1021/es8032605

Hudson, R., de Graaf, R., Rodin, M. S., Ohno, A., Lane, N., McGlynn, S. E., Yamada, Y., Nakamura, R., Barge, L., Braun, D., Sojo, V., Graaf, R. De, Strandoo, M., Ohno, A., Lane, N., & McGlynn, S. E. (2020). *CO 2 reduction driven by a pH gradient*. *117*(37). https://doi.org/10.1101/2020.03.02.973982

Inoue, K., Kwon, S. K., Kimijima, K. N. I., Kanie, K., Muramatsu, A., Shinoda, K., Suzuki, S., & Waseda, Y. (2007). Analysis of iron oxyhydroxides and oxides converted from green rust in aqueous solution. *ISIJ International*, *47*(3), 453–457. https://doi.org/10.2355/isijinternational.47.453

Inoue, K., Shinoda, K., Suzuki, S., & Waseda, Y. (2008). Reduction of copper ions in green rust suspension and oxidation of green rust containing metallic copper. *Materials Transactions*, *49*(9), 1941–1946. https://doi.org/10.2320/matertrans.MAW200818

Jackson, R. B., Abernethy, S., Canadell, J. G., Cargnello, M., Davis, S. J., Féron, S., Fuss, S., Heyer, A. J., Hong, C., Jones, C. D., Damon Matthews, H., O'Connor, F. M., Pisciotta, M., Rhoda, H. M., De Richter, R., Solomon, E. I., Wilcox, J. L., & Zickfeld, K. (2021). Atmospheric methane removal: A research agenda. *Philosophical Transactions of the Royal Society A: Mathematical, Physical and Engineering Sciences*, *379*(2210). https://doi.org/10.1098/rsta.2020.0454

Jaziri, A. Y., Charnay, B., Selsis, F., Leconte, J., & Lefèvre, F. (2022). Dynamics of the Great Oxidation Event from a 3D photochemical-climate model. *Climate of the Past*, *18*(10), 2421–2447. https://doi.org/10.5194/cp-18-2421-2022

Jia, Q. Q., Deng, J., Zhang, X., Dai, Y., Wu, F., & Huang, L. Z. (2022). Hydroxyl groups bridge the electron transfer from Fe(II) to carbon tetrachloride. *Water Research*, *221*. https://doi.org/10.1016/j.watres.2022.118791

Jia, Q.-Q., Zhang, X.-J., Zhu, L., & Huang, L.-Z. (2024). Fe(II) coordination transition regulates reductive dechlorination: the overlooked abiotic role of lactate. *Water Research*, 121342. https://doi.org/10.1016/j.watres.2024.121342

Jones, A. M., Collins, R. N., Rose, J., & Waite, T. D. (2009). The effect of silica and natural organic matter on the Fe(II)-catalysed transformation and reactivity of Fe(III) minerals. *Geochimica et Cosmochimica Acta*, *73*(15), 4409–4422. https://doi.org/10.1016/j.gca.2009.04.025

Jones, C., Nomosatryo, S., Crowe, S. A., Bjerrum, C. J., & Canfield, D. E. (2015). Iron oxides, divalent cations, silica, and the early earth phosphorus crisis. *Geology*, *43*(2), 135–138. https://doi.org/10.1130/G36044.1

Jönsson, J., & Sherman, D. M. (2008). Sorption of As(III) and As(V) to siderite, green rust (fougerite) and magnetite: Implications for arsenic release in anoxic groundwaters. *Chemical Geology*, *255*(1–2), 173–181. https://doi.org/10.1016/j.chemgeo.2008.06.036

Jorand, F., Zegeye, A., Ghanbaja, J., & Abdelmoula, M. (2011). The formation of green rust induced by tropical river biofilm components. *Science of The Total Environment*, *409*(13), 2586–2596. https://doi.org/10.1016/j.scitotenv.2011.03.030

Jordan, S., Van Zuilen, M., Martins, Z., & Lane, N. (2023). *Prebiotic membrane structures mimic the morphology of purported early traces of life on Earth*. https://doi.org/10.21203/rs.3.rs-3567744/v1

Ju, M., Chen, Z., Zhu, H., Cai, R., Lin, Z., Chen, Y., Wang, Y., Gao, J., Long, X., & Yang, S. (2023). Fe(III) Docking-Activated Sites in Layered Birnessite for Efficient Water Oxidation. *Journal of the American Chemical Society*, *145*(20), 11215–11226. https://doi.org/10.1021/jacs.3c01181

Kadyshevich, E. A., & Ostrovskii, V. E. (2023). From Minerals to Simplest Living Matter: Life Origination Hydrate Theory. *Acta Biotheoretica*, *71*(2). https://doi.org/10.1007/s10441-023-09463-9

Kanaparthi, D., Lampe, M., Zhu, B., Boesen, T., Klingl, A., Schwille, P., & Lueders, T. (2024). On the nature of the earliest known life forms. *ELife*.

Kim, J. D., Yee, N., Nanda, V., & Falkowski, P. G. (2013). Anoxic photochemical oxidation of siderite generates molecular hydrogen and iron oxides. *Proceedings of the National Academy of Sciences*, *110*(25), 10073–10077. https://doi.org/10.1073/pnas.1308958110

Kitadai, N., & Maruyama, S. (2018). Origins of building blocks of life: A review. *Geoscience Frontiers*, *9*(4), 1117–1153. https://doi.org/10.1016/j.gsf.2017.07.007

Kitadai, N., Nakamura, R., Yamamoto, M., Okada, S., Takahagi, W., Nakano, Y., Takahashi, Y., Takai, K., & Oono, Y. (2021). Thioester synthesis through geoelectrochemical CO2 fixation on Ni sulfides. *Communications Chemistry*, *4*(1). https://doi.org/10.1038/s42004-021-00475-5

Kitadai, N., Nakamura, R., Yamamoto, M., Takai, K., Yoshida, N., & Oono, Y. (2019). Metals likely promoted protometabolism in early ocean alkaline hydrothermal systems. *Science Advances*, *5*(6), 1–10. https://doi.org/10.1126/sciadv.aav7848

Klein, A. R., Basinski, J. J., Niyitanga Manzi, A., Cheng, C. X., Sanchez, M., Thongsomboon, W., & Aristilde, L. (2024). Phosphorus recycling by mineral-catalyzed ribonucleotide cleavage on iron and manganese oxides. *Environmental Chemistry Letters*. https://doi.org/10.1007/s10311-024-01754-y

Koeksoy, E., Sundman, A., Byrne, J. M., Lohmayer, R., Planer-Friedrich, B., Halevy, I., Konhauser, K. O., & Kappler, A. (2019). Formation of green rust and elemental sulfur in an analogue for oxygenated ferro-euxinic transition zones of Precambrian oceans. *Geology*, *47*(3), 211–214. https://doi.org/10.1130/G45501.1

Koga, T., & Naraoka, H. (2017). A new family of extraterrestrial amino acids in the Murchison meteorite. *Scientific Reports*, *7*(1), 1–8. https://doi.org/10.1038/s41598-017-00693-9

Konhauser, K. O., Amskold, L., Lalonde, S. V., Posth, N. R., Kappler, A., & Anbar, A. (2007). Decoupling photochemical Fe(II) oxidation from shallow-water BIF deposition. *Earth and Planetary Science Letters*, *258*(1–2), 87–100. https://doi.org/10.1016/j.epsl.2007.03.026

Konhauser, K. O., Lalonde, S. V., Amskold, L., & Holland, H. D. (2007). Was there really an archean phosphate crisis? *Science*, *315*(5816), 1234. https://doi.org/10.1126/science.1136328

Konhauser, K. O., Pecoits, E., Lalonde, S. V., Papineau, D., Nisbet, E. G., Barley, M. E., Arndt, N. T., Zahnle, K., & Kamber, B. S. (2009). Oceanic nickel depletion and a methanogen famine before the Great Oxidation Event. *Nature*, *458*(7239), 750–753. https://doi.org/10.1038/nature07858

Konhauser, K. O., Planavsky, N. J., Hardisty, D. S., Robbins, L. J., Warchola, T. J., Haugaard, R., Lalonde, S. V., Partin, C. A., Oonk, P. B. H., Tsikos, H., Lyons, T. W., Bekker, A., & Johnson, C. M. (2017). Iron formations: A global record of Neoarchaean to Palaeoproterozoic environmental history. *Earth-Science Reviews*, *172*(June), 140–177. https://doi.org/10.1016/j.earscirev.2017.06.012

Konhauser, K. O., Robbins, L. J., Pecoits, E., Peacock, C., Kappler, A., & Lalonde, S. V. (2015). The Archean Nickel Famine Revisited. *Astrobiology*, *15*(10), 804–815. https://doi.org/10.1089/ast.2015.1301

Konn, C., Charlou, J. L., Donval, J. P., Holm, N. G., Dehairs, F., & Bouillon, S. (2009). Hydrocarbons and oxidized organic compounds in hydrothermal fluids from Rainbow and Lost City ultramafic-hosted vents. *Chemical Geology*, *258*(3–4), 299–314. https://doi.org/10.1016/j.chemgeo.2008.10.034

Kopp, D. A., & Lippard, S. J. (2002). Soluble methane monooxygenase: activation of dioxygen and methane. *Current Opinion in Chemical Biology*, *6*(5), 568–576. https://doi.org/10.1016/S1367-5931(02)00366-6

Koppenol, W. H., & Sies, H. (2023). Was hydrogen peroxide present before the arrival of oxygenic photosynthesis? The important role of iron(II) in the Archean ocean. *Redox Biology*, 103012. https://doi.org/10.1016/j.redox.2023.103012

Korenaga, J. (2013). Initiation and Evolution of Plate Tectonics on Earth: Theories and Observations. *Annual Review of Earth and Planetary Sciences*, *41*(1), 117–151. https://doi.org/10.1146/annurev-earth-050212-124208

Kozin, P. A. (2014). *Charge Development at Iron Oxyhydroxide Surfaces The Interplay between Surface Structure , Particle Morphology and Counterion Identity*.

Lambert, J. F. (2008). Adsorption and polymerization of amino acids on mineral surfaces: A review. *Origins of Life and Evolution of Biospheres*, *38*(3), 211–242. https://doi.org/10.1007/s11084-008-9128-3

Lane, N. (2017). Proton gradients at the origin of life. *BioEssays*, *39*(6), 1–8. https://doi.org/10.1002/bies.201600217

Ledford, S. M., & Meredith, L. K. (2024). Volatile Organic Compound Metabolism on Early Earth. *Journal of Molecular Evolution*. https://doi.org/10.1007/s00239-024-10184-x

Lee, H.-E., Okumura, T., Ooka, H., Adachi, K., Hikima, T., Hirata, K., Kawano, Y., Matsuura, H., Yamamoto, M., Yamamoto, M., Yamaguchi, A., Lee, J.-E., Nam, K. T., Ohara, Y., Hashizume, D., Mcglynn, S. E., & Nakamura, R. (2023). Title Osmotic Energy Conversion in Deep-Sea Hydrothermal Vents. *ChemRxiv*. https://doi.org/10.26434/chemrxiv-2023-v9nc6

Lee, J.-E., Yamaguchi, A., Ooka, H., Kazami, T., Miyauchi, M., Kitadai, N., & Nakamura, R. (2021). *In situ* FTIR study of CO_2 reduction on inorganic analogues of carbon monoxide dehydrogenase. *Chemical Communications*, *57*(26), 3267–3270. https://doi.org/10.1039/D0CC07318K

Lee, S., Wang, C., & Chakrapani, V. (2023). Spontaneous Unassisted Conversion of CO 2 to Multicarbon (≥ C 2) Liquid Products on Green Rust Mineral. *ChemRxiv*. https://doi.org/10.26434/chemrxiv-2023-bch3f

Lee, W., & Batchelor, B. (2002). Abiotic reductive dechlorination of chlorinated ethylenes by iron-bearing soil minerals. 2. Green rust. *Environmental Science and Technology*, *36*(24), 5348–5354. https://doi.org/10.1021/es0258374

Legrand, L., Mazerolles, L., & Chaussé, A. (2004). The oxidation of carbonate green rust into ferric phases:solid-state reaction or transformation via solution. *Geochimica et Cosmochimica Acta*, *68*(17), 3497–3507. https://doi.org/10.1016/j.gca.2004.02.019

Leung, M., Schwieterman, E. W., Parenteau, M. N., & Fauchez, T. J. (2022). Alternative Methylated Biosignatures. I. Methyl Bromide, a Capstone Biosignature. *The Astrophysical Journal*, *938*(1), 6. https://doi.org/10.3847/1538-4357/ac8799

Li, B., Wang, S., Fessler, M., Zou, R., Su, Y., & Zhang, Y. (2024). Differential interactions between natural clay minerals and dissolved organic matter affect reactive oxygen species formation. *Water Research*, *249*. https://doi.org/10.1016/j.watres.2023.120984

Li, H., Deng, J., Jia, Q., Zhu, L., & Huang, L.-Z. (2024). Enhanced Fe(OH)2-Driven Reductive Dechlorination via Shortened Fe-O Bonds and Colloidal Medium. *Water Research*, 121589. https://doi.org/10.1016/j.watres.2024.121589

Li, Q., Fernandez, R. P., Hossaini, R., Iglesias-Suarez, F., Cuevas, C. A., Apel, E. C., Kinnison, D. E., Lamarque, J. F., & Saiz-Lopez, A. (2022). Reactive halogens increase the global methane lifetime and radiative forcing in the 21st century. *Nature Communications*, *13*(1). https://doi.org/10.1038/s41467-022-30456-8

Li, Y. L., Konhauser, K. O., & Zhai, M. (2017a). The formation of magnetite in the early Archean oceans. *Earth and Planetary Science Letters*, *466*, 103–114. https://doi.org/10.1016/j.epsl.2017.03.013

Li, Y., Wang, H., Li, Y., Ye, H., Zhang, Y., Yin, R., Jia, H., Hou, B., Wang, C., Ding, H., Bai, X., & Lu, A. (2023). Electron transfer rules of minerals under pressure informed by machine learning. *Nature Communications*, *14*(1). https://doi.org/10.1038/s41467-023-37384-1

Li, Z., Li, M., Tan, B., Du, N., Zhang, Q., Li, C., Zhang, Y., Li, J., & Li, J. (2022). Green rust (GR) and glucose oxidase (GOX) based Fenton-like reaction: Capacity of sustainable release, promoted conversion of glucose through GOX-iron and pH self-adjustment. *Environmental Research*, *208*. https://doi.org/10.1016/j.envres.2021.112656

Liu, F., Rotaru, A. E., Shrestha, P. M., Malvankar, N. S., Nevin, K. P., & Lovley, D. R. (2015). Magnetite compensates for the lack of a pilin-associated c-type cytochrome in extracellular electron exchange. *Environmental Microbiology*, *17*(3), 648–655. https://doi.org/10.1111/1462-2920.12485

Liu, R., Dai, Y., Feng, Y., Sun, S., Zhang, X., An, C., & Zhao, S. (2023). Hydroxyl radical production by abiotic oxidation of pyrite under estuarine conditions: The effects of aging, seawater anions and illumination. *Journal of Environmental Sciences*. https://doi.org/10.1016/j.jes.2023.02.016

Liu, W. (2021). *PHOTOGEOCHEMISTRY OF MINERALS UNDER ANOXIC CONDITIONS*. https://doi.org/10.7282/t3-jxb1-ke93

Liu, X., & Millero, F. J. (2002). The solubility of iron in seawater. *Marine Chemistry*, *77*(1), 43–54. https://doi.org/10.1016/S0304-4203(01)00074-3

Liu, X., Zhong, H., Wang, C., He, D., & Jin, F. (2022). CO2 reduction into formic acid under hydrothermal conditions: A mini review. *Energy Science and Engineering*, *January*. https://doi.org/10.1002/ese3.1064

Longman, J., Faust, J. C., Bryce, C., Homoky, W. B., & März, C. (2022). Organic Carbon Burial With Reactive Iron Across Global Environments. *Global Biogeochemical Cycles*, *36*(11). https://doi.org/10.1029/2022GB007447

Lovelock, J. E., & Margulis, L. (1974). Atmospheric homeostasis by and for the biosphere: the gaia hypothesis. *Tellus A: Dynamic Meteorology and Oceanography*, *26*(1–2), 2. https://doi.org/10.3402/tellusa.v26i1-2.9731

Maciuca, A. L., Dumitriu, E., Fajula, F., & Hulea, V. (2007). Catalytic oxidation processes for removing dimethylsulfoxide from wastewater. *Chemosphere*, *68*(2), 227–233. https://doi.org/10.1016/j.chemosphere.2007.01.028

Madanan, K. T., Li, Y., Boide-Trujillo, V. J., Russell, D. A., & Bonfio, C. (2024). Mg 2+-driven selection of natural phosphatidic acids in primitive membranes. *ChemRxiv*. https://doi.org/10.26434/chemrxiv-2024-199dr

Maithreepala, R. A., & Doong, R. A. (2005). Enhanced dechlorination of chlorinated methanes and ethenes by chloride green rust in the presence of copper(II). *Environmental Science and Technology*, *39*(11), 4082–4090. https://doi.org/10.1021/es048428b

Malaterre, C., ten Kate, I. L., Baqué, M., Debaille, V., Grenfell, J. L., Javaux, E. J., Khawaja, N., Klenner, F., Lara, Y. J., McMahon, S., Moore, K., Noack, L., Patty, C. H. L., & Postberg, F. (2023a). Is There Such a Thing as a Biosignature? *Astrobiology*, *23*(11), 1213–1227. https://doi.org/10.1089/ast.2023.0042

Malaterre, C., ten Kate, I. L., Baqué, M., Debaille, V., Grenfell, J. L., Javaux, E. J., Khawaja, N., Klenner, F., Lara, Y. J., McMahon, S., Moore, K., Noack, L., Patty, C. H. L., & Postberg, F. (2023b). Is There Such

a Thing as a Biosignature? *Astrobiology*, *23*(11), 1213–1227. https://doi.org/10.1089/ast.2023.0042

Mamajanov, I., & Cody, G. D. (2017). Protoenzymes: The case of hyperbranched polyesters. *Philosophical Transactions of the Royal Society A: Mathematical, Physical and Engineering Sciences*, *375*(2109). https://doi.org/10.1098/rsta.2016.0357

Martin, J. H. (1992). Iron as a Limiting Factor in Oceanic Productivity. In *Primary Productivity and Biogeochemical Cycles in the Sea* (pp. 123–137). Springer US. https://doi.org/10.1007/978-1-4899-0762-2_8

Martin, W., & Russell, M. J. (2007). On the origin of biochemistry at an alkaline hydrothermal vent. *Philosophical Transactions of the Royal Society B: Biological Sciences*, *362*(1486), 1887–1925. https://doi.org/10.1098/rstb.2006.1881

Martins-Costa, M. T. C., & Ruiz-Lopez, M. (2024). The structure of carbon dioxide at the air-water interface and its chemical implications. *Chemistry – A European Journal*. https://doi.org/10.1002/chem.202400825

Matrajt, G., & Blanot, D. (2004). Properties of synthetic ferrihydrite as an amino acid adsorbent and a promoter of peptide bond formation. *Amino Acids*, *26*(2), 153–158. https://doi.org/10.1007/s00726-003-0047-3

Matta, R., Hanna, K., & Chiron, S. (2008). Oxidation of phenol by green rust and hydrogen peroxide at neutral pH. *Separation and Purification Technology*, *61*(3), 442–446. https://doi.org/10.1016/j.seppur.2007.12.005

Mauzerall, D. C. (1990). *THE PHOTOCHEMICAL ORIGINS OF LIFE AND PHOTOREACTION OF FERROUS ION IN THE ARCHAEAN OCEANS*.

Mccollom, T. M., Ritter, G., & Simoneit, B. R. T. (1999). *LIPID SYNTHESIS UNDER HYDROTHERMAL CONDITIONS BY FISCHER-TROPSCH-TYPE REACTIONS*.

McDermott, J. M., Seewald, J. S., German, C. R., & Sylva, S. P. (2015a). Pathways for abiotic organic synthesis at submarine hydrothermal fields. *Proceedings of the National Academy of Sciences of the United States of America*, *112*(25), 7668–7672. https://doi.org/10.1073/pnas.1506295112

McDermott, J. M., Seewald, J. S., German, C. R., & Sylva, S. P. (2015b). Pathways for abiotic organic synthesis at submarine hydrothermal fields. *Proceedings of the National Academy of Sciences of the United States of America*, *112*(25), 7668–7672. https://doi.org/10.1073/pnas.1506295112

McMahon, S. (2019). Earth's earliest and deepest purported fossils may be iron-mineralized chemical gardens. *Proceedings of the Royal Society B: Biological Sciences*, *286*(1916). https://doi.org/10.1098/rspb.2019.2410

Ménez, B., Pasini, V., & Brunelli, D. (2012). Life in the hydrated suboceanic mantle. *Nature Geoscience*, *5*(2), 133–137. https://doi.org/10.1038/ngeo1359

Ménez, B., Pisapia, C., Andreani, M., Jamme, F., Vanbellingen, Q. P., Brunelle, A., Richard, L., Dumas, P., & Réfrégiers, M. (2018a). Abiotic synthesis of amino acids in the recesses of the oceanic lithosphere. *Nature*, *564*(7734), 59–63. https://doi.org/10.1038/s41586-018-0684-z

Ménez, B., Pisapia, C., Andreani, M., Jamme, F., Vanbellingen, Q. P., Brunelle, A., Richard, L., Dumas, P., & Réfrégiers, M. (2018b). Abiotic synthesis of amino acids in the recesses of the oceanic lithosphere. *Nature*, *564*(7734), 59–63. https://doi.org/10.1038/s41586-018-0684-z

Middelburg, J. J., Soetaert, K., & Hagens, M. (2020). Ocean Alkalinity, Buffering and Biogeochemical Processes. In *Reviews of Geophysics* (Vol. 58, Issue 3). Blackwell Publishing Ltd. https://doi.org/10.1029/2019RG000681

Milshteyn, D., Cooper, G., & Deamer, D. (2019). Chemiosmotic energy for primitive cellular life: Proton gradients are generated across lipid membranes by redox reactions coupled to meteoritic quinones. *Scientific Reports*, *9*(1). https://doi.org/10.1038/s41598-019-48328-5

Möller, F. M., Kriegel, F., Kieß, M., Sojo, V., & Braun, D. (2017). Steep pH Gradients and Directed Colloid Transport in a Microfluidic Alkaline Hydrothermal Pore. *Angewandte Chemie International Edition*, *56*(9), 2340–2344. https://doi.org/10.1002/anie.201610781

Moore, C. M., Mills, M. M., Arrigo, K. R., Berman-Frank, I., Bopp, L., Boyd, P. W., Galbraith, E. D., Geider, R. J., Guieu, C., Jaccard, S. L., Jickells, T. D., La Roche, J., Lenton, T. M., Mahowald, N. M., Marañón, E., Marinov, I., Moore, J. K., Nakatsuka, T., Oschlies, A., … Ulloa, O. (2013). Processes and patterns of oceanic nutrient limitation. In *Nature Geoscience* (Vol. 6, Issue 9, pp. 701–710). https://doi.org/10.1038/ngeo1765

Moore, E. K., Jelen, B. I., Giovannelli, D., Raanan, H., & Falkowski, P. G. (2017). Metal availability and the expanding network of microbial metabolisms in the Archaean eon. In *Nature Geoscience* (Vol. 10, Issue 9, pp. 629–636). Nature Publishing Group. https://doi.org/10.1038/ngeo3006

Moore, O. W., Curti, L., Woulds, C., Bradley, J. A., Babakhani, P., Mills, B. J. W., Homoky, W. B., Xiao, K. Q., Bray, A. W., Fisher, B. J., Kazemian, M., Kaulich, B., Dale, A. W., & Peacock, C. L. (2023). Long-term organic carbon preservation enhanced by iron and manganese. *Nature*, *621*(7978), 312–317. https://doi.org/10.1038/s41586-023-06325-9

Morin, G., Averseng, F., Carrier, X., Le Pape, P., Du, Y., HongE, Y., Bourbon, E., Sportelli, G., Da Silva, T. A., Mezzetti, A., Baya, C., Allard, T., Brest, J., & Rouelle, M. (2023). Phosphate Boosts Nonhydroxyl Radical Species Production upon Air Oxidation of Magnetite and Iron Sulfides at Neutral pH. *Journal of Physical Chemistry C*. https://doi.org/10.1021/acs.jpcc.3c02236

Nie, N. X., Dauphas, N., & Greenwood, R. C. (2017). Iron and oxygen isotope fractionation during iron UV photo-oxidation: Implications for early Earth and Mars. *Earth and Planetary Science Letters*, *458*, 179–191. https://doi.org/10.1016/j.epsl.2016.10.035

Nitschke, W., Farr, O., Gaudu, N., Truong, C., Guyot, F., Russell, M. J., & Duval, S. (2024). The Winding Road from Origin to Emergence (of Life). *Life*, *14*(5), 607. https://doi.org/10.3390/life14050607

Nitschke, W., McGlynn, S. E., Milner-White, E. J., & Russell, M. J. (2013). On the antiquity of metalloenzymes and their substrates in bioenergetics. *Biochimica et Biophysica Acta - Bioenergetics*, *1827*(8–9), 871–881. https://doi.org/10.1016/j.bbabio.2013.02.008

Nitschke, W., & Russell, M. J. (2009). Hydrothermal Focusing of Chemical and Chemiosmotic Energy, Supported by Delivery of Catalytic Fe, Ni, Mo/W, Co, S and Se, Forced Life to Emerge. *Journal of Molecular Evolution*, *69*(5), 481–496. https://doi.org/10.1007/s00239-009-9289-3

Nitschke, W., & Russell, M. J. (2013). Beating the acetyl coenzyme A-pathway to the origin of life. *Philosophical Transactions of the Royal Society B: Biological Sciences*, *368*(1622), 20120258. https://doi.org/10.1098/rstb.2012.0258

Nitschke, W., Schoepp-Cothenet, B., Duval, S., Zuchan, K., Farr, O., Baymann, F., Panico, F., Minguzzi, A., Branscomb, E., & Russell, M. J. (2022). Aqueous electrochemistry: The toolbox for life's emergence from redox disequilibria. *Electrochemical Science Advances*. https://doi.org/10.1002/elsa.202100192

Nizova, G. V., Süss-Fink, G., & Shul'pin, G. B. (1997). Catalytic oxidation of methane to methyl hydroperoxide and other oxygenates under mild conditions. *Chemical Communications*, *4*, 397–398. https://doi.org/10.1039/a607765j

Nutman, A. P., Bennett, V. C., Friend, C. R. L., Van Kranendonk, M. J., & Chivas, A. R. (2016). Rapid emergence of life shown by discovery of 3,700-million-year-old microbial structures. *Nature*, *537*(7621), 535–538. https://doi.org/10.1038/nature19355

Nutman, A. P., Friend, C. R. L., Horie, K., & Hidaka, H. (2007). Chapter 3.3 The Itsaq Gneiss Complex of Southern West Greenland and the Construction of Eoarchaean Crust at Convergent Plate Boundaries. *Developments in Precambrian Geology*, *15*(07), 187–218. https://doi.org/10.1016/S0166-2635(07)15033-7

Ogasawara, H., Yoshida, A., Imai, E. I., Honda, H., Hatori, K., & Matsuno, K. (2000). Synthesizing oligomers from monomeric nucleotides in simulated hydrothermal environments. *Origins of Life and Evolution of the Biosphere*, *30*(6), 519–526. https://doi.org/10.1023/A:1026539708173

O'loughlin, E. J., Boyanov, M. I., Kemner, K. M., & Burris, D. R. (2022). *Effects of Metal Amendments on the Reductive Dechlorination of Carbon Tetrachloride by Green Rust*.

O'Loughlin, E. J., & Burris, D. R. (2022). Reduction of Chlorinated Ethenes by Ag- and Cu-Amended Green Rust. *Minerals*, *12*(2), 138. https://doi.org/10.3390/min12020138

O'Loughlin, E. J., Kelly, S. D., Cook, R. E., Csencsits, R., & Kemner, K. M. (2003). Reduction of uranium(VI) by mixed iron(II)/iron(III) hydroxide (green rust): Formation of UO2 nanoparticles. *Environmental Science and Technology*, *37*(4), 721–727. https://doi.org/10.1021/es0208409

O'Loughlin, E. J., Kelly, S. D., Kemner, K. M., Csencsits, R., & Cook, R. E. (2003). Reduction of AgI, AuIII, CuII, and HgIIby FeII/FeIIIhydroxysulfate green rust. *Chemosphere*, *53*(5), 437–446. https://doi.org/10.1016/S0045-6535(03)00545-9

Onoguchi, A., Granata, G., Haraguchi, D., Hayashi, H., & Tokoro, C. (2019). Kinetics and mechanism of selenate and selenite removal in solution by green rust-sulfate. *Royal Society Open Science*, *6*(4). https://doi.org/10.1098/rsos.182147

Ooka, H., McGlynn, S. E., & Nakamura, R. (2019). Electrochemistry at Deep-Sea Hydrothermal Vents: Utilization of the Thermodynamic Driving Force towards the Autotrophic Origin of Life. In *ChemElectroChem* (Vol. 6, Issue 5, pp. 1316–1323). Wiley-VCH Verlag. https://doi.org/10.1002/celc.201801432

Ou, Y., Twight, L. P., Samanta, B., Liu, L., Biswas, S., Fehrs, J. L., Sagui, N. A., Villalobos, J., Morales-Santelices, J., Antipin, D., Risch, M., Toroker, M. C., & Boettcher, S. W. (2023). Cooperative Fe sites on transition metal (oxy)hydroxides drive high oxygen evolution activity in base. *Nature Communications*, *14*(1). https://doi.org/10.1038/s41467-023-43305-z

Park, Y. J., Jodts, R. J., Slater, J. W., Reyes, R. M., Winton, V. J., Montaser, R. A., Thomas, P. M., Dowdle, W. B., Ruiz, A., Kelleher, N. L., Bollinger, J. M., Krebs, C., Hoffman, B. M., & Rosenzweig, A. C. (2022). A mixed-valent Fe(II)Fe(III) species converts cysteine to an oxazolone/thioamide pair in methanobactin biosynthesis. *Proceedings of the National Academy of Sciences*, *119*(13). https://doi.org/10.1073/pnas.2123566119

Perez, J. P. H., Mangayayam, M. C., Rubio, S. N., Freeman, H. M., Tobler, D. J., & Benning, L. G. (2018). Intercalation of aromatic sulfonates in "green rust" via ion exchange. *Energy Procedia*, *146*, 179–187. https://doi.org/10.1016/j.egypro.2018.07.023

Perez, J. P. H., Tobler, D. J., & Benning, L. G. (2024). Synergistic inhibition of green rust crystallization by co-existing arsenic and silica. *Environmental Science: Processes and Impacts*. https://doi.org/10.1039/d3em00458a

Petrakovskii, G. A., Piskorskii, V. P., Sosnin, V. M., & Kosobudskii, I. D. (1983). Electron-paramagnetic-res of transition metal superparamagnetic particles in polymer matrices. *Sov. Phys. Solid State*, *25*, 1876–1879.

Piechota, E. J., & Meyer, G. J. (2019). Introduction to Electron Transfer: Theoretical Foundations and Pedagogical Examples. *Journal of Chemical Education*, *96*(11), 2450–2466. https://doi.org/10.1021/acs.jchemed.9b00489

Planavsky, N. J., Asael, D., Hofmann, A., Reinhard, C. T., Lalonde, S. V., Knudsen, A., Wang, X., Ossa Ossa, F., Pecoits, E., Smith, A. J. B., Beukes, N. J., Bekker, A., Johnson, T. M., Konhauser, K. O., Lyons, T. W., & Rouxel, O. J. (2014a). Evidence for oxygenic photosynthesis half a billion years before the Great Oxidation Event. *Nature Geoscience*, *7*(4), 283–286. https://doi.org/10.1038/ngeo2122

Planavsky, N. J., Asael, D., Hofmann, A., Reinhard, C. T., Lalonde, S. V., Knudsen, A., Wang, X., Ossa Ossa, F., Pecoits, E., Smith, A. J. B., Beukes, N. J., Bekker, A., Johnson, T. M., Konhauser, K. O., Lyons, T. W.,

& Rouxel, O. J. (2014b). Evidence for oxygenic photosynthesis half a billion years before the Great Oxidation Event. *Nature Geoscience*, *7*(4), 283–286. https://doi.org/10.1038/ngeo2122

Poulton, S. W., & Canfeld, D. E. (2011). Ferruginous conditions: A dominant feature of the ocean through Earth's history. *Elements*, *7*(2), 107–112. https://doi.org/10.2113/gselements.7.2.107

Pozzer, A. C., Gómez, P. A., & Weiss, J. (2022). Volatile organic compounds in aquatic ecosystems – Detection, origin, significance and applications. In *Science of the Total Environment* (Vol. 838). Elsevier B.V. https://doi.org/10.1016/j.scitotenv.2022.156155

Preiner, M., Asche, S., Becker, S., Betts, H. C., Boniface, A., Camprubi, E., Chandru, K., Erastova, V., Garg, S. G., Khawaja, N., Kostyrka, G., Machné, R., Moggioli, G., Muchowska, K. B., Neukirchen, S., Peter, B., Pichlhöfer, E., Radványi, Á., Rossetto, D., … Xavier, J. C. (2020). The future of origin of life research: Bridging decades-old divisions. *Life*, *10*(3). https://doi.org/10.3390/life10030020

Preiner, M., Igarashi, K., Muchowska, K. B., Yu, M., Varma, S. J., Kleinermanns, K., Nobu, M. K., Kamagata, Y., Tüysüz, H., Moran, J., & Martin, W. F. (2020). A hydrogen-dependent geochemical analogue of primordial carbon and energy metabolism. *Nature Ecology and Evolution*, *4*(4), 534–542. https://doi.org/10.1038/s41559-020-1125-6

Preiner, M., Xavier, J. C., Do Nascimento Vieira, A., Kleinermanns, K., Allen, J. F., & Martin, W. F. (2019). Catalysts, autocatalysis and the origin of metabolism. In *Interface Focus* (Vol. 9, Issue 6). Royal Society Publishing. https://doi.org/10.1098/rsfs.2019.0072

Preiner, M., Xavier, J. C., Sousa, F. L., Zimorski, V., Neubeck, A., Lang, S. Q., Chris Greenwell, H., Kleinermanns, K., Tüysüz, H., McCollom, T. M., Holm, N. G., & Martin, W. F. (2018). Serpentinization: Connecting geochemistry, ancient metabolism and industrial hydrogenation. In *Life* (Vol. 8, Issue 4). MDPI AG. https://doi.org/10.3390/life8040041

Proskurowski, G., Lilley, M. D., Seewald, J. S., Früh-Green, G. L., Olson, E. J., Lupton, J. E., Sylva, S. P., & Kelley, D. S. (2008). Abiogenic hydrocarbon production at lost city hydrothermal field. *Science*, *319*(5863), 604–607. https://doi.org/10.1126/science.1151194

Purvis, G., Johnson, K. L., Peacock, C., Wegorzewski, A., Sano, N., Sheriff, J., Cumpson, P., & Lopez-Capel, E. (2022). *Stable organic carbon formation accelerated by manganese oxide mineral reduction and the implications for the global carbon cycle*. https://doi.org/10.21203/rs.3.rs-2090070/v1

Purvis, G., Šiller, L., Crosskey, A., Vincent, J., Wills, C., Sheriff, J., Xavier, C., & Telling, J. (2024). Generation of long-chain fatty acids by hydrogen-driven bicarbonate reduction in ancient alkaline hydrothermal vents. *Communications Earth and Environment*, *5*(1). https://doi.org/10.1038/s43247-023-01196-4

Qian, A., Lu, Y., Zhang, Y., Yu, C., Zhang, P., Liao, W., Yao, Y., Zheng, Y., Tong, M., & Yuan, S. (2023). Mechanistic Insight into Electron Transfer from Fe(II)-Bearing Clay Minerals to Fe (Hydr)oxides. *Environmental Science & Technology*. https://doi.org/10.1021/acs.est.3c01250

Rabiu, A. M., & Yusuf, I. M. (2013). Industrial Feasiblity of Direct Methane Conversion to Hydrocarbons over Fe-Based Fischer Tropsch Catalyst. *Journal of Power and Energy Engineering*, *01*(05), 41–46. https://doi.org/10.4236/jpee.2013.15006

Rasmussen, B., Muhling, J. R., & Fischer, W. W. (2020). Greenalite Nanoparticles in Alkaline Vent Plumes as Templates for the Origin of Life. *Astrobiology*, *21*(2), 1–14. https://doi.org/10.1089/ast.2020.2270

Rasmussen, B., Muhling, J. R., Suvorova, A., & Fischer, W. W. (2021). Apatite nanoparticles in 3.46–2.46 Ga iron formations: Evidence for phosphorus-rich hydrothermal plumes on early Earth. *Geology*, *XX*(Xx), 1–5. https://doi.org/10.1130/g48374.1

Rauscher, S. A., & Moran, J. (2022). Hydrogen Drives Part of the Reverse Krebs Cycle under Metal or Meteorite Catalysis. *Angewandte Chemie International Edition*. https://doi.org/10.1002/anie.202212932

Redeker, K. R., & Kalin, R. M. (2012). Methyl chloride isotopic signatures from Irish forest soils and a comparison between abiotic and biogenic methyl halide soil fluxes. *Global Change Biology*, *18*(4), 1453–1467. https://doi.org/10.1111/j.1365-2486.2011.02600.x

Refait, P., & Génin, J. M. R. (1994). The transformation of chloride-containing green rust one into sulphated green rust two by oxidation in mixed Cl- and SO42- aqueous media. *Corrosion Science*, *36*(1), 55–65. https://doi.org/10.1016/0010-938X(94)90108-2

Rochelle M. Soo, James Hemp, Donovan H. Parks, Woodward W. Fischer, P. H. (2017). On the origin of oxygenic photosynthesis and Cyanobacteria. *Science*, *355*(4), 1436–1440. https://doi.org/10.1111/nph.16249

Rogers, K. L., & Schulte, M. D. (2012). Organic Sulfur Metabolisms in Hydrothermal Environments. *Geobiology*, *10*(4), 320–332. https://doi.org/10.1111/j.1472-4669.2012.00324.x

Rosas, J. C., & Korenaga, J. (2021). Archaean seafloors shallowed with age due to radiogenic heating in the mantle. *Nature Geoscience*, *14*(1), 51–56. https://doi.org/10.1038/s41561-020-00673-1

Ruby, C., Abdelmoula, M., Naille, S., Renard, A., Khare, V., Ona-Nguema, G., Morin, G., & Génin, J. M. R. (2010). Oxidation modes and thermodynamics of FeII-IIIoxyhydroxycarbonate green rust: Dissolution-precipitation versus in situ deprotonation. *Geochimica et Cosmochimica Acta*, *74*(3), 953–966. https://doi.org/10.1016/j.gca.2009.10.030

Ruby, C., Géhin, A., Abdelmoula, M., Génin, J. M. R., & Jolivet, J. P. (2003). Coprecipitation of Fe(II) and Fe(III) cations in sulphated aqueous medium and formation of hydroxysulphate green rust. *Solid State Sciences*, *5*(7), 1055–1062. https://doi.org/10.1016/S1293-2558(03)00121-3

Ruby, C., Géhin, A., Aissa, R., & Génin, J. M. R. (2006). Mass-balance and Eh-pH diagrams of FeII-III green rust in aqueous sulphated solution. *Corrosion Science*, *48*(11), 3824–3837. https://doi.org/10.1016/j.corsci.2006.01.002

Ruby, C., Upadhyay, C., Géhin, A., Ona-Nguema, G., & Génin, J. M. R. (2006). In situ redox flexibility of FeII-III oxyhydroxycarbonate green rust and fougerite. *Environmental Science and Technology*, *40*(15), 4696–4702. https://doi.org/10.1021/es0606834

Russell, M. (2018). Green Rust: The Simple Organizing 'Seed' of All Life? *Life*, *8*(3), 35. https://doi.org/10.3390/life8030035

Russell, M. J. (2023). A self-sustaining serpentinization mega-engine feeds the fougerite nanoengines implicated in the emergence of guided metabolism. *Frontiers in Microbiology*, *14*. https://doi.org/10.3389/fmicb.2023.1145915

Russell, M. J., & Hall, A. J. (1997). The emergence of life from iron monosulphide bubbles at a submarine hydrothermal redox and pH front. *Journal of the Geological Society*, *154*(3), 377–402. https://doi.org/10.1144/gsjgs.154.3.0377

Russell, M. J., & Nitschke, W. (2017). Methane: Fuel or Exhaust at the Emergence of Life? *Astrobiology*, *17*(10), 1053–1066. https://doi.org/10.1089/ast.2016.1599

Russell, M. J., Nitschke, W., & Branscomb, E. (2013). The inevitable journey to being. *Philosophical Transactions of the Royal Society B: Biological Sciences*, *368*(1622). https://doi.org/10.1098/rstb.2012.0254

Sagan, C. (1961). *On the Origin and Planetary Distribution of Life'*. www.jstor.org

Sánchez, M., Sabio, L., Gálvez, N., Capdevila, M., & Dominguez-Vera, J. M. (2017). Iron chemistry at the service of life. In *IUBMB Life* (Vol. 69, Issue 6, pp. 382–388). Blackwell Publishing Ltd. https://doi.org/10.1002/iub.1602

Santos-Carballal, D., Roldan, A., Dzade, N. Y., & De Leeuw, N. H. (2018). Reactivity of CO2 on the surfaces of magnetite (Fe3O4), greigite (Fe3S4) and mackinawite (FeS). In *Philosophical Transactions of the Royal Society A: Mathematical, Physical and Engineering Sciences* (Vol. 376, Issue 2110). Royal Society Publishing. https://doi.org/10.1098/rsta.2017.0065

Sasai, R., Sato, H., Sugata, M., Fujimura, T., Ishihara, S., Deguchi, K., Ohki, S., Tansho, M., Shimizu, T., Oita, N., Numoto, M., Fujii, Y., Kawaguchi, S., Matsuoka, Y., Hagura, K., Abe, T., & Moriyoshi, C. (2019). Why Do Carbonate Anions Have Extremely High Stability in the Interlayer Space of Layered Double Hydroxides? Case Study of Layered Double Hydroxide Consisting of Mg and Al (Mg/Al = 2). *Inorganic Chemistry*, *58*(16), 10928–10935. https://doi.org/10.1021/acs.inorgchem.9b01365

Sattler, T., Sörgel, M., Wittmer, J., Bourtsoukidis, E., Krause, T., Atlas, E., Benk, S., Bleicher, S., Kamilli, K., Ofner, J., Kopetzky, R., Held, A., Palm, W. U., Williams, J., Zetzsch, C., & Schöler, H. F. (2019). Natural formation of chloro- and bromoacetone in salt lakes of Western Australia. *Atmosphere*, *10*(11). https://doi.org/10.3390/atmos10110663

Schirrmeister, B. E., Gugger, M., & Donoghue, P. C. J. (2015). Cyanobacteria and the Great Oxidation Event: Evidence from genes and fossils. *Palaeontology*, *58*(5), 769–785. https://doi.org/10.1111/pala.12178

Schrauzer, G. N., & Guth, T. D. (1976). Hydrogen evolving systems. 1. The formation of molecular hydrogen from aqueous suspensions of iron(II) hydroxide and reactions with reducible substrates, including molecular nitrogen. *Journal of the American Chemical Society*, *98*(12), 3508–3513. https://doi.org/10.1021/ja00428a019

Schrödinger E. (1944). What Is Life? *Cambridge Univ Press* .

Shanker, U., Bhushan, B., Bhattacharjee, G., & Kamaluddin. (2012). Oligomerization of Glycine and Alanine Catalyzed by Iron Oxides: Implications for Prebiotic Chemistry. *Origins of Life and Evolution of Biospheres*, *42*(1), 31–45. https://doi.org/10.1007/s11084-012-9266-5

Shu, L., Nesheim, J. C., Kauffmann, K., Münck, E., Lipscomb, J. D., & Que, L. (1997). An Fe 2 IV O 2 Diamond Core Structure for the Key Intermediate Q of Methane Monooxygenase. *Science*, *275*(5299), 515–518. https://doi.org/10.1126/science.275.5299.515

Simons, M. C., Prinslow, S. D., Babucci, M., Hoffman, A. S., Hong, J., Vitillo, J. G., Bare, S. R., Gates, B. C., Lu, C. C., Gagliardi, L., & Bhan, A. (2021). Beyond Radical Rebound: Methane Oxidation to Methanol Catalyzed by Iron Species in Metal-Organic Framework Nodes. *Journal of the American Chemical Society*, *143*(31), 12165–12174. https://doi.org/10.1021/jacs.1c04766

Smith, K. (1999). METAL SORPTION ON MINERAL SURFACES: AN OVERVIEW WITH EXAMPLES RELATING TO MINERAL DEPOSITS. *Reviews in Economic Geology*, *6A, 6B*.

Song, Z., Zhao, J., Ghani, U., Liu, W., Ye, B., & Cai, X. (2024). Metal Organic Frameworks Derived Layered Double Hydroxide Nanosheets for Electrochemical Energy Storage and Conversion. *ChemElectroChem*, *11*(6). https://doi.org/10.1002/celc.202300731

Starokon, E. V., Parfenov, M. V., Arzumanov, S. S., Pirutko, L. V., Stepanov, A. G., & Panov, G. I. (2013). Oxidation of methane to methanol on the surface of FeZSM-5 zeolite. *Journal of Catalysis*, *300*, 47–54. https://doi.org/10.1016/j.jcat.2012.12.030

Sumoondur, A., Shaw, S., Ahmed, I., & Benning, L. G. (2008). Green rust as a precursor for magnetite: an in situ synchrotron based study . *Mineralogical Magazine*, *72*(1), 201–204. https://doi.org/10.1180/minmag.2008.072.1.201

Sun, L., Lechte, M., Shi, X., Zhou, X., Zhou, L., Fang, H., Xie, B., Wu, M., & Tang, D. (2022). Hexagonal magnetite in Algoma-type banded iron formations of the ca. 2.52 Ga Baizhiyan Formation, North China: Evidence for a green rust precursor? *American Mineralogist*, *107*(5), 970–984. https://doi.org/10.2138/am-2022-7981

Sun, Y., Jiang, G., Jiang, R., Lan, S., Li, Y., Yan, Y., & Zhang, Q. (2023). Effects of myo-inositol hexakisphosphate on the transformation of carbonate green rust. *Journal of Agro-Environment Science*, *42*(2), 393–402. https://doi.org/10.11654/jaes.2022-0633

Sweetman, A. K., Smith, A. J., de Jonge, D. S. W., Hahn, T., Schroedl, P., Silverstein, M., Andrade, C., Edwards, R. L., Lough, A. J. M., Woulds, C., Homoky, W. B., Koschinsky, A., Fuchs, S., Kuhn, T., Geiger,

F., & Marlow, J. J. (2024). Evidence of dark oxygen production at the abyssal seafloor. *Nature Geoscience*. https://doi.org/10.1038/s41561-024-01480-8

Switala, J., Donald, L., & Ivancich, A. (2024). A remarkable peroxidase-like behavior of the catalase KatA from the pathogenic bacteria Helicobacter pylori: The oxidation reaction with formate as substrate and the stabilization of an [Fe(IV) = O Trp•] intermediate assessed by multifrequency EPR spectroscopy. *Journal of Inorganic Biochemistry*, *257*, 112594. https://doi.org/10.1016/j.jinorgbio.2024.112594

Szécsényi, Á., Li, G., Gascon, J., & Pidko, E. A. (2018). Mechanistic Complexity of Methane Oxidation with H2O2 by Single-Site Fe/ZSM-5 Catalyst. *ACS Catalysis*, *8*(9), 7961–7972. https://doi.org/10.1021/acscatal.8b01672

Tahawy, R., Doustkhah, E., Abdel-Aal, E. S. A., Esmat, M., Farghaly, F. E., El-Hosainy, H., Tsunoji, N., El-Hosiny, F. I., Yamauchi, Y., Assadi, M. H. N., & Ide, Y. (2021). Exceptionally stable green rust, a mixed-valent iron-layered double hydroxide, as an efficient solar photocatalyst for H2 production from ammonia borane. *Applied Catalysis B: Environmental*, *286*. https://doi.org/10.1016/j.apcatb.2020.119854

Tamaura, Y. (1986). Ni(II)-bearing green rust II and its spontaneous transformation into Ni(II)-bearing ferrites. *Bulletin of the Chemical Society of Japan*, *59*(6), 1829–1832. https://doi.org/10.1246/bcsj.59.1829

Tamaura, Y., Yoshida, T., & Katsura, T. (1984). The Synthesis of Green Rust II(FeIII1–FeII2) and Its Spontaneous Transformation into Fe3O4. *Bulletin of the Chemical Society of Japan*, *57*(9), 2411–2416. https://doi.org/10.1246/bcsj.57.2411

Taran, O. (2017). Electron transfer between electrically conductive minerals and quinones. *Frontiers in Chemistry*, *5*(JUL). https://doi.org/10.3389/fchem.2017.00049

Thibon, F., Blichert-Toft, J., Tsikos, H., Foden, J., Albalat, E., & Albarede, F. (2019). Dynamics of oceanic iron prior to the Great Oxygenation Event. *Earth and Planetary Science Letters*, *506*, 360–370. https://doi.org/10.1016/j.epsl.2018.11.016

Thomas, A. N., Eiche, E., Göttlicher, J., Steininger, R., Benning, L. G., Freeman, H. M., Tobler, D. J., Mangayayam, M., Dideriksen, K., & Neumann, T. (2020). Effects of metal cation substitution on hexavalent chromium reduction by green rust. *Geochemical Transactions*, *21*(1). https://doi.org/10.1186/s12932-020-00066-8

Tosca, N. J., Guggenheim, S., & Pufahl, P. K. (2016). An authigenic origin for Precambrian greenalite: Implications for iron formation and the chemistry of ancient seawater. *Bulletin of the Geological Society of America*, *128*(3–4), 511–530. https://doi.org/10.1130/B31339.1

Tosca, N. J., Jiang, C. Z., Rasmussen, B., & Muhling, J. (2019). Products of the iron cycle on the early Earth. *Free Radical Biology and Medicine*, *140*(April), 1–16. https://doi.org/10.1016/j.freeradbiomed.2019.05.005

Tosca, N. J., & Tutolo, B. M. (2023). Hydrothermal vent fluid-seawater mixing and the origins of Archean iron formation. *Geochimica et Cosmochimica Acta*, *352*, 51–68. https://doi.org/10.1016/j.gca.2023.05.002

Trolard, F., & Bourrié, G. (2008). Chapter 5 Geochemistry of Green Rusts and Fougerite. In *Advances in Agronomy* (Vol. 99, Issue July 2016, pp. 227–288). https://doi.org/10.1016/S0065-2113(08)00405-7

Trolard, F., Duval, S., Nitschke, W., Ménez, B., Pisapia, C., Ben Nacib, J., Andréani, M., & Bourrié, G. (2022). Mineralogy, geochemistry and occurrences of fougerite in a modern hydrothermal system and its implications for the origin of life. *Earth-Science Reviews*, *225*(December 2021). https://doi.org/10.1016/j.earscirev.2021.103910

Trolard, F., Génin, J.-M. R., Abdelmoula, M., Bourrié, G., Humbert, B., & Herbillon, A. (1997). Identification of a green rust mineral in a reductomorphic soil by Mossbauer and Raman

spectroscopies. *Geochimica et Cosmochimica Acta*, *61*(5), 1107–1111. https://doi.org/10.1016/S0016-7037(96)00381-X

Tyrrell, T. (1999). The relative influences of nitrogen and phosphorus on oceanic primary production. *Nature*, *400*(6744), 525–531. https://doi.org/10.1038/22941

Ungerhofer, K. A., Plümper, O., Preiner, M., Reichart, G. J., & Kraal, P. (2024). Coupled carbon-iron-phosphorus cycling in the Rainbow hydrothermal vent field. *Chemical Geology*, *650*. https://doi.org/10.1016/j.chemgeo.2024.121994

Usman, M., Byrne, J. M., Chaudhary, A., Orsetti, S., Hanna, K., Ruby, C., Kappler, A., & Haderlein, S. B. (2018). Magnetite and Green Rust: Synthesis, Properties, and Environmental Applications of Mixed-Valent Iron Minerals. *Chemical Reviews*, *118*(7), 3251–3304. https://doi.org/10.1021/acs.chemrev.7b00224

Vallina, S. M., & Simó, R. (2007). Re-visiting the CLAW hypothesis. In *Environmental Chemistry* (Vol. 4, Issue 6, pp. 384–387). https://doi.org/10.1071/EN07055

Varma, S. J., Muchowska, K. B., Chatelain, P., & Moran, J. (2018). Native iron reduces CO2 to intermediates and end-products of the acetyl-CoA pathway. *Nature Ecology and Evolution*, *2*(6), 1019–1024. https://doi.org/10.1038/s41559-018-0542-2

Vijay, A. K., Sharma, V. K., & Meyerstein, D. (2023). Overlooked Formation of Carbonate Radical Anions in the Oxidation of Iron(II) by Oxygen in the Presence of Bicarbonate. *Angewandte Chemie International Edition*. https://doi.org/10.1002/anie.202309472

Vuillemin, A., Wirth, R., Kemnitz, H., Schleicher, A. M., Friese, A., Bauer, K. W., Simister, R., Nomosatryo, S., Ordoñez, L., Ariztegui, D., Henny, C., Crowe, S. A., Benning, L. G., Kallmeyer, J., Russell, J. M., Bijaksana, S., Vogel, H., & The Towuti Drilling Project Science Team. (2019). Formation of diagenetic siderite in modern ferruginous sediments. *Geology*, *47*(6), 540–544. https://doi.org/10.1130/G46100.1

Wander, M. C. F., Rosso, K. M., & Schoonen, M. A. A. (2007). Structure and charge hopping dynamics in green rust. *Journal of Physical Chemistry C*, *111*(30), 11414–11423. https://doi.org/10.1021/jp072762n

Wang, C., & Chakrapani, V. (2023a). Environmental Factors Controlling the Electronic Properties and Oxidative Activities of Birnessite Minerals. *ACS Earth and Space Chemistry*, *7*(4), 774–787. https://doi.org/10.1021/acsearthspacechem.2c00357

Wang, C., & Chakrapani, V. (2023b). Photocatalytic Generation of Reactive Oxygen Species on Fe and Mn Oxide Minerals: Mechanistic Pathways and Influence of Semiconducting Properties. *Journal of Physical Chemistry C*, *127*(48), 23189–23198. https://doi.org/10.1021/acs.jpcc.3c05353

Wang, C., Tao, R., Zhang, L., Walters, J., Zhu, X., Menez, B., Debret, B., Yang, K., & Lan, C. (2023, December 11). *Origins of deep abiotic hydrocarbons: Insights from fundamental redox reactions within the Fe-C-H-O system*. https://doi.org/10.7185/gold2023.14810

Wang, H., Chen, Y., Xie, W., Han, X., Feng, Q., Jiang, R., & Shang, H. (2019). *Construction of Highly Active Pt / Ni-Fe Layered Double Hydroxide Electrocatalyst towards Methanol Oxidation in Alkaline Medium*. *14*, 7961–7972. https://doi.org/10.20964/2019.08.06

Wang, J., Wu, B., Zheng, X., Ma, J., Yu, W., Chen, B., & Chu, C. (2024). Insights into the Crystallinity-Dependent Photochemical Productions of Reactive Oxygen Species from Iron Minerals. *Environmental Science and Technology*. https://doi.org/10.1021/acs.est.4c01843

Wang, P., Mou, X., Li, Y., & Shen, W. (2021). Green rusts-derived iron oxide nanostructures catalyze NO reduction by CO. *Green Energy and Environment*. https://doi.org/10.1016/j.gee.2021.06.002

Wang, Q., Barge, L. M., & Steinbock, O. (2019). Microfluidic Production of Pyrophosphate Catalyzed by Mineral Membranes with Steep pH Gradients. *Chemistry - A European Journal*, *25*(18), 4732–4739. https://doi.org/10.1002/chem.201805950

Wang, X., Liu, F., Tan, W., Feng, X., & Koopal, L. K. (2013). Transformation of hydroxycarbonate green rust into crystalline iron (hydr)oxides: Influences of reaction conditions and underlying mechanisms. *Chemical Geology*, *351*, 57–65. https://doi.org/10.1016/j.chemgeo.2013.05.003

Wang, X., Peng, J., Liang, X., Zhu, M., Lanson, B., Wang, L., Liang, X., Liu, F., Tan, W., & Feng, X. (2019). Effects of Mn2+, Ni2+, and Cu2+ on the Formation and Transformation of Hydrosulfate Green Rust: Reaction Processes and Underlying Mechanisms. *ACS Earth and Space Chemistry*, *3*(4), 519–530. https://doi.org/10.1021/acsearthspacechem.8b00187

Wang, Z., Qiu, W., Pang, S. Y., Guo, Q., Guan, C., & Jiang, J. (2022). Aqueous Iron(IV)–Oxo Complex: An Emerging Powerful Reactive Oxidant Formed by Iron(II)-Based Advanced Oxidation Processes for Oxidative Water Treatment. In *Environmental Science and Technology* (Vol. 56, Issue 3, pp. 1492–1509). American Chemical Society. https://doi.org/10.1021/acs.est.1c04530

Ward, L. M., Kirschvink, J. L., & Fischer, W. W. (2016). Timescales of Oxygenation Following the Evolution of Oxygenic Photosynthesis. *Origins of Life and Evolution of Biospheres*, *46*(1), 51–65. https://doi.org/10.1007/s11084-015-9460-3

Ward, L. M., Rasmussen, B., & Fischer, W. W. (2019). Primary Productivity Was Limited by Electron Donors Prior to the Advent of Oxygenic Photosynthesis. *Journal of Geophysical Research: Biogeosciences*, *124*(2), 211–226. https://doi.org/10.1029/2018JG004679

Weber, J. M., Czaplinski, E. C., Henderson, B. L., Barge, L. M., Castillo-Rogez, J. C., & Hodyss, R. (2024). Photochemical Stability and Reactivity of Sodium Pyruvate: Implications for Organic Analysis on Ceres. *ACS Earth and Space Chemistry*. https://doi.org/10.1021/acsearthspacechem.4c00045

Wimmer, J. L. E., Vieira, A. D. N., Xavier, J. C., Kleinermanns, K., Martin, W. F., & Preiner, M. (2021). The autotrophic core: An ancient network of 404 reactions converts H2, CO2, and NH3 into amino acids, bases, and cofactors. *Microorganisms*, *9*(2), 1–16. https://doi.org/10.3390/microorganisms9020458

Winterbourn, C. C. (1995). Toxicity of iron and hydrogen peroxide: the Fenton reaction. *Toxicology Letters*, *82–83*, 969–974. https://doi.org/10.1016/0378-4274(95)03532-X

Wittmer, J., Bleicher, S., Ofner, J., & Zetzsch, C. (2015). Iron(III)-induced activation of chloride from artificial sea-salt aerosol. *Environmental Chemistry*, *12*(4), 461–475. https://doi.org/10.1071/EN14279

Wong, M. L., Charnay, B. D., Gao, P., Yung, Y. L., & Russell, M. J. (2017). Nitrogen Oxides in Early Earth's Atmosphere as Electron Acceptors for Life's Emergence. *Astrobiology*, *17*(10), 975–983. https://doi.org/10.1089/ast.2016.1473

Wong, M. L., Cleland, C. E., Arend, D., Bartlett, S., Cleaves, H. J., Demarest, H., Prabhu, A., Lunine, J. I., & Hazen, R. M. (2023). On the roles of function and selection in evolving systems. *Proceedings of the National Academy of Sciences*, *120*(43). https://doi.org/10.1073/pnas.2310223120

Wu, S., Zhao, Y., Chen, Y., Dong, X., Wang, M., & Wang, G. (2019). Sulfur cycling in freshwater sediments: A cryptic driving force of iron deposition and phosphorus mobilization. *Science of the Total Environment*, *657*, 1294–1303. https://doi.org/10.1016/j.scitotenv.2018.12.161

Xavier, J. C., Hordijk, W., Kauffman, S., Steel, M., & Martin, W. F. (2020). Autocatalytic chemical networks at the origin of metabolism. *Proceedings of the Royal Society B: Biological Sciences*, *287*(1922). https://doi.org/10.1098/rspb.2019.2377

Xiong, Y., Guilbaud, R., Peacock, C. L., Krom, M. D., & Poulton, S. W. (2023). Phosphorus controls on the formation of vivianite versus green rust under anoxic conditions. *Geochimica et Cosmochimica Acta*, *351*, 139–151. https://doi.org/10.1016/j.gca.2023.04.032

Xue, B. W., Zhang, C. H., Wang, Y. Z., Xie, W. W., Li, N. W., & Yu, L. (2020). Recent progress of Ni-Fe layered double hydroxide and beyond towards electrochemical water splitting. *Nanoscale Advances*, *2*(12), 5555–5566. https://doi.org/10.1039/d0na00727g

Xue, X. (2009). *Fenton-like oxidation of organic pollutants in the presence of iron (II, III) oxides* [Universite Henri Poincare]. https://doi.org/NNT : 2009NAN10041

Yamaguchi, A., Yamamoto, M., Takai, K., Ishii, T., Hashimoto, K., & Nakamura, R. (2014). Electrochemical CO2 reduction by Ni-containing iron sulfides: How is CO2 electrochemically reduced at bisulfide-bearing deep-sea hydrothermal precipitates? *Electrochimica Acta*, *141*, 311–318. https://doi.org/10.1016/j.electacta.2014.07.078

Yamaguchi, K. E., Johnson, C. M., Beard, B. L., & Ohmoto, H. (2005). Biogeochemical cycling of iron in the Archean-Paleoproterozoic Earth: Constraints from iron isotope variations in sedimentary rocks from the Kaapvaal and Pilbara Cratons. *Chemical Geology*, *218*(1-2 SPEC. ISS.), 135–169. https://doi.org/10.1016/j.chemgeo.2005.01.020

Yamamoto, M., Nakamura, R., Kasaya, T., Kumagai, H., Suzuki, K., & Takai, K. (2017). Spontaneous and Widespread Electricity Generation in Natural Deep-Sea Hydrothermal Fields. *Angewandte Chemie - International Edition*, *56*(21), 5725–5728. https://doi.org/10.1002/anie.201701768

Yan, S., Boyanov, M. I., Mishra, B., Kemner, K. M., & O'Loughlin, E. J. (2018). U(VI) Reduction by Biogenic and Abiotic Hydroxycarbonate Green Rusts: Impacts on U(IV) Speciation and Stability over Time. *Environmental Science and Technology*, *52*(8), 4601–4609. https://doi.org/10.1021/acs.est.7b06405

Yao, W., Zhang, J., Gu, K., Li, J., & Qian, J. (2022). Synthesis, characterization and performances of green rusts for water decontamination: A review. In *Environmental Pollution* (Vol. 304). Elsevier Ltd. https://doi.org/10.1016/j.envpol.2022.119205

Ye, C., Zhou, X., Pu, D., Stutz, J., Festa, J., Spolaor, M., Tsai, C., Cantrell, C., Mauldin, R. L., Campos, T., Weinheimer, A., Hornbrook, R. S., Apel, E. C., Guenther, A., Kaser, L., Yuan, B., Karl, T., Haggerty, J., Hall, S., … Knote, C. (2016). Rapid cycling of reactive nitrogen in the marine boundary layer. *Nature*, *532*(7600), 489–491. https://doi.org/10.1038/nature17195

Ye, J., Hu, A., Gao, C., Li, F., Li, L., Guo, Y., Ren, G., Li, B., Rensing, C., Nealson, K. H., Zhou, S., & Xiong, Y. (2024). Abiotic Methane Production Driven by Ubiquitous Non-Fenton-Type Reactive Oxygen Species. *Angewandte Chemie International Edition*. https://doi.org/10.1002/anie.202403884

Yin, W., Ai, J., Huang, L. Z., Tobler, D. J., & Hansen, H. C. B. (2018). A Silicate/Glycine Switch to Control the Reactivity of Layered Iron(II)-Iron(III) Hydroxides for Dechlorination of Carbon Tetrachloride. *Environmental Science and Technology*, *52*(14), 7876–7883. https://doi.org/10.1021/acs.est.8b02020

Yin, W., Huang, L., Pedersen, E. B., Frandsen, C., & Hansen, H. C. B. (2017). Glycine buffered synthesis of layered iron(II)-iron(III) hydroxides (green rusts). *Journal of Colloid and Interface Science*, *497*, 429–438. https://doi.org/10.1016/j.jcis.2016.11.076

Yoo, J. M., Ingenmey, J., Salanne, M., & Lukatskaya, M. R. (2023). Anion effect in electrochemical CO 2 reduction: from spectators to orchestrators. *ChemRxiv*. https://doi.org/10.26434/chemrxiv-2023-8q0qt-v4

Yoshino, A., Fujieda, S., Shinoda, K., & Suzuki, S. (2013). Synthesis of magnetite particles by oxidation of hydroxyl-chloride green rust suspension under controlled conditions. *ISIJ International*, *53*(5), 894–899. https://doi.org/10.2355/isijinternational.53.894

Young, A. V., Robinson, T. D., Krissansen-Totton, J., Schwieterman, E. W., Wogan, N. F., Way, M. J., Sohl, L. E., Arney, G. N., Reinhard, C. T., Line, M. R., Catling, D. C., & Windsor, J. D. (2023). *Inferring Chemical Disequilibrium Biosignatures for Proterozoic Earth-Like Exoplanets*. https://doi.org/10.1038/s41550-023-02145-z

Yu, C., Ji, W., Li, X., Yuan, S., Zhang, P., & Pu, S. (2024). Critical Role of Mineral Fe(IV) Formation in Low Hydroxyl Radical Yields during Fe(II)-Bearing Clay Mineral Oxygenation. *Environmental Science and Technology*. https://doi.org/10.1021/acs.est.3c09986

Yu, C., Qian, A., Lu, Y., Liao, W., Zhang, P., Tong, M., Dong, H., Zeng, Q., & Yuan, S. (2024). Electron transfer processes associated with structural Fe in clay minerals. *Critical Reviews in Environmental Science and Technology*, *54*(1), 13–38. https://doi.org/10.1080/10643389.2023.2221154

Zang, X., Ueno, Y., & Kitadai, N. (2022). Photochemical Synthesis of Ammonia and Amino Acids from Nitrous Oxide. *Astrobiology*, *22*(4), 387–398. https://doi.org/10.1089/ast.2021.0064

Zegeye, A., Bonneville, S., Benning, L. G., Sturm, A., Fowle, D. A., Jones, C. A., Canfield, D. E., Ruby, C., MacLean, L. C., Nomosatryo, S., Crowe, S. A., & Poulton, S. W. (2012). Green rust formation controls nutrient availability in a ferruginous water column. *Geology*, *40*(7), 599–602. https://doi.org/10.1130/G32959.1

Zegeye, A., Mustin, C., & Jorand, F. (2010). Bacterial and iron oxide aggregates mediate secondary iron mineral formation: Green rust versus magnetite. *Geobiology*, *8*(3), 209–222. https://doi.org/10.1111/j.1472-4669.2010.00238.x

Zegeye, A., Ona-Nguema, G., Carteret, C., Huguet, L., Abdelmoula, M., & Jorand, F. (2005). Formation of hydroxysulphate green rust 2 as a single iron(II-III) mineral in microbial culture. *Geomicrobiology Journal*, *22*(7–8), 389–399. https://doi.org/10.1080/01490450500248960

Zhang, Y., Wei, S., Lin, Y., Fan, G., & Li, F. (2018). *Dispersing Metallic Platinum on Green Rust Enables E ff ective and Selective Hydrogenation of Carbonyl Group in Cinnamaldehyde*. https://doi.org/10.1021/acsomega.8b02114

Zhang, Z., Yan, W., Messan, O., Fang, J., & Jackson, W. A. (2021). Abiotic Reduction of Nitrate and Chlorate by Green Rust. *ACS Earth and Space Chemistry*, *5*(8). https://doi.org/10.1021/acsearthspacechem.1c00121

Zhao, G., Tan, M., Wu, B., Zheng, X., Xiong, R., Chen, B., Kappler, A., & Chu, C. (2023). Redox Oscillations Activate Thermodynamically Stable Iron Minerals for Enhanced Reactive Oxygen Species Production. *Environmental Science & Technology*. https://doi.org/10.1021/acs.est.3c02302

Zhao, J., Zhong, P., Luo, W., Zhang, S., Xu, S., Yu, Q., & Qiu, X. (2022). Insight into in-situ chemical oxidation by Fe(II)-containing minerals: The role of inherent Fe(II)-OH in Fe(II)-Al LDHs. *Chemical Engineering Journal*, *433*(P3), 133835. https://doi.org/10.1016/j.cej.2021.133835

Zhao, M., Mills, B. J. W., Homoky, W. B., & Peacock, C. L. (2023). Oxygenation of the Earth aided by mineral–organic carbon preservation. *Nature Geoscience*, *16*(3), 262–267. https://doi.org/10.1038/s41561-023-01133-2

Zhao, Y., Yang, W., Xue, Y., Wang, X., & Lin, T. (2011). Partial exfoliation of layered double hydroxides in DMSO: A route to transparent polymer nanocomposites. *Journal of Materials Chemistry*, *21*(13), 4869–4874. https://doi.org/10.1039/c0jm03975f

Zhilinskaya, E. A., Delahay, G., Mauvezin, M., Coq, B., & Aboukaïs, A. (2003). EPR Investigation of Fe-Exchanged Beta-Zeolites. *Langmuir*, *19*(9), 3596–3602. https://doi.org/10.1021/la026137f

Zhou, D., Cai, Z., Jia, Y., Xiong, X., Xie, Q., Wang, S., Zhang, Y., Liu, W., Duan, H., & Sun, X. (2018). Activating basal plane in NiFe layered double hydroxide by Mn^{2+} doping for efficient and durable oxygen evolution reaction. *Nanoscale Horizons*, *3*(5), 532–537. https://doi.org/10.1039/C8NH00121A

List of Figures

FIGURE 0.1: DIAGRAMME COMPARANT LES SIMILITUDES STRUCTURELLES ENTRE LA RG ET LA SMMO. DE GAUCHE A DROITE, UNE ILLUSTRATION D'UN SEUL CRISTAL GR, LA STRUCTURE DU CATION ET DE L'ANION LDH DU CRISTAL, LA COORDINATION OCTAEDRIQUE DES ATOMES DE FER (JAUNE) ET D'OXYGENE (ROUGE) DANS LA GR, LA STRUCTURE ATOMIQUE ANALOGUE DU CENTRE DE REACTION MMO (AZOTE = BLEU), ET UN MODELE DE L'ENZYME MMO 9
. 9

FIGURE 0.2: SCHEMA ILLUSTRANT DIVERSES INTERACTIONS CHIMIQUES AVEC LES MINERAUX D'OXYHYDROXYDE $FE^{2+}/^{3+}$ 10

FIGURE 0.3 : OXYDATION DU METHANE CH_4. **A-** AUGMENTATION DE LA CONCENTRATION DE CH_4 AVEC LA PRESSION DANS LA SOLUTION GR-CO_3. **B-** SPECTRES EPR DE GR-CO_3 AVANT (NOIR) ET APRES OXYDATION (BLEU) LORSQUE L'ACIDE PERACETIQUE ET UN PIEGE A RADICAUX ABTS SONT UTILISES. **C-** SPECTRES XPS DE LA SURFACE DE GR-CO_3 AVANT (GRIS) ET APRES (ROUGE) EXPOSITION A 1 BAR DE CH_4MONTRANT L'AUGMENTATION DE L'INTENSITE DE LA BANDE CORRESPONDANT AUX LIAISONS C=C APRES EXPOSITION. **D-** SPECTRES RAMAN DE GR-CO_3 AVANT (VERT) ET APRES EXPOSITION A 2 HEURES (BLEU) ET 48 HEURES (ROUGE ET JAUNE) DE MELANGES GAZEUX CH_4 +O_2. 11

FIGURE 0.4 : ILLUSTRATION DE RESULTATS OBTENUS A LORS D'EXPERIENCES DE REDUCTION DU CO_2. **A-** SPECTRES RMN DETAILLANT L'EFFET DE LA SORPTION DE DIFFERENTS GAZ SUR LES SOLUTIONS DE RV-SO_4, OU N_2 (BLEU), CO_2 (ROUGE), CH_4 (VERT) ET CH_4 + NO (JAUNE) SONT COMPARES. **B-** SPECTRES RMN DU DMSO INTRODUIT DANS LES SOLUTIONS DE RV-SO_4 AU COURS DU TEMPS. L'ETAT INITIAL (ROUGE) DIFFERE DE L'ETAT FINAL (BLEU CLAIR) OU L'AUGMENTATION DE LA SURFACE DES PICS A 2,1 ET 3,6 PPM IMPLIQUE LA PRODUCTION DE DMS ET DE PRODUITS DE REDUCTION GLYCOLIQUE. **C-** SPECTRES XPS DE RV-CO_3 AVANT (GRIS) ET APRES (ROUGE) L'INTRODUCTION DE CO_2. **D-** SPECTRES FTIR DE RV-SO_4 A PH=7 (ROUGE), PH=10 (BLEU) ET PH=10 AVEC K_2CO_3 (VERT). 13

FIGURE 0.4: DEMONSTRATION DE LA REPONSE DU GR AUX ESPECES REDOX EXTERNES A DIFFERENTS NIVEAUX DE COMPLEXITE. DANS LA SECTION A, LES GR SONT SUSCEPTIBLES DE TRANSFORMATION OXYDATIVE EN PRESENCE D'O_2. EN B, CELA NE SE PRODUIT PLUS EN RAISON DE LA PRODUCTION DE GLYCOLS PROTECTEURS RESULTANT DE LA REDUCTION SPONTANEE DU CO_2. DE NOMBREUSES REACTIONS PEUVENT ETRE CATALYSEES DE MANIERE NON SPECIFIQUE A CE NIVEAU DE COMPLEXITE. DANS LA DIAPOSITIVE C, EN RAISON DE PRESSIONS DE SELECTION SPECIFIQUES, LES MOLECULES ORGANIQUES SE SONT COMPLEXIFIEES EN UN HYPOTHETIQUE LIGAND POLYAMINO QUI SELECTIONNE UNIQUEMENT L'OXYDATION DU CH_4 EN CH_3OH, RESSEMBLANT A LA FONCTION ENZYMATIQUE EXISTANTE DU SMMO. LA COLORATION ROUGE ET BLEUE INDIQUE RESPECTIVEMENT LES NIVEAUX RELATIFS DE CONDITIONS REDUCTRICES ET OXYDANTES. 14

FIGURE 1.1: SECTION A DISPLAYS A 20X MAGNIFICATION IMAGE OF WET $GRCO_3$ MINERALS, DEMONSTRATING THE INTENSE GREEN COLOR AND GRANULAR PACKING. SECTION B DISPLAYS A SEM IMAGE OF $GRCO_3$ MINERALS ALONGSIDE A VIAL OF FRESHLY FLOCCULATED $GRSO_4$ FOR REFERENCE. SECTION C DISPLAYS XRD CRYSTALLOGRAPH OF $GRCO_3$ (BLUE) AND GR SO_4 (RED), WHILE SECTION D SHOWS OVERLAIN IR, RAMAN SPECTRA OF $GRCO_3$ (BLUE) AND SO_4 (RED) MINERALS. METHODS FOR COLLECTION ARE DESCRIBED IN CHAPTER 3. 29

FIGURE 1.2 : ILLUSTRATIVE DIAGRAM OF $FE^{2+/3+}$ OXYHYDROXIDE GRI, GRII, AND INFERRED MINERAL CRYSTALLINE LATTICES CONTAINING CO_3, SO4, OR VARIABLE ORGANIC INTERLAYER SPECIES. [$FE^{2+/3+}$ ARE GREENS, O ARE BLUES, C IS RED, S IS YELLOW] 30

FIGURE **2.1:** A DIAGRAM COMPARING THE STRUCTURAL SIMILARITIES BETWEEN GR AND SMMO. FROM LEFT TO RIGHT, AN ILLUSTRATION OF A SINGLE GR CRYSTAL, THE CRYSTAL'S CATION AND ANION LDH STRUCTURE, THE OCTAHEDRAL COORDINATION OF IRON (YELLOW) AND OXYGEN (RED) ATOMS IN GR, THE ANALOGOUS ATOMIC STRUCTURE OF THE MMO REACTION CENTER (NITROGEN = BLUE), AND A MODEL OF THE ENZYME MMO. 37

FIGURE 2.2: GRAPH A DISPLAYS METHANOL CONCENTRATIONS AT GIVEN CH_4 PARTIAL PRESSURE FOLLOWING 24 HOURS OF REACTION TIME IN SOLUTIONS CONTAINING $GRCO_3$, $FECL_2$, $FECL_3$, AND H_2O. GRAPH B DISPLAYS A RELATED SET OF EXPERIMENTS CONDUCTED AT [FE] = 30 MM, SHOWING METHANOL PRODUCTION OVER TIME. 40

FIGURE 2.3 : SECTION A DISPLAYS THE XRD DIFFRACTOGRAMS OF THE MINERAL SPECIES PRODUCED FOLLOWING THE EXPOSURE OF $GRCO_3$ TO PRESSURIZED CH_4/O_2 ATMOSPHERES. MAGNETITE (FE_3O_4) AND LEPIDOCROCITE (Y-FEO(OH)) WERE THE PRIMARY TRANSFORMATION PRODUCTS OF GR CORRESPONDING TO LOW (~0.1 BAR) AND HIGH (>0.1 BAR) O_2 CONTENT RESPECTIVELY. PARTIALLY TRANSFORMED PRODUCTS ARE DISPLAYED BELOW THE PRIMARY PRODUCT, WITH THE RESIDUAL GR'S LOW 2Θ D-SPACING LISTED ADJACENT. SECTION B DISPLAYS THE CORRESPONDING SEM IMAGES OF THE PURE MINERAL PHASES CHARACTERIZED IN SECTION A. 42

FIGURE S2.1 : TWO ROWS OF IMAGES FROM SEM (TOP ROW) AND TEM (BOTTOM ROW) OBSERVATIONS OF THE MINERAL PHASES DETECTED WITHIN OUR EXPERIMENTS. IMAGE A AND D SHOW GREEN RUST CARBONATE ($GRCO_3$) FRESHLY PREPARED AND OBSERVED UNDER SEM AND TEM RESPECTIVELY. IMAGE B AND E SHOW PARTIALLY OXIDIZED $GRCO_3$ FOLLOWING EXPOSURE TO CH_4/O2 MIXTURE. VISIBLE ARE GR CRYSTALS STUDDED WITH FEOOH (B, E) AND FE_3O_4 MINERALS (B). IMAGE D AND F SHOWS THE COMPLETE TRANSFORMATION OF GR INTO FE_3O_4 FOLLOWING GR'S EXPOSURE TO CH_4/O2 MIXTURE. 49

FIGURE S2.2 : GRAPH DISPLAYING GR'S ([FE] = 30 MM) PRODUCTION OF MEOH AND CHLOROCARBONS (TCM, DCM) UNDER TWO PRESSURE CONDITIONS, 10 AND 30 BAR CH_4. 50

FIGURE S2.3: GRAPH DISPLAYS DIFFERENCE IN THE PRODUCTION OF MEOH WITH DIFFERENT GR ([FE] = 30 MM) SPECIES. 51

FIGURE S2.4: GRAPH DISPLAYING THE RELATIVE EFFICIENCIES OF MEOH PRODUCTION AT A GIVEN CONCENTRATION OF FE (MEOH/FE). 52

FIGURE S2.5: GRAPH DISPLAYING THE INFLUENCE OF 1 MM H2O2 ON THE PRODUCTION OF METHANOL BY GR ([FE] = 30 MM) COMPARED TO THE PRESSURE EXPERIMENTS. 53

FIGURE SS2.1 : GRAPH A DEPICTS RECOVERED CH_4 CONCENTRATIONS FROM GR $GRSO_4$ AND $GRCO_3$ SUSPENSIONS INCUBATED WITH ~1 BAR CH_4 AND 0, 0.1, 0.15 $ATMO_2$. GRAPHS B AND C SHOW BET ANALYSIS USING N2 ADSORPTION ON $GRCO_3$ AND ITS TRANSFORMATION PRODUCT FE2O3. IMAGES D AND E ARE THE BEFORE AND AFTER IMAGES OF $GRSO_4$ AND $GRCO_3$ (RESPECTIVELY). 56

FIGURE SS2.2 : A IMAGE DEPICTING MORPHOLOGICAL CHANGES ASSOCIATED WITH THE TRANSFORMATION OF SOLUTIONS OF GR VIA HEATING AT 80C, AND A GRAPH DEMONSTRATING THE CORRESPONDING EFFECT OF HEAT OVER METHANE OXIDATION TO METHANOL. 57

FIGURE SS2.3 : AMENDMENT OF GR SOLUTIONS WITH TRANSITION METALS MODIFIED METHANOL PRODUCTION. 57

FIGURE SS2.5 : RAMAN SPECTRA OF UNKNOWN SOLID. IMAGE OF SOLIDS ADHERED TO GLASS SURFACE AND FLOATING ON MINERAL SUSPENSION UNDER SEM. 58

FIGURE 3.1: 9-GHZ EPR SPECTRUM OF $GRCO_3$ (X=.33) RECORDED AS A FUNCTION OF TEMPERATURE. THE VERY BROAD SIGNAL IS CONSISTENT WITH SUPERPARAMAGNETIC SPECIES ARISING FROM EXCHANGE INTERACTIONS OF THE FE^{2+} AND FE^{3+} IONS. EXPERIMENTAL CONDITIONS FOR SAMPLE PREPARATION AND MEASUREMENTS ARE DESCRIBED IN THE MATERIALS AND METHODS SECTION. THE INSET SHOWS A SAMPLE OF $GRCO_3$ IN THE EPR TUBE BEING FROZEN IN LIQUID NITROGEN. 64

FIGURE 3.3 : PROPOSED REACTION MECHANISM FOR THE 2 ELECTRON OXIDATION OF $FE^{2+}(^{3+})$ GREEN RUST DIMERS TO A METASTABLE FE^{4+} STATE WHICH CONDUCTS ELECTRON TRANSFER TO ABTS BACK DOWN TO FE^{3+}. 65

FIGURE 3.4: SPECTROSCOPIC CHARACTERIZATION OF $GRCO_3$ (X=0.33) SYSTEM AT 25°C WITH XRD (A) AND AT -20, 0, 20 °C WITH RAMAN(B) 66

FIGURE 4.1 : CUSTOM BUILT MS EXPERIMENTAL SET UP ATTACHED TO HIGH PRESSURE REACTION CELL INTEGRATED INTO RAMAN MICROSCOPE 71

FIGURE 4.2: EXPOSURE OF $GRSO_4$ TO N2, CO_2, CH_4, CH_4+NO ATMOSPHERES BEFORE (A) AND AFTER (B) UV IRRADIATION. THE TWO FIGURES SHOW NMR SPECTRA OF SOLUTIONS OF 0.2M $GRSO_4$ AT PH 10 WITH DIFFERENT HEAD SPACE COMPOSITIONS UNDER DARK UV IRRADIATION CONDITIONS FOR 48 HOURS. BLUE = N2, RED = CO_2, GREEN = CH_4 , YELLOW = CH_4 + NO. CHANGES TO THE SPECTRA INDICATE FORMATION OF ORGANIC COMPOUNDS. 73

FIGURE 4.3: FIGURE (A) DEMONSTRATES EVOLUTION OF N2 CONTROL OVER 48 HOURS. FIGURE (B) ARE M/Z OBTAINED VIA HEADSPACE GCMS ANALYSIS. METHANOL, PROPONIC ACID, AND ACETIC ACID WERE COMMON PRODUCTS BETWEEN EXPERIMENTS WHILE BUTANAL WERE ASSOCIATED WITH EXPOSURE TO NO. 74

FIGURE 4.4 : A & B ARE SEM IMAGES OF $GRSO_4$ CRYSTALS FOLLOWING EXPOSURE TO 6 AND 48 HOURS OF UV IRRADIATION. MINERALS ARE STUDDED WITH OXIDES. C & D ARE PICTURES OF GR SOLUTIONS WITH N_2, CO_2, CH_4, CH_4+ NO AFTER 48 HOURS OF INCUBATION IN DARK AND UV IRRADIATION CONDITONS. THE CONTROL (N_2) WAS GREEN AND THE ADDITION OF CO_2 AND CH_4 +NO RESULTED IN VISIBLE MINERAL TRANSFORMATION GIVEN COLOR CHANGE. IN ALL TESTS THE UV EXPERIMENTS LED TO VISIBLE TRANSFORMATION TO BLACK FE-OXIDE MINERALS. 75

FIGURE 4.5 : CONFIRMATION OF GLYCOL NMR SIGNATURE FOLLOWING K_2CO_3 ADDITION. IN THE MAIN FIGURE , BLUE SIGNAL CORRESPONDS TO $GRSO_4$ PRIOR TO ANIONIC REPLACEMENT BY $K2CO_3$, WHILE THE RED IS $GRCO_3$ SYNTHESIZED VIA K_2CO_3 REPLACEMENT. THE GREY SPECTRA IS CENTERED ON THE GLYCOL SIGNAL (3.6 PPM) WHICH CORRESPONDS TO ERYTHRITOL. 77

FIGURE 4.6: STACKED SPECTRA FROM A CO_2 REDUCTION EXPERIMENT WHERE THE EFFECT OF TIME (0, 10, 30, 60 MIN CORRESPONDING TO BLUE, RED, BROWN, GREEN) AND HEAT (25-80°C CORRESPONDING TO A,C,D AND B RESPECTIVELY) WAS EXPLORED DURING THE BUBBLING OF CO_2. APPROXIMATELY 1 WEEK ELAPSED BETWEEN SAMPLE COLLECTION AND ANALYSIS BY NMR. ALL SAMPLES DISPLAYED ALMOST IDENTICAL NMR SPECTRA. BUBBLING OF CO_2 INCREASED TWO TRIPLET SIGNATURES BETWEEN 4-3.8 PPM WITH NO OTHER SIGNIFICANT CHANGES TO SPECTRA. 77

FIGURE 4.7: XRD CRYSTALLOGRAMS OF THE TWO TEMPERATURE EXPERIMENTS (A:25C, B:80C) CONDUCTED USING $GRCO_3$ IN 1M KCO3. IN BOTH CASES, 30 MINUTES OF CO_2 BUBBLING DID NOT SIGNIFICANTLY ALTER THE CRYSTAL STRUCTURE OF $GRCO_3$. BY 60 MINUTES, THE HEATED EXPERIMENT RESULTED IN THE LOSS OF CRYSTALLINITY OF THE SAMPLE AND THE FORMATION OF FE-CARBONATE 78

FIGURE 4.9 : MS MEASUREMENTS OF GR DMSO INCUBATION EXPERIMENTS. GRAPH A SHOWS DMSO RECOVERED FROM $GRSO_4$ SUSPENSION WHILE B SHOWS SIMILAR SOLUTION THAT HAS BEEN AGED 3 MONTHS. A NEW SIGNAL IS WEAKLY DETECTABLE (M/Z = 52, 64, 80) BUT IS DIFFICULT TO DISTINGUISH IF IT RELATED TO THE DMS OR DMSO SIGNAL (C). 82

FIGURE 4.10: XPS SPECTRA OF $GRCO_3$ SAMPLES COMPARING OF C1S SPECTRA BEFORE (BOTTOM) AND AFTER EXPOSURE TO CO_2 (A) AND CH_4(B). GRAPH C DEPICTS PERCENT COMPOSITION OF SURFACE SPECIES. 84

FIGURE 4.11: IR SPECTRA OF OF (A) $GRSO_4$ PH 7, (B) $GRSO_4$ PH10, (C) $GRSO_4$ 10 + K_2CO_3 AMBIENT EXPOSURE TO CO_2 AND (D) $GRSO_4$ PH 7 OVER 48 HOURS OF EXPOSURE TO CH_4 ANDO_2 . LARGER CARBONATE FORMATION OCCURS AT HIGHER PH, WHILE MODIFICATION WITH K_2CO_3 APPEARS TO MODIFY CARBONATE SIGNAL. 85

FIGURE 4.13 : RAMAN SPECTRA OF $GRSO_4$ MINERALS EXPOSED TO N_2 AND CO_2 AT 25°C (DARK GREEN AND BLUE) AND -25°C TEMPERATURES.(LIGHT GREEN AND BLUE) SURFACE LOADING OF CO_2 APPEARS AS TWO DISTINCT BANDS BETWEEN 1200-1400 CM^{-1}. 86
FIGURE 4.12: FTIR SPECTRA OF 72 HOURS OF CO_2 CONTACT WITH WITH $GRCO_3$, RESULTING IN ITS DESTABILIZATION AND TRANSFORMATION INTO A MIX OF FE-OXIDES AND CARBONATE MINERALS 86
FIGURE 4.14: IR (A) AND RAMAN (B) SPECTRA OF ERYTHRITOL (RED), $GRCO_3$ (GREEN), $GRCO_3$ + CO_2 24 HOURS (BLUE), $GRCO_3$+ERYTHRITOL. 88
FIGURE 4.15: FTIR (A) AND RAMAN (B) SPECTRA OF $GRSO_4$ EXPOSED TO 1 BAR CH_4 AND 0.2 $BARO_2$. $GRSO_4$ (GREEN), $GRSO_4$ + CH_4/O2 2 HR (BLUE), 48 HR (RED & YELLOW) 89
FIGURE 4.16 : RESULTS FROM EXPERIMENT WHERE A HEADSPACE CONTAINING 8 BAR CH_4 AND 0.1ML $GRCO_3$ WAS INTRODUCED TO 1 BAR AIR. PART A SHOWS GR SOLUTION (20X MAGNIFICATION) BEFORE AND AFTER OXIDATION. B SHOWS THE DIFFERENCE IN M/Z OF 0-44 M/Z OVER 24 HOURS ADJUSTED TO 16 M/Z 91
FIGURE 4.17 : RESULTS FROM EXPERIMENT WHERE A HEADSPACE CONTAINING 8 BAR CH_4 AND 0.1ML $GRCO_3$ IN SEA WATER WAS INTRODUCED TO 1 BAR AIR. A & B COMPARES INITIAL AND FINAL M/Z COLLECTED FROM 40-100 M/Z RANGE. MARKED DIFFERENCES IN M/Z DIVERSITY ARE APPARENT WHEN COMPARING T = BEFORE AND 48 HOURS AFTER O_2 INTRODUCTION. 92
FIGURE 4.18: AN ILLUSTRATIVE DIAGRAM DEPICTING POSSIBLE REACTION PATHWAYS FOR CO_2 REDUCTION OVER $GRCO_3$ SURFACES FORMING C-C BONDS (A) OR WITHIN ITS INTERLAYER FORMING GYCOLS (B). 93
FIGURE 4.19 : AN ILLUSTRATIVE DIAGRAM DEPICTING POSSIBLE REACTION PATHWAY FOR REDUCTION OF CO_2 TO DMSO AND DMS WITHIN AND OUTSIDE THE $GRSO_4$ INTERLAYER. 94
TABLE 5.1: KNOWN PRODUCTS OF CO_2 REDUCTION AND CH_4 OXIDATION AS REPORTED BY LEE 2023 AND FARR 2023,2024. 97
FIGURE 5.1: DEMONSTRATION OF GR'S RESPONSE TO EXTERNAL REDOX SPECIES AT DIFFERENT LEVELS OF COMPLEXITY. IN SECTION A, GR IS LIABLE TO OXIDATIVE TRANSFORMATION IN THE PRESENCE OF O_2. IN B, THIS NO LONGER OCCURS DUE TO THE PRODUCTION OF PROTECTIVE GLYCOLS AS A RESULT OF SPONTANEOUS CO_2 REDUCTION. MANY REACTIONS CAN BE NONSPECIFICALLY CATALYZED AT THIS LEVEL OF COMPLEXITY. IN SLIDE C, DUE TO SPECIFIC SELECTION PRESSURES THE ORGANIC MOLECULES COMPLEXIFIED INTO A HYPOTHETICAL POLYAMINO LIGAND THAT SELECTS FOR ONLY THE OXIDATION OF CH_4 TO CH_3OH, RESEMBLING THE EXTANT ENZYMATIC FUNCTION OF SMMO. RED AND BLUE COLORATION INDICATE RELATIVE LEVELS OF REDUCING AND OXIDIZING CONDITIONS, RESPECTIVELY. 106
FIGURE 5.2 : AN ILLUSTRATIVE DIAGRAM DEPICTING THE VARIOUS CHEMICAL REACTION PATHWAYS MEDIATED BY GR REDOX CHEMISTRY AT EARLY HYDROTHERMAL VENT ENVIRONMENTS. THE INHALATION OF DISSOLVED AND GASEOUS SPECIES FROM SERPENTIZATION PROCESSES NATURALLY LEADS TO REDOX DISEQUILIBRIA WITH COLD OXIDIZED SEA WATER AT THESE MINERAL MOUNDS, PRECIPITATING REACTIVE MINERAL SPECIES LIKE GR. THESE MINERALS CONDUCT C, N, S, FE REDOX WHICH LEADS TO THE FORMATION OF SIMPLE ORGANIC COMPOUNDS WHICH COMPLEXIFY AND POLYMERIZE IN HIGH SURFACE AREA MINERAL PORES. HERE GR'S PARTICULAR CHARACTERISTICS, NAMELY ANIONIC TRANSPORT AND ORGANIC INTEGRATION, ARE SHOWN TO CROSS ORGANIC MEMBRANES AND CONDUCT H+ AND E- TRANSPORT, LEADING TO LOCAL DISEQUILIBRIA. THIS PH AND REDOX GRADIENT IS HYPOTHESIZED TO BE NECESSARY FOR LIFE TO EMERGE(DUVAL ET AL., 2019; M. J. RUSSELL, 2023). BEYOND THIS, THE PRODUCTS YIELDED FROM REDOX REACTIONS ARE EXHALED OUT INTO THE OCEAN AND INTERACT WITH SURFACE OCEAN AND ATMOSPHERIC CHEMISTRY. 111